Contents

EDITORIAL BOARD

Experimental Study of Cotton stalks Gasification in a Downdraft Reactor

دراسة عملية لتغويز حطب القطن باستخدام مفاعل السحب لأسفل

A. Khalil*, Ayman I. Bakry*, Magda K. El-Fakharany**, Karim Rabea*

* Tanta University, Faculty of Engineering, Mechanical Power Dept., Egypt.

** Kafr-Elsheikh University, Faculty of Engineering, Mechanical Power Dept., Egypt.

الملخص

تعتبر عملية تغويز الكتلة الحيوية تقنية واعدة لتحويل المخلفات الى طاقة وللقضاء على المشاكل البيئية الضخمة المصاحبة لعملية الحرق في الحقل المفتوح. الهدف من هذه الدراسة هو دراسة عملية للأداء الديناميكى لمغوز بتصميم من نوع (إمبرت) وحجم معملى بإستخدام حطب القطن. تم استخدام الهواء كعامل تغويز وكمية الكتلة الحيوية ٤ كجم دفعة واحدة. تقييم خصائص عملية التغويز يتمثل فى تحديد القيمة الحرارية السفلى وكفاءة عملية التغويز ووقت التشغيل. غطت الدراسة معدلات سريان للهواء (٦٠-١٠٠-١٥٠-٢٠٠) لتر فى الدقيقة محققة نسبة تكافؤ تتراوح بين (٠,٣٦٢ الى ٠,٢٣٢). وقد أظهرت النتائج ان نسبة التكافؤ ٠,٣٠٤ هى الأفضل لتغويز حطب القطن حيث يعطى قيمة حرارية سفلى متوسطة للغاز الناتج تساوى ٤,٣٤ ميجا جول/م^{٣} من الغاز وكفاءة تغويز ٦١,٧%.

ABSTRACT

Biomass gasification process is considered a promising waste-to-energy conversion technique to eliminate the immense environmental issues accompanied with open field burning. The objective of this study is to experimentally study the dynamic behavior of an Imbert based design manufactured bench scale gasifier using cotton stalks as a feed stock. Air was employed as a gasifying agent with a biomass batch feed of 4 kg. The gasification process characteristics are evaluated in terms of lower heating value, gasification efficiency, and operation time. The applied air flow rates are (60, 100, 150, and 200 l/m) achieving varied equivalence ratios between 0.362 – 0.232. An optimum average lower heating value and cold gas efficiency of 4.34 MJ/m^3 and 61.7 % respectively are attained at equivalence ratio, ER of 0.304.

1. Introduction

The expanding gap between demand and consumption of energy particularly in developing countries has exacerbated the energy crisis. Furthermore, the accompanied limitations related to the fossil fuels such as the expected extinction, and pollution, force to explore alternative renewable energy sources. The alternative sources, biomass gets increasing attention, thanks to its carbon neutral feature [1]. Moreover, it is the only renewable energy source which contains carbon to be converted into convenient solid, liquid and gaseous fuels, and further into heat, electricity and transport fuels [2].

Energy from biomass can be obtained via two major routes, biochemical conversion (fermentation) and thermochemical conversion (pyrolysis, gasification, combustion) [1]. Among them, gasification is an interesting technique to convert biomass into combustible gas mixture called synthesis gas (syngas). The utilization of biomass gasification is sorely wide spreading since, it is reliable and efficient technique that can use biomass with minimum pretreatments and in the same place where it is generated. Generally, gasification involves the reaction of the solid fuel with co-reactant at temperatures range of 550-1000 $^{\circ}$C. Co-reactants are introduced in sub-stoichiometric amounts in order to partially oxidize the fuel instead of complete oxidation to CO_2 and H_2O [3]. The resulting gas is a mixture of carbon monoxide, hydrogen, methane, and carbon dioxide along with small amounts of light hydrocarbons. Diverse co-reactants can be used such as air., oxygen, steam, and CO_2 [3].

Different gasifiers are employed for this process, mainly including fixed bed, fluidized bed, and entrained flow [4]. The main difference between these reactors is distinguished by how the biomass and the oxidizer are moving inside the reactor. Compared with the fluidized bed and entrained flow gasifiers, fixed bed gasifier is more suitable for small scale applications [5]. The fixed bed includes downdraft, updraft and cross-draft gasifiers. The downdraft fixed bed gasifier has the advantage of low tar generation by cracking, as the gas passes through high temperature zone [6]. Therefore, the downdraft fixed bed gasifier is chosen in this study.

Four sub-processes, namely drying, pyrolysis, oxidation (combustion), and reduction (char gasification) overlap at a particular time along the gasifier[7].

Many researches have been conducted on downdraft gasifiers for diverse types of biomass to evaluate the gasifier performance and biomass capability of gasification. Jain [8] designed and tested an open core throat-less (stratified) gasifiers with internal diameters varying from 15.2 to 34.3 cm. The optimum values of equivalence ratio (ER), gasification efficiency, and lower heating value (LHV)

were reported to be 0.40, 65%, and 4.5 MJ/m^3 respectively.

Guo et al. [6] used a reactor with an internal diameter of 0.42 m to gasify the corn stalk with continuous feeding option. They concluded that, the optimum equivalence ratio was 0.25-0.27 giving LHV of 5.4 MJ/m^3 at feeding rate of 7.5 Kg/h with gasification efficiency of 65 %.

Singh and Sekhar [9] studied experimentally and theoretically the variation in performance parameters when gasifying blends of coconut shell and rubber seed shell. The equivalence ratio range was (0.2 – 0.34) where the maximum concentration of combustible gases occurred at 0.2 and decreased at 0.3. Coconut shells conducted combustible species and conversion efficiency more than rubber seed shells.

Gai and Dong [5] studied the corn straw gasification in a stratified gasifier with two stages of air supply. The optimum ER was 0.32 giving LHV of 5.39 MJ/m^3. Yoon et al. [10] used a larger scale reactor to perform the gasification of rice husk and rice husk pellets and reported that, an optimum ER of 0.58 for rice husk and 0.29 for pellets with HHV of 4.5 and 5.5 MJ/m^3 respectively.

A co-gasification of lignite and waste wood has been investigated by Patel et al. [11] that showed a maximum LHV of 4.44 MJ/m^3 at 30 % wood to lignite ratio. Chen et al. [12] operated an electrically heated small gasifier at 800 °C using Biogas-derived digestate as a feed stock and obtained a LHV of 4.78 MJ/m^3 at ER of 0.25.

Tanczuk et al. [13] determined the influence of adding dried chicken manure to the wood pellets at constant ER of 0.21, they found that when blending wood pellets with raw chicken manure the LHV increased from 2 MJ/m^3 to 4 MJ/m^3 at 75% mixture. In order to improve the gasification process, a throat could be incorporated as referred by [14-18]

A preliminary experiment for the determination of the range of gasifying air flow rate in batch operation [16, 17] concluded that, when gasifying 9 kg and 8 kg of Oil palm fronds, the flare was observed after exceeding 200 l/m of air, then weakens after 400 l/m while the gasification time was about 34 min. Besides, preheating air upstream the gasifier enhanced the HHV from 4.66 to 5.31 MJ/m^3.

Galindo et al. [19] operated a stratified gasifier using Encalyptus wood with 12 kg/h as a feed stock at air flow rates of 300, 333.3 and 366.67 l/m which correspond with ER of 0.303, 0.279 and 289 respectively. They concluded a maximum LHV of 5.12 MJ/m^3 when operating at 0.289 equivalence ratio.

Sheth and Babu [15] studied the gasification of waste wood in batch operation of 3 kg with air flow rate varied from 30.83 to 56.67 l/m which led to 1 and 3.63 kg/h fuel consumption rate

respectively, achieving ER of 0.35 and 0.179 at different moisture content.

Machin et al. [20] created a swirl flow at the combustion zone while gasifying three different types of biomass (Olive, Peach, Pine). An optimum HHV of 3.97 MJ/m^3 for Peach at 7.6 kg batch feed with 88.3 l/m air for 2.5 hours.

Sharma and sheth [21] studied the dynamic behavior of the gasifier using wood at air flow rate varying from 25.7 l/m to 41.13 l/m and reported that, as the air flow rate increases the biomass consumption rate linearly increase. Using air-steam gasification exhibited a calorific value of (3.64 – 4.01) MJ/m^3.

Nisamaneenate et al. [22] identified the optimal operating conditions for the gasification of peanut shell waste using thermal integration unit coupled to modular downdraft gasifier. The LHV was observed to increase from 3.66 to 3.79 MJ/m^3 and cold gas efficiency from 40.17 to 41.62 % at ER of 0.12. When operating with heat recovery at ER nearly 0.21, the carbon conversion efficiency increased by 5.75 % and a maximum LHV of 3.92 MJ/m^3 was obtained.

Few researchers investigated the gasification of cotton stalk, Karatas et al. [23] investigated the gasification of cotton stalk in fluidized bed reactor, they obtained a maximum LHV of 3.24 MJ/m^3 at ER equals 0.36. Whereas, Wang et al. [24] studied the cotton stalk pellets in a throated downdraft gasifier with separated pyrolyzer and reported a LHV of 4.22 at ER of 0.21.

Hamad et al. [25] used an electric heater to externally heat the reactor for the gasification of cotton stalks, rice straw, and corn stalks with different catalysts and concluded that, cotton stalks is more suitable for gasification process. Besides, an optimum ER of 0.25 was attained.

Most of the researches have included only steady state operation [10,13,21-25]. Limited researches have been done on the dynamic behavior of the gasification process. The aim of this work is concerned with investigating the gasification with Egyptian cotton stalk waste using throated downdraft fixed bed gasifier. Hence, the dynamic behavior of cotton stalks gasification with the influence of operating parameters; air flow rate, equivalence ratio, and gasification temperature were investigated. The study was conducted by measuring temperature profiles, producer gas composition at the transient conditions inside the gasifier. In addition, the process evaluation parameters such as, produced gas calorific value and gasification efficiency are estimated.

2. Experimental Setup

2.1 Fuel material specifications

The main source of biomass waste in Egypt is the agricultural wastes (crop residues), followed by municipal solid wastes, animal wastes, and sewage wastes [26]. Therefore,

Cotton stalks as agriculture waste material is chosen for this study. The proximate and ultimate analyses of cotton stalks are presented in Table 1

Table 1: Proximate and ultimate analyses of cotton stalks [25]

Proximate Analysis, Mass Fraction %				
VM		FC		Ash
81.24		14.48		4.28
Ultimate Analysis, Mass Fraction %				
C	H	N	S	O
44.8	5.8	1.09	0.57	43.8
Higher Heating Value (MJ/kg)				
15.5				

The feed stock is shredded after open field drying to a particle size (as length) ranged from 1 to 4 cm and from 2 to 5 mm (as diameter) as shown in Fig. 1

Fig. 1: Size and shape of cotton stalks

Due to the importance of moisture content in the gasification process, it was determined based on wet basis by the oven drying method (ASTM D4442-07) [27]. The biomass is heated at 105 ˚C for 24 hours in a vented forced convection oven (Binder FD 23) and then weighed. The moisture content (MC) expressed in percentage was calculated according to equation (1) [27].

$$MC\% = \frac{m_{wet} - m_{dry}}{m_{wet}} \times 100 \qquad (1)$$

Where m_{dry} represents the mass of the fuel after heating and m_{wet} is the mass of fuel prior heating. The determined moisture content of cotton stalks was about 14 %. The feed stock was then provided to the gasification system.

Lower heating values (LHV) for biomass was calculated using the empirical formula that reported by Sarkar [28].

$$LHV = HHV - 2.44 \times (9H) \qquad (2)$$

Where H is the hydrogen content of biomass determined through the ultimate analysis.

2.2 The gasifier unit

The experimental tests are performed on a self-made downdraft gasifier. The gasification unit comprises four main parts: the reactor, the gasifier casing, the ash disposal system, and the air supply setup. A throat-type is used as the core of the gasifier reactor with the configuration and dimensions shown in Fig. 2. The core is made of a 3-mm thick steel sheet with an overall height of 0.67 m. The upper diameter of 0.32 m is tapered to 0.22 m diameter at depth of 0.46 m from the top.

This tapered section is followed by a constant diameter section of 0.22 m in diameter and 0.08 m in height. Near its lower

end, five air nozzles are regularly distributed and mounted around the same circumferential level. The reactor core is ending by a convergent-divergent section with a throat of 0.13 m where both the combustion and reduction gasification zones are situated. This constricted area provides a uniform combustion across the whole area and to force all of the pyrolysis gases to pass through this narrow passage [20].

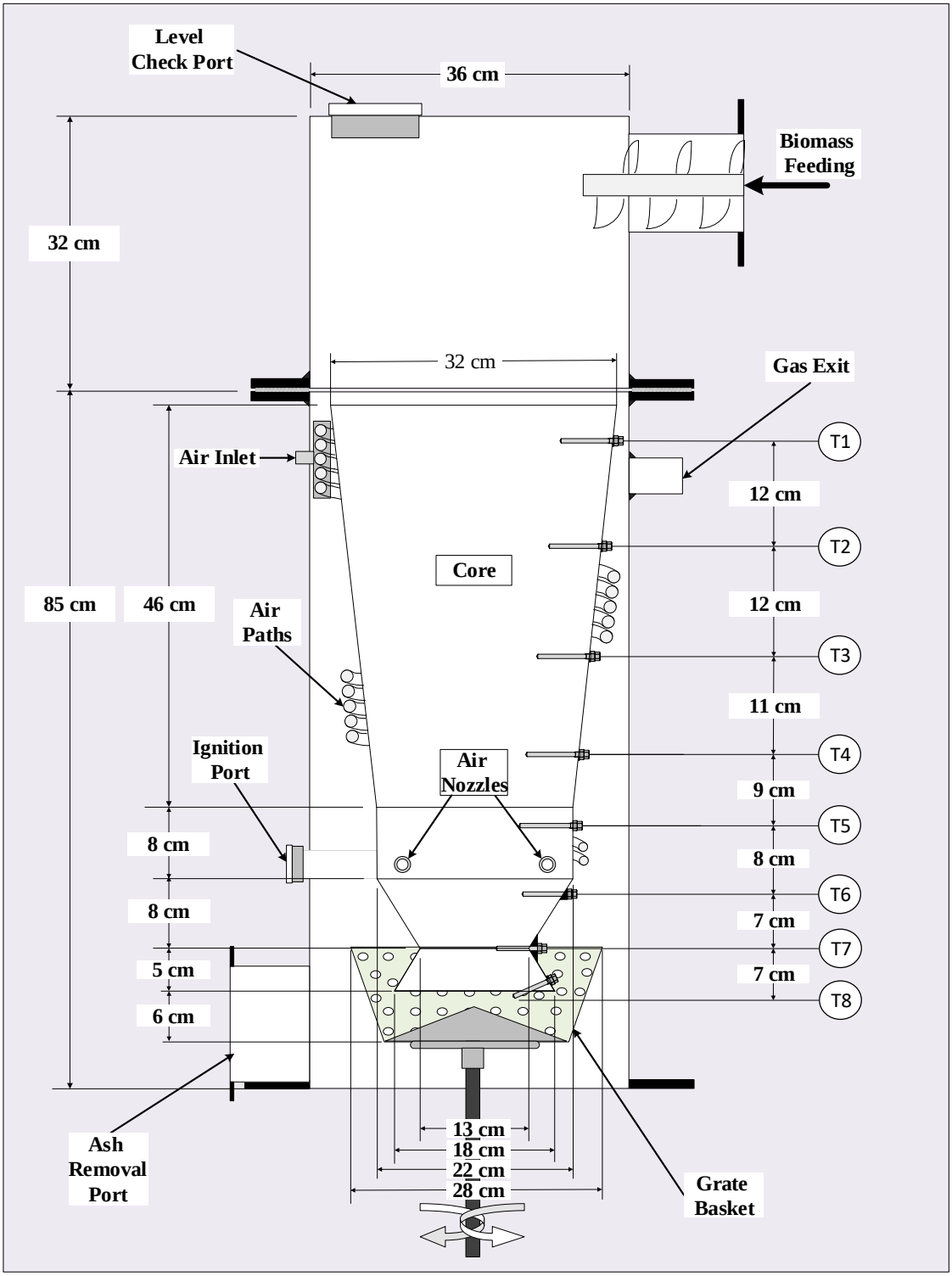

Fig. 2. The downdraft gasifier reactor

The throat is followed by the divergent part where the reduction process is commenced. The divergent part is important to lessen the gas flow velocity in order to enhance the rate of boudouard reaction and water-gas shift reaction, in order to increase the concentration of CO and H_2 in the producer gas and also decrease the gas temperature [20]. Under the divergent part, the ash grate is directly positioned to hold the hot charcoal for reduction reactions

The ash grate is made of perforated steel sheet with openings of 5 mm in diameter. The grate is formed on the shape of trapezoidal basket with upper and bottom diameters of 0.28 m and 0.20 m respectively, and a height of 0.11 m. Also, a small cone of 0.04 m in height is fixed on the floor of the basket. This small cone is used to enhance the conversion reduction reactions by keeping a thin layer of the hot charcoal in the path of the reactant gases stream. Besides, the cone is helpful in expelling the ashes out of the basket when the grate shaker system is working.

The core of the gasifier reactor is placed in a coaxial steel cylinder of 4 mm thickness with a height of 1.17 m and diameter of 0.36 m**.** the reactor cylinder is divided into two parts assembled together in the purpose of maintenance and connecting the biomass feeding system to the upper part. The lower part of the cylinder works as a shield around the reactor core. The air supply connection, the ignition port, the produced gas outlet port, and the ash removal port are installed at the cylinder side wall. The hot produced gas from the reactor is passing through the annular passage between the cylinder and the reactor core. The flowing hot produced gas is beneficial for the drying and pyrolysis zones moreover, to preheat the gasifying agent air.

The Feedstock is fed to the gasifier reactor by 4 kg batch through a controlled screw conveyor. The gasifying agent, (air) was circulated through a copper coil in five separate paths that are firmly wounded around the outer wall of the reactor core as shown in Fig. 2. These paths are ending with five nozzles of 5 mm exit diameter.

2.3 Cleaning devices

Cleaning the produced gas is often essential for downstream end-use applications. Different clean-up methodologies such as cyclone, and charcoal filter are comprised. Cyclone is connected directly to the reactor gas exit. The solid particles and some ashes are separated and collected in a collector at the lower end of the cyclone. Design and dimensions of the cyclone are based on Stairmand design [29] with main diameter (D) of 10 cm.

For further purification of the produced gas, a charcoal filter mixed with silica gel in between as a desiccator is added downstream the cyclone. The tar flowing out with the

produced gas stick at the outer surface of the char blocks.

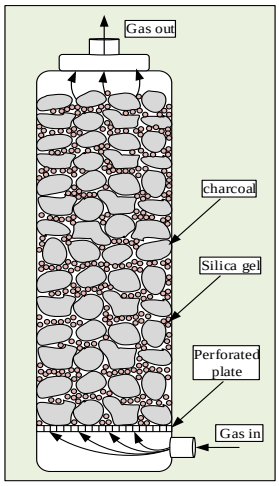

Fig. 3. Charcoal filter with silica gel

2.4 Instruments and measuring techniques

The temperatures are measured using eight K-type thermocouples positioned on the core wall with distances as illustrated in Fig. 2. Also, at the gas exit port an additional thermocouple is mounted to indicate the gas exit temperature. The thermocouples data are acquired using a multichannel multiplexer (KTA-295K) controlled by an Arduino board**.**

The air flow rate is monitored by two different flow meters connected in parallel, (Omega, FMA-A2323) is the primary flow meter providing a reading range of 0-100 SL/M and an accuracy of ±1%, besides (SMC brand, model:PFA511-F03N-Q) with the same range of flow and accuracy.

In order to characterize the produced gas, measurements of the gas compositions are carried out using gas chromatography (GC) of Perkin-Elmer, model (Clarus 580) with TCD detector. This GC is capable of detecting CO, CO_2, CH_4, H_2, N_2, O_2, C_2H_4, and C_2H_6 molecules with an accuracy of 0.01%.

A slipstream of product gas is pulled by 60 ml syringes from the bulk gas stream coming out of the charcoal filter after further sample purification by cotton.

3. Test calculations

Equivalence ratio, ER, is considered a key parameter that affects the gasification process. It relates the mass flow rate of both reactant materials including air and biomass fuel, in actual and stoichiometric conditions.

$$ER = \frac{\left[\frac{air\ flow\ rate}{biomass\ consumption\ rate}\right]_{actual}}{\left[\frac{air\ flow\ rate}{biomass\ consumption\ rate}\right]_{stoichiometric}}$$

where, the stoichiometric air to fuel ratio can be calculated as reported in [6] by Guo et al.

$$\left[\frac{\text{air flow rate}\left(^{\text{Kg}}/_{\text{h}}\right)}{\text{biomass consumption rate}\left(^{\text{Kg}}/_{\text{h}}\right)}\right]_{\text{stoichiometric}} = \frac{1.293}{0.21}\left(1.866\frac{C_{daf}}{100} + 5.55\frac{H_{daf}}{100} + 0.7\frac{S_{daf}}{100} - 0.7\frac{O_{daf}}{100}\right) \quad (3)$$

The lower heating value (LHV) of produced gas in MJ/m^3 can be estimated from the gas composition using the following empirical formula (4) [30] as follows.

$$LHV = [(10.79 \times H_2) + (12.636 \times CO) + (35.82 \times CH_4)] \quad (4)$$

Where H_2, CO, and CH_4 are the gases concentrations (% V/V), in the syngas.

Cold gas efficiency (CGE) of the gasification process is defined as the ratio of the energy in the product gas to the energy of biomass input (biomass energy). The CGE% applied in this work is based on the lower heating value (LHV) of both the product gas and biomass. Then it can be calculated as in [31].

$$CGE\ \% = \frac{[LHV]_{gas} \times V_g}{[LHV]_{biomass}} \times 100\% \quad (4)$$

Where $[LHV]_{biomass}$ is the lower heating value of biomass, MJ/kg and V_g is the volume of produced gas per unit weight of biomass (m^3/kg). It can be calculated from the concentration of nitrogen in the product gas and the total amount of nitrogen entering the reactor along with air in the gasification process as in [32] by,

$$V_g = \frac{(Q_{air} \times 79)}{(N_2 \times m_b)} \quad (5)$$

Where Q_{air} is the flow rate of air (m^3/h), N_2 is the concentration of nitrogen in the syngas (% V/V), and m_b is biomass flowrate (kg/h).

4. Test procedure

Prior each experiment, 4 kg of cotton stalk (for a specified particle size range and moisture content) is poured inside the feeding hopper and fed by the screw feeder. Now, a vacuum pump is used for the startup ignition with the aid of a fire torch. Once, some feed material became red hot, the ignition port is sealed and the adjusted air flow rate for the case study is supplied. The gas sampling starts when the flare starts and repeated randomly during the experiment until the flare disappear.

5. Results and discussion

5.1 Variation of temperature and gas composition with time.

The temperatures distribution inside the gasifier, the produced gas composition and its corresponding heating value are observed to vary with time. This variation is investigated for experimental runs at different air flow rates (60, 100, 150, and 200 l/m) that reported in Figs. 4–7 respectively. As temperatures and gas composition of produced gas are varying continuously. The dynamic behavior of temperatures and produced gas composition may provide real time interpretation of the results and hence the variation of temperatures and gas composition are presented in this study. Figures. 4–7 (a) describe the temperatures distribution while, Figs. 4–7 (b) show the gas composition with time.

5.1.1 Temperature distribution

Temperature in the gasifier increases along the length from T1 to T6 establishing zones of drying, pyrolysis, and combustion respectively then decreases at T7 and T8 representing the

reduction zone. Generally, the drying zone temperature (T1, T2) is found to be in the range of 110 °C and around 400 °C is observed for the pyrolysis zone (T3, T4). In case of batch operation, the biomass flow downward by gravity inside the reactor so, by end of the run T1-T4 increase due to biomass diminishing. Due to the bridging problem as reported by [33], an increase in T3 and T4 then decrease due to biomass collapse after bridging is noticed at some time during operation. Besides, combustion temperatures (T5 and T6) are also affected by bridging in form of T5 increase as presented in figs. 4-7 (a). While, the reduction zone temperatures (T7 and T8) showed more stability during operation with time.

Figs 4-7 (a) show that T6 represent the maximum temperature in the reactor and its maximum value is attained at 100 l/m air flow rate. When operating the gasifier at high air flow rate of 200 l/m, it is noticed that T4 and T5 jump over and exceed T6 representing expanded combustion zone up.

Meanwhile, the reduction zone temperatures (T7 and T8) are observed in relatively low range in the case of air flow rate of 60 l/m and 200 l/m than that obtained at 100 and 150 l/m as shown in figs. 4-7 (a). The average reduction zone temperatures (T7 and T8) are in the range of (635 – 455°C and 650 - 560 °C) at the air flow rates of 60 l/m and 200 l/m respectively, while, they were in the range of (710 – 590 °C and 720 - 570 °C) at air flow rates of 100 and 150 l/m respectively.

The temperatures fluctuation are observed and those may be attributed to number of reasons. One of the prominent reasons is due to the local variation of thermocouple contact with solid or gas at a particular position [21].

As, the air flow rate increases, the biomass consumption rate increases thus, the operation time of the gasification process is lessened. It was about 105 minutes at air flow rate of 60 l/m then reduced to about 20 min at 200 l/m air flow rate.

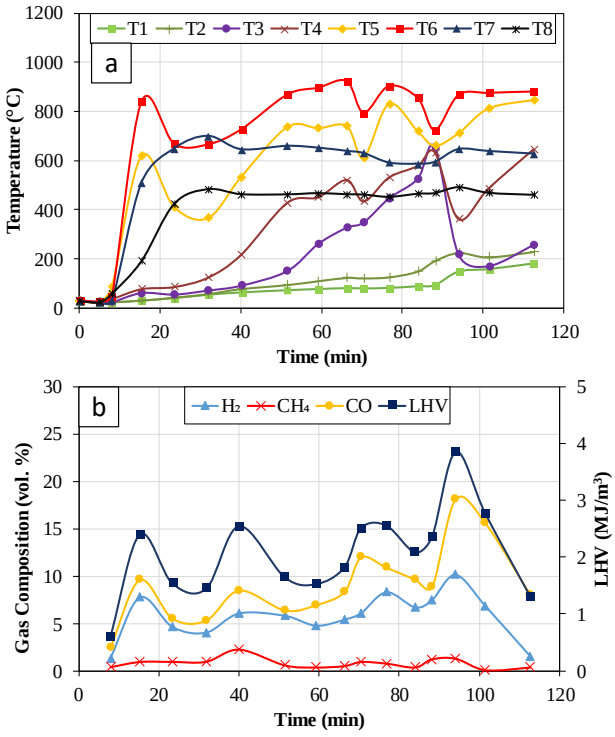

Fig. 4. Variation of temperature, gas composition and LHV over time at air flow rate of 60 l/m (ER=0.362)

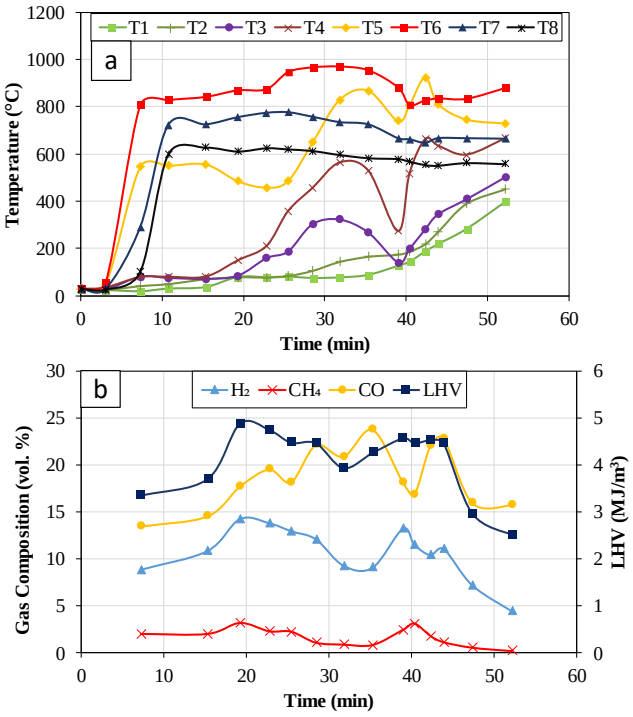

Fig. 5. Variation of temperature, gas composition and LHV over time at air flow rate of 100 l/m (ER=0.302)

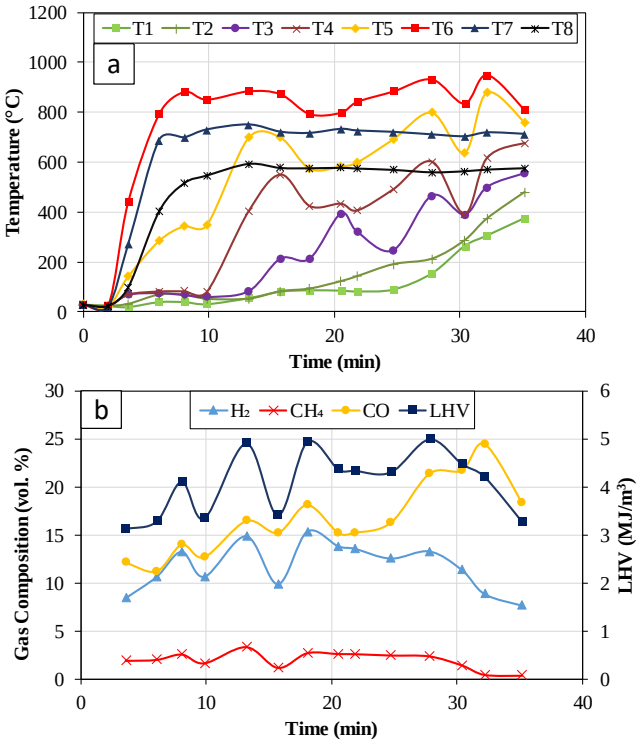

Fig. 6. Variation of temperature, gas composition and LHV over time at air flow rate of 150 l/m (ER=0.304)

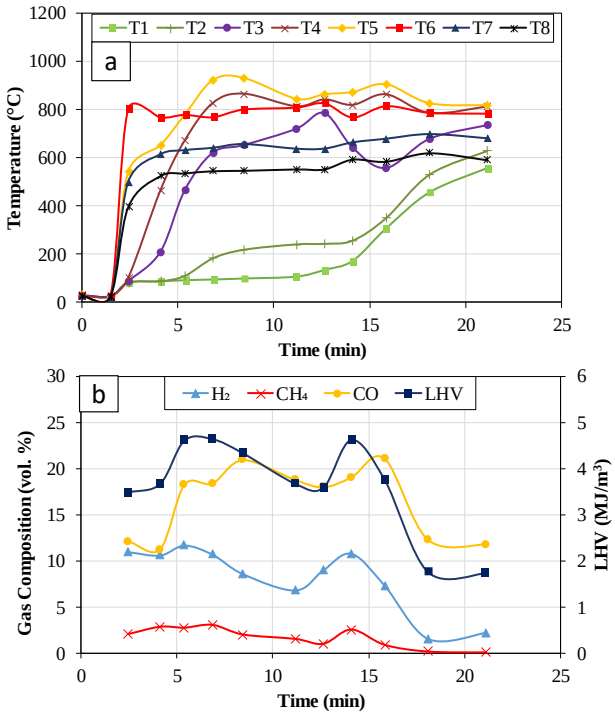

Fig. 7. Variation of temperature, gas composition and LHV over time at air flow rate of 200 l/m (ER=0.232)

5.1.2 Composition of produced gas

The produced gas composition varies with time depending on the instantaneous operating condition inside the reactor. Gas samples are taken randomly during operation with 60 ml syringes. The first sample of gas is taken with the preliminary appearance of flare. Figs 4-7 (b) show the dynamic variation of the combustible gas components including H_2, CH_4 and CO and the corresponding LHV with time. It is obvious that in batch operation, the gas components concentrations are highly affected by the temperature and the bridging problem inside the reactor. Particularly in small scale gasifiers, the moisture content, amount of biomass, and volatile matter in feed stock are diminishing with time. Thus, The CO

concentration is noticed to increase and H_2 decrease in the last period of operation time. H_2 concentration showed a relatively lower values at air flow rates of 60 and 200 l/m compared to its values at air flow rates of 100 and 150 l/m. Moreover, at 150 l/m air flow rate, CH4 indicated a considerable stable higher volumes along the run than that obtained at 60, 100 and 200 l/m.

5.1.3 Produced gas heating value

The LHV of the produced gas obtained at the different studied air flow rates exhibited fairly fluctuated values at the steady operation time as presented in figs 4-7 (b). A maximum lower heating value of 5 MJ/m^3 is attained once at 100 l/m air flow rate, while it was achieved three times at the air flow rate of 150 l/m as illustrated in fig 5 and fig 6 respectively.

5.2 Effect of air flow rate.

The effect of air flow rate on biomass consumption rate is shown in Figs. 4-7. It is found that with the increase of air flow rate, biomass consumption rate increases. The increase in the air flow rate provides more oxygen to oxidize and higher amount of biomass would get combusted. The energy released will increase the rate of drying and pyrolysis. Biomass consumption rate increases not only due to a higher combustion rate, but also due to the enhanced pyrolysis and drying rate.

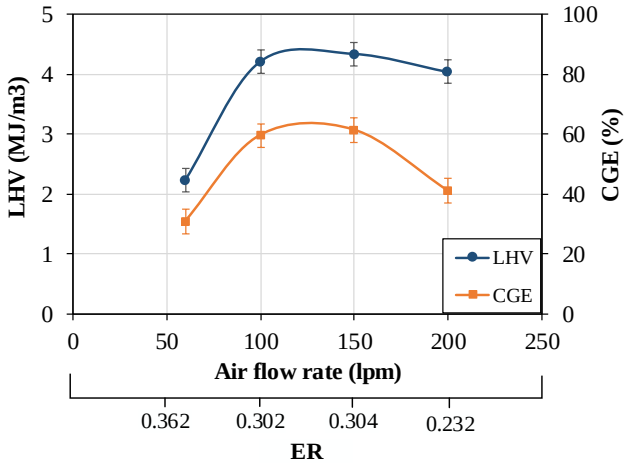

Fig. 8. Effect of ER on LHV and CGE

The average obtained values of LHV as well as the cold gas efficiency are demonstrated in Fig. 8 at different air flow rates and their corresponding ERs. LHV and CGE of the gasification process showed a significant increasing trend when the air flow rate changed from 60 l/m to 100 l/m. Almost constant values of LHV and CGE are attained till 150 l/m followed by slight decrease upon reaching 200 l/m of air flow rate. When the air flow rate is 60 l/m the combustion heat is inadequate for reduction reactions, whereas, increasing the supplied air flow rate enlarges the combustion heat to be adequate for reduction zone reactions in addition to pyrolysis and drying zones enhancement. As the air flow rate excessively increase to 200 l/m, the combustion heat being greatly enlarged compared to reduction zone requirements. Average LHVs of 2.23, 4.21, 4.34, and 4.04 MJ/m3 are attained at the air flow rates of 60, 100, 150, and 200 l/m which corresponds to a calculated ER of 0.362, 0.302,

0.304, and 0.232 respectively. While the attained average CGE values are 30.77, 59.55, 61.69, and 41.07 % at ERs of 0.362, 0.302, 0.304, and 0.232 respectively.

6. Conclusion

The experimental investigation of the dynamic behavior of cotton stalk batch gasification in an Imbert design gasifier using air as a gasifying agent was demonstrated. From the experimental results; the following conclusions are drown, In batch operation, the biomass consumption rate is proportional to the applied air flow rate as the time of operation decreases. As the pyrolysis effect decreases with time, the volume concentration of H_2 in the syngas showed a reduced values whereas the CO concentration increases due to the accumulation of char in the reduction zone. The optimum operating ER for cotton stalk gasification is (0.302-0.304) which produces a considerable high lower calorific value of (4.21-4.34) and cold gas efficiency of (59.55-61.69 %).

Nomenclature

m_{dry}	mass of fuel after heating,
m_{wet}	mass of fuel prior heating,
V_g	Produced gas yield (m^3/kg)
Q_{air}	Air flow rate (m^3/h)
m_b	Biomass feeding rate (Kg/h)

Abbreviations

ER	Equivalence Ratio
LHV	Lower Heating Value
HHV	Higher Heating Value
VM	Volatile Matter
FC	Fixed Carbon
MC	Moisture Content in feedstock
GC	Gas Chromatography
TCD	Thermal Conductivity Detector
SL/M	Standard Liter Per Minute
daf	Dry ash free

References

1. Basu, P., *Biomass gasification, pyrolysis and torrefaction: practical design and theory*. 2013: Academic press.
2. Kang, Q., et al., *Bioethanol from lignocellulosic biomass: current findings determine research priorities.* The Scientific World Journal, 2014. **2014**.
3. Rada, E.C., *Thermochemical Waste Treatment: Combustion, Gasification, and Other Methodologies*. 2017: CRC Press.
4. Raman, P. and N. Ram, *Design improvements and performance testing of a biomass gasifier based electric power generation system.* Biomass and bioenergy, 2013. **56**: p. 555-571.
5. Gai, C. and Y. Dong, *Experimental study on non-woody biomass gasification in a downdraft gasifier.* International Journal of hydrogen energy, 2012. **37**(6): p. 4935-4944.
6. Guo, F., et al., *Effect of design and operating parameters on the gasification process of biomass in a downdraft fixed bed: An experimental study.* International Journal of Hydrogen Energy, 2014. **39**(11): p. 5625-5633.
7. Ismail, T.M. and M.A. El-Salam, *Parametric studies on biomass gasification process on updraft gasifier high temperature air gasification.* Applied Thermal Engineering, 2017. **112**: p. 1460-1473.
8. Jain, A.K., *Design parameters for a rice husk throatless gasifier reactor.* Agricultural Engineering International: CIGR Journal, 2006.

9. Singh, V.C.J. and S.J. Sekhar, *Performance studies on a downdraft biomass gasifier with blends of coconut shell and rubber seed shell as feedstock.* Applied Thermal Engineering, 2016. **97**: p. 22-27.

10. Yoon, S.J., et al., *Gasification and power generation characteristics of rice husk and rice husk pellet using a downdraft fixed-bed gasifier.* Renewable Energy, 2012. **42**: p. 163-167.

11. Patel, V.R., et al., *Co-gasification of lignite and waste wood in a pilot-scale (10 kWe) downdraft gasifier.* Energy, 2017. **119**: p. 834-844.

12. Chen, G., et al., *Air gasification of biogas-derived digestate in a downdraft fixed bed gasifier.* Waste Management, 2017. **69**: p. 162-169.

13. Tańczuk, M., et al., *Experimental analysis of the fixed bed gasification process of the mixtures of the chicken manure with biomass.* Renewable Energy, 2017.

14. Olgun, H., S. Ozdogan, and G. Yinesor, *Results with a bench scale downdraft biomass gasifier for agricultural and forestry residues.* biomass and bioenergy, 2011. **35**(1): p. 572-580.

15. Sheth, P.N. and B. Babu, *Experimental studies on producer gas generation from wood waste in a downdraft biomass gasifier.* Bioresource technology, 2009. **100**(12): p. 3127-3133.

16. Guangul, F.M., S.A. Sulaiman, and A. Ramli, *Gasifier selection, design and gasification of oil palm fronds with preheated and unheated gasifying air.* Bioresource technology, 2012. **126**: p. 224-232.

17. Guangul, F.M., S.A. Sulaiman, and A. Ramli, *Study of the effects of operating factors on the resulting producer gas of oil palm fronds gasification with a single throat downdraft gasifier.* Renewable Energy, 2014. **72**: p. 271-283.

18. Omar, M.M., et al., *Downdraft gasifier structure and process improvement for high quality and quantity producer gas production.* Journal of the Energy Institute, 2017.

19. Galindo, A.L., et al., *Biomass gasification in a downdraft gasifier with a two-stage air supply: Effect of operating conditions on gas quality.* biomass and bioenergy, 2014. **61**: p. 236-244.

20. Machin, E.B., et al., *Tar reduction in downdraft biomass gasifier using a primary method.* Renewable Energy, 2015. **78**: p. 478-483.

21. Sharma, S. and P.N. Sheth, *Air–steam biomass gasification: experiments, modeling and simulation.* Energy conversion and management, 2016. **110**: p. 307-318.

22. Nisamaneenate, J., et al., *Fuel gas production from peanut shell waste using a modular downdraft gasifier with the thermal integrated unit.* Renewable Energy, 2015. **79**: p. 45-50.

23. Karatas, H., H. Olgun, and F. Akgun, *Experimental results of gasification of cotton stalk and hazelnut shell in a bubbling fluidized bed gasifier under air and steam atmospheres.* Fuel, 2013. **112**: p. 494-501.

24. Wang, Z., et al., *Gasification of biomass with oxygen-enriched air in a pilot scale two-stage gasifier.* Fuel, 2015. **150**: p. 386-393.

25. Hamad, M.A., et al., *Hydrogen rich gas production from catalytic gasification of biomass.* Renewable Energy, 2016. **85**: p. 1290-1300.

26. Abdelhady, S., et al., *Viability study of biomass power plant fired with rice straw in Egypt.* Energy procedia, 2014. **61**: p. 211-215.

27. Govett, R., T. Mace, and S. Bowe, *A practical guide for the determination of moisture content of woody biomass.* University of Wisconsin, 2010.

28. Sarkar, M., et al., *Gasification performance of switchgrass pretreated with torrefaction and densification.* Applied Energy, 2014. **127**: p. 194-201.

29. Stairmand, C.J., *The design and performance of cyclone separators.* Trans. Inst. Chem. Engrs., 1951. **29**: p. 356-362.

30. Striūgas, N., et al., *An evaluation of performance of automatically operated multi-fuel downdraft gasifier for energy production.* Applied thermal engineering, 2014. **73**(1): p. 1151-1159.

31. Basu, P., *Combustion and gasification in fluidized beds*. 2006: CRC press.

32. Sharma, A., et al., *Performance evaluation of a lab-scale fluidized bed gasifier using switchgrass as feedstock.* Transactions of the ASABE, 2011. **54**(6): p. 2259-2266.

33. Inayat, M., et al., *The study of temperature profile and syngas flare in co-gasification of biomass feedstock in throated downdraft gasifier*, in *ICGSCE 2014*. 2015, Springer. p. 203-210.

Numerical Study for Performance Evaluation of Plastic Solar Air Heater with Different Cross-Sectional Configuration

دراسة نظرية لتقييم أداء سخان هواء شمسى بلاستيكى ذو مقاطع مختلفة

A.I. Bakry *, Y.A.F. El-Samadony *, S.S. Elsayed*, A.E. Ebied **

*Tanta University, Faculty of Engineering, Mechanical Power Dept., Egypt.

** Middle Delta Electricity Production Company (MDEPC).

الملخص

فى هذا البحث تمت دراسة خمسة مقاطع مختلفة المساحة السطحية للمقطع الذى يدخل منه الهواء للسخان الهوائى الشمسى للمقارنة بينهم من ناحية الكفاءة الحرارية.المقاطع التى تمت دراستها كالأتى (دائرى ،نصف دائرة مضاف اليه مثلث متساوى الأضلاع ،نصف دائرة ،نصف دائرة مقطوع منه مثلث متساوى الأضلاع وشكل هلالي) و جميع الأشكال لها نفس مساحة مقطع السطح الماص لأشعة الشمس . وتمت الأختبارات ببرنامج أنسز 14،0 وعندما درسنا تغير السرعة من 0،25 الي 2،0 (متر/ثانية) وكانت النتائج كالأتى أن الشكل الدائرى للسخانات الهوائية الشمسية هى الأحسن من ناحية الكفاءة الحرارية بقيمة 79 ،51% .وعند ثبوت الأشعاع الشمسى عند 850 (وات/متر^2) وعند عمل الأختبار الثانى وذلك بتغير قيمة الأشعاع الشمسى من 400 الى 1200 (وات/متر^2) مع ثبوت قيمة سرعة الهواء عند 1,0 (متر/ثانية) كانت النتايج كالأتى أن الشكل الدائرى هو الأعلى كفاءة حرارية بقيمة 35،5%.

ABSTRACT

In this research, a numerical investigation was performed on five solar air heaters with different cross-sectional shape to find the best configuration relevant to thermal performance. The selected tested shapes in this study were (circular, semi-circular, half-circle plus isosceles triangle, half circle-negative isosceles triangle shape and crescent shape) and all tested shapes hade the same absorber surface area. The effect of two parameter (velocity and solar radiation intensity) on thermal performance of solar air heater were studied numerically by ANSYS 14.0. The velocity of air was changed from 0.25 to 2.0 (m.s^{-1}). Results indicated that the highest efficiencies were accomplished for the circular configuration and reached to about 51.79% at solar radiation intensity 850 (W.m^{-2}). The solar radiation intensity was changed from 400 to 1200 (W.m^{-2}). Results indicated that the highest efficiencies were accomplished for the circular configuration and reached to about 35.51% at air velocity 1.0 (m.s^{-1}).

1. Introduction

Solar air heaters (SAHs) , represent the primary component of solar energy usage systems. (SAHs) are used to convert the solar energy to thermal energy by increasing the temperature of air flow through the (SAHs).To obtain heated air we use a combustion of fuels, which have productions of (co_2, so_2, No_x) gases which cause air pollution, rain acid and damage the environment therefore all world wards to renewable energy to reduce the air pollution. The biggest source of renewable energy is the sun. The outlet temperature is used in several industrial applications [1, 2, 3], like crop drying, textile dyeing, building heating and water desalination.

1.1 Solar air heater collector's types:

- Unglazed solar air collectors or (transpired solar collectors) used primarily to heat ambient air in commercial, industrial, agriculture and process applications.

The term "unglazed air collectors" refers to a solar air heating system that consists of an absorber without any glass or glazing over top. Unglazed solar air collectors usually wall-mounted to capture the lower sun angle in the winter heating months as well as sun reflection off the snow and achieve their optimum performance.

- Glazed solar air collectors recirculating types that are usually used for space heating.

Glazed air collectors, functioning in a similar manner as a conventional forced air furnace, systems provide heat by recirculating conditioned building air through solar collector. Glazed air collectors are a simple and effective collector can be made for a variety of air conditioning or process applications, the air is ducted to the building space or to the process area where, the heated air is used for space heating or process heating needs.

A simple solar air collector consists of an absorber material sometimes having a selective surface to capture radiation from the sun and transfers this thermal energy to air.

The SAHs, have many advantages, the simple design component, no emissions, low costs to build it, longer maintenance and can built over any roof. In another side SAHs have low thermal efficiency and this is due to heat loss through the cover.

There are several studies to improve the thermal efficiency of solar air heater and all of them refer to increasing the heat transfer coefficient [4, 5] by changing the flow air through SAHs from laminar to turbulent regime by using fins or turbulators which attached over the absorber surface. Ho et al. [6] found experimentally and theoretically that

heat transfer is improved when fins were attached over the absorber surface and they found that heat transfer improve by attaching fins and thermal efficiency were increased by increasing Reynolds number (Re) .Yadav and Thapak [7] used another way to make the flow turbulent by attaching ribs on the absorber surface and they found that the flow turbulent near the wall increased and improved the heat transfer and increased the thermal efficiency. Sharma et al. [8] used ribs as artificial roughness to improve the heat transfer coefficient and they found that heat transfer improve by attaching ribs on the absorber surface and thermal efficiency were increased by increasing Reynolds number (Re) Yadav and Bhagoria [9] used transverse wire rib roughness and they found that heat transfer improve by this method and thermal efficiency were increased by increasing Reynolds number (Re). Rawat et al. [10] used 60˚ inclined V- shape ribs and they found that heat transfer improve by increasing Reynolds number (Re).

There was another method to improve the thermal efficiency by using packed bed materials were used as store heat during the day to be reused at night to increase the out let temperature. El Khadraoui et al. [11] used packed bed materials to improve the thermal efficiency they were indicated that the thermal energy which stored during the day used during the night by this ensured increasing the outlet temperature of SAHs all day. Naphon [12] used numerically method to study the effect of thermal conductivity of porous media packed bed of double- pass SAHs and they found that heat transfer improve by using packed bed method and double- pass SAHs had thermal efficiency better than one pass. Gill et al. [13] fabricated and compare between of pack bed, double glazed and single glazed and they found the results were the efficiency of pack bed is the highest and reached to 71.7%. There was another side it desired to have cheap cost to design the SAHs, many paper had been studied for thermal efficiency with low cost of component. Njomo [14] compared the plastic and glasses cover thermal performance and cost for them. The results found that using plastic cover decrease the cost of designing the SAHs. Janjai et al. [15] also used plastic cover and they concluded that thermal efficiency was increased as the length of SAHs increased till reached to 20 m whiles increasing length more than 20 m there was no notable increase in thermal efficiency. Bansal et al. [16] applied two solar air heaters with low cost absorber materials one with black textile absorber and the other with black PVC foil they found that the thermal efficiency was increase about 18% and the increase of the outlet temperature was about 10 °C. Ahmad [17] designed a solar air heater with cheap plastic cover with air bubbles they found that the thermal efficiency was increase about 12.5% and the increase of the outlet

temperature was about 10 °C. Abdullah and Bassiouny [18] used flexible cylinder type plastic SAH, with circular shape with 0.5 m diameter. They concluded that the outlet temperature increased as the mass flow rate was increased. Abdullah et al. [19] used different cross sectional for solar air heater (circle, semi-circle and half circle-plus isosceles triangle) had same absorber surface area with plastic cover, the thermal performance studied with varied mass flow rate experimentally. They concluded that the highest efficiencies were accomplished for circular shape and reached to about 82.2% at mass flow rate 0.25 ($kg.s^{-1}$).

To the author's knowledge effect of inlet air velocity and solar radiation intensity on thermal performance of solar air heater with different five cross sectional area were studied numerically.

Different cross sectional shapes were studied were (circle, semi-circle, half circle-plus isosceles triangle, half circle-negative isosceles triangle and crescent shape).

All the SAHs had the same absorber area semi-circle with (diameter D= 0.3 m and length L=20 m), the all shapes had the same plastic cover with emissivity coefficient 0.98 and all of them were studied at same boundary conditions.

2. Numerical Work

A numerical simulating program is used in the current search is ANSYS 14.0, it is used to solve set of equations which describe the processes of momentum, the steady-state equations of heat and mass transfer. The ANSYS 14.0 CFX is based on finite volume techniques to solve these equations. In this technique the region which tested, divided into small sub-regions called control volumes. The equations discretized and solved iteratively for each control volume. As a result, an approximation of the value of each variable at specific points throughout the domain can be obtained. In this way, a full picture obtained of the behavior of the flow. The geometry of the region of interest is then defined. The mesh is then created after importing the mesh into the pre-processor other elements of the simulation including the boundary conditions (inlets, outlets, etc.) and fluid properties were defined. The flow solver was run to produce a file of results that contains the variation of velocity, temperature and any other variables throughout the region was studied. Results can be providing the engineer an understanding of the behavior of the fluid throughout the region of interest. This can lead to design modifications which can be tested by changing the geometry of the CFD model and seeing the effect.

The process of performing a single CFD simulation can be divided into.

1. Creating the Geometry/Mesh, as shown in Fig. (1, 2).
   Table (1) shown how to select mesh properties.

2. Defining the Physics of the Model and boundary conditions created (inlet, outlet, absorber wall and fluxed wall).

3. Solving the CFD Problem.

4. Visualizing the Results in the Post-processor, as shown in Fig. (3).

Five different cross-sectional shapes as shown in Fig. (4,5) were studied under the same boundary conditions and same physics model used and one variable varied to study the effect of this variation with the thermal performance.

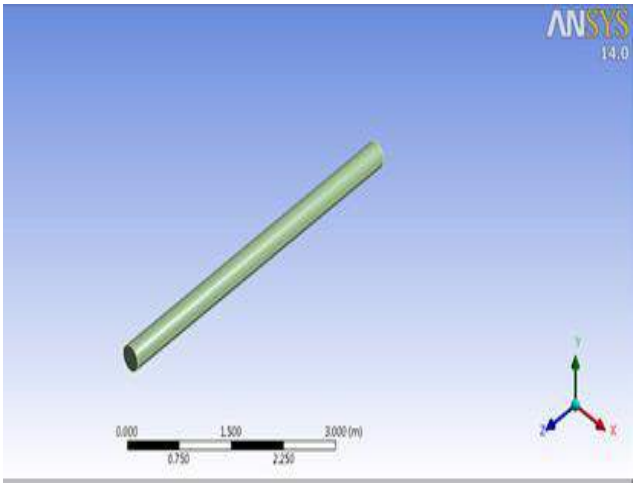

Fig. 1. The geometry of circular air heater.

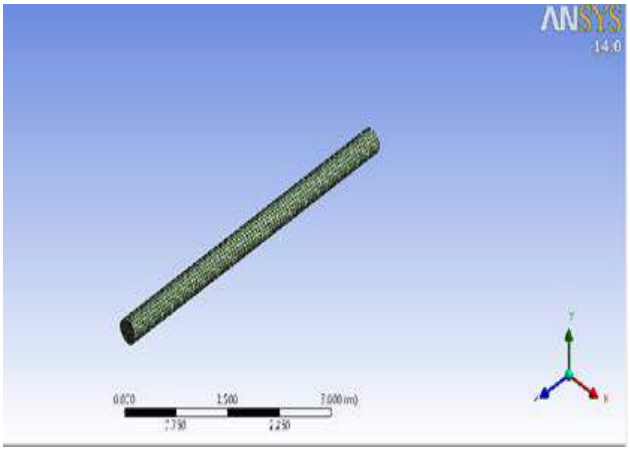

Fig. 2. Mesh of circular air heater.

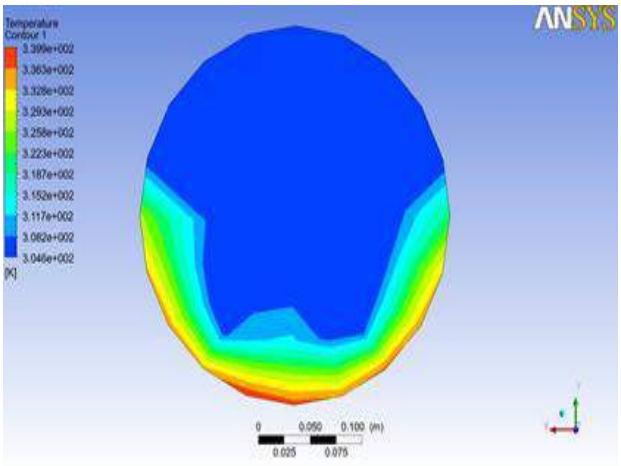

Fig. 3. Out let profile obtained in one of the simulation.

Table 1. selection of mesh sizing for tested simulating.

Max face size	No. of grids		Outlet temperature	Error %
	Nods	Element		
0.035	60321	55221	345.18	-
0.045	40495	35076	346.42	0.35
0.055	37620	33352	346.796	0.1
0.065	21948	18356	346.852	0.01
0.075	18630	14792	346.858	0.0017

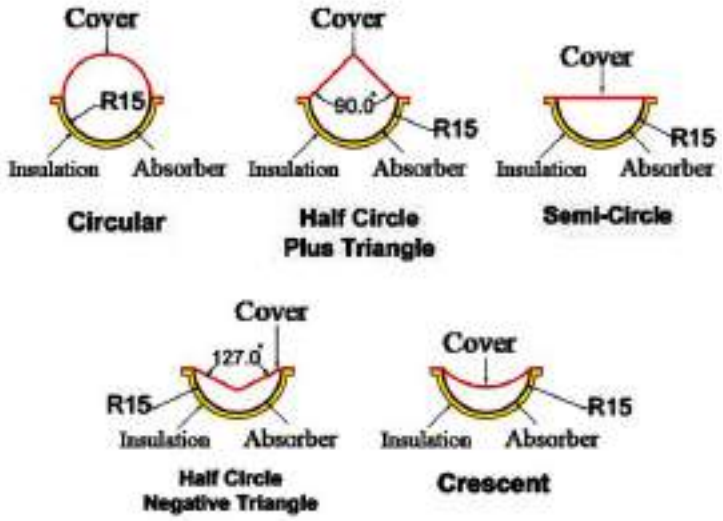

Fig. 5. The different five cross section area of tested solar air heaters.

Table 2: Definition for studied five shapes

parameter	Circular	Half circle + triangle	Semi-circle	Half circle - triangle	Crescent
Cross section area (A_c) , m^2	0.071	0.058	0.035	0.024	0.023
Premeter (p), m	0.942	0.896	0.771	0.807	0.805
$D_{hydraulic}$, m	0.3	0.258	0.18	0.118	0.1143
Diameter , m	0.3	0.3	0.3	0.3	0.3
Cover surface area , m^2	9.42	8.48	6.0	6.72	6.66
Absorber surface area (A_p) , m^2	9.42	9.42	9.42	9.42	9.42

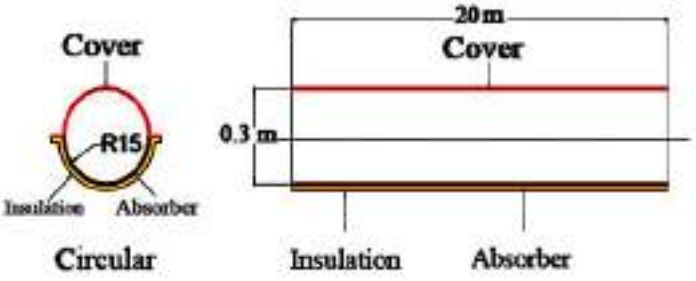

Fig .4. Circular model (L=20m, D=0.3m)

.

2.1 Effect of inlet air velocity:

Studding the effect of variation of air inlet velocity through SAHs from 0.25 to 2.0 ($m.s^{-1}$) with a constant solar radiation intensity flux I= 850 ($W.m^{-2}$) on the thermal performance of solar air heaters. The boundary condition for this tested case is shown in table (3). In this study the outlet temperatures (T_{out}) represent the main parameter.

Table 3: The boundary condition for studding the effect of air inlet velocity.

Domain	Boundary conditions	Value
Inlet	Temperature	32.9 ˚C
	Air flow velocity	0.25, 0.5, 1.0, 1.5, 2.0 $m.s^{-1}$
Outlet	Ref. Pressure	1.0 atm
Absorber	Heat transfer	0.0 $W.m^{-2}$
cover	Heat transfer	850 $W.m^{-2}$

2.2 Effect of solar radiation:

Studding the effect of variation of solar radiation intensity from 400 to 1200 ($W.m^{-2}$) with a constant inlet air velocity V= 1.0 ($m.s^{-1}$), on the thermal performance of solar air heaters. The boundary condition for this tested case is shown in table (4). In this study the outlet temperatures (T_{out}) represent the main parameter.

Table 4: The boundary condition for studding the effect of solar radiation intensity.

Domain	Boundary conditions	Value
Inlet	Temperature	32.9 ˚C
	Air flow velocity	1.0 $m.s^{-1}$
Outlet	Ref. Pressure	1.0 atm
Absorber	Heat transfer	0.0 $W.m^{-2}$
cover	Heat transfer	400, 600, 800, 1000, 1200 $W.m^{-2}$

2.3 Comparison between present numerical results and previews experimental data at same conditions:

Abdullah et al. [19] used different cross sectional for solar air heater (circle, semi-circle, half circle-plus isosceles triangle) as shown in figure (6,7). The thermal performance studied with varied mass flow rate experimentally they concluded that the highest efficiencies were accomplished for circular shape and reached to about 80.2% at mass flow rate 0.25 ($kg.s^{-1}$) and at the same working conditions the efficiencies for the other shapes were respectively (70.6% and 50.6% for half circle-plus isosceles triangle and semi-circle), in this case we studied the same three shape (circle, semi-circle and half circle-plus isosceles triangle) with absorber length 5.0 m , diameter 0.3 m and emissivity coefficient 0.98 at same worked condition of their experimental search they varied the mass flow rate through the SAHs from 0.05 to 0.25 ($kg.s^{-1}$) with a constant solar radiation intensity 950 ($W.m^{-2}$) to make a comparison between a numerical studied and their experimental studied. The boundary condition for this tested case is shown in table (5).

Table 5: The boundary condition for studding the effect of mass flow rate through in SAHs.

Domain	Boundary conditions	Value
Inlet	Temperature	32.9 C°
	Air mass flow rate	0.05, 0.1, 0.15, 0.2, 0.25 kg. s^{-1}
Outlet	Ref. Pressure	1.0 atm
Absorber	Heat transfer	0.0 $W.m^{-2}$
cover	Heat transfer	950 $W.m^{-2}$

Fig .7. The different three cross section area of tested solar air heater for verification. [19]

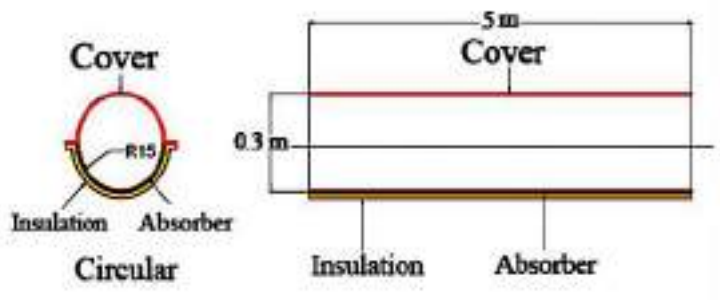

Fig .7. Circular model (L=5m, D=0.3m). [19]

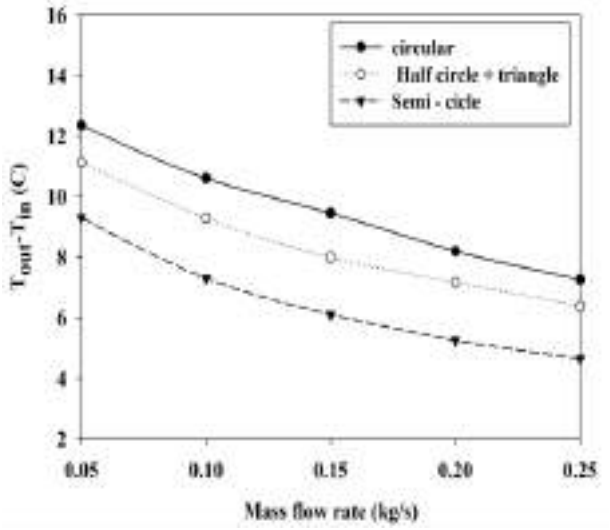

Fig.8.The variations of temperature difference with mass flow rate at constant solar radiation intensity 950 (W/m^2) for different tested shape.

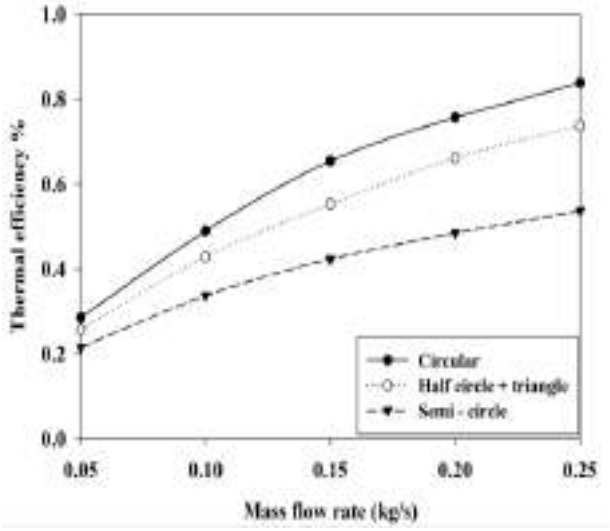

Fig.9.The variations of thermal efficiency with mass flow rate at constant at constant solar radiation intensity 950 (W/m^2) for different tested shapes.

The variation of mass flow rate at constant solar radiation intensity was done at various plastic solar heaters cross sectional Shapes to acquire the best efficiency. A comparison between the variations of temperature difference, between inlet and outlet air temperature (T_{out} - T_{in}) with mass flow rate ($\dot{m}$) at constant solar radiation intensity 950 ($W.m^{-2}$) for circular, half-circle plus isosceles triangle, semi-circular is shown in Figure

(8).The figure indicated that the temperature difference decreases as mass flow rate (ṁ) increase at a constant solar radiation intensity 950 ($W.m^{-2}$). It was found that the temperature difference for the circular shape is higher than half circle-plus isosceles triangle, by the same way the half circle-plus isosceles triangle is higher than semi-circle. Also from Figure (8). It could be noted that at mass flow rate 0.05 ($kg.s^{-1}$) and solar radiation 950 ($W.m^{-2}$) the temperature differences was about 12.36 ˚C for circular shape air heater.

A comparison between the thermal efficiency for the three cross section shapes (circular shape, half circle-plus isosceles triangle and semi-circular) had the same absorber cross section area. The tested solar air heaters as a function of mass flow rate (ṁ) through air heaters at constant solar radiation intensity 950 ($W.m^{-2}$) is shown in Figure (9). As shown it can be noticed that by increasing mass flow rate (ṁ) the thermal efficiency for the air solar heaters increases. Also, it can also be observed that the rate of increasing the thermal efficiency is very high at lower air flow rate range 0.05–0.15 (kg. s^{-1}). The energy loss by heat transfer to fluid increases with increasing the mass flow rate (i.e. increasing the Reynolds number).The figure indicated that the circular solar air heater had better efficiency compared with semi-circular plus triangle air heaters and semi-circular air heaters. This due to the circular solar air heater had the highest energy transfer because of having the largest cross section area.

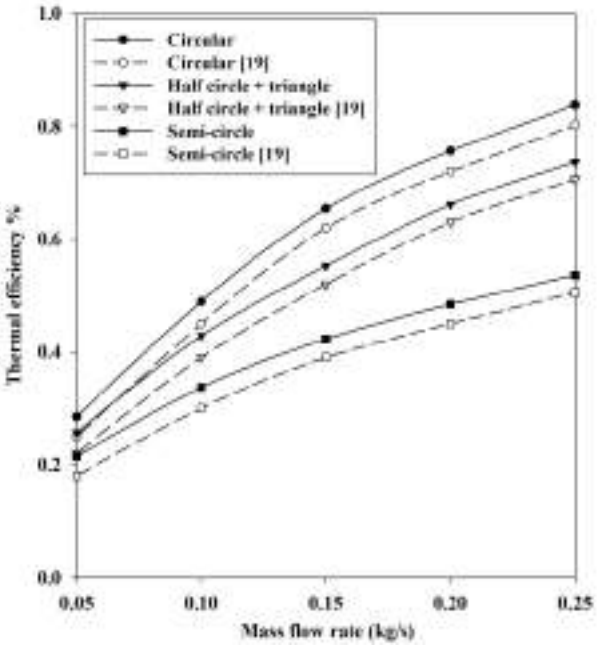

Fig.10.The variations of thermal efficiency with mass flow rate at constant at constant solar radiation intensity 950 ($W.m^{-2}$) for different tested shapes numerical and experimental results verification.

A comparison between present work and Abdullah, et al. [19] experimental study at same boundary conditions is shown in Figure (10) As shown it can be noticed that the circular shape had the best thermal efficiency numerically and experimentally and the results for the both searches were converged and the error between them as shown in figure (10) at range from 2.96% to 3.80%.

2.4. Governing Equations

Governing equations which are used by the ANSYS software are illustrated here.

2.4.1. Continuity equation

$$\partial\rho/\partial t + \nabla \cdot (\rho\, U) = 0 \qquad (1)$$

2.4.2. Momentum equation

$$\frac{\partial(\rho \mathrm{U})}{\partial t} + \nabla \cdot (\rho\, U \times U) = -\nabla P + \nabla \cdot \tau + \mathrm{S_M} \qquad (2)$$

Where the stress tensor, τ, is related to the strain rate by

$$\tau = \mu\left(\nabla U + (\nabla U)^T - \frac{2}{3}\,\delta\,\nabla \cdot U\right) \qquad (3)$$

2.4.3. Total energy equation

$$\frac{\partial(\rho h_{tot})}{\partial x} - \frac{\partial \rho}{\partial t} + \nabla \cdot (\rho\, U\, h_{tot}) = \nabla \cdot (\lambda \nabla T) + \nabla \cdot (U \cdot \tau) + U \cdot \mathrm{S_M} + \mathrm{S_E} \qquad (4)$$

Where h_{tot} is the total enthalpy, related to the static enthalpy h(T, P) by.

$$h_{tot} = h + \frac{1}{2}\,\mathrm{U}^2 \qquad (5)$$

The term $\nabla \cdot (\mathrm{U} \cdot \tau)$ represents the work due to viscous stresses and is called the viscous work term.

The term $\mathrm{U} \cdot \mathrm{S_M}$ represents the work due to external momentum sources and is currently neglected.

2.4.4. Reynolds no (Re). Calculation

$$\mathrm{Re} = \rho \mathrm{V} D/\mu \qquad (6)$$

$$D = \frac{4A}{P}$$

2.4.5. Mass flow rate ($\dot{m}$) through the SAHs can calculate from

$$\dot{m} = \rho \mathrm{V} A_c \qquad (7)$$

2.4.6. The SAHs thermal efficiency obtained as follow:

$$\zeta = \frac{\text{Useful energy delivered}}{\text{Total incoming solar energy}} = \frac{\dot{m}\, C_P\, (T_{out} - T_{in})}{A_P\, I_C} \qquad (8)$$

Where, A_p the absorber area

$A_p = \pi\, r\, L$

3. Results and Discussions

3.1 The variation of inlet air velocity at constant solar intensity radiation:

The variation of inlet air velocity at constant solar intensity radiation was done at various plastic solar heaters cross sectional Shapes to acquire the best thermal efficiency. A comparison between the variations of temperature difference between inlet and outlet air temperature (T_{out}-T_{in}) with velocity of air flow through solar air heater cross sectional shapes shown in Figure (11). The figure indicated that the temperature difference decreases as the velocity of flow air increases because of increasing the Reynolds number. Higher Reynolds number increases the turbulent flow that improves energy transfer to air. It is found that the temperature difference for the crescent shape was the highest, this is because of the crescent shape has the smallest mass flow rate due to the crescent shape had the smallest cross section area . Also, from Figure (11) it could be noted that solar intensity 850 ($W.m^{-2}$) and air flow velocity

0.25 ($m.s^{-1}$) the temperature differences was about 86.16 ˚C for crescent shape air heater.

A comparison between the thermal efficiency for the five tested solar air heaters as a function of inlet air velocity at constant solar radiation intensity 850 ($w.m^{-2}$) shown in Figure (12). It can be noticed from that by increasing velocity of air flow the thermal efficiency for the air solar heaters increases. The figure indicated that the circular solar air heater had the best thermal efficiency compared with others four cross sectional shapes. Because of the circular shape have the largest cross-sectional area so the circular solar air heater has higher energy transfer than the other four shapes.

3.2 The variation of solar radiation intensity at constant inlet air velocity:

The variation of solar radiation intensity at constant velocity was done at various plastic solar heaters cross sectional Shapes to acquire the best thermal efficiency. A comparison between the variations of temperature difference between inlet and outlet air temperature (T_{out} - T_{in}) with solar radiation intensity at a constant air velocity 1.0 ($m.s^{-1}$) as shown in Figure (13). The figure indicated that the temperature difference increases as solar radiation intensity increase at a constant velocity 1.0 ($m.s^{-1}$).It is found that the temperature difference for the crescent shape was the highest compared with others shapes This is because at velocity of air flow1.0($m.s^{-1}$) the mass flow rate (ṁ) within crescent the shape 0.0393 ($Kg.s^{-1}$) is lower than that for half circle-negative isosceles triangle 0.041($Kg.s^{-1}$), semi-circular shape 0.059 ($Kg.s^{-1}$), half circle-plus isosceles triangle 0.099 ($Kg.s^{-1}$) and circle shape 0.121 ($Kg.s^{-1}$). And every cross-sectional shape the mass flow rate (ṁ) through in was a constant whatever solar intensity varied from 400 to 1200 ($w.m^{-2}$). Also, from this figure it could be noted that solar intensity 1200 ($W.m^{-2}$) and air flow velocity 1.0 ($m.s^{-1}$) the maximum temperature differences was about 89.09 ˚C for crescent air heater.

A comparison between the thermal efficiency for the five tested solar air heaters as a function of solar radiation intensity at constant inlet air flow velocity 1.0 ($m.s^{-1}$) as shown in figure (14). As shown it can be noticed from that by increasing solar radiation intensity the thermal efficiency for the air solar heaters increases. The figure indicated that the circular solar air heater had the best efficiency compared with other four cross sectional shapes Because of the circular shape had the largest cross-sectional area so it had higher energy transfer than the other four shapes.

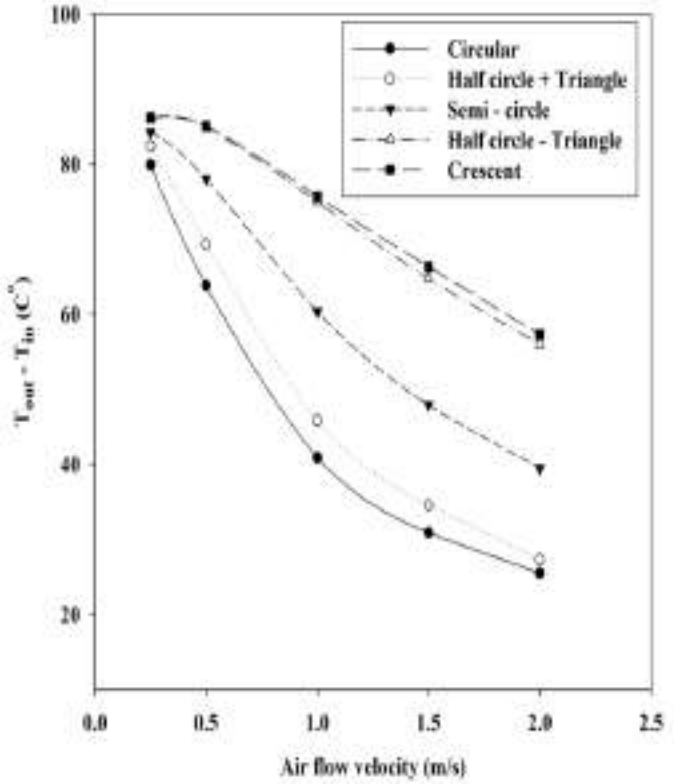

Fig.11.The variations of temperature difference with air inlet velocity at constant solar radiation intensity 850 (W/m^2) for different tested shapes.

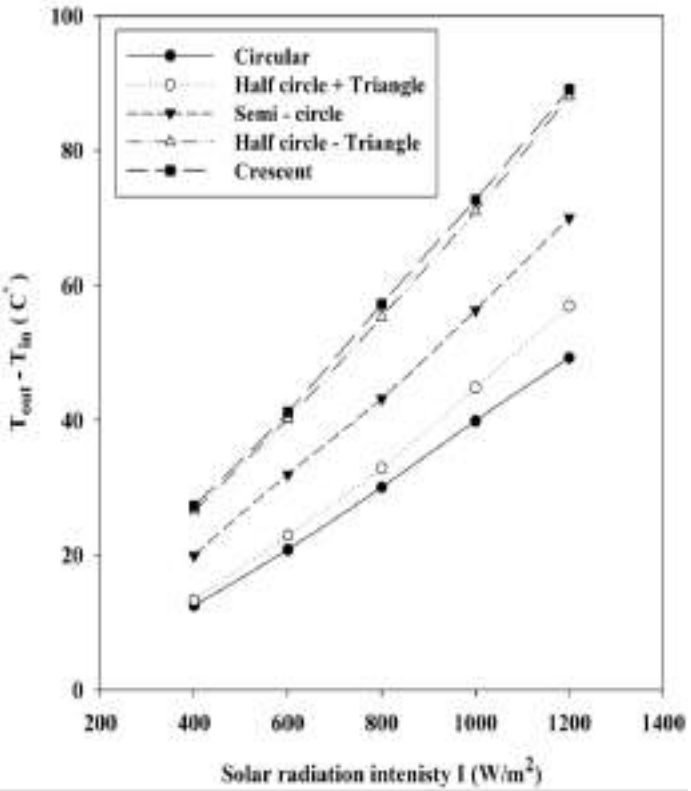

Fig.13.The variations of temperature difference with solar radiation intensity at constant inlet air velocity 1.0 (m/s) for different tested shapes.

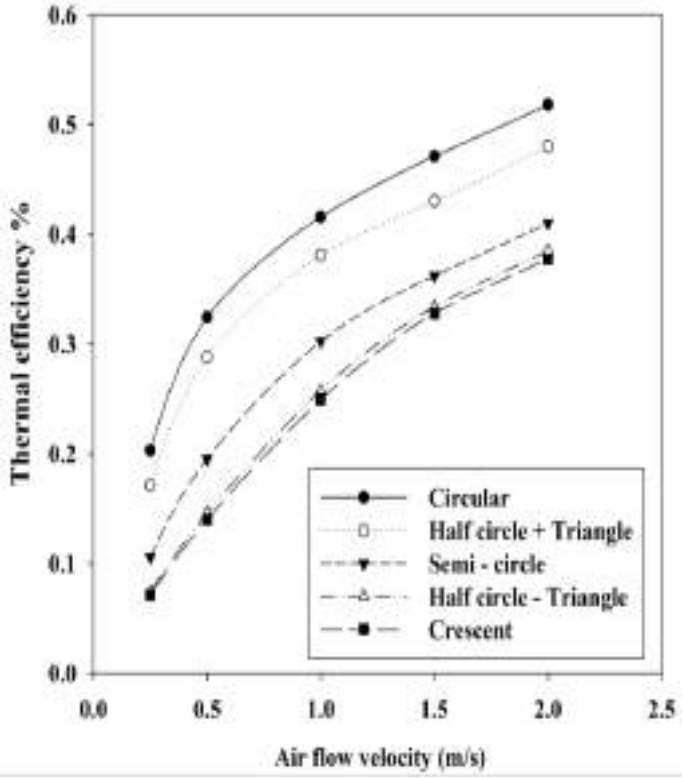

Fig.12.The variations of thermal efficiency with air inlet velocity at constant solar radiation intensity 850 (W/m^2) tested SAHs shapes.

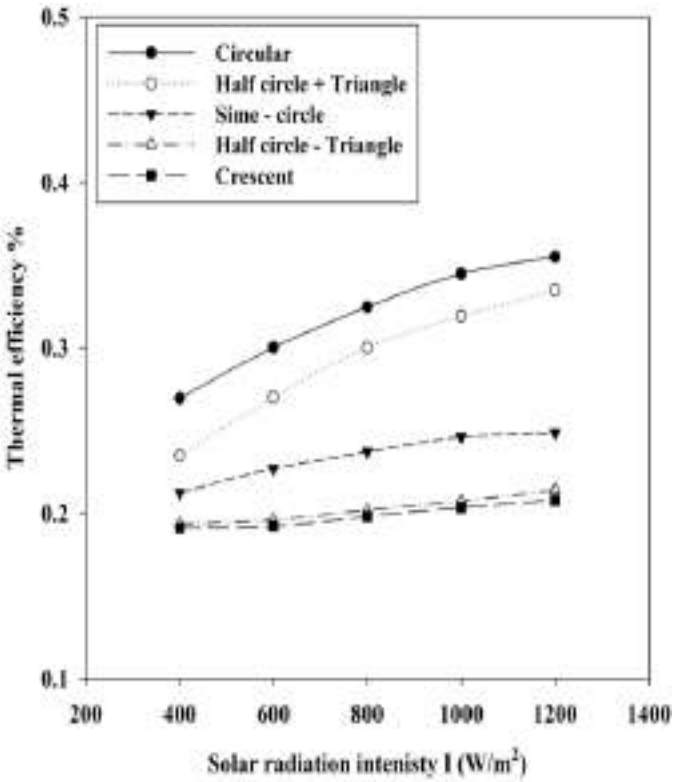

Fig.14.The variations of thermal efficiency with solar radiation intensity at constant air inlet velocity 1.0 (m/s) tested SAHs shapes.

4. Conclusions

The numerical study of plastic SAHs with different configurations was tested by ANSYS 14.0, the effect of variation the inlet air flow velocity at constant solar radiation intensity and the effect of variation solar radiation intensity at constant air flow velocity on the thermal performance of the plastic SAHs were examined.

- The results indicated that the highest efficiencies were achieved for the circular configuration and reach about 51.79% at air flow velocity of 2.0 ($m.s^{-1}$) and a constant solar radiation of 850 ($W.m^{-2}$). The thermal efficiency reached about 41.3% for half-circle plus isosceles triangle shape, 38.48% for semi-circular shapes, 38.4% for half circle-negative isosceles triangle shape and 37.72% for crescent shape.
- At solar radiation 1200($w.m^{-2}$) and a constant air flow velocity 1.0 ($m.s^{-1}$) the circular air heater had thermal efficiency about 35.51%, half circle-plus isosceles triangle air heater about 33.47%, semi-circular air heater about 24.85%, half circle-negative isosceles triangle air heater about 21.41% and crescent air heaters about 20.78%.
- The verification between present work and Abdullah et al. [19] indicated that results were converged and the error between them at range from 2.96% to 3.80%.

Nomenclature

A_c: Cross section area of solar air heaters.

A_p: Absorber surface area (m^2).

C_p: Specific heat of air ($J.kg^{-1}.K^{-1}$).

D: The hydraulic diameter of the cross sectional shapes (m).

I_c: The solar radiation intensity ($W.m^{-2}$).

L : The solar air heater absorber length.(m)

$\dot{m}$: The mass flow rate ($kg.\ s^{-1}$).

P: Premeter of sectional shapes (m).

T_{out}: The outlet temperature (K˚).

T_{in}: The inlet temperature (K˚).

V: The velocity of air flow ($m.s^{-1}$).

ρ: The density of air flow ($kg.\ m^{-3}$).

μ: The viscosity of air flow ($N.s.m^{-2}$).

ζ: The thermal efficiency.

Abbreviations

SAH: Solar air heater.

SAHs: Solar air heaters.

A CFD: computational fluid dynamics.

References

[1] C.Arkar, T.Šuklje, B.Vidrih and S.Medved, "Performance analysis of asolar air heating system with latent heat storage in a lightweight building", Applied Thermal Engineering .95(2016)281–287.

[2] M.A.Karim and M.Hawlader, "Performance evaluation of a v-groove solar

air collector for drying applications", Applied Thermal Engineering. 26 (2006) 121–130.
[3] A. Sreekumar, "Techno-economic analysis of a roof-integrated solar air heating system for drying fruit and vegetables", Energy Conversion and Management. 51 (2010) 2230–2238.
[4] D. Peng, X. Zhang, H. Dong and K. Lv, "Performance study of a novel solar air collector", Applied Thermal Engineering. 30 (2010) 2594–2601.
[5] M. Karim, E. Perez and Z.M. Amin, "Mathematical modeling of counter flow vgroove solar air collector", Applied Renewable Energy .67 (2014) 192–201.
[6] C.D. Ho, H. Yeh, T. Cheng, T. Chen and R. Wang , "The influence of recycle on the performance of baffled double pass flat plate solar air heaters with internal fins attached", Applied Energy 86 (2009) 1470–1478.
[7] A.S. Yadav and M.K. Thapak, "Artificially roughened solar air heater: experimental investigation", Renewable and Sustainable Energy Reviews. 36 (2014) 370–411.
[8] A. Sharma, Varun, P. Kumar and G. Bharadwaj, "Heat transfer and friction characteristics of double pass solar air heater having V-shaped roughness on the absorber plate", Journal of Renewable and Sustainable Energy (2013) 023109.
[9] A.S. Yadav and J. Bhagoria , "A CFD (computational fluid dynamics) based heat transfer and fluid flow analysis of a solar air heater provided with circular transverse wire rib roughness on the absorber plate", Energy 55 (2013) 1127–1142.
[10] D.Rawat, A. Jaurker, K. Gunasekaran, M.N. Mohana, D. Rathore, S. Kumar, X. Quan, G. Bian, B. Shao and B. Gayathiri , "Performance evaluation of two pass solar air heater using 60_ inclined v shaped ribs on absorber plate", Int. J. Eng. Sci. Invent. 3 (8) (2014) 01–10.
[11] A. El Khadraoui, S. Bouadila, S. Kooli, A. Guizani and A. Farhat, "Solar air heater with phase change material: an energy analysis and a comparative study", Applied Therml Engineering. 107 (2016) 1057–1064.
[12] P. Naphon , "Effect of porous media on the performance of the double pass flat plate solar air heater" , International communications in heat and mass transfer 32 (2005) 140–150.
[13] R. Gill, S. Singh and P.P. Singh, "Low cost solar air heater", Energy Conversion and Management. 57 (2012) 131–142.
[14] D. Njomo, "Techno-economic analysis of a plastic cover solar air heater", Energy conversion and management. 36 (10) (1995) 1023–1029.
[15] S. Janjai, A. Esper and W. Mühlbauer., "Modelling the performance of a large area plastic solar collector", Renewable energy. 21 (3–4) (2000) 363–376.
[16] N. Bansal and R. Uhlemann, "Development and testing of low cost solar energy collectors for heating air", Solar Energy 33 (1984) 197–208.
[17] N.Ahmad, "Agricultural solar air collector made from low-cost plastic packing film", Renewable Energy 23 (2001) 663–671.
[18] A. Abdullah and M. Bassiouny, "Performance of cylindrical plastic solar collectors for air heating", Energy Conversion and Management 88 (2014) 88–95.
[19] A. Abdullah, Y. El-Samadony and Z. Omara , "Performance evaluation of plastic solar air heater with different cross sectional configuration", Applied Thermal Engineering, 121 (2017) 218-223.

Performance of a pyramid solar still with stepped trays: Experimental approach

A.I. Bakry[a], Y.A.F. El-Samadony[a,b], , H.M. El-Gohari[c] and M. Ismail[c, a]

[a] *Faculty of Engineering, Tanta University, Egypt.*

[b] *Faculty of Engineering, BAU, Lebanon*

[c] *Faculty of Petroleum and mining Engineering, Suez University, Egypt.*

Abstract

The present experimental work aims to enhance the daily productivity of solar stills. A stepped pyramidal still with three trays was fabricated and tested under Tanta conditions, Egypt in September 2016. The still was tested with the brine feed being uninterrupted in one experiment, and with intermittent brine supply in another experiment. For continuous brine supply, the accumulated distillate was 4.95 L. For intermittent brine supply, the accumulated distillate was 4.6 L. Per unit total area, the average daily distillate water productivity is 5.5 and 5.11 L/m^2 for the continuous and the intermittent feed stills, respectively. In the two ways, the still yielded a greater productivity than that of conventional pyramid solar still which is 4.4 L/m^2.

1. Introduction

Along with the growth of population, the demand for fresh water is increasing in parallel. Unfortunately, the resources of fresh water on the earth are being over depleted, thus the call for making the abundant saline water suitable for domestic, irrigation and especially for drinking purposes is rising. One of the solutions on the table is solar desalination. Taking advantage of the renewable solar radiation, the solar desalination has been attractive for so long, and much research is being done in this area.

Solar still is one of the solutions that have been thought to be reliable and cost effective. Solar stills take advantage of two resources available abundantly almost everywhere on the earth, saline water and the sun. The principle of solar stills depends mainly on evaporating the brackish or saline water kept in the basin and condensing the vapor later when getting with the glass cover. The condensed droplets are being collected in a separate reservoir as distillate [1]. Conventional solar still is simple in construction as it consists of a basin covered with a tilted transparent cover. Unfortunately, conventional solar still has low capacity due to loss of latent heat of condensation to surrounding and the difficulty in increasing the evaporation temperature of water [2]. So, great efforts have been done to increase the productivity of distillate by investigating the development of some design parameters such as the shape, the material used and the depth of water in the basin.

Solar stills may be classified as either passive or active according to the source of the thermal energy used to evaporate the water. Both of passive and active stills are further classified as single effect (SE) and multi effect (ME) still according to the number of glazing layers.

In passive solar stills, the only used source of thermal energy is the direct solar radiation. Its simplest design is SE passive solar still having conventional basin of rectangular in top view and trapezoidal in front view. However, different shapes of passive solar stills were investigated with the aim of collecting more solar radiations such as triangular stills, tubular stills, hemispherical stills, vertical stills and pyramidal still [3]. In a multiple-slope solar still, the optimum tilt angle for the cover was believed to be 23° [4]. To overcome the problem of heat losses to the surrounding, ME solar still is used as the multi-glass layers utilize more heat and the efficiency is enhanced.

In active solar stills, other sources of energy, rather than solar radiation, acquire much more increasing in the water temperature and hence the evaporation is enhanced. The inclined solar still was investigated. It is inclined to the horizontal surface with the aim of producing larger productivity through acquiring long flow path, long retention time and high rate of evaporation [3]. It can be mainly classified as wick type and basin type inclined solar stills. In wick type, the saline water is slowly fed through a porous, radiation-absorbing pad (the wick) which can be made of cotton, jute, metal pieces, stones etc. [5]. Its simplest design is the single wick still [6]. Due to its small heat capacity, the time required to evaporate the water is decreased, and the productivity in turn, can be enhanced by 16 - 50 % as compared to basin solar still [7]. Other designs of wick inclined still have been investigated [3]. One of them is that investigated by Minasian et al. [8] which consists of small conventional solar still integrated with a wick-type solar still in such a manner that hot water leaving the wick-type still would directly feed basin-type still. The productivity of this still is 8.477 l/m^2/day with efficiency of 78% as compared to a sole wick type with productivity of 5.970 l/m^2/day with efficiency of 64 %.

The basin type inclined solar still is a conventional basin still but the whole basin is inclined to enhance the productivity. The angle of inclination depends on the latitude of location and the season. It can be further classified as multi-effect, stepped and cascade solar stills [3]. Abdullah et al. [9] experimented a stepped solar still with cooling the glass cover by flowing a small stream of cold water. The productivity was raised to 5.7 l/m^2/d with efficiency of 59%, as compared to a productivity of 3.35 and efficiency of 34% for the conventional solar still [3]. Moreover, integrating stepped solar still, basin type still, and a mini solar pond has was thought of and put into action by Velmurugan et al. [10]. The productivity was enhanced as a result of preheating the water by the solar pond. Going further, integrating the still furtherly with fins and sponges was observed to raise the productivity to 6.12 with efficiency of 87 %. As reviewed in [11], efficiency increases by inclining the basin referred with the sun angle. In addition, thin layer of water flowing over glass cover produces more distillate. Moreover, high efficiency can be achieved by combining wick and basin type still.

Inclined solar stills have also been designed in various miscellaneous stills. One still is integrated with a sun tracking system to improve the performance of the still [12], another uses a hybrid solar still in which an evacuated solar water heater with the desalination still to preheat the saline water [13]. Further effort was exerted trying to study the effect of forced convection on the productivity of solar stills.

Pyramid solar still is the kind in which top cover has the shape of pyramid. There were basically two shapes covers and basin offered in pyramid solar still: triangular and square pyramid solar still. Hamdan et al. [14] made an experimental and theoretical comparisons on the performance of different multiple basin solar stills, having top cover in shape of squared pyramid. The three stills were constructed using a 0.96×0.96 m^2 base area, and the cover of each still is of a pyramid shape and inclined at 45^o. They concluded that the distillate output from triple basin solar still was approximately 24% and 5.8% greater than that of single basin, double basin respectively. They obtained that the maximum daily efficiencies of triple basin, double basin and single basin solar still were 44 %, 42 % and 32 % respectively. Kabeel [15] developed a solar still with pyramid shaped cover. He used concave-shaped basin covered with wick to enhance the daily productivity of the simple pyramid solar still. Yield of 4100 ml and 2100 ml per m^2 per day was observed for the pyramid shaped concave wick solar still and traditional solar still respectively. He recorded instantaneous efficiency of 45 % whereas average daily efficiency of 30% for the pyramid solar still. Taamneh and Taamneh [16] studied the effect of forced convection on the daily productivity of a pyramid type solar still with a low power consumption fan integrated with a still with a basin area of 0.95 m^2. They found that the productivity was raised by 25% as compared to free convection solar stills. To evaluate the impact of water amount (expressed as depth of water) in basin on the productivity of single basin square solar still, Al-Hassan and Algarni [17] designed and tested three similar square pyramid solar still. For the experimentations, three different amounts of saline water were used: as 3 l, 6 l and 9 l in the models 1, 2 and 3 respectively. Average daily output found to be 3.924 l/m^2 per day, 3.116 l/ m^2 per day and 2.408 l/ m^2 per day for 3 l, 6 l and 9 l of saline water in basins. From this result, it has been observed that the lower quantity of saline water gives higher productivity. Sathya murthy et al. [18] experimentally studied the parameters affecting the performance of triangular pyramid solar still. They got daily yield of 4.3 kg/m^3 for 2 cm water depth, 2.3 kg/m^2 for 4 cm, 1.2 kg/m^2 for 6 cm, 0.9 kg/m^2 for 8 cm and 0.5 kg/m^2 for 10 cm.

From the previous works, it has been observed that, the pyramid solar still acquires more productivity than the conventional still. So, the study aimed to investigate the pyramid solar still with some configurations either in the geometry or in the water feeding. Stepped trays were used in the pyramid still as a new modification. Besides that, two water feeding methods were considered. The first method is the continuous water feeding while the other is the intermittent feeding. The system has been provided with suitable instrumentations to measure the study parameters like the solar radiation, different temperatures of the still elements (absorbers and glass covers), the inlet water temperature and the productivity.

2. Experimental set-up, procedure and instrumentations

The test-rig is designed and fabricated from commercial available materials. It consists from three main parts (feeding system, solar still system and collecting system). Also, the test-rig is provided with instrumentations to measure the parameters affecting the performance and the productivity (solar radiation and temperatures at various positions). The design configurations, fabrication, construction of the tested unit, the instrumentation and measuring techniques are described in the following sections.

2.1 Experimental set-up description

Fig. 1 illustrates a photograph of the present work test-rig. The first part of the test-rig is the solar still system, which consists of two main components; glass covers, absorber and the stepped trays. Four glass covers are mounted stably on the structural frame. Each cover is inclined to the horizontal by an angle of 72° to attain the most reliable conjunction with the plates. The dimensions of each glass cover and corresponding frame 1 m × 1.5 m with a thickness of 5 mm. In addition, three trays are mounted on a vertical rod, on at the base (absorber) and the others at two different heights, as shown in Fig. 2. The bottom tray is insulated as it is considered as absorber plate while the other plates, upper and middle, are not insulated as they are just considered as stepped trays. This rode acts as supporting to the horizontal trays and partially supporting the weight of the inclined glass covers. The areas of the absorber and the two trays vary from lower plate to the upper plate according to the pyramidal sectional area at the absorber height. The area of absorber is 0.9 m^2 while areas of the trays are 0.36 and 0.11 m^2 at the middle and the upper, respectively. So, the total surface area is 1.37 m^2. The vertical distance between each subsequent two plates is about 35 cm. The solar still system is well-sealed to avoid the leakage of water vapor to the outside . The second part of the unit is the distilled water collecting system, Fig. 3. It consists of four small tray channels inclined and attached to each glass cover. Each one is inclined to help the collecting of the condensed water to the collecting hose attached at the end of each deflector. Each hose is connected to a calibrated collecting tank.

Finally, the feeding saline water system, Fig. 4, through which water is fed to the apparatus through three hoses with 1 cm diameter each. One end of each hose is connected to a separate, manually-operated valves. These valves are mounted on a highly elevated water tank. The feeding system has two different configurations, one is for the continuous brine supply and the other is for the intermittent brine supply. K-type thermocouples are used for measuring the glass covers, inlet saline water, brine temperature and the absorber surfaces. . Thermocouples are fixed on the surface of the absorbers and at the upper side of glass covers. Fig. 5 Shows the locations of the thermocouples .

Fig. 1 A photograph of test-rig

Fig. 2 A photograph of the absorber plates.

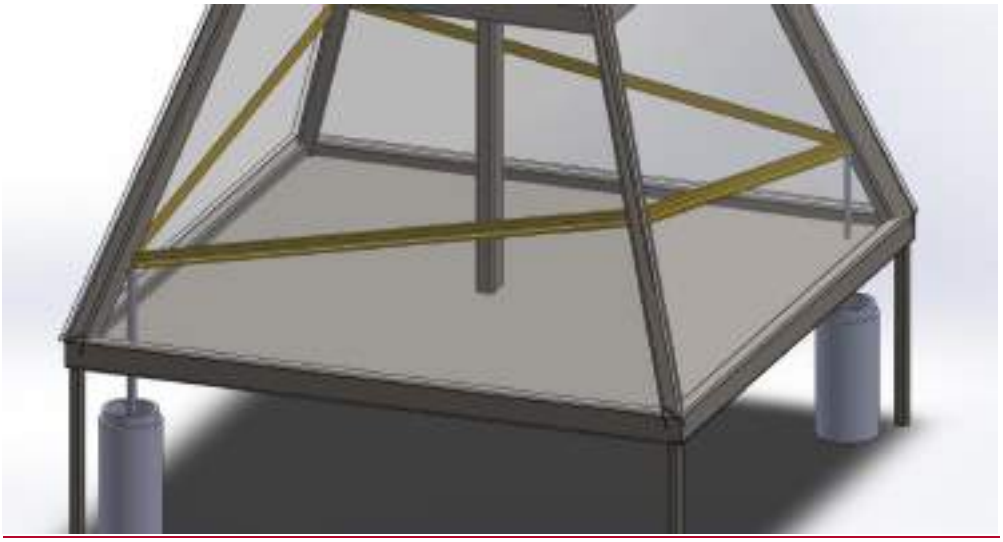

Fig. 3 A schematic diagram of the collecting system

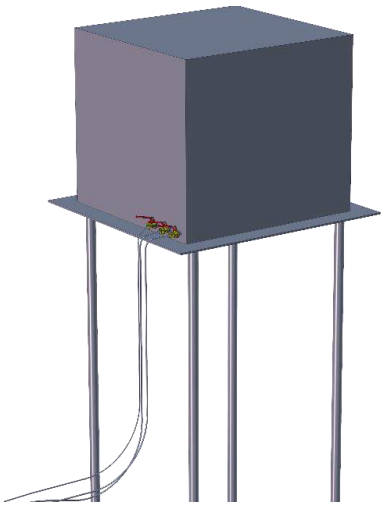

Fig. 4 A schematic diagram of the feeding system

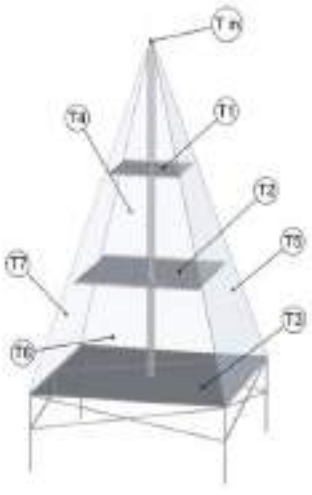

symbol	Temperature of ..
T1	Upper absorber plate
T2	Middle absorber plate
T3	Lower absorber plate
T4	Northern cover
T5	Eastern cover
T6	Southern cover
T7	Western cover
T in	Inlet stream

Fig. 5 The positions of the thermocouples

2.2. Experimental procedure and instrumentations

Stepped pyramidal solar still is experimentally tested in outdoor environment. The experiments were conducted in two different ways. The first way is intermittent brine supply, which depends on attaining an almost constant water level over the trays through manually adjustable valves at the hoses inlets. In the second way, the valves are always opened and the hoses are plugged at the end with some filler. Near these ends though, a tiny hole is cut in each hose acting as a choke to restrict the flow rate. Water delicately flows out of these holes spreading over the horizontal trays continuously compensating for the distilled water. The Experiments were conducted at the Faculty of Engineering, Tanta University, Egypt and carried out from 9 am to 5 pm during the period of September 2016. Solar radiation and temperature of absorbers surface, saline water, glass covers, and distilled water are measured every 1 h. The depth of the saline water, H = 5 mm in the solar stills is kept constant during the experiment according to the results of [19]. The temperatures were measured using calibrated K-type thermocouples. The readout of the thermocouples is monitored by Avometer. The global incident solar irradiation on the surface is measured by means of data logging solar meter.

3. Experimental results

As previously mentioned, the stepped pyramidal solar still has been tested for brine distillation in two different configurations, one with continuous feed ant the other with intermittent feed. The apparatus has been experimentally tested with the feed being intermittent for 3 days in a row, and then tested with continuous feed for other 3 sequential days. The apparatus was under test from 8:30 am to 5:30 pm each day. The temperatures of the four glass-covers as well as the solar intensity falling on each were recorded. The temperatures of both three trays' surface and the inlet brine were also measured. Finally, the volume of the distilled water was measured then the cumulative volume distilled during the whole period of test was calculated. These parameters have been measured each hour during the day of test, and then plotted over the time.

3.1 Intermittent feeding

3.1.1 Solar radiation and temperatures variation

Fig. 6 shows the solar radiation intensity falling onto the four glass covers with time. The maximum radiation was noticed to be 145, 688, 777 and 732 W/m^2, for the northern, southern, eastern and western plates respectively.

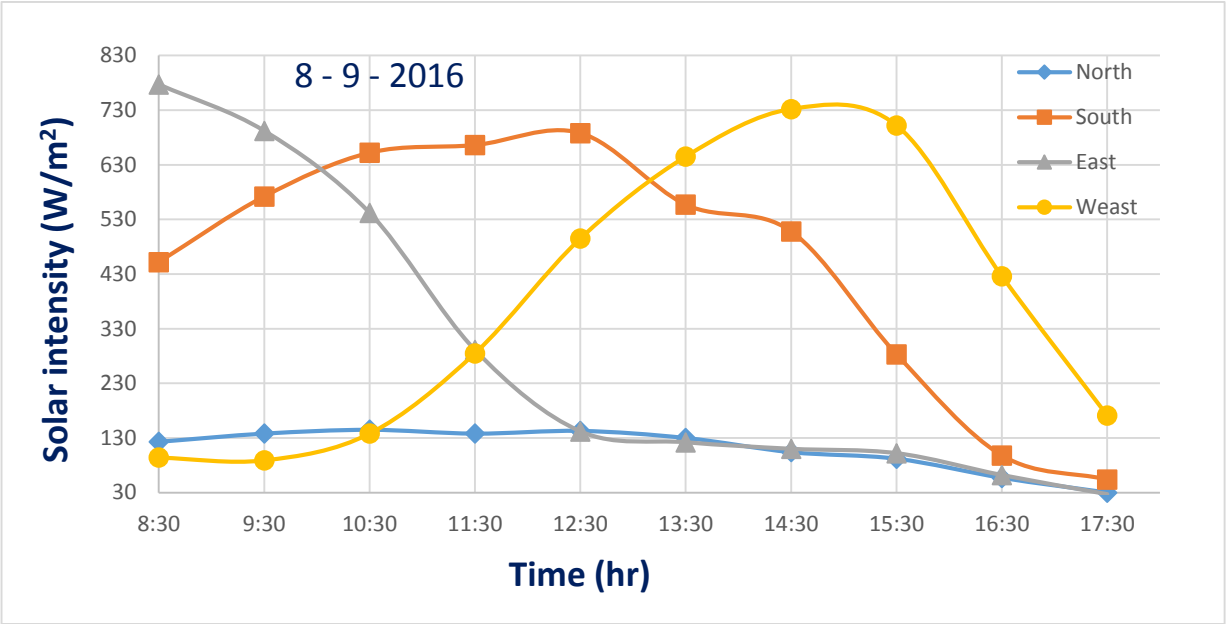

Fig. 6 Solar radiation of the intermittent feeding.

Fig. 7 shows a plot of the temperature of the glass covers with time. The maximum temperature measured was 53, 57, 54 and 60 °C, for the northern, southern, eastern and western glass covers respectively. These temperatures were recorded at 13:30 for the northern and eastern covers and at 14:30 for the western and southern covers.

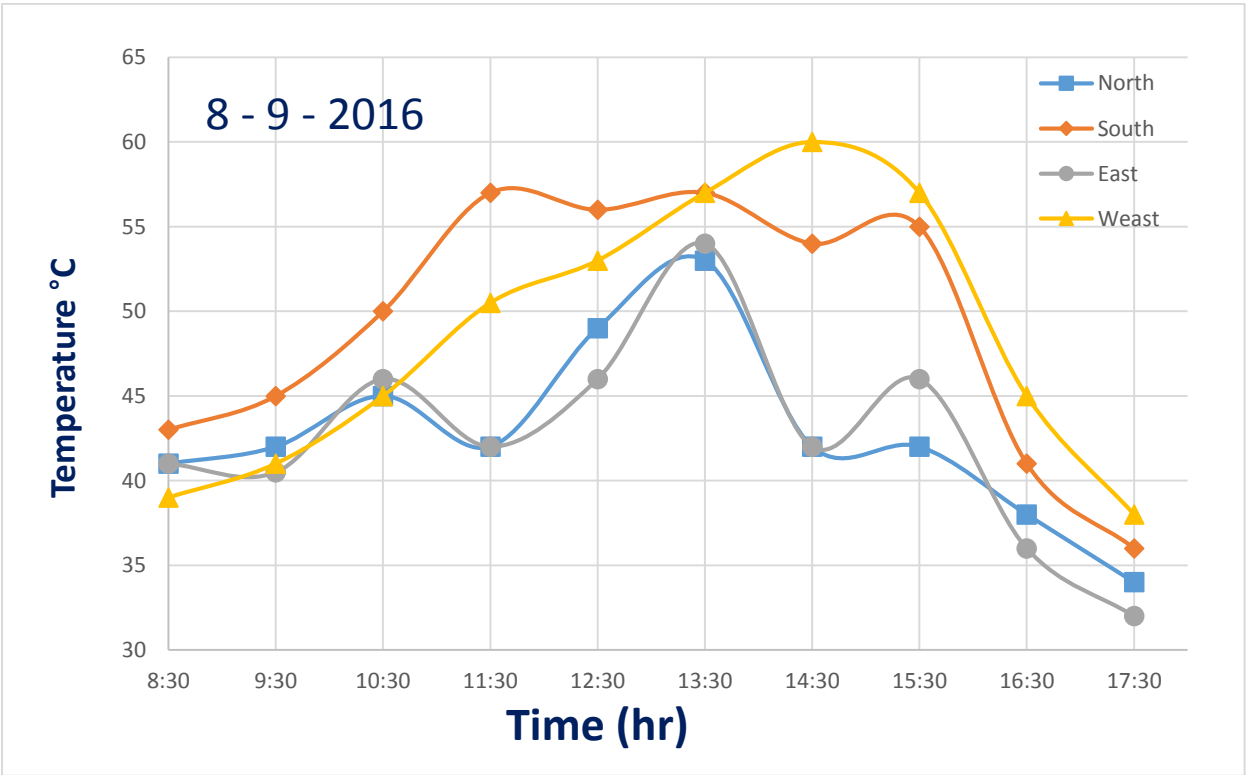

Fig. 7 Temperature variation of the glass covers of the intermittent feeding.

Fig. 8 shows the temperature of the lower, middle, top absorber plates and that of the inlet stream with time during the second day. The maximum temperatures on the surfaces of bottom, middle and top plates, were 62, 65 and 62 °C, respectively. These temperatures were recorded at 13:30, 14:30 and 12:30 respectively. The inlet temperature reached a maximum of 44 °C at 13:30.

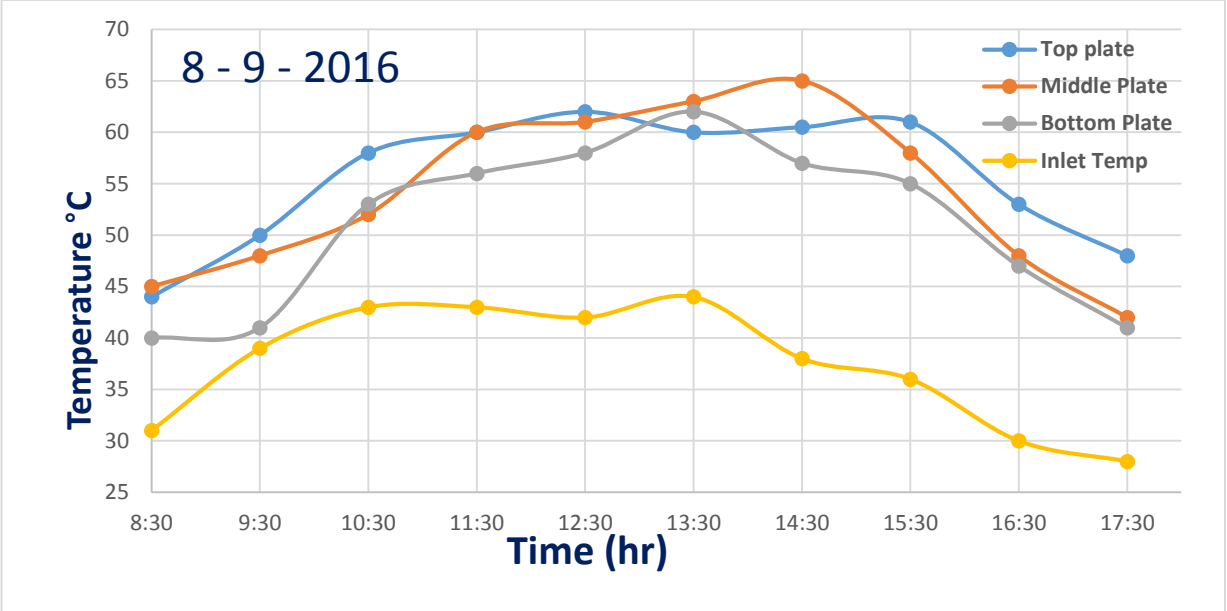

Fig. 8 Temperature variation of the trays' surface of the intermittent feeding.

3.1.2 Productivity

Fig. 9 shows the productivity over time, the maximum productivity occurred between 13:30 and 14:30, whereas Fig.10 shows a plot of the accumulative production during that day. The daily accumulative productivity was 5.11 L/m^2. The productivity reached the peak also at 1:30 P.M. of 0.89 L/m^2

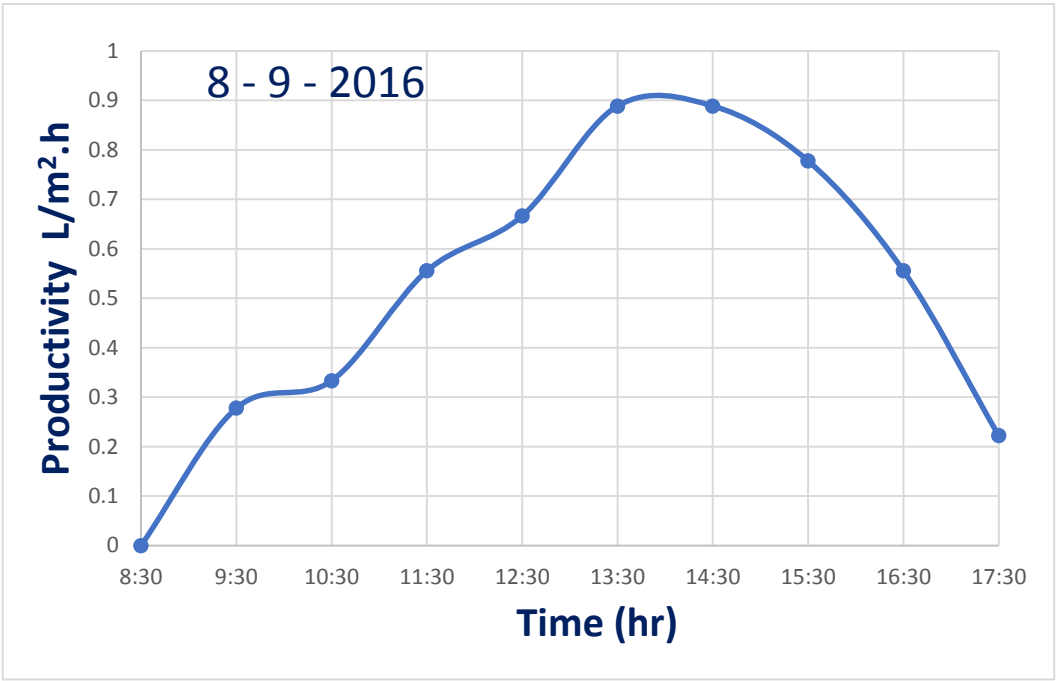

Fig. 9 Hourly productivity of intermittent feeding.

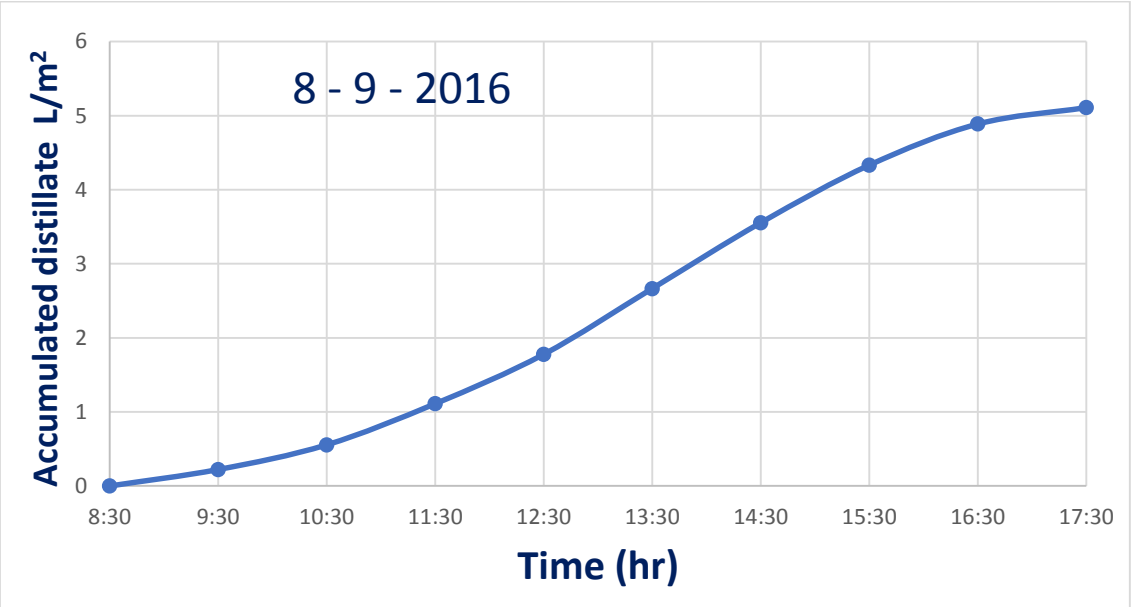

Fig. 10 Accumulative productivity of intermittent feeding.

3.2 Continuous feeding

3.2.1 Solar radiation and temperatures variation

Fig. 11 shows the solar intensity of the radiation falling onto the four glass covers versus time. The maximum radiation was 150, 690, 770 and 735 W/m^2, for the northern, southern, eastern and western plates respectively.

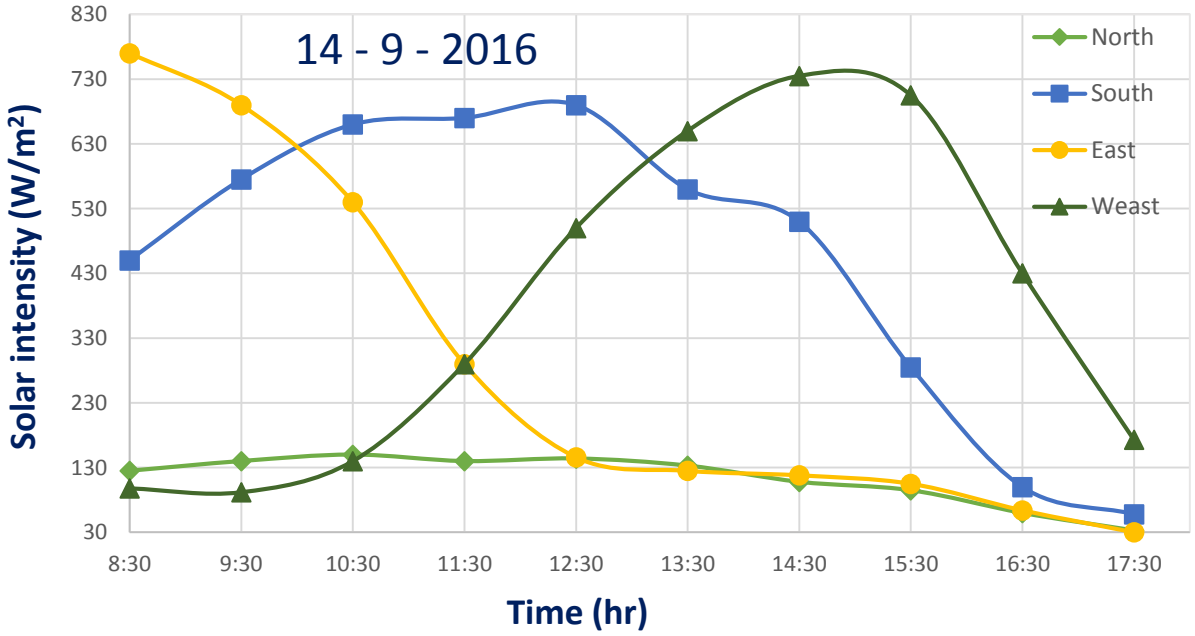

Fig. 11 Solar radiation of the continuous feeding.

Fig. 12 shows the temperature of the glass covers versus time. The maximum measured temperatures were 52, 57, 52 and 59 °C, for the northern, southern, eastern and western plates respectively. These temperatures were recorded at 13:30 14:30 13:30 and 14:30, respectively.

Fig. 13 shows the temperature of the lower, middle, top absorber plates and that of the inlet stream versus time. The maximum obtained temperatures on the bottom, middle and top plates, were 60, 62 and 62.5 °C, respectively. These temperatures were recorded at 13:30, 14:30 and 14:30 respectively. The inlet temperature reached a maximum of 41.5 °C at 10:30 and a minimum point of 29.5 °C at 17:30.

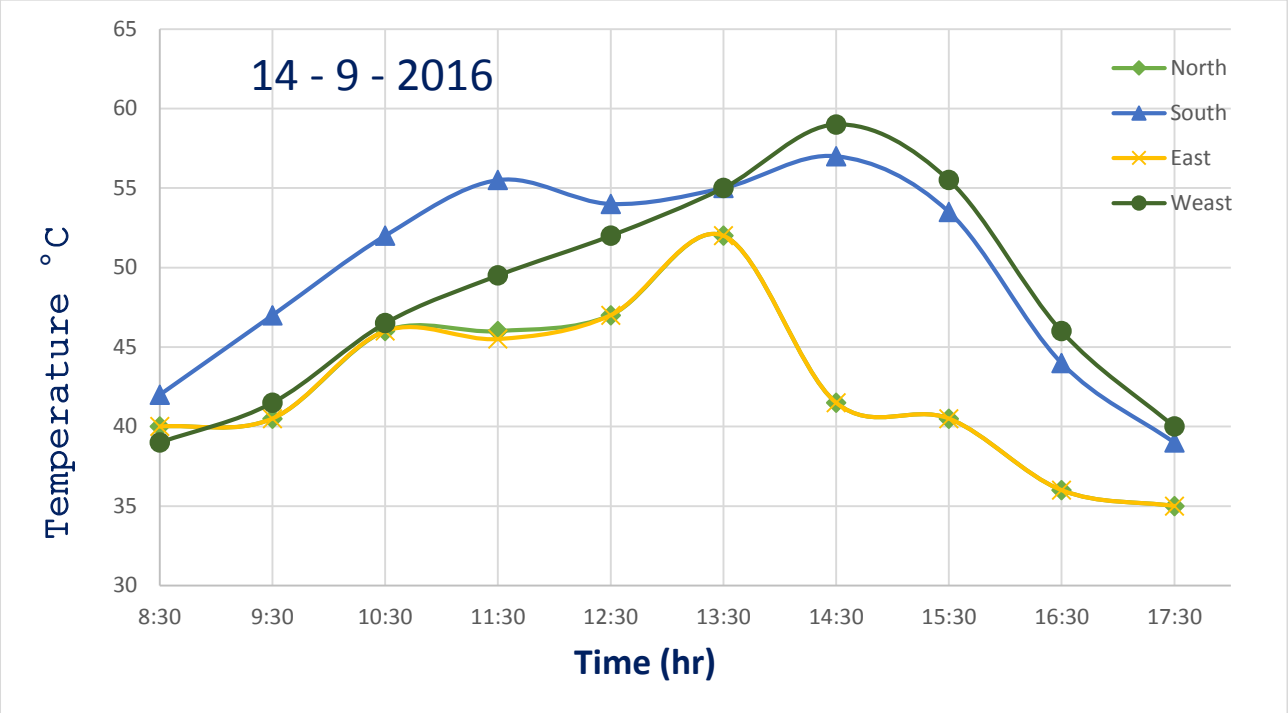

Fig. 12 Temperature variation of the glass covers of the continuous feeding.

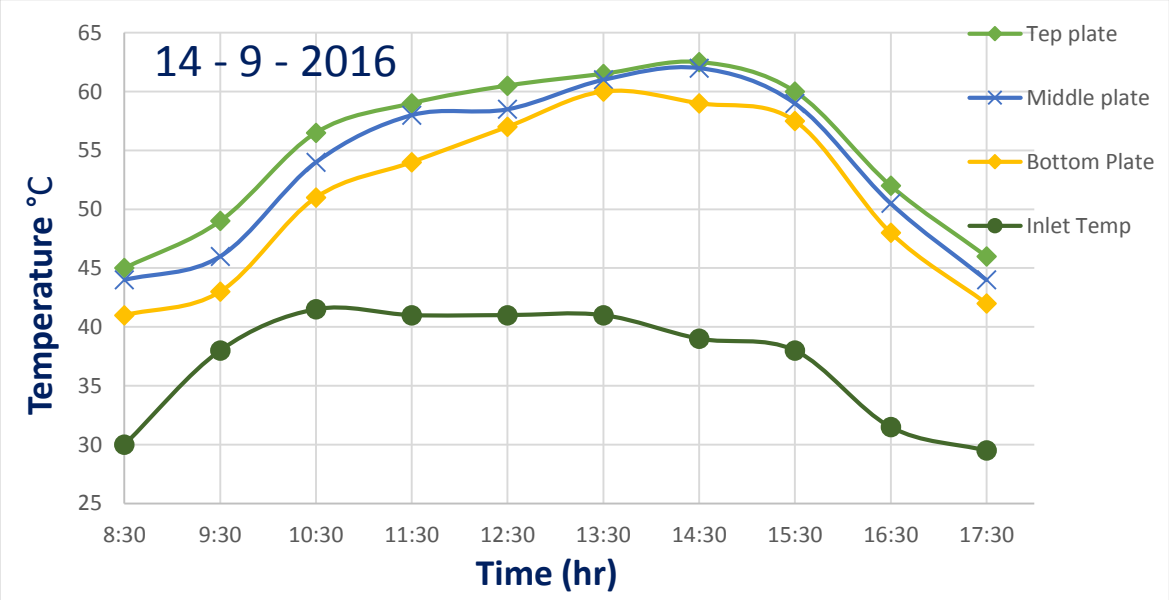

Fig. 13 Temperature variation of the trays' surface of the continuous feeding.

3.2.2 Productivity

Fig. 14 shows the productivity over time, the maximum productivity occurred between 13:30 and 14:30, whereas Fig .15 shows a plot of the accumulative production during that day. The still has yielded an accumulative volume of the distilled brine of 5.5 L/m^2. Maximum productivity was acquired at 1:30 pm. The volume distilled from 12:30 to 1:30 was 0.94 L/m^2.

One of the findings is that continuous water feeding is better than intermittent feeding. This is due to the continuous drop of water droplets which works to disturb the water surface and stimulate the surface molecules to evaporate faster than the intermittent feeding state in which the surface is completely stationary.

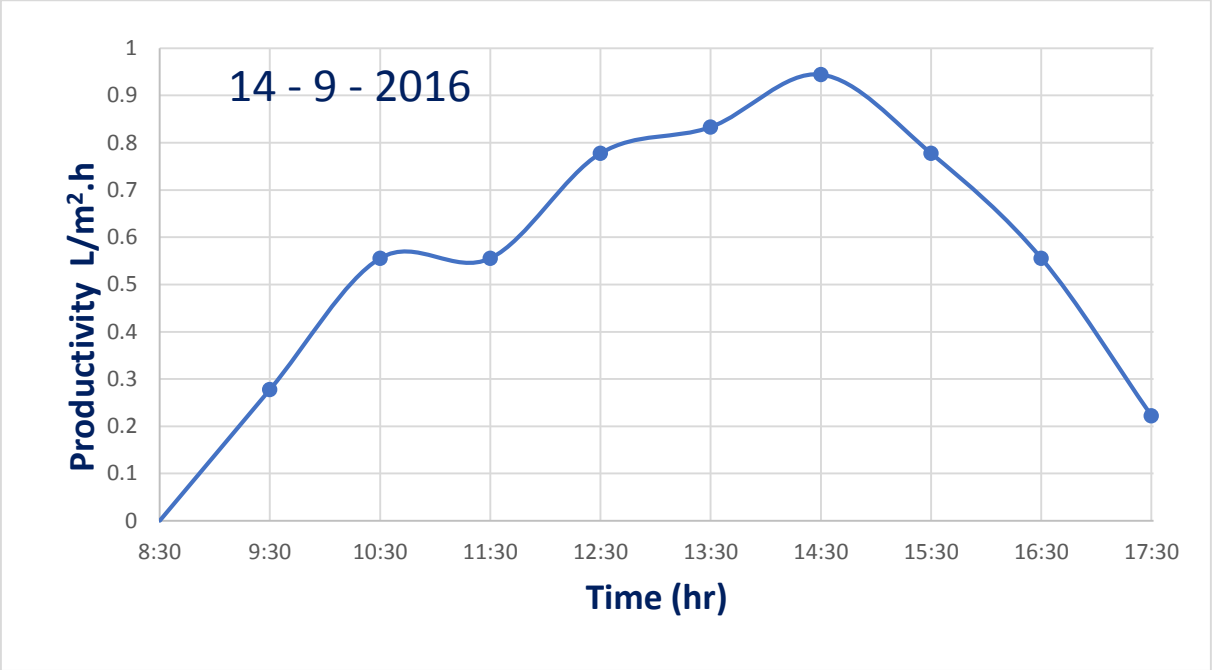

Fig. 14 Hourly productivity of continuous feeding.

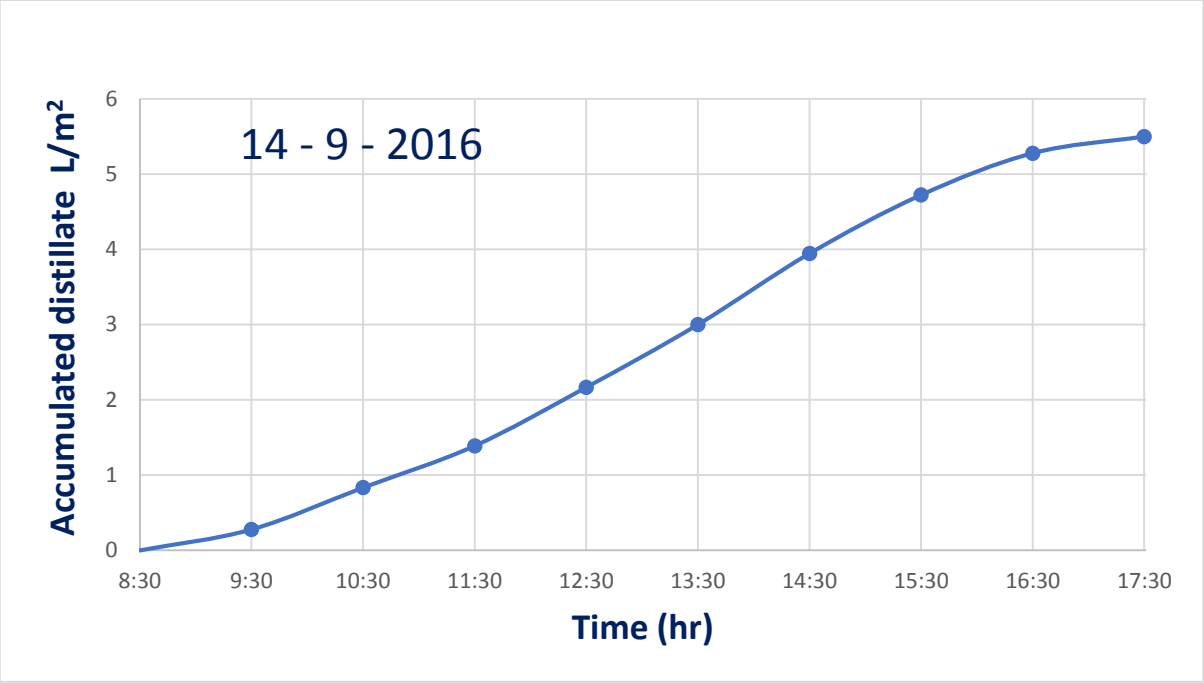

Fig .15 Accumulative productivity of continuous feeding.

The proposed configurations of pyramid solar still showed an accepted performance compared to some other studied systems as illustrated in Table 1.

Table 1 Comparison between the productivity of the present system and some other systems

Study	**Design configurations**		**Daily Productivity (L/m^2)**
Present study	• Pyramid solar still • With two stepped trays • Dimensions of basin = (0.95 × 0.95) m^2 • The glass cover angle is 72 degrees to the horizontal	Intermittent feeding	5.11
		Continuous feeding	5.5
Kabeel [15]	• Pyramid solar still • The basin is concave • Dimensions of basin = (1.2 × 1.2) m^2 • The glass cover angle is 45 degrees to the horizontal		4.1
Taamneh and Taamneh [16]	Pyramid solar still	With a fan	2.99
		Without a fan	2.485

Arun kumar et al. [20]	• Pyramid solar still • Dimensions of basin = (0.95 × 0.95) m^2		3.3
Kabeel et al. [21]	• Pyramid solar still • With different glass cover angles • Dimensions of basin = 0.64 m^2	30.47°	4.13
		40°	3.5
		50°	`2.93

3.3. Pyramid solar still efficiency

The instantaneous efficiency, η_i, defined as the ratio between the hourly distillate productivity m multiplied by the latent heat h_{fg} and the summation of solar radiation over the absorber area A.

The daily efficiency, η_d, is defined as the ratio between the summation of the hourly distillate productivity m multiplied by the latent heat h_{fg} and average solar radiation I(t) over the absorber area A.

$$\eta_i = \frac{m \times h_{fg}}{(\sum I) \times A} \quad (1)$$

$$\eta_d = \frac{\sum m \times h_{fg}}{I_{avg} \times A} \quad (2)$$

Assume that, the latent heat h_{fg} = 2350 kJ/kg.

The instantaneous efficiency of pyramid solar still calculated using Eq. (1) during the selected days of intermittent and continuous feeding is shown in Fig. 16. The instantaneous efficiency increases in the morning time until a maximum value at 4:30 pm and then decreases. It can be observed that the efficiency after 3 pm is increasing, while the solar radiation decreases, this may be due the stored energy in the still, which is not considered in calculation, may increase the evaporation process. The efficiency of the pyramid solar still reached about 0.55 for continuous feeding and 0.56 for intermittent feeding. The calculated daily efficiency from Eq. (2) equals 0.37 for continuous feeding and 0.35 for intermittent feeding.

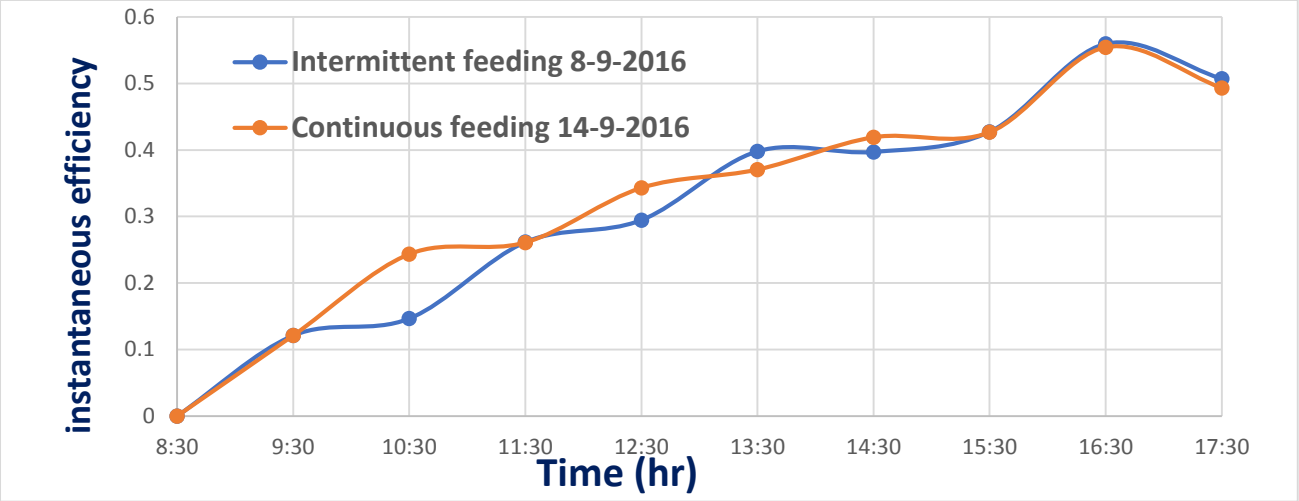

Fig .16 The hourly variation of the instantaneous efficiency for intermittent and continuous feeding

4. Conclusion

The current work achieved good enhancement in the daily productivity of solar stills. A stepped pyramidal still with multi trays was fabricated and tested. Two different ways of feeding were tested. The first way is continuous feeding while the second way is intermittent feeding. From the results, it can be concluded that:

- For continuous feeding, the accumulative productivities were 5.5 L/m^2 and the efficiency reached about 0.55.
- For intermittent feeding, the accumulative productivities were 5.11 L/m^2 and the efficiency reached about 0.56.

References

[1] P. K. Abdenacer and S. Nafila, "Impact of temperature difference (water-solar collector) on solar-still global efficiency," *Desalination*, vol. 209, pp. 298–305, 2007. [2] T. He and L. Yan, "Application of alternative energy integration technology in seawater desalination," *Desalination*, vol. 249, no. 1, pp. 104–108, 2009.

[3] A. K. Kaviti, A. Yadav, and A. Shukla, "Inclined solar still designs: A review," *Renew. Sustain. Energy Rev.*, vol. 54, pp. 429–451, 2016.

[4] V. S. V. BAPESHWARARAO, U. SINGH, and G. N. TIWARI, "Transient analysis of double basin solar still*," *Energy Convers. Manag.*, vol. 23, no. 2, pp. 83–90, 1983.

[5] P. Vishwanath Kumar, A. Kumar, O. Prakash, and A. K. Kaviti, “Solar stills system design: A review,” *Renew. Sustain. Energy Rev.*, vol. 51, pp. 153–181, 2015.

[6] B. Janarthanan, J. Chandrasekaran, and S. Kumar, “Performance of floating cum tilted-wick type solar still with the effect of water flowing over the glass cover,” *Desalination*, vol. 190, pp. 51–62, 2006.

[7] Z. N. He., “Solar thermal utilization,” *China Press Univ. Sci. Technol. China*, vol. 404, pp. 48–52, 2009.

[8] A. N. MINASIAN and A. A. AL-KARAGHOULI, “AN IMPROVED SOLAR STILL: THE WICK-BASIN TYPE,” *Energy Convers. Manag.*, vol. 36, no. 3, pp. 213–217, 1995.

[9] A. S. Abdullah, “Improving the performance of stepped solar still,” *DES*, vol. 319, pp. 60–65, 2013.

[10] V. Velmurugan, S. Pandiarajan, P. Guruparan, L. H. Subramanian, C. D. Prabaharan, and K. Srithar, “Integrated performance of stepped and single basin solar stills with mini solar pond,” *Desalination*, vol. 249, no. 3, pp. 902–909, 2009.

[11] K. Kalidasa Murugavel, P. Anburaj, R. Samuel Hanson, and T. Elango, “Progresses in inclined type solar stills,” *Renew. Sustain. Energy Rev.*, vol. 20, pp. 364–377, 2013.

[12] S. Abdallah, O. Badran, and M. M. Abu-khader, “Performance evaluation of a modified design of a single slope solar still,” *Desalination*, vol. 219, pp. 222–230, 2008.

[13] Z. M. Omara, M. A. Eltawil, and E. A. Elnashar, “A new hybrid desalination system using wicks / solar still and evacuated solar water heater,” *DES*, vol. 325, pp. 56–64, 2013.

[14] M. A. Hamdan, A. M. Musa, and B. A. Jubran, “Performance of solar still under Jordanian climate,” *Energy Convers. Manag.*, vol. 40, no. 5, pp. 495–503, 1999.

[15] A. E. Kabeel, “Performance of solar still with a concave wick evaporation surface,” *Energy*, vol. 34, no. 10, pp. 1504–1509, 2009.

[16] Y. Taamneh and M. M. Taamneh, “Performance of pyramid-shaped solar still: Experimental study,” *Desalination*, vol. 291, pp. 65–68, 2012.

[17] G. A. Al-hassan and S. A. Algarni, “Exploring of Water Distillation by Single Solar Still Basins,” vol. 2013, no. March, pp. 57–61, 2013.

[18] R. Sathyamurthy, H. J. Kennady, P. K. Nagarajan, and A. Ahsan, “Factors affecting the performance of triangular pyramid solar still,” *Desalination*, vol. 344, pp. 383–390, 2014.

[19] A. E. Kabeel, A. Khalil, Z. M. Omara, and M. M. Younes, “Theoretical and experimental parametric

study of modi fi ed stepped solar still," *DES*, vol. 289, pp. 12–20, 2012.

[20] T. Arunkumar, K. Vinothkumar, A. Ahsan, R. Jayaprakash, and S. Kumar, "Experimental Study on Various Solar Still Designs," *ISRN Renew. Energy*, vol. 2012, pp. 1–10, 2012.

[21] A. E. Kabeel, M. Abdelgaied, and N. Almulla, "Performances of pyramid-shaped solar still with different glass cover angles: Experimental study," *IREC 2016 - 7th Int. Renew. Energy Congr.*, 2016.

AUTOMATED OPTIMIZATION OF CENTRIFUGAL COMPRESSORS "ECKARDT ROTOR O"

Aly M. Elzahaby
Professor,
Mechanical power Engineering Department
Tanta, Egypt

Mohamed K. Khalil
Lecturer,
MTC A/C Mechanical Engineering Department
Cairo, Egypt

Mohammed E. AlMoghazy
Teaching Assistant
Mechanical Engineering Department
Kafr ElSheikh, Egypt

ABSTRACT

Centrifugal compressors play an important role in many industries. Improving the efficiency of centrifugal compressors and extending their range has been an important subject for both engineers and researchers working in the turbomachinery field. This paper discusses the optimization of Eckardt O impeller through changing its blade angles distribution to increase its efficiency. the optimization process is performed using an automated procedure performed within ANSYS workbench. The geometry is parameterized using ANSYS design modeler, the mesh is generated using ANSYS Turbogrid and steady flow CFD results are obtained using ANSYS CFX. Optimization by genetic algorithm is done using a surrogate model generated through a sample of designs selected through Design of experiments "DOE" sampling. The performance of the optimized and the original designs are compared both qualitatively and quantitatively, the optimized design efficiency successfully increased from 87.994 % to 88.481% based on CFD results.

NOMENCLATURE

p_0	Total pressure, Pa
T_0	Total temperature, K
R	Radius, m
PR	Pressure ratio

Greek symbols

η	Efficiency
β	Relative blade angle
Θ	Corrected total temperature
δ	Corrected total pressure
$\dot{m}_{cor}$	Corrected mass flow rate, kg/s
n	Rotational speed, rpm

Subscript

tt	Total to total

Abbreviations

DOE	Design of Experiments

INTRODUCTION

Centrifugal compressors are characterized by their high-pressure ratio per stage, robustness and stability over a wide operating range [1]. These characteristics make them ideal for many important applications including sophisticated industrial, aerospace and automotive industries. Designers of centrifugal compressors use the latest tools and methodologies to design aerodynamically efficient compressors that meet the structural, manufacturability and costs constraints imposed by the specific application for which they are designed. Designing a centrifugal compressor rotor starts from calculating its main dimensions, this is done utilizing simple 1D or 2D methods [2]. The next stage is defining the 3D geometry of the compressor blades. The 3D blade geometry is specified through the definition of the hub, shroud, blade angle distribution and thickness distribution curves. These curves are generally defined as Bezier or spline curves for which the coordinates of the defining points are parameterized [3],[4]. There are no available analytical methods to specify the blade defining curves to give optimal performance. It is rather an iterative process where an optimization workflow is used [2]. The optimizer varies the parameters controlling the blade defining curves. The aerodynamic performance is calculated using CFD. Finally, the optimizer introduces the best candidate designs according to the predetermined objective function and constraints.

For optimization, surrogates or metamodels are used to approximate computationally expensive functions to provide computationally inexpensive reasonable predictions of the real functions. Standard polynomial response surfaces, Kringing model and artificial neural networks are popular in the turbomachinery design discipline. The design of experiments “DOE” techniques are used to introduce proper samples to construct an approximate metamodel that is as accurate as possible and covers the required region of the design space with the least design points to save the computational resources[5], [6].

In this paper optimization of the Eckardt O compressor is introduced. The blade angle distributions curves of the Eckardt O are redesigned to get optimum aerodynamic performance at the operating point of the original Eckardt O compressor. The workflow is performed using ANSYS software package and optimization is performed using surrogate model and Design of experiments methods.

AUTOMATED OPTIMIZATION WORK FLOW

The automated optimization workflow scheme, Figure 1, includes the following modules:

- **Geometry module**: this module contains the parametric CAD geometry to be controlled through the accessible geometrical parameters.
- **TurboGrid module**: uses the geometry in the geometry module as an input and generates a suitable mesh according to a set of user-defined settings.
- **CFX module:** This module calculates the 3D flow field and calculates specific centrifugal compressor performance parameters according to a set of predefined equations.
- **Response surface optimization module:** Optimizes the compressor geometry to get the best performance according to a user-defined objective function and without violating a set of pre-defined constraints. It uses the response surface model and design of experiments for sampling.

The optimization process works in the following order: the optimization module selects a sample of compressor geometries which cover the entire design space, this set is defined using a suitable design of experiments techniques. The geometry is used to generate a suitable mesh, then the performance of the design is calculated, and the output performance parameters are stored. This process continues till the performance of each of the designs in the initial sample is calculated. The stored data is used by the optimization module to generate a surrogate model (also called a response surface) with the compressor performance parameters as outputs (responses) and geometrical variables as inputs.

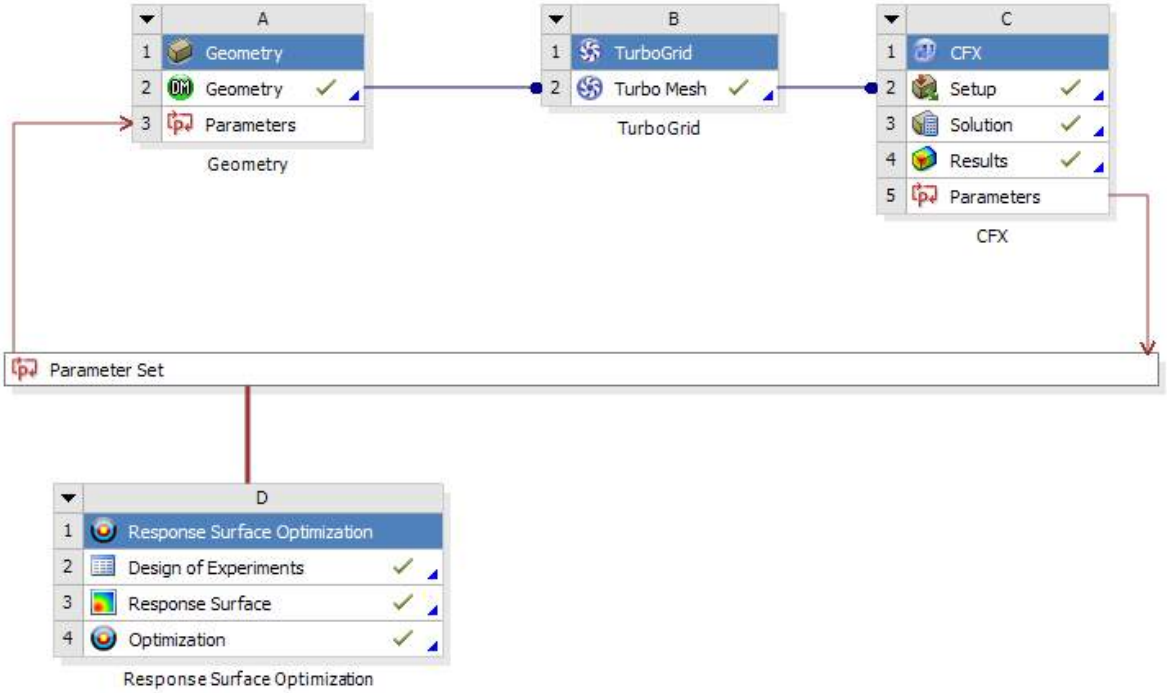

Figure 1: Automated optimization workflow schematic in ANSYS workbench

Using an automated optimization workflow saves time and effort, but the following requirements should be fulfilled so that the automated workflow can work:

- Preparation of a robust parametric CAD model of compressor.
- Setting up a mesh configuration that achieves a good balance between accuracy, computational time and robustness.
- Proper specification of the CFX setup, solution parameters and defining the equations for the calculated performance parameters.
- Validation of the CFX setup and solver settings through using the Eckard O compressor geometry and comparing the calculated parameters to the experimental results.

GEOMETRICAL MODEL

Two CAD models are required for the analysis, the first one is the Eckardt O compressor 3D model, it is required for the CFD setup validation step, the second model is the parametric model used in the automated optimization workflow.

Rotor of the original Eckardt O compressor

The Eckardt Rotor O geometry was modeled using siemens NX CAD package, the rotor hub and shroud curves are circular arcs, blade elements are radial, and the blade camber lines are elliptical curves in cylindrical sections. Figure 2 shows the main dimensions of the meridional contour of the Eckardt O rotor, the elliptical blade camber curves in cylindrical sections are defined using the following equation:

$$\frac{(Y-a)^2}{a^2}+\frac{X^2}{b^2}=1 \qquad (1)$$

Where: a = 4.7693R mm, b= 220.579 mm

No data was found in the literature regarding the blade thickness of the Eckardt O rotor, so it was assumed following the design recommendations used at the time the original compressor was designed, Blade thickness was assumed constant for stream-wise sections and increasing linearly from the shroud to the hub along the blade span, the blade thickness was assumed 1.25 mm at the shroud and 2.5mm at the hub. Figure 3 shows the created CAD model of the compressor.

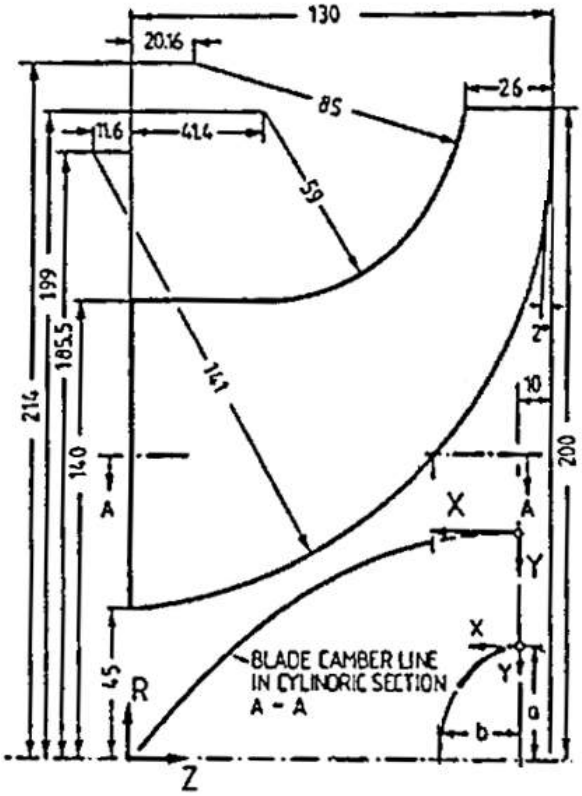

Figure 2: Meridional contour and mean camber line [7]

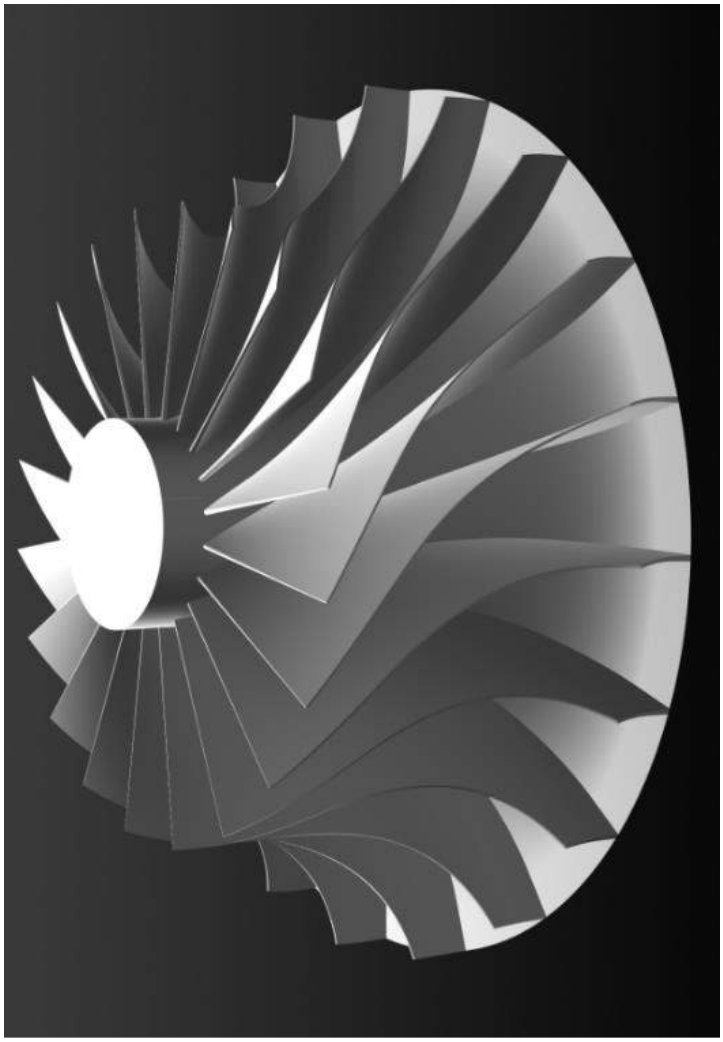

Figure 3: The developed CAD model of Eckardt O rotor

Rotor of the parametric CAD model

The parametric CAD model used in the optimization workflow is defined in the ANSYS design modeler module. It shares the same meridional contour with the original Eckardt O rotor. For the blade, Radial element surface construction is used, this makes the definition of the blade camber line at only one cylindrical section at any radius from the rotor axis sufficient to define the whole blade camber surface. In ANSYS blade modeler the blade camber lines can be defined at stream-wise sections by defining their blade angles values along the meridional length [4]. For the developed parametric CAD model, A Bezier curve with 6 control points was used to define the blade stream-wise camber line at the shroud section. The range through which the coordinates of each of the control points could be varied is carefully selected to avoid the generation of distorted blade geometries. three of the control point are kept fixed and the meridional coordinates of the other three points were also kept fixed, leaving only three parameters controlling blade angles as variables to be controlled by the optimizer during the automated optimization workflow. Figure 4 shows the blade angles distribution at the shroud stream-wise section, the control points designated by "+"

kept fixed and only the angle values for the control points designated by "o" are used as parameters to be controlled by the optimizer, these parameters are named beta1, beta2, beta3 and the range of their values is specified in Table 1.

Table 1 upper and lower bounds of geometrical parameters

Variable	Lower bound	Upper bound
beta1	-30°	-15°
beta2	-30°	-5°
beta3	-5°	5°

The thickness distribution applied was assumed in the same way previously used to create the Eckardt O CAD model.

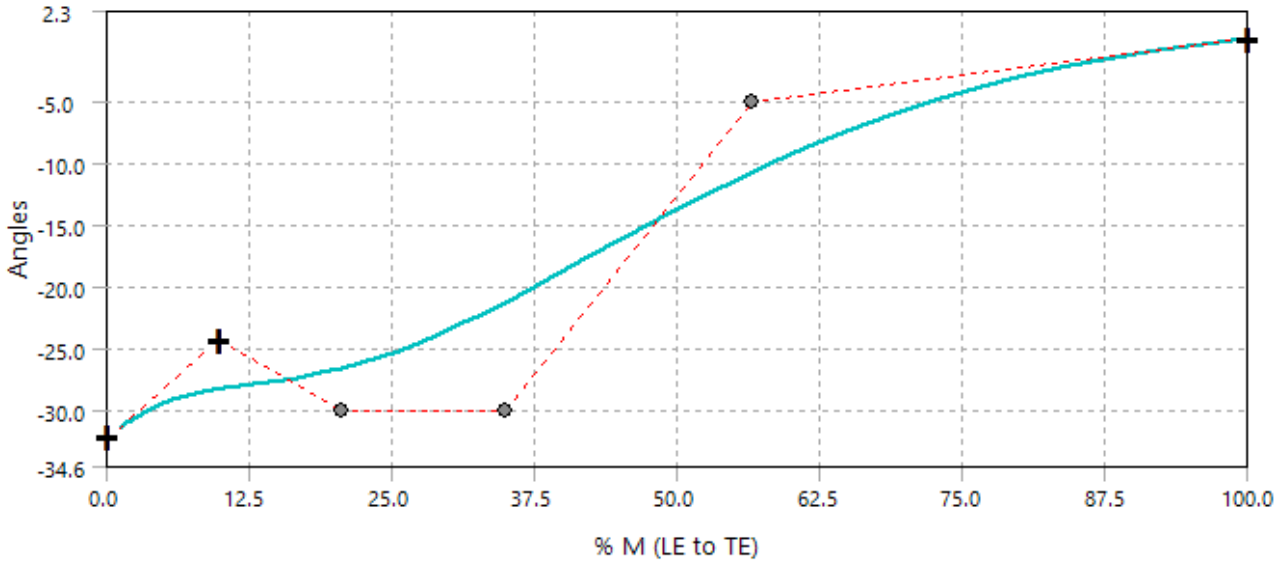

Figure 4: Blade angle distribution at the shroud stream-wise section

Diffuser Geometry for the CFD verification CAD model

The original Eckardt O diffuser is vaneless with constant flow area up to a radius equal to twice the impeller tip radius (R/R2 = 2), followed by a bend to turn the flow into an annular settling chamber as shown in Figure 5, the experimental results reported are based on inlet conditions at station 0 and outlet conditions at station 4 (R/R2 = 1.69) [8], thus, the vaneless diffuser used in the CAD setup verification was modeled only up R/R2 = 1.69 such that the CFD results could be validated against the published experimental results. The same diffuser geometry was also used with the parametric rotor model used in the automated optimization work flow such that the results obtained could be directly compared to the experimental results achieved by the original Eckardt rotor O. Figure 6 shows the meridional contour of the flow path in ANSYS design modeler.

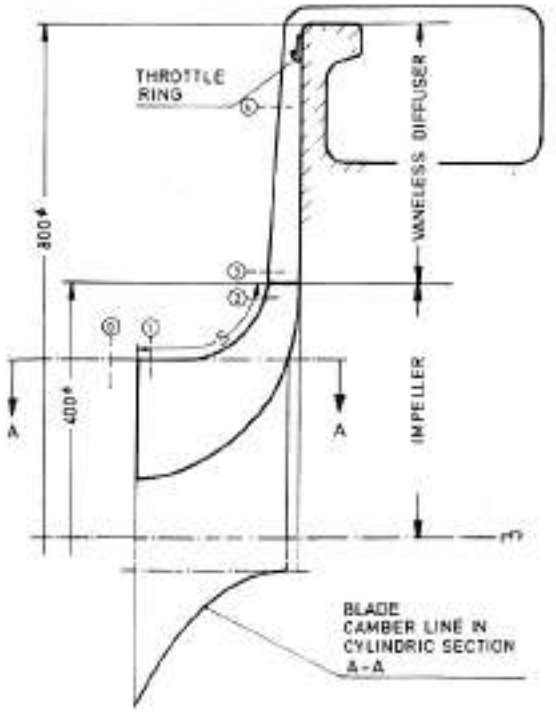

Figure 5: Meridional contour of the compressor stage [9]

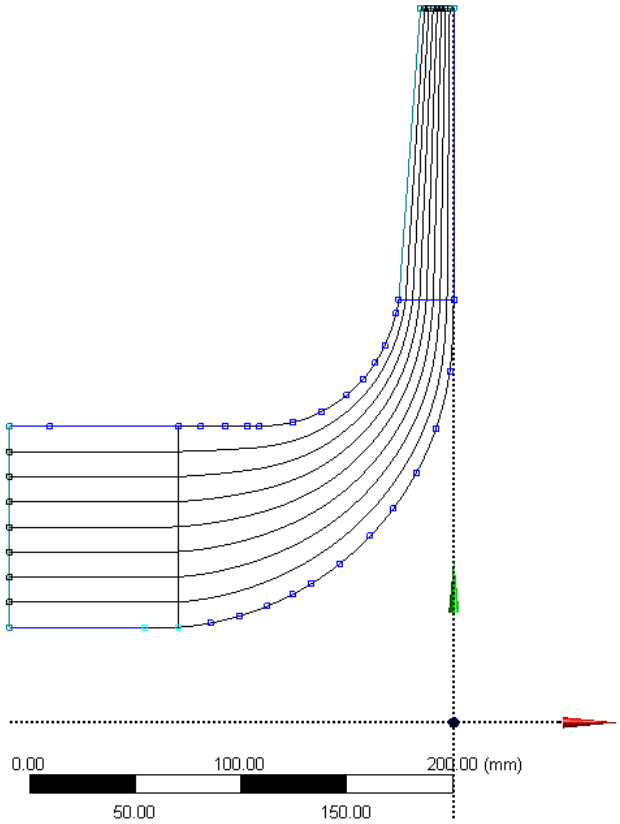

Figure 6: Meridional contour of the flow path in ANSYS design modeler

CFD MODEL SETUP & VALIDATION

The selected computational tool for CFD calculation is ANSYS CFX®. This commercial simulation software package is selected for its proven accuracy in turbomachinery applications including centrifugal compressors, also it can be used integrally with geometry, meshing and optimization modules within the ANSYS workbench environment to create a stable integrated and automated optimization workflow.

Frame of reference

A single frame of reference can be used when calculating the compressor stage, that is, a frame of reference that is fixed with respect to the rotor, this makes the flow steady with respect to this frame of reference which greatly simplifies the analysis, despite the fact that the vaneless diffuser is rotating with respect to this single frame of reference, using the single frame of reference is still possible because the vaneless diffuser consists of only two surfaces of revolution around the impeller axis of rotation [10], using a rotating frame of reference for the rotor and a stationary frame of reference for the diffuser is also possible by adding a suitable interface, but it adds unnecessary complexity to the analysis and yields almost no differences in the results.

Boundary conditions

The flow simulation is performed using a single flow passage between two adjacent blades by using rotational periodicity to calculate the performance of the whole compressor, this reduces the computational time significantly and gives accurate results. Figure 7 shows the computational domain boundaries definitions.

Inlet Boundary conditions:

- Total pressure at inlet (P_0) = 101325 Pa
- Total Inlet Temperature (T_0) = 288.15 K

Outlet Boundary conditions:

- Mass Flow rate = 5.31 kg/s

Wall Boundary condition:

- Blade surfaces.
- Inlet Hub and impeller hub surfaces.
- Diffuser hub surface (with wall velocity: counter rotating).
- Shroud (with wall velocity: counter rotating).

Periodicity Boundary conditions:

- Between the periodic sides 1 and 2 of the hub, passage and shroud.

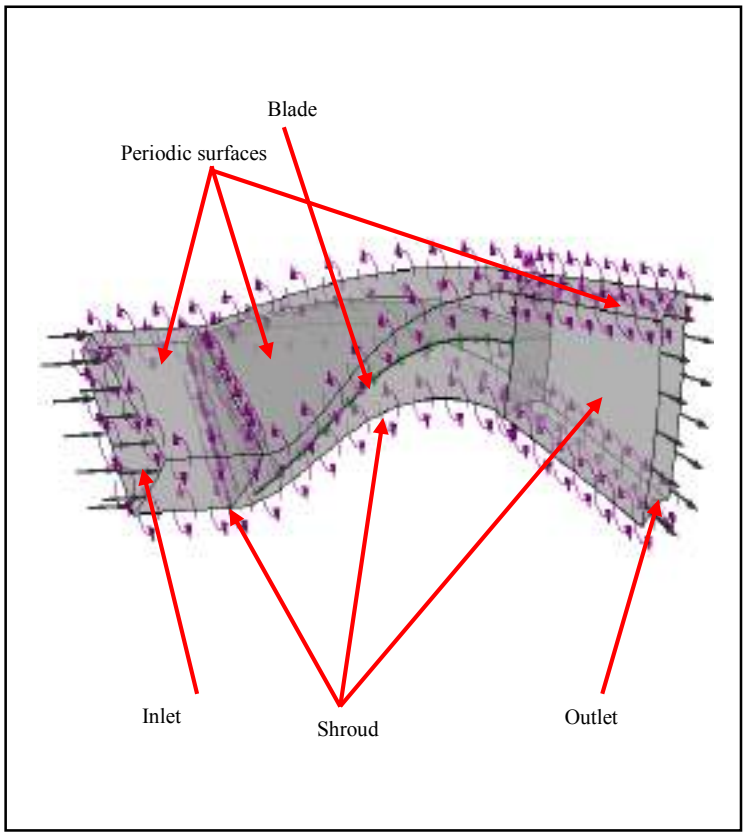

Figure 7 Boundaries definition

Turbulence model selection

For an automatic optimization workflow, many designs are evaluated using a computationally expensive CFD solver, the simulation time and robustness are both important factors. Accuracy of the CFD solver is also critical to obtain a design that performs as expected. Investigators compared between different turbulence models for centrifugal compressors applications [11] SST model proved to offer a good balance between robustness, speed and accuracy. It is also recommended by ANSYS for turbomachinery applications [12], so it was chosen for this analysis.

Mesh generation.

Mesh generation is carried out using ANSYS TurboGrid, whereas structured type mesh is used. ANSYS TurboGrid has the capability of producing high quality meshes with the least number of elements, thus helps in obtaining fast and accurate results.

Method: Global size factor, this was varied from 1.1 to 1.3 during the grid independence study, the final mesh has a global size factor of 1.1.

Topology: The mesh topology is defined using the ATM optimized option in ANSYS TurboGrid and the selected method is the single round cut-off refined, Figure 8

Boundary Layer: Different methods for near wall element size specification during the grid independence study, for the final mesh an absolute First element offset of 0.5 mm was applied with target maximum expansion rate of 1.3.

Passage data: the method is “Proportional” with Factor =1.

Inlet domain: mesh type is H-Grid, defined by a maximum expansion rate of 1.2, the total node count of the final mesh is 800000 and it proved to be valid through the grid independence test.

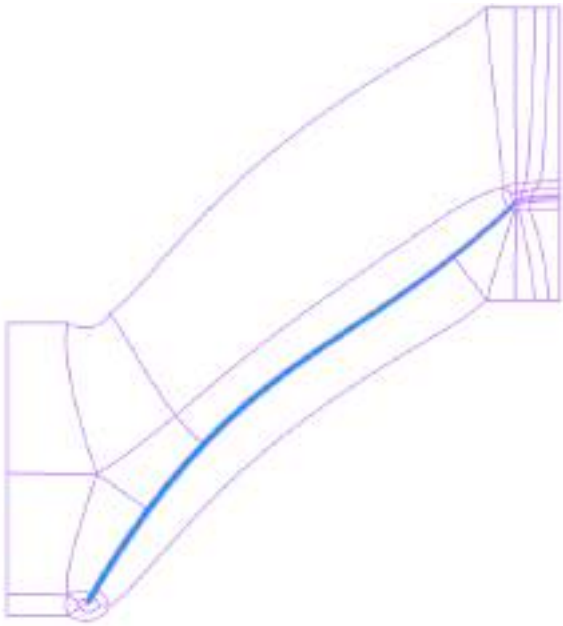

Figure 8 Turbogrid Mesh Topology (Single Round Cut-off refined)

Grid independence study

Grid independence study is performed at the performance point m =5.31 kg/s at 14000 rpm for the Eckardt O rotor, Table 2. The experimental values of the total to total pressure ratio and isentropic efficiency are 2.094 and 88% respectively. Therefore, the mesh with 8E05 nodes is selected as the final mesh which gives relative errors of -0.468 %for pressure ratio prediction and -0.0068% for efficiency compared to the experimental values.

Table 2 Grid independence study

Passage mesh elements	Total temperature ratio	Total pressure ratio	η_{tt}	Compressor mass flow rate
400000	1.2672	2.0816	87.849	5.31
800000	1.2672	2.0842	87.994	5.31
1100000	1.2665	2.0825	88.13	5.31
1800000	1.2669	2.0849	88.16	5.31

The produced mesh offers Non-dimensional wall distance values, "Y+" suitable for good accuracy with the SST model, Figure 9 shows the Y+ contours on the hub and the blades, the y+ value doesn't exceed 5 almost over all the surfaces

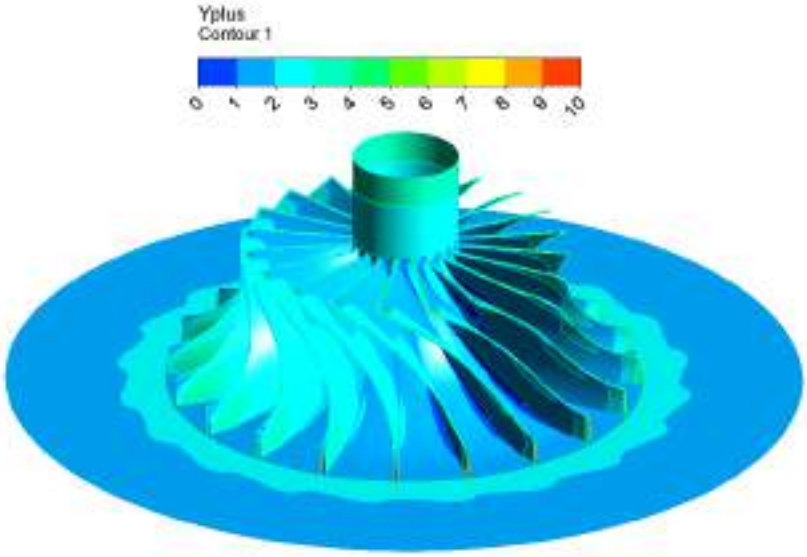

Figure 9 Y plus contours on the rotor and diffuser hub

CFX-pre-setup

High resolution option is selected for advection scheme and turbulence numerics, the maximum number of iterations is set to 500 (the solver terminates even if the convergence criteria is still not met). Automatic time scale factor is used. Timescale factor is set to 5.

The convergence is achieved if the RMS residuals reach 1E-07, a conservation target is set to 0.01 and interrupt control is activated, it defines a better criterion for convergence compared to the RMS residuals. It terminates the solution earlier if all the following conditions are met:

- Current time step>20
- Standard deviation over a moving interval of 40 iterations of isentropic efficiency >0.05.
- Standard deviation over a moving interval of 40 iterations of outlet total pressure <1 Pa
- Standard deviation over a moving interval of 40 iterations of stage mass flow rate < 0.05 kg/s

Calculated parameters

Total pressure ratio: $PR_{tt_4} = \frac{P_{t_4}}{P_{t_1}}$

Corrected mass flow rate: $\dot{m}_{cor} = \dot{m}\sqrt{\theta_0}/\delta_0$

Corrected total temperature: $\theta_0 = \frac{T_{t_0}}{288.15\ K}$

Corrected total pressure: $\delta_0 = \frac{P_{t_0}}{1\ atm}$

Total to total isentropic efficiency: $\eta_{tt_{04}} = \frac{\left(P_{t_4}/P_{t_1}\right)^{\frac{k-1}{k}}-1}{T_{t_4}-T_{t_1}}$

Computational tool validation

The validation process starts with the comparison between CFD results and the experimental results at n = 14000 rpm, reported by D. Eckardt, the performance parameters of the compressor at the three test points are summarized in Table 3.

Table 3 Summary of Eckardt's O performance at the CFD1, CFD2 & CFD3 Test points

Test Point	$n/\sqrt{\Theta_0}$ [rpm]	$\dot{m}\sqrt{\Theta_0}/\delta_0$ [kg/s]	$PR_{tt_{04}}$ [--]			$\eta_{tt_{04}}$ [%]		
			Measured	CFD	Relative Error	Measured	CFD	Relative Error
1	14000	6.09	2.061	2.0605	-0.024 %	86.8	87.399	0.69 %
2	14000	5.31	2.094	2.0842	-0.468 %	88.0	87.994	-0.0068%
3	14000	4.53	2.086	2.0608	-1.208 %	86.5	86.531	0.035%

Comparison between measured and CFD impeller tip conditions

Table 4 shows the comparison between the CFD and Experimental impeller tip conditions reported by Japikse & Baines [1],

Table 4 Experimental and calculated impeller tip conditions

	Measured	CFD	Deviation
T_{t_2}	363.5 K	364.7 K	0.330%
p_{t_2}	220.5 kPa	216.314 kPa	-1.898%
p_2	144.7 kPa	143.422 kPa	-0.883%

The results obtained show a good agreement between experimental and calculated CFD results, thus the illustrated mesh settings are applied to the CFD calculations within the automated optimization workflow

OPTIMIZATION MODULE SETUP

Design of experiments (DOE)

The first step is the determination of the upper and lower bounds of the input parameters, the upper and lower bounds are specified in Table 1. The selected design of experiments type is the "Latin Hypercube Sampling Design", whereas the selected samples type is "CCD ". The number of design points generated using this methodology is 15 design points. The output parameters calculated and stored for each design point are the mass flow rate, total to total isentropic efficiency and total to total pressure ratio.

Response surface

Kringing auto refinement is used for response surfaces generation. This method uses the CFD results of the DOE samples for metamodel construction, then checks the accuracy of the response surface through comparing the CFD calculated results of a new, automatically selected performance point to the predicted results from the current metamodel, if the results give an error exceeding the user defined maximum relative error, more automatically selected, CFD calculated performance points are added to construct a more accurate metamodel, this process continues till the response surface accuracy reaches the user defined target. in this analysis the maximum relative error specified is 5%.

Optimization objectives & constraints

The objective of the optimization process is to maximize the total to total isentropic efficiency of the compressor while keeping the total to total pressure ratio constrained between 2 and 2.2. Figure 10 shows the objectives and constrains set in the design explorer component.

Figure 10 Optimization objectives and constraints

Optimization Algorithm and results

The Multi-Objective Genetic Algorithm (MOGA) is used, it is a variant of the NSGA-II algorithm, it aims at finding the global optimum and supports multiple objectives and constraints.

The optimization component is configured to generate initial 500 samples using 150 samples per iteration to find three candidates that deliver the best performance, the performance predicted through the response surface is verified via CFD calculations. The obtained optimum design has the following geometrical variables values, Table 5.

Table 5: Optimum design geometrical variables values

Variable	Value (Degree)
beta1	-15^o
beta2	-5^o
beta3	0.12^o

RESULTS & DISCUSSION

The selected optimized design has the highest efficiency in the design space, compared to the performance of the original Eckardt rotor under the same operating conditions (N =14000 rpm & $\dot{m}$ = 5.31 kg/s). The efficiency has increased from 87.994 % to 88.481%, that is, about 0.487 %. Changing the blade angles distribution improved the blade loading leading to less losses and improved efficiency.

Figure 11 and Figure 12 show a comparison between the blade to blade Mach number contours of the original and the optimized compressors at 60 % span. It is obvious that changing the blade angle distribution changes the blade shape such that the Mach number inside the passage generally decreases leading to a reduction in losses and increase in efficiency. The Mach number reduction is more obvious at 90% span. Comparing Figure 13 and Figure 14 a significant reduction in the Mach number in the inducer section is seen, leading to efficiency improvement.
it can be noticed that the wake region seems to be larger in the optimized impeller, but its severity is less compared to the wake in the original impeller.

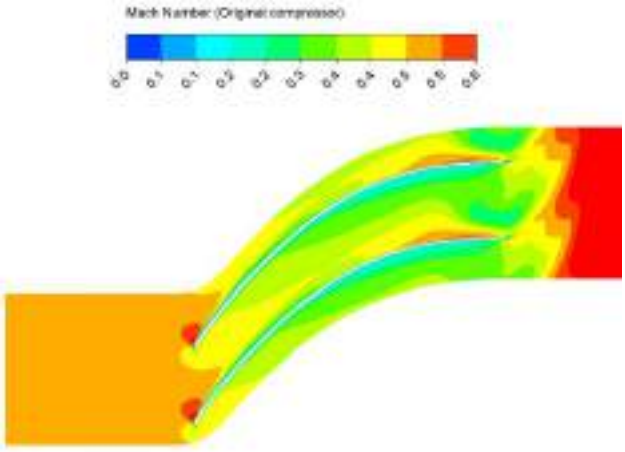

Figure 11: Original compressor blade to blade Mach No. Contours at 60% span

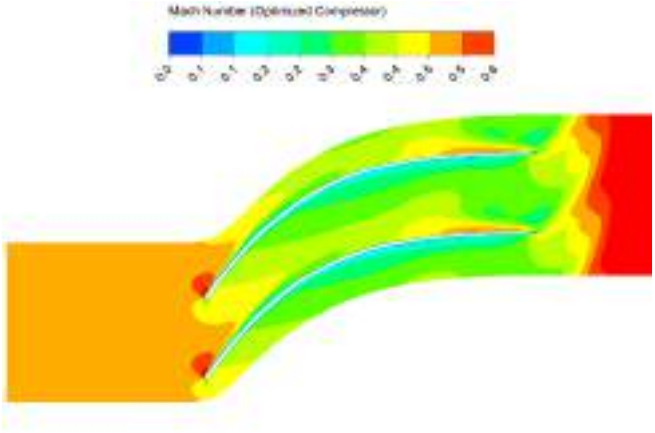

Figure 12 Optimized compressor Blade to blade Mach No. Contours at 60% span

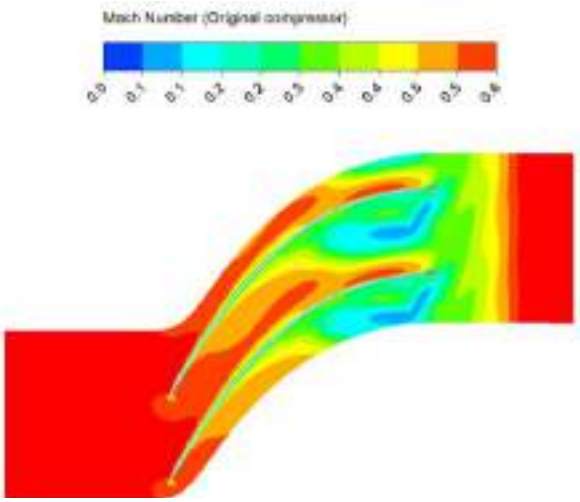

Figure 13: Original compressor Blade to blade Mach No. Contours at 90% span

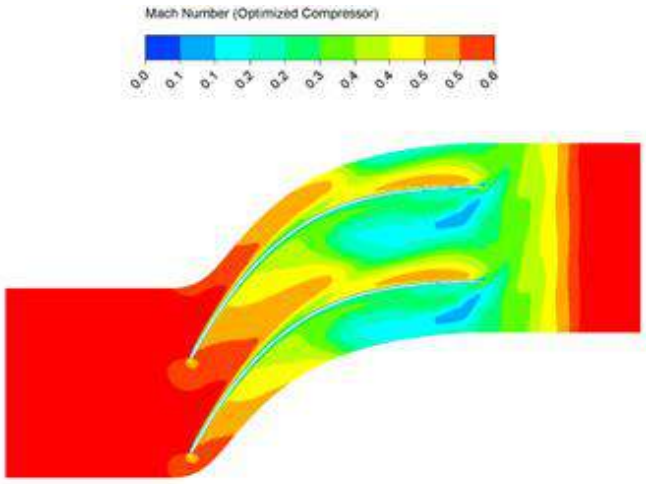

Figure 14: Optimized compressor Blade to blade Mach No. Contours at 90% span

CONCLUSION

The optimization of the rotor of the Eckardt O compressor is performed through variation of the blade angle distribution while keeping the blade angles at the impeller inlet and outlet unchanged. An automated optimization is performed based on a surrogate model exploiting DOE for sampling and using CFX as the fluid flow solver. The design point performance for the original and optimized compressors are evaluated and compared both quantitatively and qualitatively, where 0.487% of efficiency improvement is reached. It can be shown that varying the blade angles distribution modifies the blade loading such that a sound improvement in the Mach number distribution is achieved leading to a mild improvement in the compressor total to total efficiency for the same pressure ratio and mass flow rate.

REFERENCES

[1] D. Japikse and N. C. Baines, *Introduction to turbomachinery*. Concepts ETI, 1994.

[2] D. Japikse, *Centrifugal compressor design and performance*. Concepts ETI, 1996.

[3] R. H. Aungier, *Centrifugal compressors : a strategy for aerodynamic design and analysis*. ASME Press, 2000.

[4] ANSYS, "ANSYS TurboSystem User Guide," vol. 15317, no. October. pp. 724–746, 2012.

[5] Z. Li and X. Zheng, "Review of design optimization methods for turbomachinery aerodynamics," *Prog. Aerosp. Sci.*, no. May, p. , 2017.

[6] I. Lepot, "Complements on Surrogate Based Optimization for Engineering Design," vol. 41, no. 1, pp. 1–12, 2009.

[7] A. TOURLIDAKIS, "Numerical Modelling Of Viscous Turbomachinery Flows With a Pressure Correction Method," Cranfield Institute of Technology, 1992.

[8] D. Eckardt, "Instantaneous Measurements in the Jet-Wake Discharge Flow of a Centrifugal Compressor Impeller," *J. Eng. Power*, vol. 97, no. 3, pp. 337–345, 1975.

[9] D. Eckardt, "Detailed Flow Investigations Within a High-Speed Centrifugal Compressor Impeller," *J. Fluids Eng.*, vol. 98, no. 3, pp. 390–399, 1976.

[10] ANSYS, "Module 5: Multiple Zone Modeling." 2016.

[11] S. Gibson, L, Galloway, L, Kim, S & Spence, "Assessment of turbulence model predictions for a centrifugal compressor simulation GPPF-2017-0138," 2017.

[12] ANSYS, "ANSYS CFX Reference Guide," *Elements*, vol. 15317, no. November. pp. 724–746, 2011.

STRUCTURAL PERFORMANCE FOR WIDE-SHALLOW BEAM IN SHEAR (COMPARATIVE STUDY)

By

Abd El-Hakim Khalil[1], Emad Etman[1], Ahmed Atta[1], A.T. Baraghith[2] and R.N.Behiry[3]

[1] Professor, Structural Engineering Dept., Faculty of Engineering, Tanta University, Tanta, Egypt
[2] Assistant Professor, Structural Engineering Dept., Faculty of Engineering, Tanta University, Tanta, Egypt
[3] Assistant Lecturer, Structural Engineering Dept., Faculty of Engineering, Tanta University, Tanta, Egypt

Abstract: Many floor systems contain wide shallow beams to carry floor loads and transfer it to columns. For example, in bridge construction, a system of wide shallow beams (WSBs) may provide a simple and economical system to transfer loads from the slab deck to columns. In many of these design situations, it is often advantageous to use different member widths to minimize reinforcement conflicts and reduce overall congestion. This geometrical peculiarity deserves some attention and caution while dealing with the behaviour at ultimate limit states for shear and flexure. Seven wide-shallow beams with edge columns specimens were used to investigate the effect of width to depth ratios (b/d) and column width to beam width ratios (c/b) on the performance of shear capacity. The performances were measured in terms of deflection, ultimate loads, crack patterns, web reinforcement strains, and shear strain distribution a cross width. The results revealed that, the contribution of concrete formals of the international codes must be recalibrated.

1 INTRODUCTION

Many floor systems contain wide shallow beams to carry floor loads and transfer it to columns. For example, in bridge construction, a system of wide shallow beams may provide a simple and economical system to transfer loads from the slab deck to columns. In many of these design situations, it is often advantageous to use different member widths to minimize reinforcement conflicts and reduce overall congestion. Common practice is to use beams which are wider than the supporting columns as illustrated in Fig.1, the geometric differences in member width between beam and column will create a difference force flow in the beam compared with the beams that support on columns with the same width.

Recently, some researchers directed their efforts to study the shear behavior of wide shallow beams. Lubell et al., 2009 and Serna et al., 2002 investigated the influence of the stirrups cross spacing on the shear capacity of wide shallow RC beams. The study concluded that the effectiveness of stirrups increases as the spacing of web reinforcement legs across the width of decreases and also the mode of failure is more brittle when widely spaced up to a distance of approximately twice the effective depth. Sherwood et al., 2007carried out an experimental study to compare between the behavior of the wide shallow beams and thick slabs in shear. They tested five specimens of normal strength concrete with a nominal thickness of 470 mm and varied in width from 250 to 3005 mm. The study ended to that the failure shear stresses of narrow beams, wide beams, and slabs are all very similar.

Figure 1: Wide shallow beams application in bridges

The influence of member width on the shear behavior was studied also by Antonio et al., 2015. The test series compared the capacities of wide specimens to narrow specimens having the same effective depth and longitudinal reinforcement ratio. Thus, Antonio concluded that member width was a significant parameter in predicting the shear stress at failure. S. E. Mohammadyan et al., 2014 investigated the shear capacity of six reinforced concrete wide beams with diverse types of reinforcement. The results revealed that using some numbers of independent bent-up bars significantly improved the shear capacity of wide beams. The combination of independent bent-up bars with stirrups led to higher shear capacity and gradual failure of the specimen.

2 RESEARCH SIGNIFICANCE

The objective of this study is to determine the effect of the following parameters on the shear behaviour of wide shallow wide beams: (i) The effect of member width to depth ratio (b/d) and (ii) The effect of columns width to beam width ratio (c/b). On the other hand, the study addressed the adequacy of international codes requirements for shear design of wide shallow beams. A similar comparison is made between the experimental test results and analytical results obtained through the proposed model.

3 EXPERIMENTAL PROGRAM

3.1 Specimen's description:

Seven RC beams were tested under a four point loading system and a shear span-to-depth ratio (a/d) of 2.25 to achieve shear failure for all specimens. All beams had the same height (250 mm) and gross cover (50 mm), corresponding to an effective depth of 200 mm. Moreover, all beams reinforced with the minimum amount of transverse shear reinforcement, was also produced: four-leg stirrups having a diameter of 8 mm at a longitudinal distance of 200 mm .The longitudinal reinforcement was placed with a same reinforcement area; in particular, seven rebar's having a diameter of 22 mm were disposed in tension zone for all beams to prevent flexure failure and seven rebar's having a diameter of 12 mm were used in the compression zone to hold the stirrups in position. Also, for considering the effect of shear on bar force at support, 90o hooked anchorages were used at both ends, with a development length of 200 mm. Table 1 summarizes all specimens geometry details. It should be noticed that, the column parts were reinforced properly with stirrups

and axial reinforcement using appropriate anchorage length of bars in order to resist the applied load at failure.

3.2 Materials properties

All specimens were cast in plywood formwork simultaneously and cured under moist gunny. Seven standard cylindrical molds 150 mm in diameter and 300 mm high, one cylinder for each specimen, were cast at same time as the specimens and cured for control tests. Concrete samples were tested according to ASTM: C39/C39M-14, 2014 and the average compressive strength was 28.47 MPa .Steel bars of 8, 12, and 22 mm were used for stirrups, compression reinforcement, and tension reinforcement, respectively. The actual yield and ultimate stress for the used bars of different diameters evaluated according to ASTM A615 / A615M – 16, 2016. The yield strength for steel bars 8, 12, and 22 mm were 355,446, and 406 respectively.

Table1: Main characteristics of test specimens

Group (I)								
specimen	b mm	d mm	c mm	b/d	c/b	Tension R.F.T	Compression R.F.T	Shear R.F.T
B1	250	200	250	1.25	1.00	7Ø22	7Ø12	Ø8@200mm
B2	600	200	600	3.00	1.00	7Ø22	7Ø12	Ø8@200mm
B3	800	200	800	4.00	1.00	7Ø22	7Ø12	Ø8@200mm
B4	1000	200	1000	5.00	1.00	7Ø22	7Ø12	Ø8@200mm
B5	1400	200	1400	7.00	1.00	7Ø22	7Ø12	Ø8@200mm
Group (II)								
specimen	b mm	d mm	c mm	b/d	c/b	Tension R.F.T	Compression R.F.T	Shear R.F.T
B6	800	200	200	4.00	0.25	7Ø22	7Ø12	Ø8@200mm
B7	800	200	400	4.00	0.50	7Ø22	7Ø12	Ø8@200mm
B3	800	200	800	4.00	1.00	7Ø22	7Ø12	Ø8@200mm

Where: b= the width of beam section, d= the effective depth of beam section, and c= the width of column section, perpendicular length to centerline of beam.

3.3 Testing setup and instrumentations

All tested beams were loaded symmetrically with two equal concentrated loads, which resulted in a region of nearly constant moment over the central part of the beam. Instrumentations for all specimens were designed to capture the load-deformation behaviour, and determine variations in reinforcement strains, for the different beam widths and support configurations. A manual hydraulic jack with maximum capacity 1200 kN loaded the beam by applying downward load by increment of 1.0 kN up to failure and measured by the load cell attached to the jack. Vertical displacement measurements were recorded from LVDTs to capture differential deformations across the width of the members. Test setup for loaded specimens was depicted in Fig.2a.Shear strains were measured on the side faces of each specimen at mid line from face of column to the load point using one circular rosette of four side-mounted linear variable differential transformers (LVDTs) as shown in Fig.2.b. A system of LVDTs-based bulging gauges was used to measure the shear stress distribution cross the beam width by measuring the vertical increase of member thickness caused by diagonal cracking as shown in Fig.2.c. The holes through the concrete for the bulging gauge were formed with 6mm diameter flexible plastic tubing that removed prior to the tests. The free movement of the LVDTs piston prevented the gauge from action as a force – resisting element. For all beams, each stirrup in the shear span was instrumented with an electrical resistance strain gauge.

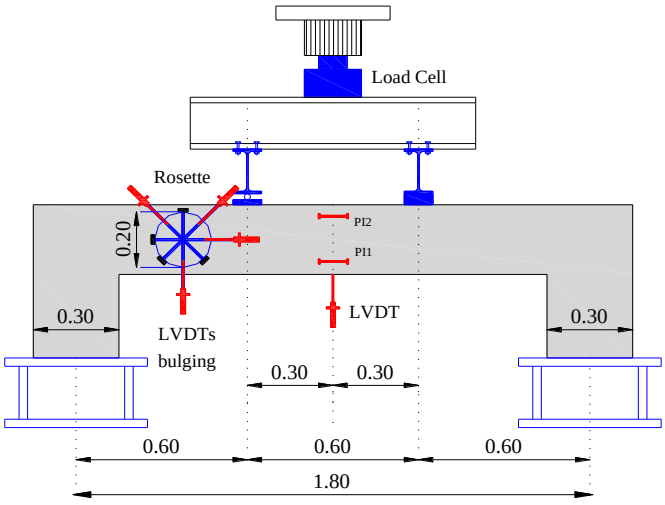

2.a) Sketch for dimension of test setup

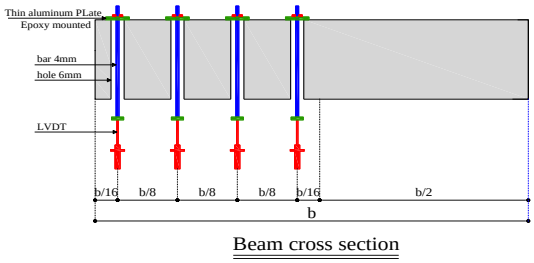

2.b) The system of LVDTs-based bulging gauges

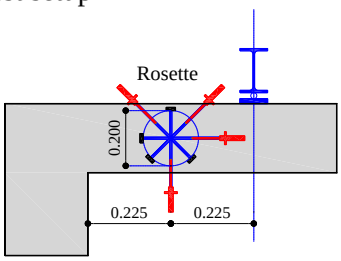

2.c) The system of LVDTs to obtain shear stress

Figure 2: Instrumentation and test set up

4 EXPERIMENTAL RESULTS AND DISCUSSIONS

4.1 Crack patterns and failure modes

In the early stages of loading, the beams were free of cracks. When a maximum tensile stress in the concrete was reached, vertical flexural cracks formed from the tension surface of the beam at intervals along the constant moment region. After the flexural cracks had extended upward a short distance above the longitudinal reinforcement, they extended further vertically in the pure moment zone. Shortly after the flexural crack formed, a small diagonal crack appeared suddenly slightly above the main steel level and at approximately the middle of the shear span. As the load increased, the inclined shear crack developed further towards the loading points and the supports. The rate of propagation of the inclined shear crack was different as b/d changed. Correspondingly the ultimate failure of the tested beams took different forms with a variation of width to depth ratio (b/d). The crack patterns for all specimens are shown in Fig.3.

For narrow beam (B1) with b/d ratio equals 1.25, the inclined shear crack propagated very gradually toward the load point, and eventually crushing occurred somewhat above the crack in the reduced section. When the inclined shear crack reached a point somewhere above the neutral axis, several local diagonal cracks were formed at the level of the tension reinforcement, and gradually connected each other. For this beam the formation of the inclined shear crack did not

cause failure; substantial additional load was resisted after the inclined shear crack initiated. The failure was sudden and loud, this failure mode is conventionally called shear compressive failure. For wide – shallow beams (B2), (B3), (B4), and (B5), it appears that the failure modes are directly related to the stability of the inclined shear cracks, which depends on b/d ratio. The inclined shear crack in beam B2 can be classified as an unstable crack because it propagated quickly without any additional load, resulting in separation of the member into two pieces. Whereas in beams B3, B4 and B5, an additional load was needed to extend the inclined shear crack, so that these cracks may be identified as stable cracks.

In group II, for all three specimens, flexural cracks near mid-span were detected first during initial load stages. Then, new flexural cracks formed in the shear spans and curved diagonally towards the loading point. The diagonal crack widths gradually increased as the applied load at mid-span increased. At the last stages of loading before failure ($P > 0.9\ P_{max}$), an existing diagonal crack rapidly widened and extended upwards to the loading plate. During the shear failure and after the occurrence of the crushing mechanism in the compressive concrete, cracking along the longitudinal reinforcement towards the support region was also observed in specimens. A significant difference in performance was related to the crack development on the side faces of the members. For specimens (B3) with where the support width extended to the specimen edge, the shear cracks terminated at the edge of the loading plate. However, when a narrow support was used, the shear crack extended horizontally past the centerline of the specimen. The difference in crack extent is explained by the lack of confining pressure in the latter case, which allows tensile splitting cracks to form. The results of all tested specimens are summarized in Table 2, which includes the load at the initiation of the flexural crack (flexural cracking load), at the initiation of the inclined shear crack (diagonal cracking load), and the failure (ultimate load). The flexural and diagonal cracking loads were determined from the direct observation of the crack patterns during the test. The stirrup strain measurements were also used to determine the diagonal cracking load as the load at which first significant increase of the stirrup strain crossing the inclined crack occurred.

Table 2: Specimen properties and test results

specimen	b mm	d mm	c mm	b/d	c/b	Flexural Cracking Load (kN)	Shear Cracking Load (kN)	Ultimate Load (kN)	Max. Deflection (mm)
Group (I)									
B1	250	200	250	1.25	1.00	35	171	397	11.62
B2	600	200	600	3.00	1.00	73	407	735	12.20
B3	800	200	800	4.00	1.00	95	540	809	9.45
B4	1000	200	1000	5.00	1.00	116	648	884	7.71
B5	1400	200	1400	7.00	1.00	160	869	1035	10.72
Group (II)									
B6	800	200	200	4.00	0.25	75	528	655	17.99
B7	800	200	400	4.00	0.50	80	537	736	13.73
B3	800	200	800	4.00	1.00	95	540	809	9.45

3.a) Final crack pattern of specimen (B1)

3.b) Final crack pattern of specimen (B2)

3.c) Final crack pattern of specimen (B3)

3.d) Final crack pattern of specimen (B4)

3.e) Final crack pattern of specimen (B5)

3.f) Final crack pattern of specimen (B6)

3.g) Final crack pattern of specimen (B7)

Figure 3: Final crack pattern of tested specimens

4.2 Load-deflection relationships

The load-deflection curves for the tested specimens of group I at mid-span are presented in Fig.4. As presented in this Figure, the general trend of the load-deflection curves was similar among the tested specimens of this group despite the change of the width to depth ratio (b/d). The load-deflection curves of specimens may be roughly described by a bilinear relationship. The first stage starts from the beginning of loading to the point at which an inclined shear crack was first observed. In this stage, the beams acted linearly and the slopes (stiffness) were dependent on b/d ratio. The second stage starts from the point of the inclined shear crack initiation to the point of the ultimate load. Around the inclined shear cracking load, the stiffness generally started to decrease more rapidly. For narrow beam (B1) with b/d ratio equals 1.25, the stiffness was little changed. However, for other specimens, the stiffness was considerably changed just after the inclined shear cracks were initiated. Noted that the vertical axis indicates the machine load over the ultimate maximum load to normalize the results for different widths.

The load-deflection response of specimens of group II are shown in Fig.5. In contrast to the typical behaviour of RC members in flexure, the specimens in this group did not exhibit a sudden or large change of slope in the load-deflection plot at the initiation of flexural cracking. A non-linear relationship with gradually reducing slope was observed for specimens to shear failure. The load-deflection response for specimen (B3) started to exhibit a plateau after reaching the ultimate load, mainly due to the non-linear behaviour of the longitudinal reinforcement. After some additional deformation in specimen, a significant diagonal crack formed leading to a shear failure, then a sudden and large drop in load was recorded at failure.

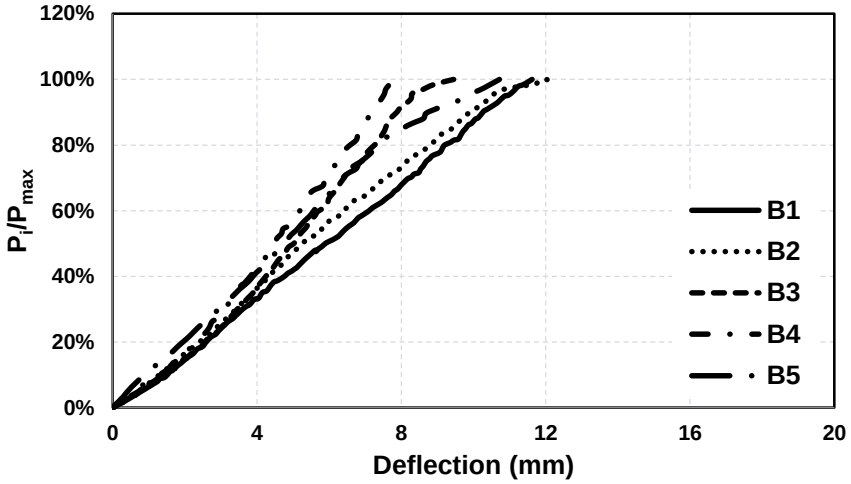

Figure 4: Experimental curves of the machine load vs. mid-span deflection for Group (I)

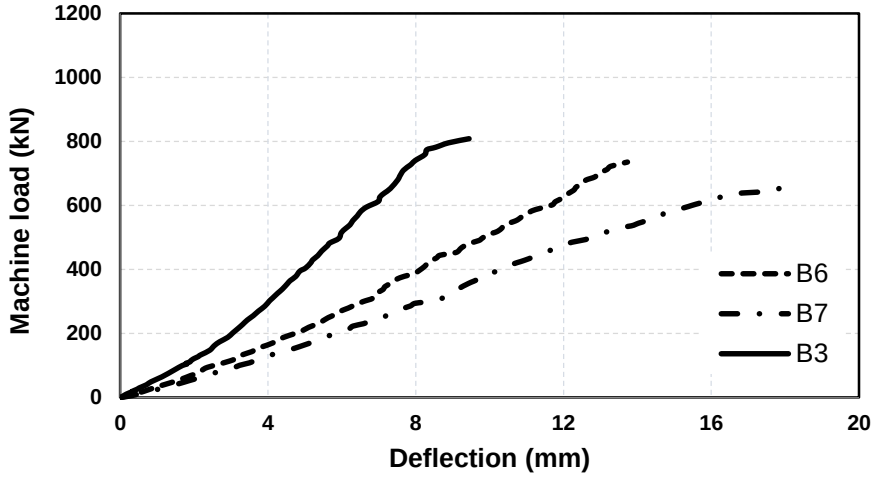

Figure 5: Experimental curves of the machine load vs. mid-span deflection for Group (II)

4.3 Strains

In all specimens, the trend of the shear stress-strain plots for strain gauges installed on the web reinforcement could be described by a tri-linear relationship. The first part of this relationship is defined by a line starting at the origin and extending along the vertical axis up to the appearance of the first inclined cracking. This behaviour indicates that, initially, the stirrups did not contribute to the shear strength of the beam until an inclined crack developed. However after inclined

cracking, the second region of the shear stress-strain relationship started and extended up to the yielding strain of stirrups. At the beginning of this region, a small plateau related to the sudden opening of an inclined crack could be observed in some strain gauges. The third region in the shear stress-strain plots could be observed if the strain gauges installed on stirrups corresponds to a yielding plateau that extended up to failure of the specimen or the de-bonding of the gauge.
For curves relative to narrow beam (B1), it appears that the tensile strain in inner stirrups the same tensile strain in outer stirrups and equal to the 800 micro strain, it is clear that the shear stress distribution on the width of the cross section is constant. However, for another wide-shallow beams the average tensile strain in inner stirrups is 33% the average tensile strain in outer stirrups so that indicates that the shear strain distribution on the width of the section is variable as shown in Fig.6. For specimen (B6) with support width equal to 25% of the beam width, the inner stirrups tensile strain reached to yield strain (1209 micro strain), however the tensile strain of the outer stirrups is 460 micro strain, 38% of yield strain. On the other hand, the behaviour of strains for specimen (B3), full width supporting, is in the opposite way, the inner stirrups tensile strain reached to 417 micro strain (35% of yield strain), however the tensile strain of the outer stirrups reached to yield strain as shown in Fig.7.

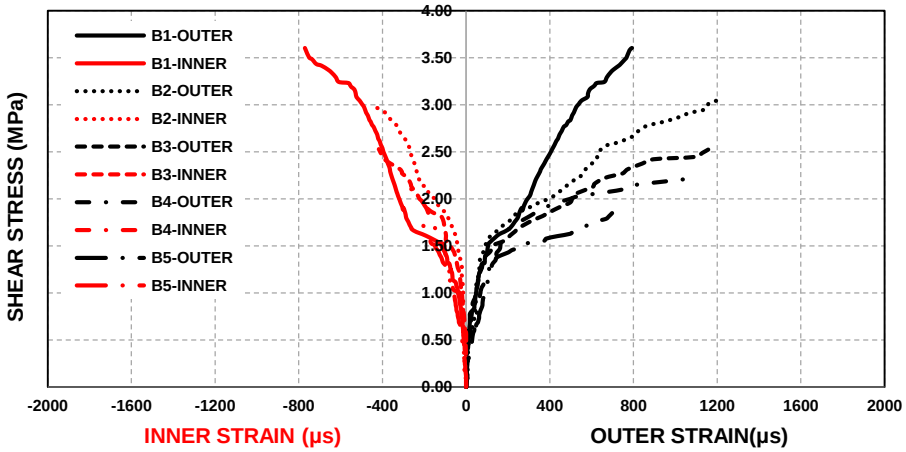

Figure 6: Shear stress vs. shear strain in outer and inner stirrups for Group (I)

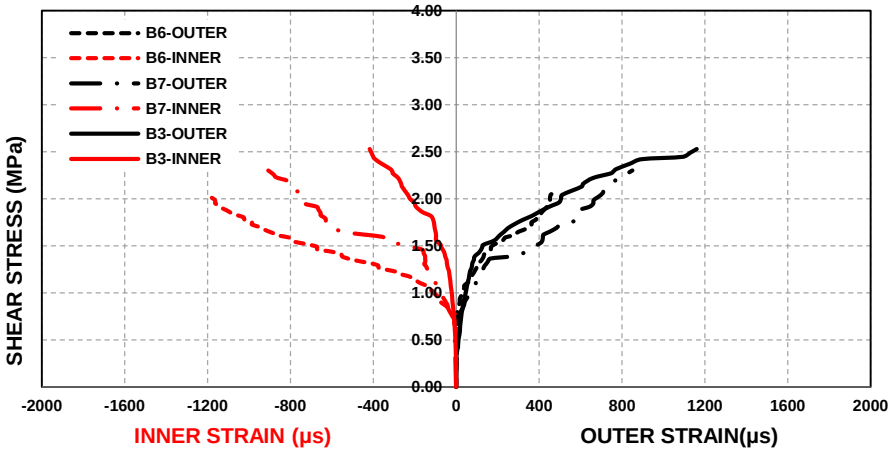

Figure 7: Shear stress vs. shear strain in outer and inner stirrups for Group (II)

4.4 Strain distribution on width of cross section

Fig.8 shows the strain distribution on width of cross section that was measured using a system of LVDTs-based bulging gauges by measuring the vertical increase of member thickness caused by diagonal cracking. By analyzing the curve of narrow beam (B1), the shear stress is approximately constant over the cross section. However, the shear stresses for wide shallow beams have the minimum values at mid-point and the maximum values of the outer face. For wide-shallow beams (B2-,B3, B4 and B5), the shear stress at mid-point decrease by an average 27% compared with the value at the outer face and this conclusion lead to that the width of the cross section is very important parameter in design implication for shear. However, the changing of the column width to beam width (c/b) from 25% to 100% has a strong effect on the shear behaviour of reinforced concrete wide-shallow beams. Fig.9 shows a prominent influence on the shear strain distribution. The shear strain trend of narrow column is contrasting to the trend of wide column, the maximum strain at mid-width for narrow column but the maximum strain at face of the width for wide columns.

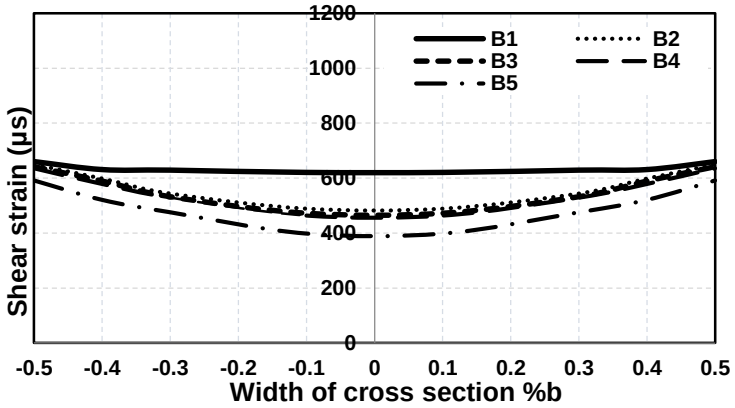

Figure 8: Shear strain distribution on cross width for specimens in Group (I)

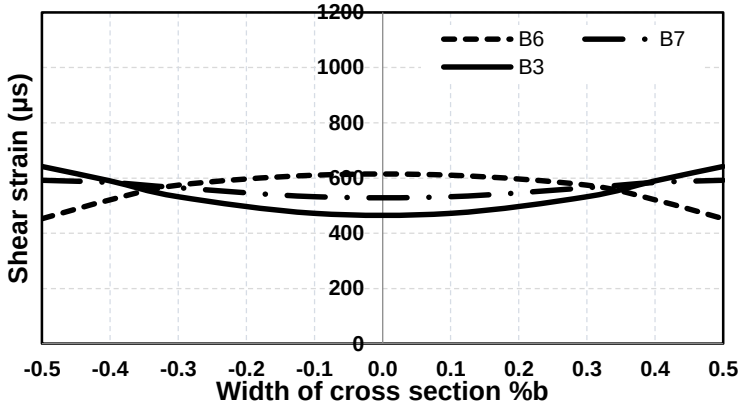

Figure 9: Shear strain distribution on cross width for specimens in Group (II)

5 COMPARISONS WITH INTERNATIONAL CODES

Table 3 shows a number of predictive equations for the shear design formulas for beams in different design codes. Fig. 10 reports the comparison between the experimental shear crack load and the shear strength predicted by shear design formulas. It can be observed that ACI318-08,

AASHTO LRFD-2005, and EC2-04 codes are un-conservative, however the estimations that obtained by using CSA-A23.3-04 is conservative. This conclusion confirms the fact that the contribution of concrete formals of the international codes must be recalibrated.

Table 3 Predictive equations for shear strength of RC beams

Reference	Predictive equation
ACI 318-08,2008	$V_c = 0.17\sqrt{f'_c}\, b\, d$
AASHTO LRFD,2005	$V_c = 0.083\beta\sqrt{f'_c}\, b\, d$
EC2,2004	$V_{Rd,c} = \left[C_{Rd,c} k \left(100\rho\, f_{ck}\right)^{1/3}\right] b\, d$
CSA A23.3-04,2004	$V_c = \phi_c \lambda \beta \sqrt{f'_c}\, b\, d$

Where

V_c, $V_{Rd,c}$	The nominal shear strength provided by concrete.
f_c'	The concrete compressive cylinder strength (MPa).
f_{ck}	The characteristic concrete cube strength (MPa).
b	The web width of section (mm).
d	The distance from the extreme compression fiber to the central axis of the longitudinal reinforcement (mm).
β	The factor indicating the ability of diagonally cracked concrete to transmit tension.
λ	The strength reduction factor.
$Ø_c$	The resistance factor for concrete.
ρ	The tensile reinforcement ratio.
γ_c	The concrete partial safety factor.

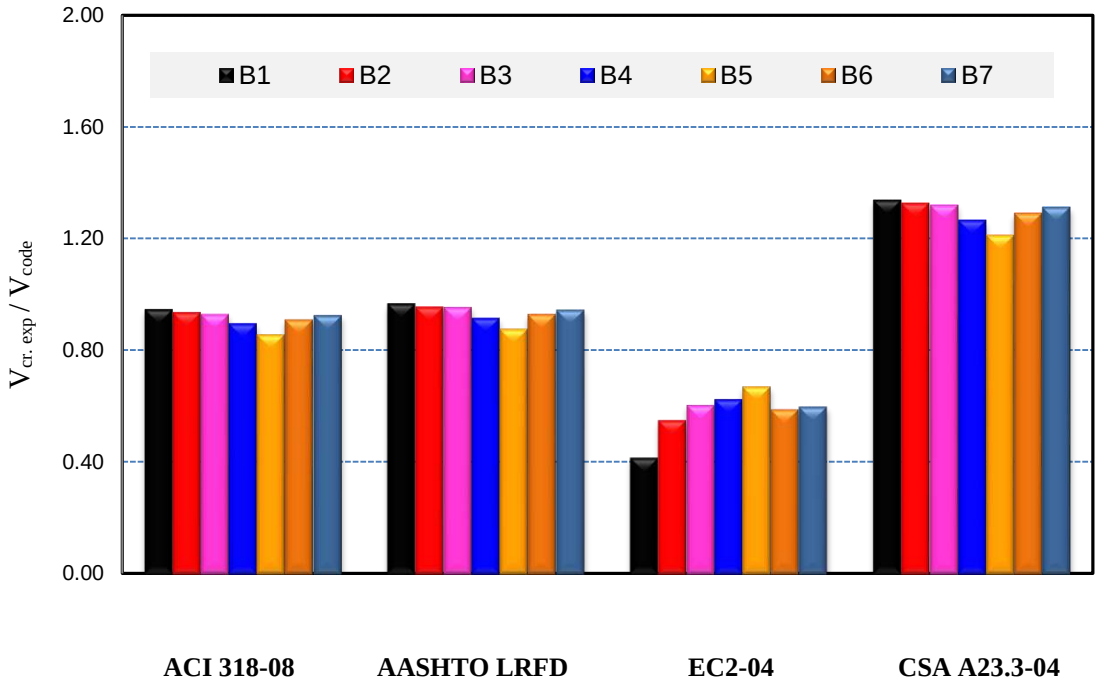

Fig. 10 Expermental vs. Predicted shear force

6 CONCLUSIONS

The behaviour of reinforced concrete wide-shallow beams under shear loading has been analyzed in this manuscript, focusing on the influence of width-to-effective depth ratio and support width to beam width. Based on the experimental test results obtained in this study, the following conclusions can be drawn:

1. The ratio between width-to-effective depth ratios (b/d) in wide-shallow beams seems to significantly influence the mechanism of failure and the shear capacity.
2. Wide-shallow beams that were supported over a portion of their width had a decrease in shear capacity over members with full width conditions. Capacity prediction models must account for this influence, to accurately estimate the failure strength of wide members.
3. For a wide- shallow beams, simply-supported member supported on columns with partial width, the distribution of strains in the concrete varies across the member width. Furthermore, this distribution changes from that of typically higher strains in the outer point to higher strains in the middle point near the supports.
4. Most of current analytical formulations for shear disregarded the losses in shear resistance due to different values of width-to-effective depth ratio (b/d) and support width to beam width ratio (c/b).

REFERENCES

ACI Committee 318, "Building Code Requirements for Structural Concrete (ACI 318-08) and Commentary," American Concrete Institute, Farmington Hills, MI, 2008, 473 pp.

Antonio Conforti, Fausto Minelli, Andrea Tinini, Giovanni A. Plizzari, "Influence of polypropylene fibre reinforcement and width-to-effective depth ratio in wide-shallow beams'', Engineering Structures 88(2015)12-21.

ASTM A615/A615M-16: Standard Specification for Deformed and Plain Carbon-Steel Bars for Concrete Reinforcement, 2016.

ASTM Standers: C39-C39M-14, ASTM committee C09 on concrete and concrete aggregates, 2014.

Bentz, E. C. (2005). "Empirical modeling of reinforced concrete shear strength size effect for members without stirrups." ACI Struct. J., 102(2), 232–241.

CSA Committee A23.3: Design of concrete structures, CSA A23.3-04, Rexdale, Ontario, Canada: Canadian Standards Association, 2004.

Euro code 2, "Design of Concrete Structures-Part 1-1: General Rules and Rules for Buildings (EN1992-1-1)," European Committee for Standardization, Brussels, Belgium, Dec. 2004, 451 pp.

L.R.F.D. AASHTO, Bridge Design Specifications and Commentary, third ed., American Association of State and Highway Transportation Officials, Washington, DC, 2005.

Lubell, A. S.; Bentz, E. C.; and Collins, M. P., "Shear Reinforcement Spacing in Wide Members," ACI Structural Journal, V. 106, No. 2, Mar.-Apr. 2009, pp. 205-214.

S. E. Mohammadyan-Yasouj, A. K. Marsono, R. Abdullah, and M. Moghadasi, 2014, "Wide Beam Shear Behavior with Diverse Types of Reinforcement," ACI Structural Journal, V. 111, No. 1-6, Dec.-Jan. 2014.

Serna-Ros, P.; Fernandez-Prada, M. A.; Miguel-Sosa, P.; and Debb, O. A. R., "Influence of Stirrup Distribution and Support Width on the Shear Strength of Reinforced Concrete Wide Beams," Magazine of Concrete Research, V. 54, No. 3, 2002, pp. 181-191. doi: 10.1680/macr.2002.54.3.181.

Sherwood, E. G.; Bentz, E. C.; and Collins, M. P., "Effect of Aggregate Size on Beam-Shear Strength of Thick Slabs," ACI Structural Journal, V. 104, No. 2, Mar.-Apr. 2007, pp. 180-190.

Evaluation Structural Strength for Beams and Two-Way Roof Slab Systems using Core Test and load Test and Analyzing the Causes of Their Failure.

Mohammad A. Al Zuhaili [1], Khalid Y. A. Al Mazrouei [2]

[1] *M.Sc. Civil Engineering, Trainrr of Construction Training Institut, Public Authority of Applied Education and Training, Kuwait, E-mail: ma.alzuhaili@paaet.edu.kw*

[2] *M.Sc. Civil Engineering, Maneger of Construction Training Institut , Public Authority of Applied Education and Training, Kuwait E-mail:maz.Khalid@gmail.com*

ملخص: تناقش هذه الورقة اختبار القلب الخرساني واختبار التحميل كطريقة لتقييم القوة الانشائية للنظام الانشائي القائم . الهدف الرئيسي للطريقتين هو تقييم القوة الانشائية والسلامة والخدمة. وتتطلب الفشل في الجسور والأسقف تحديد أسباب الفشل ، وتم إجراء مزيد من التحليل لاقتراح أفضل الطرق لإصلاح النظام الانشائي المعيب. في هذه الورقة تم فحص نظام بلاطات السقف ذات اتجاهين لفيلتين مختلفتين في مدينة الكويت ، في فترات زمنية مختلفة من البناء. ونتيجة لذلك ، كان الضعف في قوة الخرسانة موجودًا ، كما ظهر هبوطات في بلاطات الاسقف ، كما ظهرت بعض التشققات في بعض البلاطات والجسور ولذلك ، تم اتخاذ قرار بإجراء مزيد من التحقيقات في السلامة الانشائية ، ودراسة أسباب هذا الفشل. تم إجراء اختبار التحميل والاختبار القلب الخرساني وفقًا لـ ACI-318 ، لقياس وتقييم قوة الخرسانة القائمة.
تشير النتيجة إلى أن العناصر الانشائية دعم إضافي للهيكل الانشائي. من خلال التحقيق والتحليل ، تم العثور على العديد من الأسباب التي تؤدي إلى الفشل في قوة الخرسانة. وأخيرا ، يتم تقديم توصيات لتقييم سلامة تصميم الهيكل.

Abstract: This paper discusses Core Test and Load Test as a method to evaluate Structural Strength for existing structural system. The primary objective of the two methods is to assess structural strength, safety and serviceability. Failure in beams and roof Slabs structural strength were targeted to determine the causes of the failure, and further analysis has been done to suggest the best methods to repair the defected structural system. In this paper a two-way roof slab system for two different vacant villas in Kuwait City was inspected, at different construction time intervals. As a result, weakness in concrete strength was present, and a deflection appears in roof slabs, also cracks appeared in some of slabs and beams. Therefore, decision was made to do further structural safety investigation, and study the causes of such failure. Load test and core test according to ACI-318, were carried out to measure and evaluate the strength of the existing concrete. The result indicates that the structural elements is unsafe, so a necessitate procedure should be carried-out to support these elements, like re-design, re-casting, adding additional structure support. Through investigation and analysis, several reasons were found that leads for failure in concrete strength. Finally, recommendations to assess the safety of the structure design is given.

Keyword: *Concrete structure; Field test; Load test; Core test; In situ test; Two-way slab system.*

1) Introduction

Structure concrete member, designed to resist different applied forces. Where the compressive strength value for that member indicates concrete properties. Standard test specimens (according to standard specifications and codes) are examined during construction, to ensure concrete quality and potential strength. Repeated arguments in whether the specimens standard test can represent in-situ strength of concrete,

especially when the specimens result indicates noncompliance with the specification. In such cases, a complicated problem is generated and immense argue will present, as the conflict between the two parties (Contractor, Engineer consultancy Office) can end up in worse positions than when they started the investigation. Compressive concrete strength test is done by drilling cylinder specimens from suspected structural member, then sent to a specialized laboratory to determine the compressive strength, it is very useful to get result from different kind of tests. Core test is the most popular way to assess the properties of the concrete in the structure [1]. The test result will be shown as a PSI Number, that must be processed, and the strength value should be cautiously interpreted, because core strengths are affected by a number of factors such as diameter, l/d ratio and moisture condition of the core specimen, the direction of drilling, the presence of reinforcement steel bars in the specimen and the strength level of the concrete [4]. From general prospective, core test is ultimately needed to assess the following:

1. Concrete potential strength.
2. Concrete actual strength.
3. Structure member capacity load design, actual loads and new additional load.
4. Structure deterioration factors like fatigue, chemical reaction, fire, and explosion.

2) Literature survey:

Core testing and Load testing of concrete structures in the United States is a century old tradition with one of the earliest well-documented cases are found in the 1890s Birkmire 1894 [6] [7].

The American Concrete Institute began formalizing load test for concrete structures in 1920 [8] ACI [9]. At that time, the evaluation criteria for passing the load test focused on maximum deflection under sustained load combined with the recovery of deflection after the test load removed. Subsequent Codes ACI 1936 defined the deflection evaluation criterion as a function of the span length squared and divided by the total depth of the member cross section [1]. This form of the deflection criterion is still in effect ACI 2005. Notable investigations into load testing of concrete structures are documenting the practice of the last decades can be found in the literature Fitz Simons and Longinow 1975; RILEM 1984; Bungey 1989.[1],[10],[11],[12], [13]

3) Case Study:

In this research a site evaluation preformed on two-way solid roof slabs for two villas, to identify the load level for each structure and causes of failure, with consideration to the design and Implementation of Load Test and Core Test, also its focuses on evaluation criteria and their significance, limitations and applicability. Those structure elements were chosen carefully to represent an ideal case study. Site evaluation shows a deflection in the center and diffuse cracks in top and Bottom faces of slabs, the slabs dimension is (6.90 m x 5.25 m, 6.00 m x 6.20 m) and it supported by beams (6.00 m x 5.00 m).

The following summarizes the preliminary assessment of the structure and the sources for the information used in designing the core test and load test.

First Case:

1. General description of the building:

A typical concrete frame and brick walls house, consists of basement, ground, 1st and 2nd floor. The building was constructed in conventional method, built from reinforcement concrete and the cement block walls (Figure 1, 2, 3). This study is carried out to assess the

integrity of the Structural system of an existing building in Bayan area. An architectural, structural drawings, and data available, as well results of concrete core tests.

Figure 1 General view of the building

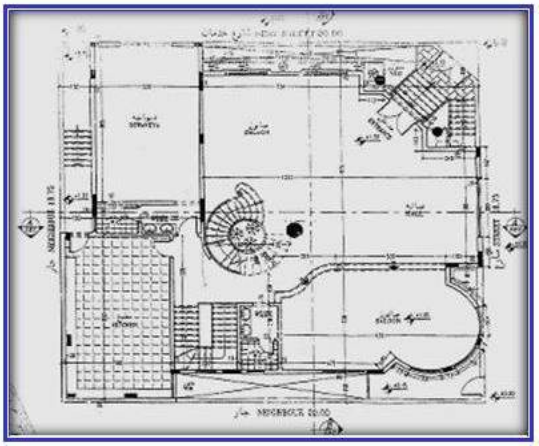

Figure 2 Ground floor plan

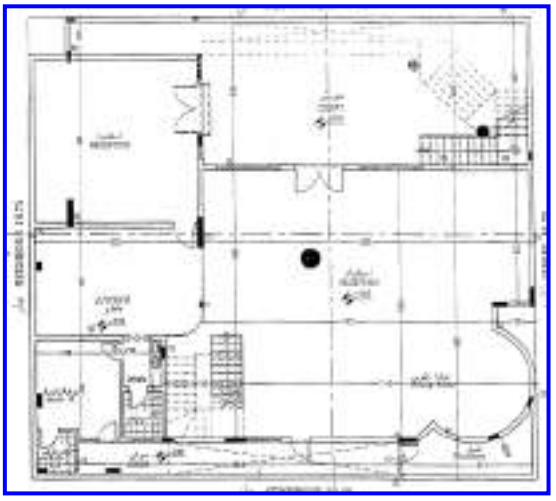

Figure 3 basement floor plane

2. Optical inspection results

The cracks distributed at the positive and negative moment regions, and deflection in center of slabs. Core test carried out of slabs and beam for assess the strength of the existing concrete and look for reasons If its fail. A detailed optical inspection was carried out to identify the apparent structural defects, and to compare between the actual structural elements dimensions executed on site, and the design dimensions on the drawings. Some information was gathered as follow:

- Inclined cracks in some beams type B17, CB1and CB5 in the ground roof.
- Cracks in some slabs, at the bottom in the ground roof (Figure 4).
- Changes in the color of the concrete slab roof in various places (Figure 5)
- Vertical cracks in beam B3 (Figure 6).

Concrete core samples were taken from various parts of the building. The results show concrete compressive strength for beam CB5 is 130 kg/cm2, for beam B18 is 140 kg/cm2, and for the ground floor roof is 168 kg/cm2. The results indicate a weak concrete.

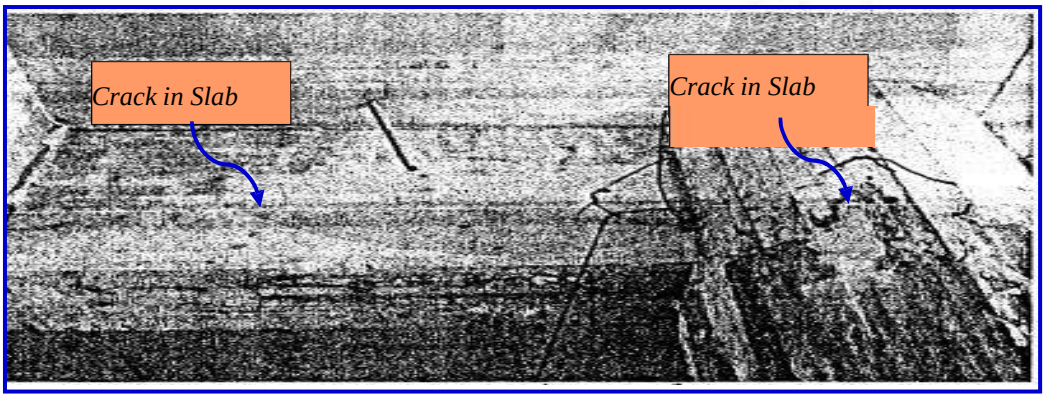

Figure 4 Cracks at the bottom of the slabs

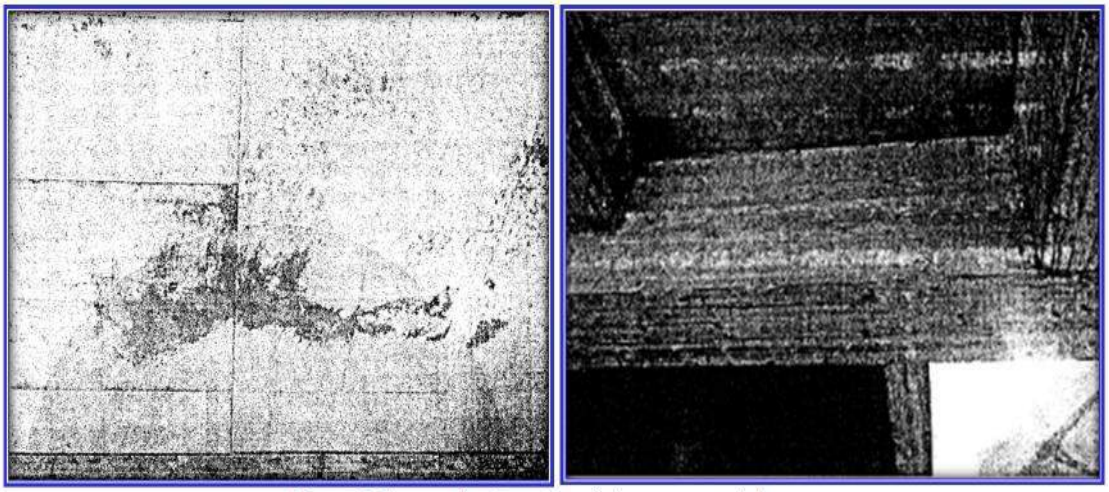

Figure 5 Changes in the color of the concrete slab

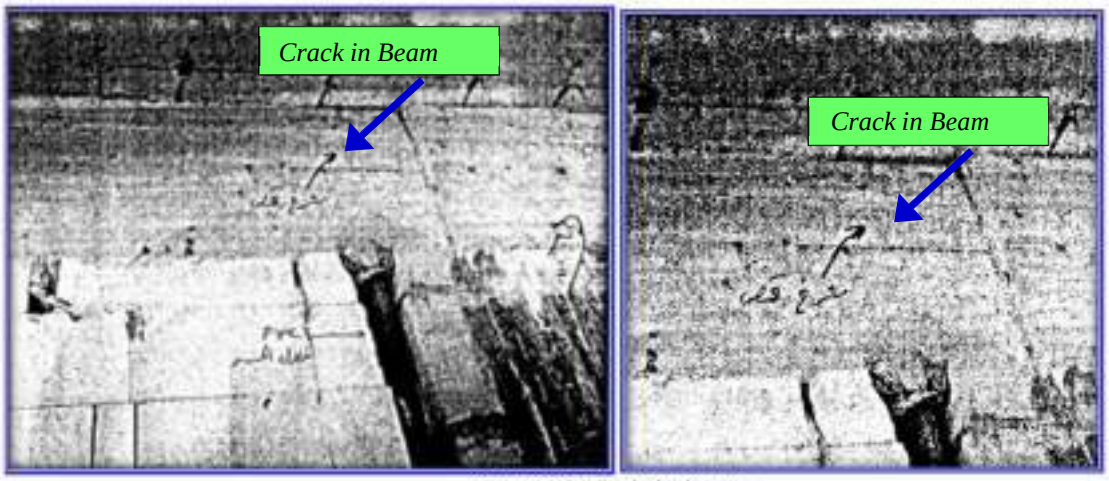

Figure 6 Cracks in the beams

3. Concrete tests

According to chapter 5.6.5.4. of ACI-318 specifications as follows: Concrete is considered as constructively valid if the core test samples are provided with the following two conditions:

- The strength average of three samples not less than 85% of concrete strength design.
- No sample presented with strength less than 75% of concrete strength design.

Five concrete samples core was taken from various places in the building (3 samples from the beams and 2 from the ground roof slab) to determine the concrete's ability to bearing the compressive strength of concrete and its quality. And for measure the actual strength of the concrete. They were examined after 24 hours from extraction. The following table shows the detailed results of concrete samples (Figure 7, 8, Table 1)

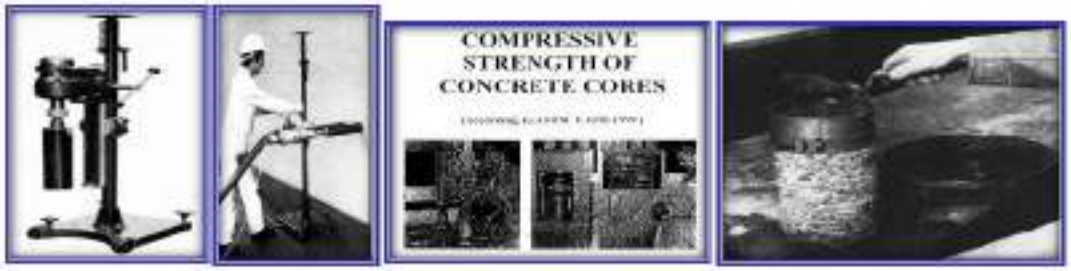

Figure 7 Instruments of concrete core test (according to ASTM C42M-1999)

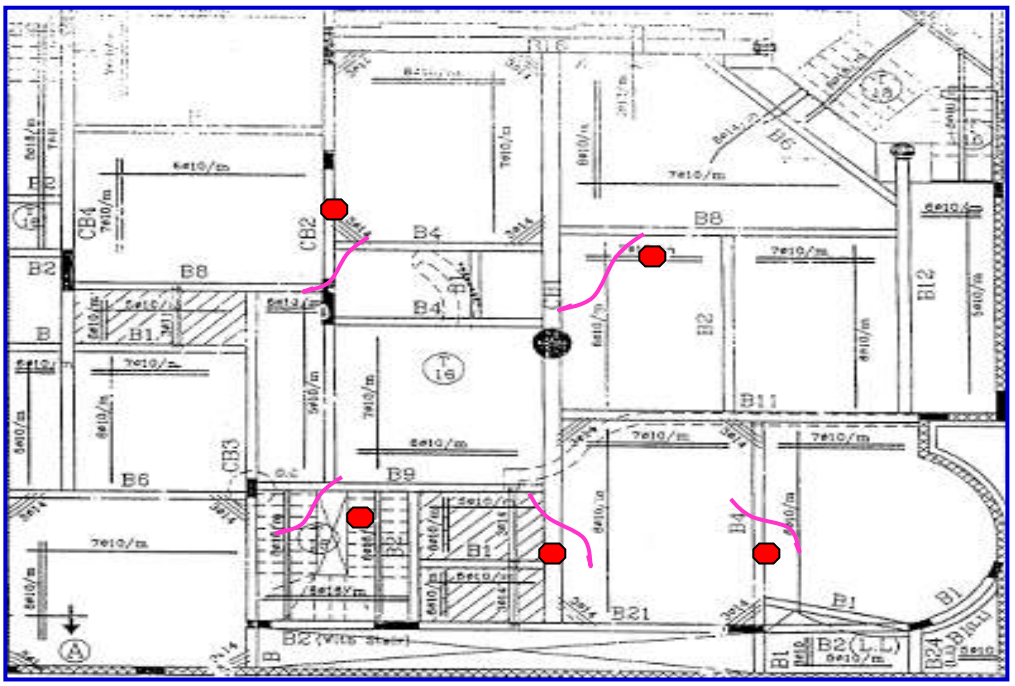

Figure 8 Location of core test & Crack in Slab

4. Concrete compressive strength:

The specifications of the building stipulate that the compressive strength of concrete for the slabs and beams should be not less than 250 kg/cm2 and columns 300 kg/cm2.
The results were 208, 130, 205 kg/cm2 in the beams and 168, 170 kg/cm2 in the slab.

Samples CB3 and GS1 contain bars of reinforcement, which significantly affect the result, and should be taken into consideration when using it in structural analysis. The strength of GB2 beam decreases to 130 kg/cm2, about 52% of the required strength (Table 1,2). The results show that the average strength of the beam and slabs samples is 188 kg/cm2, which is equivalent to 75% of the imposed design strength of 250 kg/cm^2. It is also noted that three samples are less than 75% of the design strength imposed (Table 1, 2,3)

Table 1. Results of core test from INCO-LAB, KWAIT

DETERMINATION OF COMPRESSIVE STRENGTH OF CONCRETE CORE

Method of end preparation by saw Machine & Sulphur capping

Test No.		1	2	3	4
Length Recovered (max)/(min.)	(cm)	18.6/16.0	18.9/16.7	15.5/14.0	18.9/17.9
Identification of Core		CB 5	B 18	CB 6	B 19
Location		Beam			
Direction of Drilling		Horizontal			
Average Diameter	(cm)	9.4	9.4	9.4	9.4
Weight in Air	(gm)	1950.7	2051.3	1839.1	1949
Length after cutting	(cm)	12.4	12.9	11.6	12.6
Length after preparation	(cm)	13.0	13.7	12.2	13.1
Volume of core	(cm^3)	857.41	895.59	805.34	874.76
Density of specimen	(gm/cm^3)	2.275	2.290	2.284	2.228
Length/Diameter ratio		1.383	1.457	1.298	1.394
Factor for estimated in-situ cube strength		1.125	1.144	1.101	1.127
Diameter of the reinforcement	(cm)	N.A.	N.A.	1.1	N.A.
Distance of axis of bar from nearer end	(cm)	N.A.	N.A.	1.3	N.A.
Correction factor for reinforcement		N.A	N.A	1.019	N.A
Sectional area	(cm^2)	69.43	69.43	69.43	69.43
Max. Load at Failure	(kN)	53.6	58.7	69.1	102.2
Measured compressive strength	(Kg/cm^2)	78.75	86.24	101.52	150.15
Estimated in-situ cube strength	(Kg/cm^2)	**88.6**	**98.6**	**113.9**	**169.3**
Estimated in-situ cube strength	(N/mm^2)	**8.7**	**9.7**	**11.2**	**16.6**

CONDITION OF CORES WHEN RECEIVED : (VISUAL EXAMINATION)

Sample No.	1	2	3	4
Cement Appearance	Yes	Yes	Yes	Yes
Max Size of Aggregate	3/4"	3/4"	3/4"	3/4"
Voids	Small	Small	Small	Small
Honeycombs	Nil	Nil	Nil	Nil

Note:- The results of this test represent only for the samples received from client.

TEST COMPLETED : 22.01.2007

Senior Lab. Technician

Material Engineer

Project : Construction of Villa at Bayan Blk# 5, Plt# 352

Owner : Yaqub Mahmood Hussain Shams Al Din

Consultant : Al Hadiya Office

Contractor : Yaqub Mahmood Hussain Shams Al Din

Determination of Compressive Strength of Conc. Core
BS 1881 : Part 120: 1983

INCO - LAB

For Testing: Materials, Soil, Surveying, & Environmental Research

P.O.Box 21073, Safat 13071, Kuwait. Tel (965) 4710780 Fax (965) 4710525

J.O # 0639

Table 2. Results of core test

	Specimen	BC1	GC1	FC-1	GS-2
1	- Identification of the specimen:	Beam			
2	- Location: Axes	CB5	B18	CB6	B19
3	- Average diameter (cm):	9.4	9.4	9.4	9.4
4	- Weight in Air (gm)	1950.7	2051.3	1839.1	1949
5	-Volume of core	857.41	895.59	805.34	874.76
6	- Density of specimen (kg/m2)	2.275	2.290	2.284	2.228
7	-Factor for estimated in situ cube strength	1.1.25	1.144	1.101	1.127
8	- Sectional area (cm2)	69.43	69.43	69.43	69.43
9	- Maximum load of failure (KN)	53.6	58.7	69.1	102.2
10	-Measured compressive strength	78.75	86.24	101.52	150.15
11	-Estimated in-situ cube strength (N/mm^2)	8.7	9.7	11.2	16.6
12	**- Estimated insitu cube strength (kg/cm2)**	**88.6**	**98.6**	**113.9**	**169.3**

Table 1. Results of core test

Tests results indicate that ground roof slab design didn't met the code ACI-318. Also, the concrete mixture test result show weakness in concrete strength, due to failure in water percentage in the mixture. It is necessary to verify the slabs in other ways as a load test (Figure 9).

Table 3. Analysis of core test results

No	-Strength of core test (kg/cm^2)	BC1	GC1	FC-1	GS-2
1	-Strength design value	250			
2	-Min. Computing =0.85* Fc	212.5			
3	-Average Strength	117.6			
4	-Strength Not Less Than0.75*Fc	187.5			
5	-Test Reading (insitu)	88.6	98.6	113.9	169.3
6	-Result	Unverified	Unverified	Unverified	Unverified

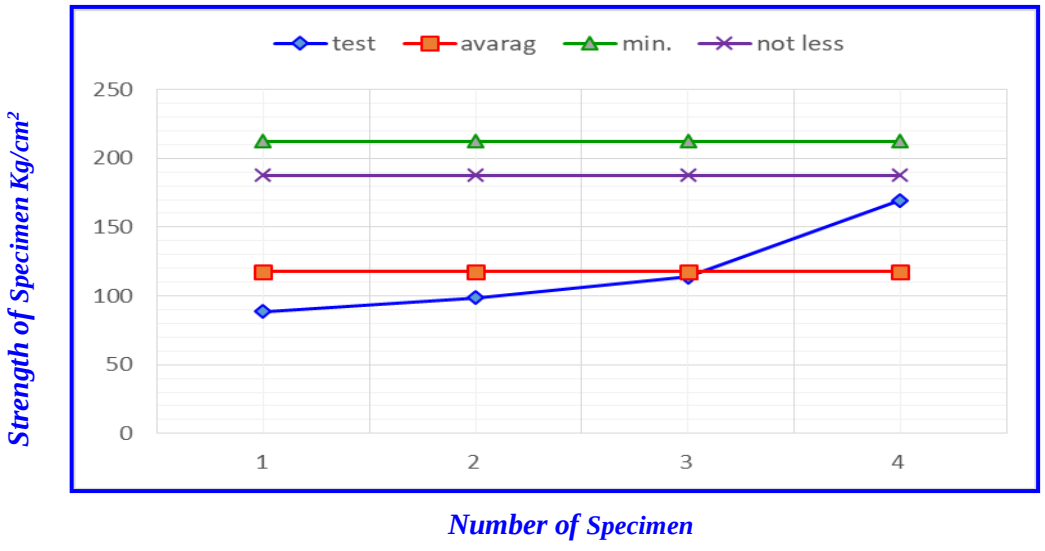

Figure 9 Strength of core test, average, min., not less

5. Study and Analysis:

It is clear from the study that the thickness of the slabs is insufficient as well as the reinforcing steel in both directions. Absence of upper reinforcement steel, resulting in cracks around the slabs and the sides of the beams, as there is no reinforcing in the corners of the slabs causing additional cracks. The reduction of the cross-sectional reinforcing steel in the B11 and the CB5 beam was also shown to be unsafe due to the design and the weakness of the concrete, resulting in clear cracks. It is noted from the design that the slabs are designed as *simple support* and should be designed as *continuous slabs* with the knowledge that the reinforcing steel is properly positioned and properly designed. The upper reinforcing steel was not extended to 22% of the larger beam's length in the adjacent beam, which is failure to follow ACI-318 design code.

6. First case analysis:

The study shows that the structural elements in the building need supporting and strengthening to enable the building to carry out the structural role required to ensure the structural safety required for the building: The repair process should be designed for defective structural elements by a consulting engineering firm specializing in repairs
Beams and slabs in which a landing by a specialized company and engineering supervision should be repaired.

Second Case:

1. General description of the building:

The study was conducted for an existing building (villa) in the Salmiya area. The information and data available are architectural and structural drawings, as well as the results of concrete core tests and load test.
The building consists of a basement, ground, first, second floors, and a roof with two rooms. The building was constructed as the structure shown (Figure 10)

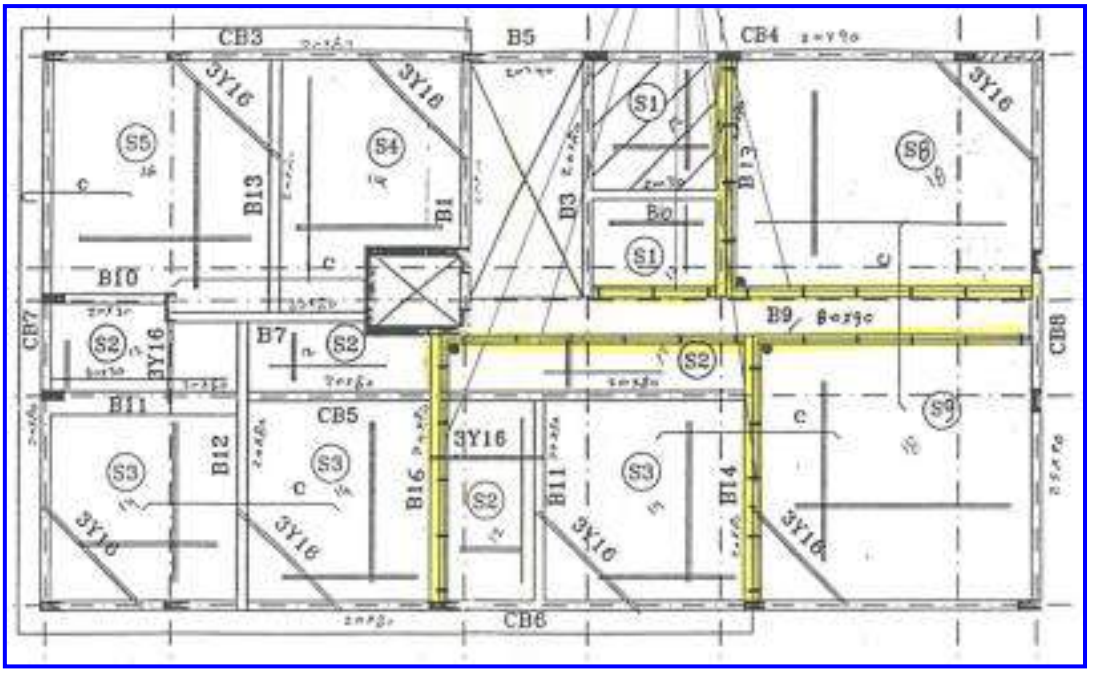

Figure 10 first floor roof slabs plan

Optical inspection results:

From the observation and visual inspection of the building, there are many damages and defects in structural elements:

1.1. Beams:

1.1.1. The air conditioning duct openings are near the beams support points (at the high shear points), causing fractures and cracks in these places. (Figure 11).

1.1.2. The concrete cover of the steel reinforcing of the beams is insufficient as the stirrups steel reinforcing have appeared from the bottom of the beam.

1.1.3. There are cracks around most of the air conditioning duct openings in the beams.

1.1.4. Nesting and voids (honey comb) in concrete

1.1.5. Adhesion the bars of steel reinforcing in some beams, which prevents the passage of concrete, causing a lack of cohesion between concrete and steel

1.1.6. There are inclined in some beams and lack of straightness (Figure 11)

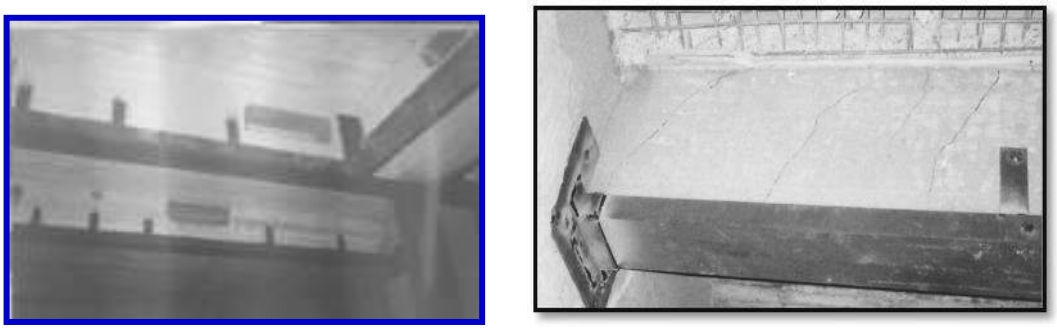

Core Location

Crack in beam

Figure 11 Core Location & Cracks in beams

1.2. Slabs:

1.2.1. The presence of water in many areas in most of the slabs, indicating the presence of cracks and deep fractures on the whole thickness of the slab

1.2.2. There are cracks and cracks up in some places to display 2 mm

1.2.3. There is a large deflection in the floors of the first floor (roof of the ground floor) up to 5 cm in slabs S5, S8 and S9 in addition to the presence of deep and many cracks on the perimeter of the slab sometimes reach the full thickness of the slab (Figure 12)

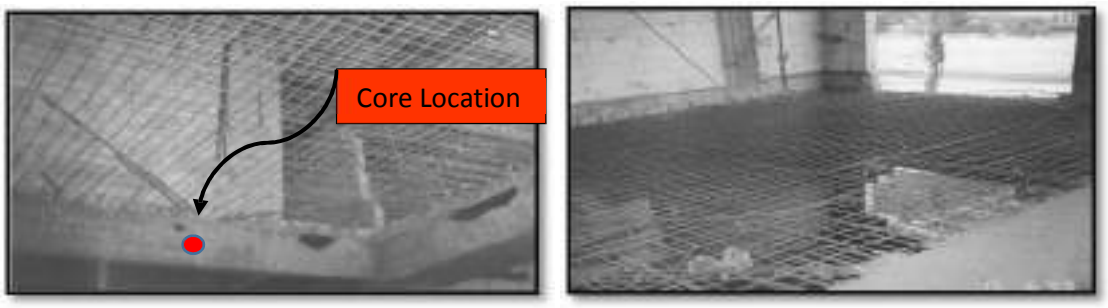

Figure 12 Slabs S9, S8 after demolishing

2. Core test:

10 concrete core test samples were taken from all parts of the building to verify the quality and safety of the concrete in all floors, taking into consideration that they are distributed so that each floor and all structural elements are represented, and the following table shows in Table (4,5)

Table 4. Results of core test from MPW, KWAIT (N/mm^2)

21.2	15.9	الجسر B9 في سقف الدور الأرضي على المحور D	B6	9
21.2	17.5	الجسر B14 في سقف الدور الارضي على المحور 6	B7	10
21.2	18.3	البلاطة S3 في سقف الدور الارضي على المحاور B-C 5-6	S8	11
21.2	17.1	البلاطة S9 في سقف الدور الارضي على المحاور B-D 6-8	S9	12
21.2	16.9	البلاطة S5 في سقف الدور الارضي على المحاور D-F 2-3	S10	13
21.2	22.1	العمود C1 في الدور الاول على المحاور F/5	C11	14
21.2	13.1	العمود C1 في الدور الاول على المحاور D/2	C22	15
21.2	13.3	العمود C5 في الدور الاول على المحاور B/6	C23	16
21.2	22.8	الجسر B9 في سقف الدور الأول على المحور D	B12	17
21.2	17.1	الجسر CB8 في سقف الدور الأول على المحور 8	B13	18
21.2	13.9	البلاطة S8 في سقف الدور الأول بين المحاور D-F 6-8	S14	19
21.2	11.1	البلاطة S5 في سقف الدور الأول بين المحاور D-F 2-3	S15	20

Table 5: results of core test

No.		Location of the specimen	Identification	Number	Cubic Strgh (kg/cm^2)	Result
1	9	Ground slab roof	Beam	B9	187	Unverified
2	10	Ground slab roof	Beam	B14	206	Verified
3	11	Ground slab roof	Slab	S3	215	Verified
4	12	Ground slab roof	Slab	S9	202	Verified
5	13	Ground slab roof	Slab	S5	199	Verified
6	15	First slab roof	column	C11	155	Unverified
7	16	First slab roof	column	C5	156	Unverified
8	18	First slab roof	Slab	S9	201	Verified
9	19	First slab roof	Slab	S8	164	Unverified
10	20	First slab roof	Slab	S5	150	Unverified

2.1. Measuring the actual thickness of the slabs

The actual thickness of the slabs that were taken from the core test specimen was measured and compared with the design thickness. The following (table 6) shows the actual thickness and the thickness of the design:

Table 6. Actual thickness of the slabs

No	specimen	slab	design thickness (cm)	actual thickness (cm)
1	S3	S3	14	15
2	S9	S9	18	13
3	S10	S5	16	13.5
4	S18	S9	18	15
5	S14	S8	18	15
6	S15	S5	16	13.5

2.2. Concrete strength of core tests

According to the data above and to chapter 5.6.5.4. Of ACI-318 specifications conditions for concrete core tests, it can be concluded as following:

2.2.1. In basement, the average concrete strength of the slab is 67.2% of the design value. In some area the concrete strength value as low as 59% of the design value, which considered a failure in the concrete slab.

2.2.2. In ground floor, the average concrete strength of the slab is less than 82% of the design value, which considered a failure in the concrete slab.

2.2.3. In first floor, the average concrete strength for the slab is equivalent 76.4% of the design value. In some area the concrete strength value is 52% of the design value, which considered a failure in the concrete slab. The thickness of roof slabs was measured in the concrete core test samples and compared with the design thickness according to the drawings and it was found 10% less.

2.3. Study and Analysis:

By comparing structural analysis of the core test results with the structural design provided by the Engineering Consulting Office, it can be concluded as following:

2.3.1. Beams: The reinforcement ratio of some beams is greater than the permissible, reinforcement ratio according to ACI-318, which makes the method of failure surprising (Brittle mode of failure) in the case of increasing the stresses of what the structural elements

2.3.2. Slabs: In the ground and first floor the slabs (S5, S8, S9) are unsafe structure. Table (5,7), Figure 13

Table 7. Analysis of results core test

	specimen	B9	B14	S3	S9	S5	C11	C5	S9	S8	S5
1	Strength design value	250									
2	Min. Computing =0.85* Fc	212.5									
3	Average Strength	183.5									
4	Strength Not Less Than0.75*Fc	187.5									
5	Test Reading (in-situ)	187	206	215	202	199	155	156	201	164	150
	Result	Unver	Verifie	Verifi	Verifi	Verifi	Unver	Unver	Verifie	Unver	Unver

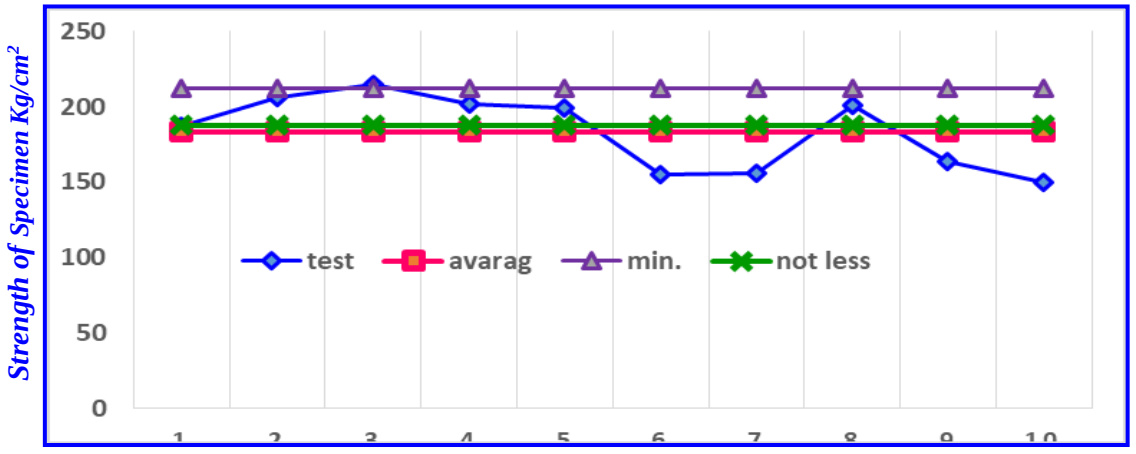

Figure 13 Strength of core test, average, min., not less

3. Load Test:

3.1. Testing Procedure:

The next section shows the conceptual steps followed to:

- Determine the value of the total test load magnitude during a preparatory phase.
- Obtain the continuous structural assessment, during the load test performance.
- Obtain the real-time calibration of the test load according to the continuous assessment of the boundary conditions through the measurement of selected structural parameters.

3.1.1. Applying load Intensity test levels as recommended in Chapter 20 of ACI-318

3.1.2. Applying Load Test Protocols as recommended ACI standard, two variables are considered for the principle evaluation:

- Dead load effect.
- Live load effect.

Total load (weight) applied on the tested deck slab calculated as recommended in ACI- 318/318R [17], [18].

The Value test load shall be calculated as follow

Test load W = 0.85 x (1.4 D + 1.7 x L) (1)

3.1.3. Load Configuration

The load was distributed uniformly on the three floor slabs, measurement came the exact as in load testing resulting from factored uniformly-distributed load, in terms of negative moment.

The ACI requirements and standards for the structural using condition must be considered and limited by two variables that are [16],[17],[18]:

- Maximum Deflection and.
- Rebound Deflection or Residual Deflection.

According to ACI 318/318R, the maximum deflection and the rebound deflection are

$$\Delta \text{ max} \leq L2 / 20000\ h \quad (2)$$

$$\Delta \text{ rebound} \leq \Delta \text{ max} / 4 \quad (3)$$

Where: $\Delta\ max$ is the maximum deflection

$\Delta\ rebound$ is the rebound deflection or Residual Deflection

L is *length of slab* on the short side, and h is thickness of slab

3.1.4. Load Testing Procedure

- Dial gauges with magnetic base, installs into the slab structure in several points, where dial gage no.3 (G1) is installed at the middle of the slab. (Figure 13).
- Initial deflections, and temperature prior the testing should be recorded.
- Load should be increased gradually (0% - 25% - 50% - 75% - 100%) of the maximum load, while each load stage held for 1 hour, and for the maximum load (100%) it should held for 24 hours.
- After 24 hours, load is decreased gradually (100%- 75%- 50%- 25% - 0%)
- each released stage is held for 1 hour, and after releasing all load it must held for 24 hours.

The load test for the roof slabs and beams results as follows Figure 14 and Table 8:

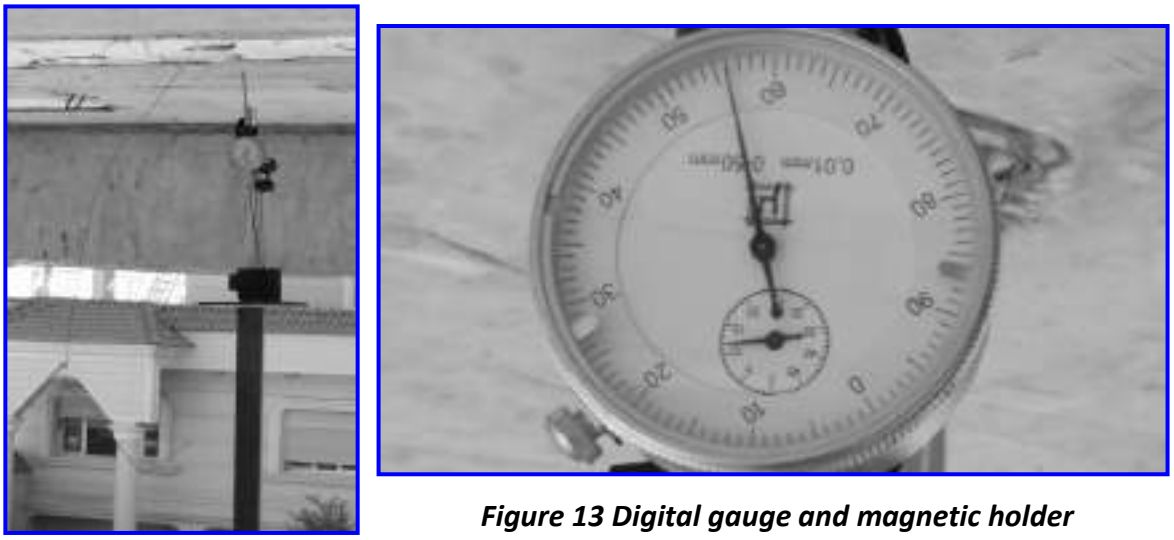

Figure 13 Digital gauge and magnetic holder

(The load test was carried out by the Government Inspection Center of the Ministry of Public Works-Kuwait)

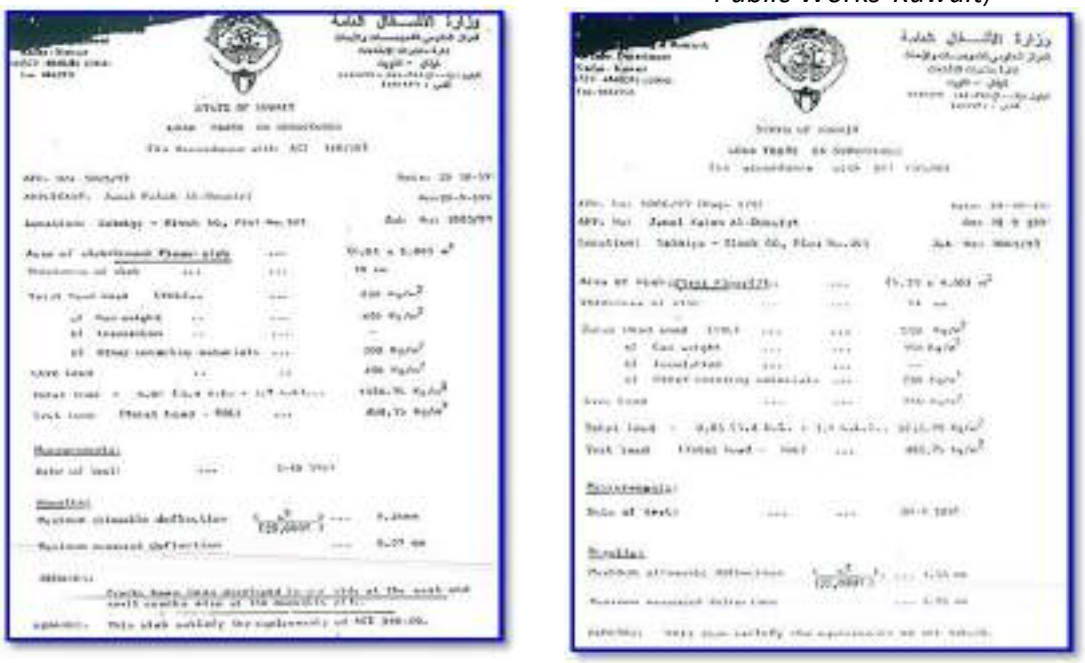

Figure 14 Ministry of Public work inspection reports

Table 8. Analysis of load test results

No	Statement	Slab1	Slab2	Slab3
1	Identification of the specimen &Location	S5	S8	S9
2	Dimensions (m):	6.05*5.80	5.25*4.60	4.50*4.00
3	Thickness (cm) :	18	14	14
4	Dead Load :1) Own Weight (Kg/m^2)	450	350	350
5	2)Covering Load (Finishing) (Kg/m^2)	200		
6	Total Dead Load (TDL) (Kg/m^2)	650	550	550
7	Live Load (Kg/m^2)	250		
8	Total Load (Kg/m^2) = 0.85 x (1.4 D. L + 1.7 L.L)	1134.75	1015.75	1015.75
9	Test Load =Total Load – TDL (Kg/m^2)	484.75	465.75	465.75
10	**Max. Allowable Deflection =L^2/20000*T(mm)**	**9.34**	**5.7**	**7.56**
11	**Max. Measured Deflection (mm)**	***8.27***	***5.05***	***6.95***
12	***Remarks: This slab as Requirement of ACI-318***	***Satisfy***	***Satisfy***	***Satisfy***

After the test, cracks have been developed in one side and smaller one at opposite side. Deflection values that occurred after the tests was acceptable according to the ACI-318 code. The ratio of the existing reinforcing steel is greater than the maximum percentage, it indicates that the concrete strength will reach its maximum value before the steel reaches to the yield point.

4. Second Case Identification of damage causes:

According to drawing design, and core test and load test analysis for the concrete, with reference to the nature of the damage and its shape. Damage causes can be summarized as follows:

4.1. Concrete is Non-conforming to the required specifications in the roof slabs.

4.2. Poor roofs slabs implementation, where thickness of many slabs does not match the drawings, causing distortions and large cracks in slabs.

4.3. Poor installation of steel bars, where the required distances between the bars were not considered, which led to a weak link between the concrete and steel, where voids occurred in concrete.

4.4. Lack of sufficient concrete cover for many structural elements

4.5. Un satisfactory fitting of air-conditioning openings, especially in the high cut points of beams.

5. Methods of treatment and repair:

5.1. Due to the weak of concrete and many cracks in the slabs of the ground and first roof, it must be demolished and re-poured, with proper reinforcement procedures that extend to adjacent slabs.

5.2. Strengthening the identified beams, using appropriate steel section, and strong adhesive materials like (epoxy materials).

5.3. Reinforcing the defected columns with appropriate steel sections.

5.4. Apply epoxy layer to the old concrete faces where they are bonded with the new concrete before casting directly [15].

6. Conclusions and Recommendations:

This paper presented methods to evaluate Structural Strength, using Load and Core Tests, it also present methods to analysis the Causes of Structural Strength failure: based on the results obtained from the tests, site investigation, and structural design drawing. For the two vacant villas, structure strength tests were conducted, and data has been analysis. As a result, Core test and the load test in-situ prove that the ACI-318 code gives logical results and expressive status, for structural component strengths. The causes of weak slabs and beams resulted from weak of design and defect in implementation. The tests showed that the concrete slabs were more elastic as the recovery deflection was relatively large compared to the initial deflection. quality control and weak audit of these designs. Failure to fulfill the requirements and specifications of the international codes and feeble monitoring, neglection to apply technical conditions, and weak Supervision on the construction site, was the main causes to failure in the structure.

In the first building (Bayan), beams should be supported by steel beams to support the structure to withstand the loads. Cracks should be repaired by epoxy products. The second building (Salmiyah), slabs (S5, S8, S9) should be demolished and recasting concrete accordance to ACI-318 specifications.

References

[1]. Tuncan, M., et al., *Assessing concrete strength by means of small diameter cores.* Construction and Building Materials, 2008. **22**(5): p. 981-988.

[2]. ASTM, C., *42/C 42M-90.* Test for obtaining and testing drilled cores and sawed beams of concrete, Annual Book of ASTM Standards, 2008.

[3]. Nikbin, I., M. Eslami, and D. Rezvani, *An experimental comparative survey on the interpretation of concrete core strength results.* Eur J Sci Res, 2009. **37**(3): p. 445-456.

[4]. Gibbs, J. and W. Zhu. *Strength of hardened self-compacting concrete*. in *Proceedings of First international RILEM Symposium on Self-Compacting Concrete (PRO 7), Stockholm, Suede*. 1999.

[5]. Khoury, S., A.A.-H. Aliabdo, and A. Ghazy, *Reliability of core test–Critical assessment and proposed new approach.* Alexandria Engineering Journal, 2014. **53**(1): p. 169-184.

[6]. Friedman, D., *Historical building construction: design, materials, and technology*. 2010: WW Norton & Company.

[7]. Galati, N., et al., *In-situ evaluation of two concrete slab systems. I: Load determination and loading procedure.* Journal of Performance of Constructed Facilities, 2008. **22**(4): p. 207-216.

[8]. Goble, G.G., *Geotechnical related development and implementation of load and resistance factor design (LRFD) methods*. Vol. 276. 1999: Transportation Research Board.

[9]. Galati, N. and T. Alkhrdaji, *In Situ Evaluation of Structures Using Load Testing*, in *Forensic Engineering 2009: Pathology of the Built Environment*. 2010. p. 657-667.

[10]. Mettemeyer, M. and A. Nanni, *CENTER FOR INFRASTRUCTURE ENGINEERING STUDIES.*

[11]. Luping, T. and L.-O. Nilsson, *Rapid determination of the chloride diffusivity in concrete by applying an electric field.* Materials Journal, 1993. **89**(1): p. 49-53.

[12]. Ridge, A.R. and P.H. Ziehl, *Evaluation of strengthened reinforced concrete beams: cyclic load test and acoustic emission methods.* ACI Structural Journal, 2006. **103**(6): p. 832.

[13]. Abdulahad, E., *Developing a national system for the investigation of the structures* in *Symposium of the Bulgarian construction chamber Bulgaria*. 2014: Sofia ,Bulgaria

[14]. Illidge, F.A.B., *Acoustic emission techniques and cyclic load testing for integrity evaluation of self-compacting normal and self-compacting lightweight prestressed concrete girders*. 2010, University of South Carolina.

[15]. Abdulahad, E., *Essence and issues affecting the operation of the National Service of operational reliability*, in *Symposium of the Bulgarian construction chamber Bulgaria* 2014: Sofia Bulgaria

[16]. Committee, A., A.C. Institute, and I.O.f. Standardization. *Building code requirements for structural concrete (ACI 318-08) and commentary*. 2008. American Concrete Institute.

[17]. Committee, A., *Building code requirements for structural concrete (ACI 318-14) and commentary.* ACI, Farmington Hills, United States, 2014.

[18]. ACI Committee 318, American Concrete Institute, , *Building Code Requirements for Structural Concrete and Commentary, (ACI 318-95)*. 1995,

Membership function based on similarity and dissimilarity

E.Elsodany [1] and A.M.Kozae [2]

[1] Department of Physics and Engineering Mathematics, Faculty of Engineering, Tanta University, Tanta, Egypt
[2] Department of Mathematics, Faculty of Science, Tanta University, Tanta, Egypt

Abstract

Deciding membership function of an object to uncertain class of objects in an information system is essential particularly, all things considered, displaying issues. This paper will present a comparison between different ways of constructing membership function of an object. We initiate a concept based on dissimilarity and similarity between objects using values of their features. The fundamental tool is classes resulted from dissimilarity and similarity. We will also express a classification relation and minimum and maximum memberships correspond to these classifications.

Keywords: rough membership, dissimilarity measures and similarity.

1. Introduction

Organizations need information to analyze problems, control their work, make decisions and produce new services. The information system handles and processes information which can be considered the backbone of organizations. Information systems are in every branch of our daily life such as education, finance, healthcare, businesses, and government. A tool to deal with the uncertainty of these systems became an utmost necessity. Rough set theory was presented by Pawlak [1-3] in 1980's to deal with uncertain data or incomplete knowledge. Rough sets handled the uncertainty of data depending on approximations and equivalence relations. Another issue of classification is clustering which has many methods and the more similar objects in the same cluster than the dissimilar objects in a different cluster under a specific condition. The nature of collected data determines the measuring criteria of similarity. Algorithms of quantitative and qualitative data, graph diagrams, and similarity and dissimilarity measures were presented [4-7]. Membership of an object to a set is an important issue to identify participation of each object in this set. Membership was discussed [8] from a topological view which was extended from the definition of rough membership function[9].Topological space has an intersection between basis but rough set classes have no intersection. [10] discussed the opinion of classes intersection in rough set and introduced a membership of an object to a class. In this case, an object can belong to more than one class, so it has different memberships minimum, maximum and average. From this point of view, we will introduce a membership function of an object to a set depending on the dissimilarity measures and similarity between objects. We will also define relations or classes then determine the membership of an object to a set. Comparison between minimum, maximum and membership of topological view will be mentioned. The decision of most, least membership value can be chosen by the expert.

The next sections of this paper is developed to preliminaries used in the paper, section two presents main definitions, results and examples. Section three is reserved for the more results and illustrations.

2. Preliminaries

In this section, we will mention some essential basics and definitions of rough set and information system representation. The dissimilarity and similarity between attributes of objects esteem are presented. Likewise, the membership of rough set and topology is also mentioned.

Definition 2.1 [1]

The information system is a pair $S = (U, A)$, where U is a nonempty finite set called the universe and A is a nonempty finite set of attributes. Every attribute $a \in A$ is a total function $a: U \to V_a$, where V_a is the set of values of a called the domain of a.

Definition 2.2 [1]

Let B be a subset of attributes A ($B \subset A$) , a binary relation $IND(B)$ called indiscernibility relation is defined as follows:

$$IND(B) = \{(x, y) \in U^2 : \forall\, a \in B, a(x) = a(y)\}$$

So $IND(B)$is an equivalence relation and $IND(B) = \bigcap_{a \in B} IND(a)$

This view classify the objects depends on the equal features between objects as a result of this there is no intersection between relations.

Definition 2.3[7]

Let an information system $S = (U, A)$ and two objects $x, y \in U$ described by a_k attributes subset of . Mismatches of the attributes between two objects are the dissimilarity measures which is defined as

$$d(x, y) = \sum_{i=1}^{k} \delta(a_i(x), a_i(y))$$

Where

$$\delta(a_i(x), a_i(y)) = \begin{cases} 0 : a_i(x) = a_i(y) \\ 1 : a_i(x) \neq a_i(y) \end{cases}$$

This can be considered as another view of an information system classification. The produced classes are relations of dissimilarity between objects. The similarity between objects is the opposite way of dissimilarity or simply the number of matches between two objects.

Definition 2.4 [9]

Let $S = (U, A)$ be an information system and let $\emptyset \neq X \subset U$. The rough S-membership function of the set X, denoted by μ_X^S is defined as follows

$$\mu_X^S(x) = \frac{|[x]_A \cap X|}{|[x]_A|} \text{ for } x \in U$$

Definition 2.5 [8]

Let τ be a topology on a finite set U, where its base is β,then the rough membership function is

$$\mu_X^\tau(x) = \frac{|\{\cap\beta_x\} \cap X|}{|\cap\beta_x|} \ , \ \beta_x \in \beta \ , x \in U$$

We will call this definition rough-topology membership function in the following section.

3. Results

In this section, we will illustrate the previous definitions and introduce a comparison between membership views. We will also work on the resulted relations of the dissimilarity and similarity relations.

Definition 3.1

Let an information system $S = (U, A)$ and two objects $x, y \in U$ are described by a_k attributes subset of . The matches of the attributes between two objects is the similarity between objects which is defined as

$$s(x, y) = \sum_{i=1}^{k} \lambda(a_i(x), a_i(y))$$

Where

$$\lambda(a_i(x), a_i(y)) = \begin{cases} 0 : \ a_i(x) \neq a_i(y) \\ 1 : \ a_i(x) = a_i(y) \end{cases}$$

Definition 3.2

Let $S = (U, A)$ be an information system, x_i and x_j subset of objects and $x_i \ R \ x_j$ represents the relation between them which is resulted from the dissimilarity measures and similarity representation can be defined as

$$x_i \ R = \{x_j : x_i \ R \ x_j\} \text{ where } d(x_i, x_j) \neq 0 \text{ and } s(x_i, x_j) \neq 0$$

These relations are considered a classification of objects with respect to dissimilarity and similarity between objects. We will use these classes instead of the classical classes of an indiscernibility relation.

Example 3.1

The following information system in Table 1 consists of 5-objects $\{x_1, x_2, x_3, x_4, x_5\}$ and 3-attributes $\{a_1, a_2, a_3\}$.

U	attributes		
	a_1	a_2	a_3
x_1	1	5	20
x_2	1	9	10
x_3	1	5	10
x_4	4	8	15
x_5	3	5	20

Table 1 an information system

	x_1	x_2	x_3	x_4	x_5
x_1	0	2	1	3	1
x_2	2	0	1	3	3
x_3	1	1	0	3	2
x_4	3	3	3	0	3
x_5	1	3	2	3	0

Table 2 dissimilarity measures representation

Table 2 represents the dissimilarity measures of an information system of Table 1 and we apply Definition 2.3. This table represents the number of different attributes which can be considered dissimilarity representation of an information system. Each value in this table represents the number of the corresponding attributes of objects are far away from each others. Each value of Table 2 takes 4-values 0,1,2 and 3 because we have only 3-attributes. The value 0 means the corresponding 2-objects have an identical value for all attributes. The value 1 means only 1-mismatch attribute between the 2-objects. The value 2 means 2-mismatches between attributes but, value 3 means there is no match at all between objects.

It's obvious that similarity between objects is the complement of dissimilarity measures. Similarity can be obtained using Definition 3.1 to take 1 if the two objects have the same value and vice versa.

	x_1	x_2	x_3	x_4	x_5
x_1	3	1	2	0	2
x_2	1	3	2	0	0
x_3	2	2	3	0	1
x_4	0	0	0	3	0
x_5	2	0	1	0	3

Table 3 similarity representation

Table 3 shown represents the similarities between objects of table 1. We can observe that this table is the opposite of Table 2. The number of matches between objects is calculated instead of the number of mismatches. So the value 3 means the two objects are identical, but value 0 means there are no matches between objects. The value 1 and 2 mean there is one-match and two-match between objects, respectively.

The resulting classes of Table 2 using Definition 3.2 are

$x_1\ R = \{x_2, x_3, x_4, x_5\}, x_2\ R = \{x_1, x_3, x_4, x_5\}, x_3\ R = \{x_1, x_2, x_4, x_5\}$

$x_4\ R = \{x_1, x_2, x_3, x_4\},\ x_5\ R = \{x_1, x_2, x_3, x_4\}$

And classes of Table 3 are

$x_1\ R = \{x_1, x_2, x_3, x_5\}, x_2\ R = \{x_1, x_2, x_5\}, x_3\ R = \{x_1, x_2, x_3, x_5\}$

$x_4\ R = \{x_4\}, x_5\ R = \{x_1, x_3, x_5\}$

We also observed the intersection between classes of dissimilarity and similarity alike classes of an indiscernibility relation.

Membership function is an important concept which identifies the participation of an object with respect to a set. From the above relations, we can observe that an object participates in more than one class so it can have more than one membership value with respect to the class. In the following, we will calculate rough membership of Definition 2.4 according to the classes of dissimilarity and similarity representation, respectively.

To calculate the membership, we should choose a set X so we will choose random sets, then we will apply Definition 2.4.

Case 1: $\boldsymbol{X = \{x_1, x_2\}}$

objects	$\mu_X^S(x_i)$ with respect to $x_i\ R$				
	$x_1\ R$	$x_2\ R$	$x_3\ R$	$x_4\ R$	$x_5\ R$
x_1	–	$\frac{1}{4}$	$\frac{1}{2}$	$\frac{1}{2}$	$\frac{1}{2}$
x_2	$\frac{1}{4}$	–	$\frac{1}{2}$	$\frac{1}{2}$	$\frac{1}{2}$
x_3	$\frac{1}{4}$	$\frac{1}{4}$	–	$\frac{1}{2}$	$\frac{1}{2}$
x_4	$\frac{1}{4}$	$\frac{1}{4}$	$\frac{1}{2}$	–	$\frac{1}{2}$
x_5	$\frac{1}{4}$	$\frac{1}{4}$	$\frac{1}{2}$	$\frac{1}{2}$	–

Table 4 membership of case 1 dissimilarity representation

Case 2: $\boldsymbol{X = \{x_1, x_2, x_3\}}$

objects	$\mu_X^S(x_i)$ with respect to x_i R				
	x_1 R	x_2 R	x_3 R	x_4 R	x_5 R
x_1	–	$\frac{1}{2}$	$\frac{1}{2}$	$\frac{3}{4}$	$\frac{3}{4}$
x_2	$\frac{1}{2}$	–	$\frac{1}{2}$	$\frac{3}{4}$	$\frac{3}{4}$
x_3	$\frac{1}{2}$	$\frac{1}{2}$	–	$\frac{3}{4}$	$\frac{3}{4}$
x_4	$\frac{1}{2}$	$\frac{1}{2}$	$\frac{1}{2}$	–	$\frac{3}{4}$
x_5	$\frac{1}{2}$	$\frac{1}{2}$	$\frac{1}{2}$	$\frac{3}{4}$	–

Table 5 membership of case 2 dissimilarity representation

Case 3: $\boldsymbol{X = \{x_1, x_2, x_3, x_4\}}$

objects	$\mu_X^S(x_i)$ with respect to x_i R				
	x_1 R	x_2 R	x_3 R	x_4 R	x_5 R
x_1	–	$\frac{3}{4}$	$\frac{3}{4}$	$\frac{3}{4}$	1
x_2	$\frac{3}{4}$	–	$\frac{3}{4}$	$\frac{3}{4}$	1
x_3	$\frac{3}{4}$	$\frac{3}{4}$	–	$\frac{3}{4}$	1
x_4	$\frac{3}{4}$	$\frac{3}{4}$	$\frac{3}{4}$	–	1
x_5	$\frac{3}{4}$	$\frac{3}{4}$	$\frac{3}{4}$	$\frac{3}{4}$	–

Table 6 membership of case 3 dissimilarity representation

From Table 4 to Table 6, we can say that each object has a membership to X with respect to the corresponding x_i R which contains the object. And membership value of all objects belongs to x_i R with respect to X are equal. We need to have only one membership value of an object so we can choose minimum or maximum membership. In the following, we will apply Definition 2.5 in each case and compare the result with our previous results considering the minimum and maximum membership.

objects	Rough membership		Rough-topology membership
	Min	Max	
x_1	$\frac{1}{4}$	$\frac{1}{2}$	1
x_2	$\frac{1}{4}$	$\frac{1}{2}$	1

x_3	$\frac{1}{4}$	$\frac{1}{2}$	0
x_4	$\frac{1}{4}$	$\frac{1}{2}$	0
x_5	$\frac{1}{4}$	$\frac{1}{2}$	0

Table 7 dissimilarity representation membership comparison of case 1

objects	Rough membership		Rough-topology membership
	Min	Max	
x_1	$\frac{1}{2}$	$\frac{3}{4}$	1
x_2	$\frac{1}{2}$	$\frac{3}{4}$	1
x_3	$\frac{1}{2}$	$\frac{3}{4}$	1
x_4	$\frac{1}{2}$	$\frac{3}{4}$	0
x_5	$\frac{1}{2}$	$\frac{3}{4}$	0

Table 8 dissimilarity representation membership comparison of case 2

objects	Rough membership		Rough-topology membership
	Min	Max	
x_1	$\frac{3}{4}$	1	1
x_2	$\frac{3}{4}$	1	1
x_3	$\frac{3}{4}$	1	1
x_4	$\frac{3}{4}$	1	1
x_5	$\frac{3}{4}$	1	0

Table 9 dissimilarity representation membership comparison of case 3

From Table 7 to Table 9 we illustrate the comparison in each case and topological view of classes taking into account the intersection between them. But in our case resulting classes only intersect on one object. As a result of this, the membership is 1 and 0 according to the object belongs or not belongs to X, respectively. This makes the membership like the case of the classical crisp set. In some cases the maximum rough membership value equal to the topological rough membership value. This gives a chance to choose between more than membership value according to the problem we have.

In the following, we will also make a comparison of each case, but we will take into account similarity between objects and their corresponding classes. Tables will consider

the resulting minimum and maximum of rough membership then we will compare them with the topological view of rough membership.

objects	Rough membership		Rough-topology membership
	Min	Max	
x_1	$\frac{1}{3}$	$\frac{1}{2}$	$\frac{1}{2}$
x_2	$\frac{1}{3}$	$\frac{1}{2}$	$\frac{2}{3}$
x_3	$\frac{1}{3}$	$\frac{1}{2}$	$\frac{1}{3}$
x_4	0	0	0
x_5	$\frac{1}{3}$	$\frac{1}{2}$	$\frac{1}{2}$

Table 10 similarity representation membership comparison of case 1

objects	Rough membership		Rough-topology membership
	Min	Max	
x_1	$\frac{2}{3}$	$\frac{3}{4}$	$\frac{1}{2}$
x_2	$\frac{2}{3}$	$\frac{3}{4}$	$\frac{2}{3}$
x_3	$\frac{2}{3}$	$\frac{3}{4}$	$\frac{2}{3}$
x_4	0	0	0
x_5	$\frac{2}{3}$	$\frac{3}{4}$	$\frac{1}{2}$

Table 11 similarity representation membership comparison of case 2

objects	Rough membership		Rough-topology membership
	Min	Max	
x_1	$\frac{1}{2}$	$\frac{3}{4}$	$\frac{1}{2}$
x_2	$\frac{1}{3}$	$\frac{2}{3}$	$\frac{2}{3}$
x_3	$\frac{1}{2}$	$\frac{3}{4}$	$\frac{2}{3}$
x_4	1	1	1
x_5	$\frac{1}{2}$	$\frac{3}{4}$	$\frac{1}{2}$

Table 12 similarity representation membership comparison of case 3

We can conclude from the above comparison that in some cases, there is a match among minimum or maximum membership and topological membership values. In other cases, the value of topological membership is 0 but minimum and maximum values are not and

the opposite is true. This gives us a variety of choice and we can take a decision according to our desire.

Conclusion

The proposed strategy for developing another view of membership function based on dissimilarity and similarity can help in decision making of uncertain issues. This view is constantly hard to be developed so our technique can take care of new issues of areas in social, financial aspects, arithmetic, and so on.

References

[1] Z. Pawlak, "Rough sets," *International Journal of Computer & Information Sciences*, vol. 11, pp. 341-356, 1982.

[2] Z. Pawlak, *Rough Sets: Theoretical Aspects of Reasoning about Data*: Kluwer Academic Publishers, 1992.

[3] Z. Pawlak and W. Marek, "Rough sets and information systems," *ICS. PAS. Reports*, vol. 441, pp. 481-485, 1981.

[4] T. Alharthi and M. Elsafty, "Discovery of Similarity and Dissimilarity," *Journal of Mathematics Research*, vol. 8, p. 105, 2016.

[5] S. Coppock and L. Mazlack, "Rough sets used in the measurement of similarity of mixed mode data," in *Fuzzy Information Processing Society, 2003. NAFIPS 2003. 22nd International Conference of the North American*, 2003, pp. 197-201.

[6] J. Han, J. Pei, and M. Kamber, *Data mining: concepts and techniques*: Elsevier, 2011.

[7] Z. Huang, "A fast clustering algorithm to cluster very large categorical data sets in data mining," *DMKD*, vol. 3, pp. 34-39, 1997.

[8] E. F. Lashin, A. M. Kozae, A. A. A. Khadra, and T. Medhat, "Rough set theory for topological spaces," *Int. J. Approx. Reasoning*, vol. 40, pp. 35-43, 2005.

[9] Z. Pawlak and A. Skowron, "Rough membership functions," in *Advances in the Dempster-Shafer theory of evidence*, 1994, pp. 251-271.

[10] Y. Yao and J. Zhang, "Interpreting fuzzy membership functions in the theory of rough sets," in *International Conference on Rough Sets and Current Trends in Computing*, 2000, pp. 82-89.

Removing of Toxic Cr (VI) Ions from wastewater using different adsorbents.

A.M. Ahmed[1], Ahmed A. ABD EL-KHALEK[2], Mona A. Derweesh[3*] and Eman M. yousef[2].

1- Alex. University, Faculty of Science.

2- Beni-Suef University, Faculty of Science.

3- Tanta University, Faculty of Engineering.

* Corresponding author E-mail: mona_ahmed_dar2006@yahoo.com

A B S T R A C T

The removal of hexavalent chromium from wastewater on the Na-bentonite and activated carbon has been studied under static conditions. Experiments were carried out as a function of solution pH, dosage of Na-bentonite and activated carbon contact time, agitation speed and temperature. The adsorption equilibrium for hexavalent chromium on to Na-bentonite is reached in 120 min. the adsorption of hexavalent chromium is pH dependent in the pH range 1-4, the kinetic process of adsorption can be described by the pseudo-second order kinetic equation excellently and the adsorption isotherm be fitted to the langmuir and freundlich model by means of regression analyses very well. Finally it can be seen that Na-bentonite was favorite to be effective for removal of hexavalent chromium than activated carbon under the same experimental conditions.

Keywords

Na-bentonite; Hexavalent Chromium; Adsorption; Isotherm; Kinetics

1.INTRODUCTION

Industrial wastewater contaminated with heavy metal is commonly produced from many kinds of industrial processes there for, is this wastewater is not treated with a suitable process; it can cause a serious environmental problem in the natural eco-system [1, 2]. Tannery effluent is a major source of aquatic pollution in Egypt with high hexavalent chromium [3]. Water of high quality is essential to human life and of acceptable quality is essential for agriculture, industrial, domestic and commercial uses. All this activities are also responsible for polluting the water. Billions of gallons of waste from all this sources are thrown to fresh water bodies everyday [4].

The requirement for water is increasing while slowly all the water resources are becoming unfit for use due to improper waste disposal [5]. The task of providing proper treatment facility for all polluting sources is difficult and also expensive; hence there is pressing demand for innovative technologies which are low cost, require low mentainence and are energy efficient [6]. The adsorption technique is economically

favorable and technically easy to separate as the requirements of the control system is minimum [7].

Hexavalent chromium Cr (VI) compounds are being used in a wide variety of commercial processes and unregulated disposal of the chromium containing effluents has led to the contamination of soil, sediment, surface and ground waters. In trace amounts, chromium is considered an essential nutrient for numerous organisms, but at higher level, it is toxic and mutagenic. nearly80% of the tanneries is engaged in the chrome tanning processes. Most of them discharge untreated water into the environment. In such aqueous waste, Cr (VI) is present as either dichromate $(Cr_2O_7)^{-2}$ in acidic environments or as chromate $(CrO_4)^{-1}$ in alkaline environments. Chromium compounds were employed in textile coloring and leather tanning processes. The principle chromium emissions into surface waters are from metal finishing processes such as electro- plating, pickling and bright dipping [8].

Pollution of soils occurs as result of the dumping of chromate wastes such as those from tanniers or electroplating and from sewage sludge disposal on land [9]. Uncontrolled emissions have greater potential for contaminating the fresh waters with relatively toxic from Cr (VI) , which exists only as oxy species and is strongly oxidizing other small discharges of Cr (VI) are from the additive in circulating waters, Landry chemicals [10].

In this article, the technical feasibility of low cost (adsorption), and locally available adsorbents bentonite and activated carbon for heavy metal removal Cr (VI) ion, from contaminated water has been reviewed. This work is intended to remove Cr (VI) from aqueous solutions on to bentonite and activated carbon as an effective and low cost.

In the present investigation, to estimate the amount of chromium ions present in its aqueous solutions after treatment and the removal of chromium from wastewater using bentonite and activated carbon as an adsorbents are attempted.

The present work is also aimed at fixing the optimal conditions such as pH, equilibrium time (for batch mode technique), dosages of adsorbent and initial concentration on the adsorption efficiency of Cr (VI) ion from wastewater by bentonite and activated carbon besides for effective removal of chromium; To evaluate the equilibrium of adsorption process using Langmuir and freundlich isotherms. Meanwhile, the kinetics of Cr (VI) ion adsorption on bentonite and activated carbon also analyzed using pseudo-second order kinetic models[11].

2. MATERIALS AND METHODS

2.1. MATERIALS AND REAGENTS

All chemicals used in the present investigation were either of analytical reagent (AR) or laboratory reagent (LR) grade and were used as received. $K_2Cr_2O_7$, H_2SO_4 (98% w/w) supplied by BDH chemicals Ltd. Distilled water was used in all preparations. Potassium dichromate ($K_2Cr_2O_7$) with 99% purity and deionized water were used to prepare synthetic chromium containing wastewater. Powder activated carbon (PAC) produced from natural origin by ADWIC was used as adsorbent as well as American Wyoming calcium bentonite used in Alexandria Company for Refractories.

2.2 ADSORBENTS ANALYSIS

Two different materials were used in order to examine the removal of Cr^{+6} from aqueous solutions. Powder activated carbon (PAC) and bentonite (clay) were supplied from ADWIC and Alexandria Company for Refractories, respectively. The surface area and particle size analyses for the two adsorbents were checked (Table 1). Elemental analysis for bentonite was evaluated using x-ray fluorescence (Philips PW 1390) as shown in (Table 2).

Table 1. Surface area and particles size analysis of activated carbon and bentonite.

Adsorbents / **Analysis**	**Activated Carbon**		**Bentonite**	
Surface Area (BET) Nova 2000 Quantachrome	931.9 m^2/g		119.8 m^2/g (dry)	
	Size	Wt. %	Size	Wt. %
Particle size (XRD)	(micrometer)	2.75	(micrometer)	1
Philips PW 1730	32-16	55.89	>63	1
	16-8	16.03	63-32	2
	8-4	4.19	32-16	3
	<2		16-8	2
			8-4	4
			4-2	87
			< 2	

Table 2. Elemental analysis for bentonite was evaluated using x-ray fluorescence (Philips PW 1390).

Oxides (wt.%)	Bentonite
SiO_2 (%)	55.89
Al_2O_3 (%)	16.03
Fe_2O_3 (%)	4.19
CaO (%)	3.25
MgO (%)	2.75
K_2O (%)	0.49
Na_2O (%)	0.34
TiO_2 (%)	0.15
P_2O_5 (%)	0.086
SO_3 (%)	0.23
LOI (%)	17.2

2.3 APPARATUS AND TECHNIQUE

Magnetic hot plate stirrer was used to stir the heavy metal solution with adsorbents (activated carbon or bentonite). A definite volume of heavy metal ion solution with a known initial concentration is stirred with a definite amount of adsorbent for certain time at fixed temperature and agitation rate. pH of the solution was measured by digital pH meter (Model μ pH system-361, India).

2.4 EXPERIMENTAL PROCEDURES

Potassium dichromate ($K_2Cr_2O_7$) and redistilled water were used to prepare a stock solution with a concentration of 1000 ppm Cr(VI) which was diluted for preparation of standard and test solutions. Several solutions with different initial concentrations of potassium dichromate (50, 100, 200, 300 and 400 ppm) were prepared. The required pH was adjusted by drop wise addition of 0.1 N H_2SO_4 depending on the acidity of the sample. All experiments were carried out at 25°C by adding different amounts of adsorbents (0.1, 0.3, 0.5, 0.7 and 1.0 g) to different concentrations of 250 ml of heavy metals ions solution. The agitation rate for all experiments was 200 rpm and the residence time was (0, 15, 30, 45, 60, 75, 90 and 120 min).

1 ml of Sample was taken from reaction solution and diluted to 10 ml by redistilled water, the solution is then separated from the adsorbents by using filter paper (Watman No. 40) and the residual Cr^{+6} concentration in the solution is then determined by atomic-absorption spectrophotometer (AAS).

The effects of several parameters, such as contact time, initial concentration, adsorbent doses, pH and temperature on the adsorption of Cr(VI) ions on activated carbon and bentonite were studied.

2.5 ANALYTICAL METHOD

Atomic absorption spectrophotometry utilizes the phenomenon that atoms absorb radiation of particular wavelength. By atomic-absorption spectrophotometer AAS (Model, AA55; Varian Inc., USA), The metals in water sample can be analyzed. It detects the concentration of Cr(VI) in ppm level in the solution and the volume of sample required is only 1 ml for one analysis.

2.6 DATA ANALYSIS

The uptake of Cr(VI) ions was calculated from the mass balance, which was stated as the amount of solute adsorbed onto the solid. It equals the amount of solute removed from the solution. Mathematically, it can be expressed by Eq. (1):

$$q_e = (C_i - C_e)/S \qquad (1)$$

where:

q_e the heavy metal ions concentration adsorbed by an adsorbent at equilibrium (mg of metal ion/g of adsorbent)

C_i is the initial concentration of metal ions in the solution (mg/L).

C_e is the equilibrium concentration or final concentration of metal ions in the solution (mg/L).

S the dosage concentration and it is expressed by Eq. (2):

$$S = m/V, \qquad (2)$$

where V is the initial volume of metal ions solution used (L) and m is the weight of dried used adsorbent (g).

The percentage of adsorption (%) is calculated using equation (3):

$$\% \text{ adsorption} = [(C_i - C_e)/C_i] \times 100 \quad (3)$$

3. RESULTS AND DISCUSION

3.1 EFFECT OF CONTACT TIME

The experiment of adsorption as a function of contact time was conducted at known initial concentration of Cr(VI) metal ion, dose of 4 g/L for both activated carbon and bentonite (Fig 1). It is easily seen from Fig 1 that the percentage removal of Cr(VI) metal ions increased with increasing the contact time. The % removal was 73% for activated carbon and 77% for bentonite after 120 min. It is clear that, at the beginning % removal increased rapidly in few minutes. By increasing contact time, % removal increased lightly and slowly till reach maximum value and this can be explained on the basis that, initially a large number of vacant surface sites may be available for adsorption of metal ions, and by time the surface sites become exhausted [12]. These results indicate that the activated carbon and bentonite have a very strong capacity for adsorption of Cr(VI) ions in solution.

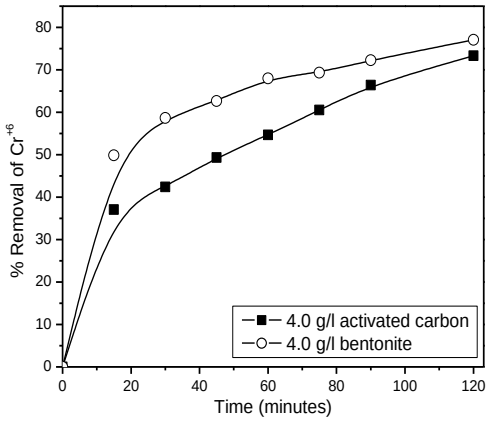

Fig 1. Effect of contact time on Cr^{+6} removal (conditions; adsorbate initial conc., 400 mg/L; pH, 2.0; adsorbents dose, 4 g/L; agitation speed, 200 rpm and temperature, 25 $^{\circ}$C).

3.2 Effect of Adsorbent Dose

The percentage adsorption of Cr^{+6} on activated carbon and bentonite was studied at different adsorbent doses (0.4, 1.2, 2.0, 2.8 and 4.0 g/L), keeping pH (2), temperature (25°C), contact time (120 min) and initial Cr^{+6} ions

concentration of (400 mg/L) constant Fig 2. The results showed that with increasing in adsorbent dose, percentage adsorption of Cr^{+6} was increased and the maximum removal was observed with adsorbent 4 mg/L for activated carbon and bentonite. Increasing the percentage of adsorption with adsorbent dose may be due to the increase in adsorbent surface area and availability of more adsorption sites [13,14]. But unit adsorption was decreased with increasing in adsorbent dose Fig 3. This is may be due to overlapping of adsorption sites as a result of overcrowding of adsorbent particles [14].

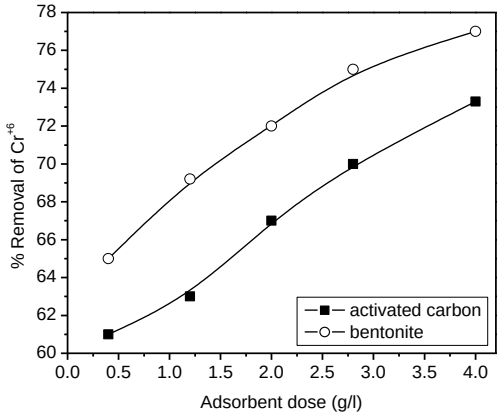

Fig 2**.** The effect of variant activated carbon or bentonite adsorbent dosage (0.4, 1.2,2.0, 2.8, and 4.0 g/l) on the removal of 400 mg/l Cr^{+6} ions from wastewater at contact time, 2 h, temperature, 25°C and agitation speed, 200 rpm.

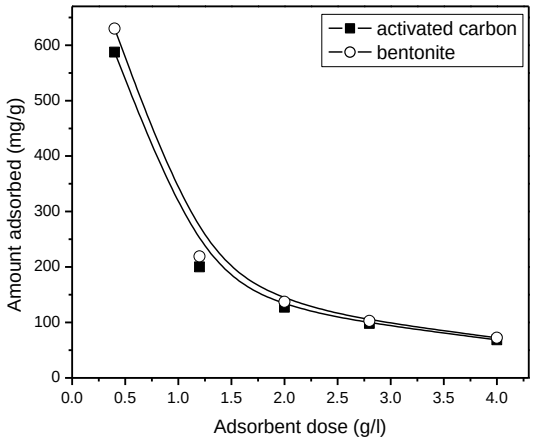

Fig 3. The effect of variant activated carbon or bentonite adsorbent dosage (0.4, 1.2, 2.0, 2.8, and 4.0 g/L) on the quantity adsorbed of 400 mg/L Cr^{+6} ions from wastewater at contact time, 2 h, temperature, 25°C and agitation speed, 200 rpm.

3.3 EFFECT OF INITIAL CHROMIUM (VI) IONS CONCENTRATION

The initial heavy metal ion concentration is an important parameter in adsorption since a certain amount of adsorbent can adsorb a certain amount of heavy metal. The percentage removal of Cr^{+6} was studied by varying Cr^{+6} concentration from 50 to 300 mg/L with 4 g/L adsorbent doses of activated carbon and bentonite at pH (2), temperature (25°C) and contact time (120 min) is illustrated in Fig 4.

The results presented in Fig.4, showed that the percentage Cr^{+6} adsorption was decreased with increasing in initial concentration. But the actual amount of Cr^{+6} adsorbed per unit mass of the adsorbent was increased with increasing in Cr^{+6} concentrations in the test solution, Fig 5. According to these results, the initial Cr^{+6} ions concentration plays an important role in the adsorption capacities. Higher concentrations of metal ion were used to study the maximum adsorption capacity of adsorbent [15, 16].

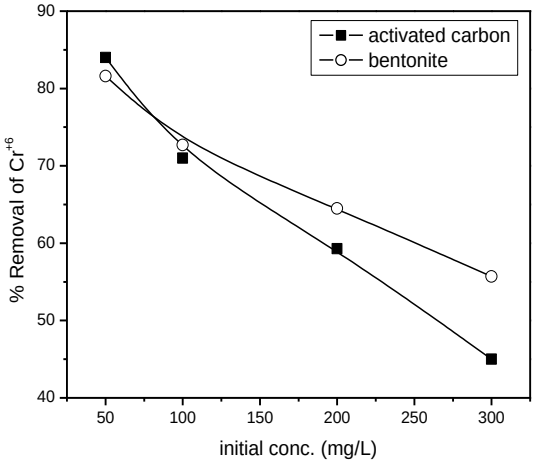

Fig 4. The effect of initial concentration (namely 50, 100, 200 and 300 mg/l) on removal of Cr^{+6} ions (conditions; adsorbents dose, 4 g/l; agitation speed, 200 rpm and temperature, 25°C).

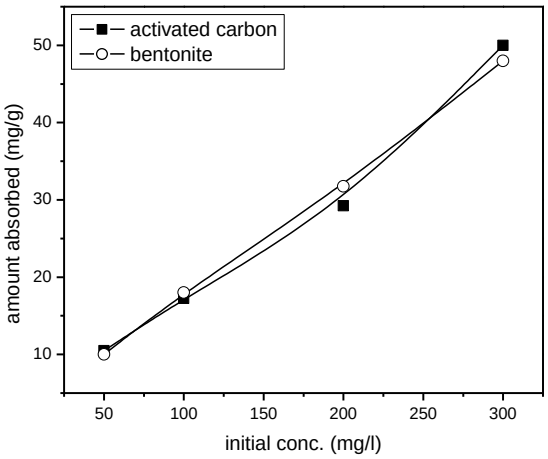

Fig 5. The effect of initial concentration (namely 50, 100, 200 and 300 mg/l) on quantity adsorbed of Cr^{+6} ions (conditions; adsorbents dose, 4 g/l; agitation speed, 200 rpm and temperature, 25°

3.4 EFFECT OF pH ON THE UPTAKE OF Cr^{+6}

The pH of the solution is an important variable which controls the adsorption of the metal ions at the solid-water interface. Hence, the influence of pH on the adsorption of Cr^{+6} on activated carbon and bentonite was examined in the pH range 1-4. The results were presented in Fig 6, it showed that the adsorption capacities of Cr^{+6} onto both adsorbents increases significantly with decreasing pH value and the maximum removals of Cr^{+6} by both adsorbents for contact time (120 min) were carried out at pH (2). The improved removal of chromium(VI) at low pH is probably due to reduction of hexavalent chromium to trivalent chromium [17], Eq. (4) .

$$Cr_2O_7^{-2} + 14H^+ + 6e^{-1} \rightarrow 2Cr^{+3} + 7H_2O \qquad (4)$$

Also at low pH, there is presence of a large number of H^+ ions, which in turn neutralize the negatively charged adsorbent surface thereby reducing hindrance to the diffusion of dichromate ions [18].

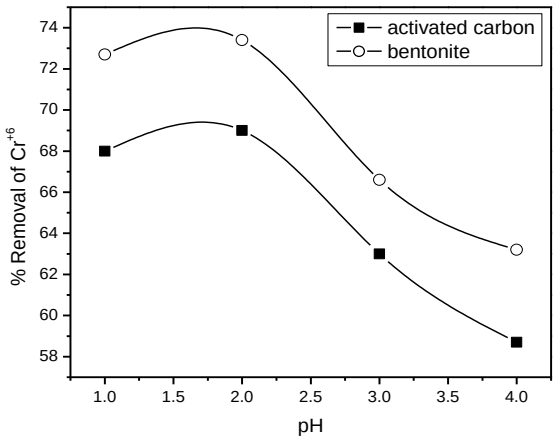

Fig 6. Effect of pH for the adsorption of Cr(VI) ions onto activated carbon and bentonite at 25°C.

3.5 EFFECT OF TEMPERATURE

Fig 7 indicates the effect of temperature on the removal efficiency of Cr^{+6} ions from wastewater using activated carbon and bentonite. Four different temperatures were considered in this study (25, 30, 35 and 40°C). The figure showed that the removal efficiency increases by increasing the temperature, where the maximum adsorption (76% approx.) is achieved at 40°C in case of activated carbon. The augmentation of the removal efficiency by stepping up the temperature are due to: Firstly, the higher temperature activates the metal ions for enhancing adsorption at the coordinating sites of the adsorbent, and the metal cation more faster [19, 20]. Secondly, acceleration of some originally slow step(s) and creation of some new activation sites on the adsorbent surface [21]. Herein, the phenomenon can be observed in both adsorbents, but activated carbon is affected much higher than in case bentonite Fig 7.

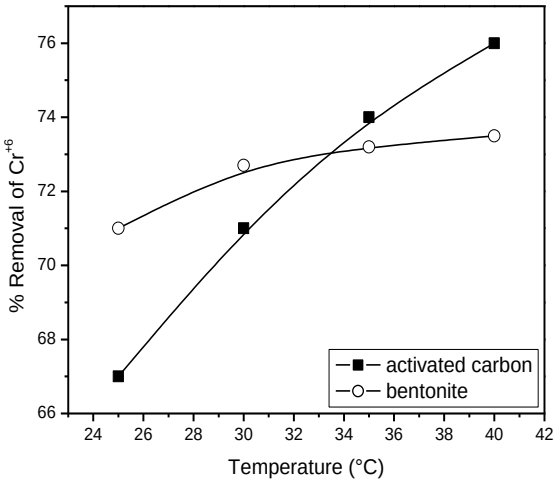

Fig 7. The effect of temperature between 25 and 40 ˚C for the removal of Cr^{+6} ions from wastewater (conditions; adsorbate initial conc., 400 mg/L; pH, 2.0; adsorbents dose, 4 g/L; agitation speed, 200 rpm and contact time 2 h).

3.6 ADORPTION ISOTHERMS

Several models have been used in the literature to describe the experimental data of adsorption isotherm. The Langmuir and Freundlich models are the most frequently employed to describe equilibrium [22]. The Langmuir isotherm is based on the theoretical principle that only a single adsorption layer exists on an adsorbent and it represents the equilibrium distribution of metal ions between the solid and liquid phases. The basic assumption of the Langmuir adsorption process is the formation of a monolayer of adsorbate on the outer surface of the adsorbent and after that no further adsorption take place. The Langmuir-type isotherm remains to be the most widely used for practical application. The Langmuir isotherm for pure component adsorption can be obtained from Eq. (5):

$$C_e/q_e = 1/(q_{max}b) + (1/q_{max})\, C_e \qquad (5)$$

Where q_{max} is the maximum metal ions uptake per unit mass of adsorbent (mg/g), which is related to the adsorption capacity and b is Langmuir constant (L/mol) which is exponentially proportional to the heat of adsorption and related to the adsorption intensity. Therefore, a plot of C_e/q_e versus C_e gives a straight line of slop $1/q_{max}$ and intercept $1/(q_{max}\, b)$ as shown in Fig 8.

Zeldowitsch (1934) [22], assuming an exponentially decaying function of site density with respect to heat of adsorption and obtained the classical empirical isotherm, Eq. (6):

$$\ln q_e = \ln K_f + 1/n \ln C_e \qquad (6)$$

This is known as Freundlich isotherm. The Freundlich adsorption isotherm is an indicator of the extent of heterogeneity of the adsorbent surface, where the Freundlich constants K_f and n, which respectively indicating the adsorption capacity and the adsorption intensity, were calculated from the intercept and slope of the plot of $\ln q_e$ versus $\ln C_e$ as shown in Fig 9.

This Freundlich type behavior is indicative of surface heterogeneity of the adsorbents, i.e the adsorptive sites (surface of activated carbon and bentonite) are made up of small heterogeneous adsorption patches that are homogeneous in themselves. The activation of adsorption site takes place, leading to increased adsorption probably through the surface exchange mechanism.

The calculated results of Langmuir and Freundlich isotherm constants are given in table 3.

It can be seen that the Freundlich model yields a much better fit than the Langmuir model, when the R^2 values are compared in table 3. This suggests that the boundary layer thickness is increased. The Freundlich constant K_f indicates the sorption capacity of the sorbent. From table 3, the values of K_f are 1.84 and 1.58 for activated carbon and bentonite, respectively.

Furthermore, the value of n is 2.26 and 1.78 for activated carbon and bentonite, respectively. It is noted that the values of n are bigger than 1, reflecting the favorable adsorption. On the other hand, the q_{max} and the adsorption intensity values of bentonite are higher than activated carbon. The calculated b values indicate the interaction forces between bentonite surface and Cr^{+6} ions are stronger than in case of activated carbon, this means that the bentonite is more powerful adsorbent than activated carbon. These results indicate that both adsorbents have a very strong adsorption capacity towards Cr^{+6} ions.

Table 3.Langmuir and Freundlich isotherm constants for the adsorption of Cr^{+6} on activated carbon and bentonite at constant temperature 25˚C.

Adsorbent	Langmuir Isotherm constants			Freundlich Isotherm constants		
	q_{max} (mg/g)	b (L/mol)	R^2	K_f (mg/g)	n	R^2
Activated Carbon	38.17	0.0252	0.9686	1.8446	2.26	0.9953
Bentonite	48.83	0.0377	0.9658	1.5826	1.78	0.9995

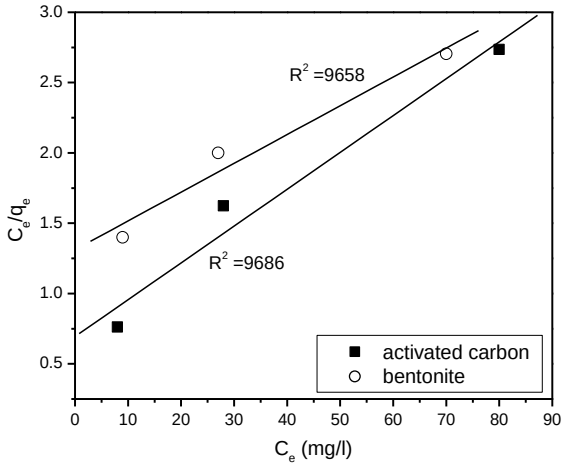

Fig 8. The linarized Langmuir adsorption isotherm for Cr^{+6} ions adsorption by activated carbon and bentonite at constant temperature 25˚C and contact time 2 h.

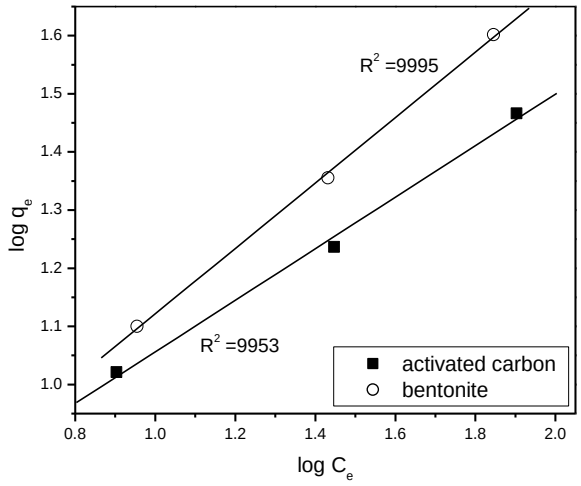

Fig 9. The linarized Freundlich adsorption isotherm for Cr^{+6} ions adsorption by activated carbon and bentonite at constant temperature 25°C and contact time 2 h.

3.7 THERMODYNAMIC PARAMETERS

Thermodynamic parameters such as free energy (ΔG°), enthalpy (ΔH°) and entropy (ΔS°) changes of adsorption can be evaluated from the following equations (7, 8):

$$K_c = C_{Ae}/C_e \qquad (7)$$

$$\Delta G^\circ = -RT \ln K_c \qquad (8)$$

Where K_c is the equilibrium constant and C_{Ae} and C_e (both in mg/L) are the equilibrium concentrations for solute on the sorbent and in the solution, respectively. The K_c values are used in Eqs. (7) and (8) to determine the ΔG°, ΔH° and ΔS° the K_c may be expressed in terms of the ΔH° (kj mol^{-1}) and ΔS° (kj $mol^{-1}K^{-1}$) as a function of temperature, Eq. (9):

$$\ln K_c = - \Delta H^\circ/RT + \Delta S^\circ/R \qquad (9)$$

Thermodynamic parameters such as free energy of sorption (ΔG°), the heat of sorption (ΔH°) and standard entropy (ΔS°) changes during the sorption process were calculated using Eqs. (7) and (8) on a temperature range of 25-40°C at initial concentration 50 mg/L of Cr^{+6} and dose 4 g/L for activated carbon and bentonite.

(ΔH°) and (ΔS°) were obtained from the slope and intercept of a plot of $\ln K_c$ against 1/T (Fig 10). The values of these parameters were recorded in table 4.

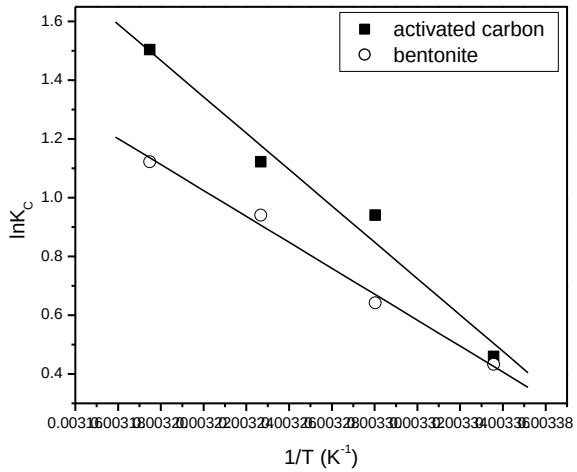

Fig 10. A plot of $\ln K_C$ against 1/T for Cr^{+6} adsorption for 50 mg/l initial concentration at constant adsorbents dose 4 g/L.

Table 4.Thermodynamic parameters for the adsorption of Cr(VI) onto activated carbon and bentonite.

Adsorbent	ΔH°(kj mol^{-1})	ΔS°(kj $mol^{-1}K^{-1}$)	ΔG°(kj mol^{-1})			
			25°C	30°C	35°C	40°C
Activated carbon	51.45	0.1776	-1.24	-2.12	-3.00	-3.89
Bentonite	36.72	0.1268	-1.06	-1.70	-2.33	-2.71

The negative values of ΔG° indicate the spontaneous nature of the process and more negative value with increase of temperature shows that an increase in temperature favors the sorption process. The positive values of ΔH° indicate that the sorption process was endothermic in nature and the positive values of ΔS° show the increased randomness at solid/solution interfaces during the adsorption of metal on both adsorbents and also reflects the affinity of activated carbon and bentonite toward Cr^{+6} ions under consideration. It is also suggested that the positive values of entropy indicate some structural changes in the adsorbate and adsorbent [23-25].

4. COCLUSION

Both adsorbents can be successfully used for removing of chromium (VI) ions from wastewater. The maximum adsorption percentage of Cr(VI) ions using both adsorbents were achieved within 120 min. The adsorption percentages of Cr^{+6} ions increase sharply by increasing adsorbent doses. As the initial concentration of ions increase the percentage removal using activated carbon and bentonite decreases. The best temperature for the maximum adsorption is found to be 30-40°C for activated carbon, while the adsorption using bentonite is less affected by increasing temperature. The maximum removals of Cr(VI) by both adsorbents were carried out at pH 2. The obtained experimental data has been well described by Langmuir and Freundlich isotherm models into both activated carbon and bentonite.

Different thermodynamic parameters, viz., ΔH°, ΔS° and ΔG° have also been evaluated and it has been found that the sorption was feasible, spontaneous and endothermic in nature. The positive value of the entropy change, suggests the increased randomness.

5. REFERENCES

[1] Ayad M. jebur almamoori*, fikrat m. hassana and thaer i. kassimb,2012" impact of industrial waste on the properties of one major drainage in the region of the middle euphrates / Iraq" int. j. chem. Sci.: 10(4)(2012) 1785-1798

[2]Park Heung Jai, Jeong Seong Wook,Yang Jae Kyu, Kim Boo Gil, Lee Seung Mok" Removal of heavy metals using eggshell", Journal of Environmental Sciences 19(2007) 1436-1441.

[3]Mohamed Nasif Abbas, Firas Saeed Abbas, Hala Husham Nussarat, Safaa Neamat Hussein, "Synthesis of Promoted Catalyst from Iraqi rice"

[4]Mohamed Ali Zulfikar, EdehDieke Mariske, and samitha Dewi Djajanti,"Adsorption of Ligosulfnate compounds using powder eggshell",songkanakarin

j.sci.Technol,34(3),May – June (2013) 309-316

[5]Suresh Gupta and BV Babu, 2013,"Adsorbtion of chromium (VI) by low-cost adsorbent prepared from tamarind seeds" Birla institude of technology and science, india,2013

[6]Rajendran. A and C.Mansiya,2011, "Extraction of Chromium from tannery effluents using waste eggshell materials as adsorbent" , British Journal of environment and climate change ,1(2),(2011) 44-52

[7]Renge,V.C. S.V. Khedkar and Shraddha V Pande, " Removal of heavey metals from waste water using low-cost adsorbent" Sci. Revs. Chem. Common,: 2(4) , (2012) 580 -584 ISSN 2277-2669

[8] Rajendran, A. (2010). Applicability of an ionic liquid in the removal of chromium from tannery effllluents: Agreen chemical approch, Affrican journal of pure and Applied Chemistery., 4(6) ,100-103

[9]Ambasht , R.S. (1983). Ecological Consideration of water pollution , Souvenir and abstract , National Conference on Revier pollution and Human Health. PP.3-4

[10] Ananthakrishna Nader, P., Balasubramanian. N., Venkatachlam, T., Parabakaran , T.R.(1992). Pollution Load of Cauvery revier water . Jornal. Of Nacton.42,91-104.

[11] Areej Dalf Abbas, 2012,"Influnce of Operating Condition on adsorbtion of lead (II) From Contaminated water using different adsorbent" Eng& Tech.Journal,Vol.3.NO.6,2012.

[12]Y. B. Zhan, A. Shukla, S. Shukls, K. L. Dorris, The removal of heavy metal from aqueous solutions by sawdust adsorption-removal of Copper, J. Hazard. Mater. 80(2000) 33-42.

[13]C. Namasivayam, K. Kadirvelu, M. Kumuthu, Removal of direct red and acid brilliant blue by adsorption on to banana pith, Bioresour. Technol. 64 (1998) 77-79.

[14]U. K. Garg, M. P. Kaur, V. K. Garg, D. Sud, Removal of hexavalent chromium from aqueous solution by agricultural waste biomass, Hazard. Mater. 140 (2007) 60-68.

[15]K. Mohanty, M. Jha, B. C. Meikap, M. N. Biwas, Biosorption of chromium(VI) from aqueous solution by Eichhornia Crassipis, Chem. Eng. J. 117 (2006) 71-77.

[16]T. Karthikeyan, S. Rajgopal, L. R. Miranda, Chromium adsorption from aqueous solution by Hevea Brasilinesis sawdust activated carbon, J. Hazard. Mater. B124 (2005) 192-199.

[17]Anon, Standard Methods for the examination of Water and Wastewater, 19th ed., Washington, DC, USA, 1995.

[18]D.C. Sharma, C.F Forster, The treatment of chromium wastewaters using the sorptive potential of leaf mould, Biores. Technol. 49 (1994) 31-40.

[19]S. Babel, T. A. Kurniawan, Low-cost adsorbents for heavy metals uptake from contaminated water: a review, J. Hazard. Mater. B97 (2003) 219-243.

[20]V. J. Inglezakis, M. D. Loizidou, H. P. Grigoropoulou, Ion exchange studies on natural and modified zeolites and the concept of exchange site accessibility, J. Colloid Interface Sci. 275 (2004) 570-576.

[21]a) P. A. Domenico, F. W. Schwartz, Physical and Chemical Hydrogeology 1st Ed., John Wiley and Sons, New York, 1990; b) L. N. Reddi, H. I. Inyang, Geo-Environmental Engineering Principles and Applications, Marcel Decker Inc. New York, 2001; c) O. Nitzsche, H. Vereecken, Modelling Sorption and Exchange Processes in Column Experiments and Large Scale Field Studies, Mine Water Environ. 21 (2002) 15-23.

[22]J. Zeldowitsch, Űber den Mechanismus der Katalytischen Oxydation von CO an MnO_2, Acta Physiochim. URSS 1 (1934) 364-449.

[23]H. S. Altundogan, S. Altundogan, F. Tumen, M. Bildik, Arsenic removal from aqueous solution by adsorption on red mud. Waste Mange. 20(2000) 761-767.

[24]H. G. Fuhrman, J. C. Tjell, D. Mcconchie, Adsorption of arsenic from water using activated neutralized red mud. Environ. Sci. Technol. 38(2004) 2428-2434.

[25]M. Ajmal, R. A. K. Rao, S. Anwar, J. Ahmed, R. Ahmed, Adsorption studies on rice husk: removal and recovery of Cd(II) from wastewater. Bioresour. Technol. 86(2003) 147-149.

Topological approximations based on relations induced from differences

Rukaia M. Rashed

Department of Mathematics, Faculty of Education, Al-Zawia University, Libya

A. A. azzam

Department of Mathematics, Faculty of Science, Assuit University, New Valley, Egypt

Abstract

The starting point of rough set theory is the indiscernibility relation, which is generated by information about objects of interest. The indiscernibility relation is intended to express the fact that due to the lack of knowledge we are unable to discern some objects employing the available information. Therefore, generally, we are unable to deal with single object. Nevertheless, we have to consider clusters of indiscernible objects.

In this paper, a relationship was created through a table of given data. This relationship is based on the expert's opinion in the field of data. Based on this relationship, we constructed a topological under the lowest possible conditions. This topology describes the roughness of the set and shows that the intermittent topology obtained is stronger and more precise than others Other studies, also in this paper, compared the approximations obtained using the precision scale to determine the best.

Introduction

Rough set theory, proposed by Pawlak in 1980's as a result of a long term program on mathematical fundamental research can be seen as a new mathematical approach to vagueness (set) and uncertainty (element) from databases (information systems) [3]. One of the important issues in rough set-based database analysis is discovering dependencies between attributes. An attribute dependency states that the value of an attribute is uniquely determined by the values of some other attributes. The objective of discovering attribute dependency is to find the relationship among attributes in information systems. A rough set model in databases may therefore be considered as a method for constructing a topological space using indiscernibility relation on the set of objects [2]. In a reverse process, we can generalize the notions of rough sets based on the topological space.

Definable sets, *i.e.*, a family of union of one or more equivalence classes are substituted by open sets in defining the lower approximations, and by closed sets in defining upper approximations, as the basic concepts of rough set theory.

In this paper, we focus on the dependency of attributes in information systems. We show that a dependency of attributes in information systems determines a finer quasi-discrete topology which can be considered as a quasi-discrete topological subspace. Then, we use the notion of the topology to characterize the roughness of a set. The rest of this paper is organized as follows. Section 3 describes the rough set theory in information systems. Section 4 describes the notion of topological space and several topological aspects of sets.

Note

In each part of this paper we used the same example data.

1- Preliminaries

The concept of topological space structures is one the most powerful notions in system analysis. The notions of topological space, open set and closed set, closure of a set, interior of a set, exterior of a set, boundary of a set and base of a topological space has been handled in [**1**, **7**].

Example 1.1

Suppose that data about 6 students is given, as shown in table (1)

Student	Analysis	Algebra	Statistics	Decision
1	bad	good	medium	accept
2	good	bad	medium	accept
3	good	good	good	accept
4	bad	good	bad	reject
5	good	bad	medium	reject
6	bad	good	good	accept

Table (1)

From table (1) we have

$U = \{1,2,3,4,5,6\}, A = \{\text{Analysis}, \text{Algebra}, \text{Statistics}, \text{Decision}\}$, where

$$C = \{\text{Analysis}, \text{Algebra}, \text{Statistics}\} =, D = \{\text{Decision}\}\&$$

$$V_{\text{Analysis}} = \{\text{bad}, \text{good}\}, \qquad V_{\text{Algebra}} = \{\text{bad}, \text{good}\},$$

$V_{\text{Statistics}} = \{\text{bad}, \text{medium}, \text{good}\} \& V_{\text{Decision}} = \{\text{accept}, \text{reject}\}$, in the information system $S = (U, A, V, f)$ where $U$is the universe, A is the set of attributes, $V = \bigcup_{a \in I} V_a, V_a$ is the domain (value set) of attribute a, $f: U \times A \longrightarrow V$ is a total function such that $f(u, a) \in V$, for every $(u, a) \in U \times A$, called information (knowledge) function.

2- Indiscernibility relation

From table (1), it is noted that students 2, 3 & 5 are indiscernible with respect to the attribute Analysis, meanwhile, students 3& 6 are indiscernible with respect to the attribute Algebra and Decision, and students 2 & 5 are indiscernible with respect to the attribute Analysis, Algebra and Statistics. Now I will make the schedule of the relation as the following, from the previous table we determine the number of times between element until the group ends then we get a symmetrical table the elements of its diameter are zeros.

	1	2	3	4	5	6
1	0	2	2	2	3	1
2	2	0	2	4	1	3
3	2	2	0	3	3	1
4	2	4	3	0	3	2
5	3	1	3	3	0	4
6	1	3	1	2	4	0

Table (2)

Definition 2.1[**8**, **9**]

Let $S = (U, A, f)$ be an information system and let B be any subset of A. Two elements $x, y \in U$ are be B −indiscernible (indiscernible by the set of attribute $B \subseteq A$ in S) if and only if $f(x, a) = f(y, a)$, for every $a \in B$.

Definition 2.1

Let R be a general relation over U, and $S = (U, A, V, f)$, be an information system, B any subset of A then the minimal a construction set is the family of all after sets of Rcontaining an element$x \in U$, and denoted by $(m.s)$ where $(m.s) = \{xR: x \in U\} \& xR = \{y: xRy, y \in U\}$.

Now we conclusion the a after sets or before sets with the all numbers of the table (2) as follows

With respect to a relationship that yields results less than 2

$$1R0 = \{1,6\},\ \ 2R0 = \{2,5\},\qquad 3R0 = \{3,6\},\ \ 4R0 = \{4\},\ \ 5R0 = \{2,5\},$$

$$6R0 = \{1,3,6\} \Longrightarrow R_1 = \begin{Bmatrix}(1,1),(1,6),(2,2),(2,5),(3,3),(3,6),\\(4,4),(5,2),(5,5),(6,1),(6,3),(6,6)\end{Bmatrix},$$

The first after set is

$$S_1 = \{\{4\},\{1,6\},\{3,6\},\{2,5\},\{1,3,6\}\}$$

With respect to a relationship that yieldsresults less than 3

$$1R1 = \{1,2,3,4,6\}, 2R1 = \{1,2,3,5\}, 3R1 = \{1,2,3,6\}, 4R1 = \{1,4,6\},$$

$$5R1 = \{2,5\}, 6R1 = \{1,3,4,6\}$$

$$\Longrightarrow R_2 = \begin{Bmatrix}(1,1),(1,2),(1,3),(1,4),(1,6),(2,1),(2,2),(2,3),(2,5),(3,1),(3,2),\\(3,3),(3,6),(4,1),(4,4),(4,6),(5,2),(5,5),(6,1),(6,3),(6,4),(6,6)\end{Bmatrix},$$

The second after set is $S_2 =$

$\{\{1,2,3,4,6\},\{1,2,3,5\},\{1,2,3,6\},\{1,4,6\},\{2,5\},\{1,3,4,6\}\}$.

With respect to a relationship that yieldsresults less than 4

$$1R3 = U, 2R3 = \{1,2,3,5,6\}, 3R3 = U, 4R3 = \{2,3,4,5,6\}, 5R3 = \{1,2,3,4,5\},$$

$$6R3 = \{1,2,3,4,6\}$$

$$\Longrightarrow R_3 = \begin{Bmatrix}(1,1),(1,2),(1,3),(1,4),(1,5),(1,6),(2,1),(2,2),(2,3),(2,5)(2,6),\\(3,1),(3,2),(3,3),(3,4),(3,5),(3,6),(4,2),(4,3),(4,4),(4,5),(4,6),\\(5,1),(5,2),(5,3),(5,4),(5,5),(6,1),(6,2),(6,3),(6,4),(6,6)\end{Bmatrix}$$

The third after set is$S_3 = \{U,\{1,2,3,5,6\},\{1,2,3,4,5\},\{1,2,3,4,6\},\{2,3,4,5,6\}\}$.
Now we define minimal a construction$(m.s)$as

$(m.s)_1 = \{\{4\},\{1,6\},\{3,6\},\{2,5\},\{1,3,6\}\}$,

$(m.s)_2 = \{\{1,2,3,4,6\},\{1,2,3,5\},\{1,2,3,6\},\{1,4,6\},\{2,5\},\{1,3,4,6\}\}$,

$(m.s)_3 = \{U,\{1,2,3,5,6\},\{2,3,4,5,6\},\{1,2,3,4,5\},\{1,2,3,4,6\}\}$,

Also, $(m.s)_1^C = \{\{2,3,4,5\},\{1,3,4,6\},\{1,2,4,5\},\{1,2,3,5,6\},\{2,4,5\}\}$,

$$(m.s)_2^C = \{\{5\},\{4,6\},\{4,5\},\{2,3,5\},\{1,3,4,6\},\{2,5\}\},$$

$$(m.s)_3^C = \{\emptyset,\{4\},\{1\},\{6\},\{5\}\}$$

3- Rough set approximations

Rough set theory [**4**] proposes a new mathematical approach to imperfect knowledge, i.e. to vagueness (or imprecision).In this approach vagueness is expressed by region of a set.

Rough set concept can be defined by means of topological operations, interior and closure, called approximations.

Definition 3.1 $[\mathbf{4},\mathbf{5}]$

Let $X \subseteq U$ and R be an equivalence relation, then we denotes the boundary of X in Uas $BND_R(X) = \overline{R}(X) - \underline{R}(X)$and,

1- X is an exact if $\underline{R}(X) = \overline{R}(X) \Rightarrow BND_R(X) = \Phi$.

2- If $BND_R(X) \neq \Phi$ then$\underline{R}(X) \subset X \subset \overline{R}(X)$, the set X is called a rough set.

Definition3.1

Let R be a general relation over U, and $S = (U, A, V, f)$, be an information system, B any sub set of A&X is any subset of U, then the $B - lower$ approximation of Xdenoted by $\underline{B}(X)$ and $B - upper$ approximation of Xdenoted by $\overline{B}(X)$, respectively are defined by

$\underline{B}(X) = \cup\{x \in U: (m.s) \subseteq X\},\ \overline{B}(X) = \cap\{x \in U: (m.s) \cap X \neq \emptyset\}$.

From above definition we obtained the results

1- The boundary region $BND_B(X) = \overline{B}(X) - \underline{B}(X)$.

2- The positive region $POS_B(X) = \underline{B}(X)$.

3- The negative region $NEG_B(X) = U - \overline{B}(X)$.

X is said to be $R - exact$ if $\underline{R}(X) = \overline{R}(X)$ otherwise X is said to be $R - rough$.

Now, in this part we will generate a topological space and we will find the minimal a construction for all the relationships as in the following example where we can find a topology and its base as follows:

Example 3.1

From example 1.1, we have:

$R_1 = \begin{Bmatrix}(1,1),(1,6),(2,2),(2,5),(3,3),(3,6),\\(4,4),(5,2),(5,5),(6,1),(6,3),(6,6)\end{Bmatrix}, \frac{U}{R_1} = \{\{4\},\{1,6\},\{3,6\},\{2,5\},\{1,3,6\}\}$,

the minimal base for T_1 is $\beta_1 = \{U, \emptyset, \{4\},\{6\},\{1,6\},\{3,6\},\{2,5\},\{1,3,6\}\}$.

$$T_1 = \begin{Bmatrix} U,\emptyset,\{4\},\{1,6\},\{3,6\},\{2,5\},\{4,6\},\{1,3,6\},\{1,4,6\},\\ \{6\},\{2,4,5\},\{2,5,6\},\{1,3,4,6\},\{1,2,5,6\},\{2,3,5,6\},\\ \{3,4,6\},\{2,4,5,6\},\{1,2,3,5,6\},\{1,2,4,5,6\},\{2,3,4,5,6\}\end{Bmatrix},$$

$$T_1^C = \begin{Bmatrix} U,\emptyset,\{1,2,3,5,6\},\{2,3,4,5\},\{1,2,4,5\},\{1,3,4,6\},\\ \{1\},\{3\},\{4\},\{1,2,3,5\},\{2,4,5\},\{2,3,5\},\{1,2,3,4,5\},\\ \{1,3,4\},\{1,3,6\},\{2,5\},\{3,4\},\{1,4\},\{1,2,5\},\{1,3\}\end{Bmatrix}$$

It is obvious that $\emptyset$ & U are closed and open (clopen) sets, Also the sets $\{1,3,6\}$&$\{2,5\}$ are clopen sets, the set $\{1,4,6\}$ is open, the set $\{1\}$ is closed and the set $\{2,5\}$ is neither open nor closed.

Table (3) summarizing interior, exterior, closure and boundary of sets with respect to T_1

Set	Interior	Exterior	Closure	Boundary
$\{5\}$	$\emptyset$	$\{1,3,4,6\}$	$\{2,5\}$	$\{2,5\}$
$\{1,3,4\}$	$\{4\}$	$\{2,5,6\}$	$\{1,3,4\}$	$\{1,3\}$
$\{2,3,4\}$	$\{4\}$	$\{1,6\}$	$\{2,3,4,5\}$	$\{2,3,5\}$
$\{1,2,5,6\}$	$\{1,2,5,6\}$	$\{4\}$	$\{1,2,3,5,6\}$	$\{3\}$

Table (3)

With respect to T_2

$R_2 = \{(1,1),(1,2),(1,3),(1,4),(1,6),(2,1),(2,2),(2,3),(2,5),(3,1),(3,2),(3,3),(3,6),(4,1),(4,4),(4,6),(5,2),(5,5),(6,1),(6,3),(6,4),(6,6)\}$, $\frac{U}{R_2} = \{\{1,2,3,4,6\},\{1,2,3,5\},\{1,2,3,6\},\{1,4,6\},\{2,5\},\{1,3,4,6\}\}$, the minimal base for T_2 is

$\beta_2 = \{U,\emptyset,\{1\},\{2\},\{1,3\},\{1,6\},\{2,5\},\{1,2,3\},\{1,3,6\},\{1,2,3,5\},\{1,2,3,6\},\{1,4,6\},\{1,3,4,6\},\{1,2,3,4,6\}\}$,

$T_2 = \{U,\emptyset,\{1\},\{2\},\{1,2\},\{1,3\},\{1,6\},\{2,5\},\{1,2,3\},\{1,2,5\},\{1,2,3,5\},\{1,2,3,4,6\},\{1,2,6\},\{1,3,6\},\{1,4,6\},\{1,2,3,6\},\{1,2,4,6\},\{1,2,5,6\},\{1,3,4,6\},\{1,2,3,5,6\}\}$,

$T_2^C = \{U,\emptyset,\{4\},\{5\},\{2,5\},\{3,4\},\{3,5\},\{4,5\},\{4,6\},\{2,4,5\},\{2,3,5\},\{3,4,5\},\{3,4,6\},\{4,5,6\},\{3,4,5,6\},\{2,4,5,6\},\{2,3,4,5\},\{1,3,4,6\},\{1,3,4,5,6\},\{2,3,4,5,6\}\}$.

It is obvious that $\emptyset$ & U are closed and open (clopen) sets, Also the sets $\{2,5\}$&$\{1,3,4,6\}$ are clopen sets, the set $\{1,4,6\}$ is open, the set $\{5\}$ is closed and the set $\{1,3,4\}$ is neither open nor closed.

Table (4) summarizing interior, exterior, closure and boundary of sets with respect to T_2

Set	Interior	Exterior	Closure	Boundary
$\{5\}$	$\emptyset$	$\{1,2,3,4,6\}$	$\{5\}$	$\{5\}$
$\{1,3,4\}$	$\emptyset$	$\{2,5\}$	$\{1,3,4,6\}$	$\{1,3,4,6\}$
$\{2,3,4\}$	$\emptyset$	$\emptyset$	U	U
$\{1,2,5,6\}$	$\{2,5\}$	$\emptyset$	U	$\{1,3,4,6\}$

Table (4)

With respect to T_3

$$R_3 = \begin{Bmatrix} (1,1),(1,2),(1,3),(1,4),(1,5),(1,6),(2,1),(2,2),(2,3),(2,5),(2,6), \\ (3,1),(3,2),(3,3),(3,4),(3,5),(3,6),(4,2),(4,3),(4,4),(4,5),(4,6), \\ (5,1),(5,2),(5,3),(5,4),(5,5),(6,1),(6,2),(6,3),(6,4),(6,6) \end{Bmatrix},$$

$\frac{U}{R_3} = \{U, \{1,2,3,5,6\}, \{1,2,3,4,5\}, \{1,2,3,4,6\}, \{2,3,4,5,6\}\}$, the minimal base for$T_2$ is

$\beta_3 = \{U, \emptyset, \{1\}, \{2\}, \{3\}, \{4\}, \{1,2\}, \{1,3\}, \{1,6\}, \{2,3,4\}\}$.

$$T_3 = \begin{Bmatrix} U, \emptyset, \{1\}, \{2\}, \{4\}, \{1,2\}, \{1,3\}, \{1,4\}, \{1,6\}, \{2,3\}, \{2,4\}, \\ \{3,4\}, \{1,2,3\}, \{1,2,4\}, \{1,2,6\}, \{1,3,4\}, \{1,3,6\}, \{1,4,6\}, \\ \{2,3,4\}, \{1,2,3,4\}, \{1,3,4,6\}, \{1,2,4,6\}, \{3,4,5\} \end{Bmatrix},$$

$$T_3^C = \begin{Bmatrix} U, \emptyset, \{2,5\}, \{3,5\}, \{5,6\}, \{1,2,6\}, \{1,5,6\}, \{2,3,5\}, \{2,4,5\}, \{2,5,6\}, \\ \{3,4,5\}, \{3,5,6\}, \{4,5,6\}, \{1,2,5,6\}, \{1,3,5,6\}, \{1,4,5,6\}, \{2,3,4,5\}, \\ \{2,3,5,6\}, \{2,4,5,6\}, \{3,4,5,6\}, \{1,2,3,5,6\}, \{1,3,4,5,6\}, \{2,3,4,5,6\} \end{Bmatrix},$$

It is obvious that $\emptyset$ & U are closed and open (clopen) sets, Also the sets $\{1,2,6\}$&$\{3,4,5\}$ are clopen sets, the set $\{1,3,6\}$ is open, the set $\{5,6\}$ is closed and the set $\{5\}$ is neither open nor closed.

Table (5) summarizing interior, exterior, closure and boundary of sets with respect to T_3

Set	Interior	Exterior	Closure	Boundary
$\{5\}$	$\emptyset$	$\{1,2,3,4,6\}$	$\{2,5\}$	$\{2,5\}$
$\{1,3,4\}$	$\{1,3,4\}$	$\{2\}$	$\{1,3,4,5,6\}$	$\{5,6\}$
$\{2,3,4\}$	$\{2,3,4\}$	$\{1,6\}$	$\{2,3,4,5\}$	$\{5\}$
$\{1,2,5,6\}$	$\{1,2,6\}$	$\{3,4\}$	$\{1,2,5,6\}$	$\{5\}$

Table (5)

Also we have $\mathbb{R} = R_1 \cap R_2 \cap R_3 = R_1$& $T = T_1$

Definition 3.2

The accuracy of approximation (accuracy of roughness) of any subset $X \subseteq U$, with respect to $B \subseteq A$ denoted by $\alpha_B(X)$ is measured by $\alpha_B(X) = \left|\frac{\underline{R_B}(X)}{\overline{R_B}(X)}\right|$.

Example 3.2

Let us show accuracy of approximation notion by example referring in Table (1).

With respect to T_1

If $X = \{5\} \Longrightarrow \underline{R}(X) = \emptyset,\ \overline{R}(X) = \{2,5\},\ \alpha(X) = \left|\frac{\underline{R}(X)}{\overline{R}(X)}\right| = 0,$

$X = \{1,3,4\} \Longrightarrow \underline{R}(X) = \{4\}, \overline{R}(X) = \emptyset\ , \alpha(X) = \left|\frac{\underline{R}(X)}{\overline{R}(X)}\right| = 0\ ,$

$X = \{2,3,4\} \Longrightarrow \underline{R}(X) = \{4\}$, $\overline{R}(X) = \emptyset$, $\alpha(X) = \left|\frac{\underline{R}(X)}{\overline{R}(X)}\right| = 0$,&

if $X = \{1,2,5,6\} \Longrightarrow \underline{R}(X) = \{1,2,5,6\}$, $\overline{R}(X) = \emptyset$, $\alpha(X) = \left|\frac{\underline{R}(X)}{\overline{R}(X)}\right| = 0$

With respect to T_2

If $X = \{5\} \Longrightarrow \underline{R}(X) = \emptyset$, $\overline{R}(X) = \{2,5\}$, $\alpha(X) = \left|\frac{\underline{R}(X)}{\overline{R}(X)}\right| = 0$,

$X = \{1,3,4\} \Longrightarrow \underline{R}(X) = \emptyset$, $\overline{R}(X) = \emptyset$, $\alpha(X) = \left|\frac{\underline{R}(X)}{\overline{R}(X)}\right| = 1$,

$X = \{2,3,4\} \Longrightarrow \underline{R}(X) = \emptyset, \overline{R}(X) = \emptyset$, $\alpha(X) = \left|\frac{\underline{R}(X)}{\overline{R}(X)}\right| = 1$&

if $X = \{1,2,5,6\} \Longrightarrow \underline{R}(X) = \{2,5\}$, $\overline{R}(X) = \emptyset$, $\left|\frac{\underline{R}(X)}{\overline{R}(X)}\right| = 0$.

With respect to T_3

If $X = \{5\} \Longrightarrow \underline{R}(X) = \emptyset$, $\overline{R}(X) = \{2,5\}$, $\left|\frac{\underline{R}(X)}{\overline{R}(X)}\right| = 0$,

$X = \{1,3,4\} \Longrightarrow \underline{R}(X) = \emptyset$, $\overline{R}(X) = \emptyset$, $\left|\frac{\underline{R}(X)}{\overline{R}(X)}\right| = 1$,

$X = \{2,3,4\} \Longrightarrow \underline{R}(X) = \emptyset$, $\overline{R}(X) = \{2,3\}$, $\left|\frac{\underline{R}(X)}{\overline{R}(X)}\right| = 0$&

if $X = \{1,2,5,6\} \Longrightarrow \underline{R}(X) = \emptyset$, $\overline{R}(X) = \{2,5\}$, $\left|\frac{\underline{R}(X)}{\overline{R}(X)}\right| = 0$.

It is clear that the relations R_2 are the best among the differences we created for the selected set X according to the accuracy scale $\alpha_B(X)$, where $\alpha_B(X)$ =1, and this means that the set *X* is crisp(precise) with respect to *B*, otherwise the set *X* is rough (imprecise) with respect to *B* . But for the next set, all differences are perfect because the precision scale gives the best measurement and therefore the set X is crisp with respect to *B*.

4- Quasi Discrete Topology

In this section, we show that a topological space generated by minimal a construction relation in an information system is a special type of topology called a clopen (quasi discrete) topology.

Definition 4.1

A subset $X \subseteq U$ called a rough set in (U, T_R), if $X^{\circ} \neq \overline{X}$. Otherwise X is crisp in (U, T_R).

Notions 4.1

Let (U, T_R) be a topological space, $X \subseteq U$ in (U, T_R), then we have

i- A set $X \subseteq U$ is rough in (U, T_R) if $BN(X) \neq \emptyset$.

ii- A set $X \subseteq U$ is rough in (U, T_R) if $X^{\circ} \subset X \subset \overline{X}$.

iii- A set $X \subseteq U$ is rough in (U, T_R) if $X \notin T$.

Definition 4.2

Let (U, T_R) be a general knowledge base, $X \subseteq U \& R \in \mathbb{R}$.

(1) X is totally $R - definable$ (exact) set if $X^{\circ} = X = \overline{X}$.

(2) X is totally $R - undefinable$If $X^{\circ} = \Phi \& \overline{X} = U$.

(3) X is internally R-definable set if $X^{\circ} = X,\ \overline{X} \neq X$.

(4) X is internally $R - undefinable$ set if $X^{\circ} = \Phi\ \& \overline{X} \neq U$.

(5) X is externally $R - definable$ set if $X^{\circ} \neq X,\ \overline{X} = X$.

(6) X is externally $R - undefinable$ set if $X^{\circ} \neq \Phi\ \& \overline{X} = U$.

(7) X is roughly $R - definable$ set if $X^{\circ} \neq \Phi\ \& \overline{X} \neq U$.

(8) X is $R - indefinable$ (rough) set if$X^{\circ} \neq X, \overline{X} \neq X$.

Proposition 4.3[**6**]

Let $K = (U, \mathbb{R})$ be a general knowledge base, $X \subseteq U$ and $R \in \mathbb{R}$.

(1) Set X is $R - definable$ (roughly $R - definable$, totally$R - undefible$) if and only if soX^C.

(2) Set X is externally (internally) $R - undefible$ if X^C is internally (externally) $R - undefinble$.

Proof

(1) If X is $R - definable$ then$\underline{R}(X) \neq \Phi \& \overline{R}(X) \neq U$, we show that

(2) $\underline{R}(X^C) \neq \Phi \& \overline{R}(X^C) \neq U$ since$\underline{R}(X) \neq \Phi \Longrightarrow \underline{R}(X) = \left(\overline{R}(X^C)\right)^C \neq \Phi$

$\Longrightarrow \overline{R}(X^C) \neq U$, and since $\overline{R}(X) \neq U \Longrightarrow \overline{R}(X) = \left(\underline{R}(X^C)\right)^C \neq U \Longrightarrow \underline{R}(X^C) \neq \Phi$ i.e. X^C is R- $definble$.

Also if X is totally $R - undefinable$ then$\underline{R}(X) = \Phi \& \overline{R}(X) = U$, we show that

$\underline{R}(X^C) = \Phi, \& \overline{R}(X^C) = U$ since$\underline{R}(X) = \Phi \Longrightarrow \left(\overline{R}(X^C)\right)^C = \Phi$

$\Longrightarrow \overline{R}(X^C) = U$. And since $\overline{R}(X) = U \Longrightarrow \left(\underline{R}(X^C)\right)^C = U \Longrightarrow \underline{R}(X^C) = \Phi$.

(2) X is externally$R - undefinable \Leftrightarrow X^C$ is internally $R - undefinable \Longrightarrow$ $\underline{R}(X) \neq \Phi\ \& \overline{R}(X) = U \Leftrightarrow \underline{R}(X^C) = \Phi\ \& \underline{R}(X^C) \neq U \Longrightarrow \underline{R}(X) \neq \Phi \Leftrightarrow \left(\overline{R}(X^C)\right)^C \neq$ $\Phi \Leftrightarrow \overline{R}(X^C) \neq U \& \overline{R}(X) = U \Leftrightarrow \left(\underline{R}(X^C)\right)^C = \Phi \Leftrightarrow \underline{R}(X^C) = \Phi$.

Also X is internally $R-undefinable$- $\Leftrightarrow X^C$ is externally$R-undefinable \Longrightarrow$ $\underline{R}(X)=\Phi \Leftrightarrow \left(\overline{R}(X^C)\right)^C = U \Leftrightarrow \overline{R}(X^C)=U \& \overline{R}(X) \neq U \Leftrightarrow \left(\underline{R}(X^C)\right)^C \neq \Phi \Leftrightarrow$ $\underline{R}(X^C) \neq \Phi$.

From above example we have

Table summarizing interior, closure, boundary, Exterior, Category, and Accuracy of roughness of sets, W, X, Y, Z in (U, T_R), such that

$$W=\{2\}, X=\{2,3,4\}, Y=\{1,2\}, Z=\{2,5\}.$$

w.r.t. T_1

Set	Int	Clo	BN	EX	Category	Accuracy
W	$\emptyset$	$\{2,5\}$	$\{2,5\}$	$\{1,3,4,6\}$	Internally R-$indefinable$	0
X	$\{4\}$	$\{2,3,4,5\}$	$\{2,3,5\}$	$\{1,6\}$	Roughly R-$definable$	0
Y	$\emptyset$	$\{1,2,5\}$	$\{1,2,5\}$	$\{3,4,6\}$	Internally$R$-$indefinable$	1
Z	$\{2,5\}$	$\{2,5\}$	$\emptyset$	$\{1,3,4,6\}$	Roughly$R$-$definable$	1

Table (8)

w.r.t. T_2

Set	Int	Clo	BN	EX	Category	Accuracy
W	$\emptyset$	$\{2,5\}$	$\{2,5\}$	$\emptyset$	Internally$R$-$indefinable$	0
X	$\emptyset$	U	U	$\emptyset$	Totally$R$-$indefinable$	1
Y	$\emptyset$	U	U	$\emptyset$	Totally$R$-$indefinable$	1
Z	$\{2,5\}$	$\{2,5\}$	$\emptyset$	$\emptyset$	Roughly R-$definable$	0

Table (9)

$$T_3 = \begin{Bmatrix} U, \emptyset, \{1\}, \{2\}, \{4\}, \{1,2\}, \{1,3\}, \{1,4\}, \{1,6\}, \{2,3\}, \{2,4\}, \\ \{3,4\}, \{1,2,3\}, \{1,2,4\}, \{1,2,6\}, \{1,3,4\}, \{1,3,6\}, \{1,4,6\}, \\ \{2,3,4\}, \{1,2,3,4\}, \{1,3,4,6\}, \{1,2,4,6\}, \{3,4,5\} \end{Bmatrix},$$

$$T_3^C = \begin{Bmatrix} U, \emptyset, \{2,5\}, \{3,5\}, \{5,6\}, \{1,2,6\}, \{1,5,6\}, \{2,3,5\}, \{2,4,5\}, \{2,5,6\}, \\ \{3,4,5\}, \{3,5,6\}, \{4,5,6\}, \{1,2,5,6\}, \{1,3,5,6\}, \{1,4,5,6\}, \{2,3,4,5\}, \\ \{2,3,5,6\}, \{2,4,5,6\}, \{3,4,5,6\}, \{1,2,3,5,6\}, \{1,3,4,5,6\}, \{2,3,4,5,6\} \end{Bmatrix}.$$

w.r.t. T_3

Set	Int	Clo	BN	EX	Category	Accuracy
W	$\emptyset$	$\{2,5\}$	$\{2,5\}$	$\{1,3,4,6\}$	Internally $R-undefinable$	1
X	$\{2,3,4\}$	$\{2,3,4,5\}$	$\{5\}$	$\{1,6\}$	Roughly $R-definable$	$\frac{3}{4}$
Y	$\{1,2\}$	$\{1,2,3,5,6\}$	$\{3,5,6\}$	$\{4\}$	Roughly $R-definable$	$\frac{2}{5}$
Z	$\emptyset$	$\{2,5\}$	$\{2,5\}$	$\{1,3,4,6\}$	Internally $R-undefinable$	0

Table (10)

Conclusion

We have shown in this paper that the rough set is a standard model in information systems. This model has helped to constructing a topological space by using relationships resulting from the difference and generating the minimum of the construction set and we proved that the topological resulting is more accurate and stronger and is used to study the characteristics of the rough set. where some approximations were compared using the precision scale in order to determine the best.

Reference

[1] Kelley J.L. (1975),***General topology***, Graduate Texts in Mathematics,ISSN 0072-5285, Editorial universitaria de Buenos Aires.

[2] Lashin E.F., Kozae A.M., Khadra A. and Medhat A. A. (2005), ***Rough set theory for topological spaces***, International Journal of Approximate Reasoning, vol. 40, pp. 25-43.

[3] Pawlak Z. (1982), ***Rough sets***, International Journal of Computer and Information Science, vol. 11, no.,pp. 341-356.

[4]Pawlak Z. (1982), ***Rough sets***,International Journal of Information And Computer Science, vo.11: no.(5) pp. 341-356.

[5] Pawlak Z. (1991), ***Rough sets theoretical aspects of reasoning about data***,Vo.9 of System Theory, Knowledge Engineering and Problem Solver Kluwer Academic Publishers, Dordrecht.

[6] Rashed R. (2013), ***On Some Topological Approximations in Information Systems*** , Mathematics Department, Al-zawia University, Libya.

[7] Sierpenski W. and Krieger C. (1952), ***General topology***, University of Torranto Press.

[8] Yao Y. Y., ***Two views of the theory of rough sets in finite universes***, International Journal of Approximate Reasoning, vol.15, no.4, (1996), pp.191-317.

[9] Yao Y. Y., ***Information granulation and rough set approximation***, International Journal of Intelligent Systems, vol.16, no.1, (2001), pp. 87-104.

Combined DMS and DGS Techniques for Compact and Low Cutoff Frequency LPF Design

Sara M. Meeper, Amr H. Hussein, Mahmoud A. Attia

Electronics and Electrical Communications Engineering Department, Faculty of Engineering, Tanta University, Tanta, Egypt

***Abstract*- high performance and compact size low pass filters with narrow stopband and sharp cutoff characteristics are highly required in numerous wireless communication systems for noise and interference suppression. In this paper, a compact microstrip LPF with sharp cutoff characteristics is introduced. Defected ground structure (DGS) and defected microstrip structure (DMS) have been used to obtain wide stopband. The proposed filter is composed of two arc-shaped DGS units in the ground plane and a shaped microstrip line where stub and inset feed matching techniques is attached to enhance the pass band characteristics. This structure allows sharp cutoff frequency response and high harmonics suppression. Furthermore, it provides compact filter size without the need for cascading periodic DGS structures. The stop band attenuation is controlled by adjusting the depth of the inset feed and the length of the stub sections. It has a 3 dB cutoff frequency at 1.3725 GHz and it is as small as 20 mm × 19 mm.**

Keywords: Defected ground structure (DGS), Defected microstrip structure (DMS), arc-shaped, low pass filter (LPF).

1. INTRODUCTION

Microwave low pass filters are essential devices in RF wireless communication systems to remove noise, harmonics and other spurious signals. For these circuits, size compactness and high power attenuation levels throughout a broad stopband spectral range are desired properties to efficiently accomplish this task. Different techniques have been investigated i.e. using resonators, shaped transmission lines, and defected ground structures to achieve miniaturization of microwave filter. In [1-3] numerous low pass filters having wide stopband for moderate attenuation levels of about $-15dB$ to $-17dB$ are introduced. But as the attenuation level is increased to -20dB, the widths of the stopband of these filters are reduced. A compact asymmetric shaped microstrip low pass filter (LPF) with ultra wide stopband characteristics was introduced in [4]. The filter is based on Stepped Impedance Resonator (SIR). The asymmetric structure allows the suppressing cell to be located within the resonator structure without occupying a large area. So that the resulting filter occupies only a small area of about ($0.156\,\lambda_g \times 0.128\,\lambda_g$), where λ_g is the guided wavelength at $2.92\,GHz$. On the other hand, defected ground structures DGS are widely used to implement compact filters with good passband and stopband characteristics [5,6]. In [6] a compact LPF using double U-shaped DGS units at the ground plane and a shaped microstrip structure DMS on the top was introduced. It provides compact filter size without the need for cascading periodic DGS structures. But, it has relatively high cutoff frequency which equals 2.7 GHz. In [7], a sharp cutoff low pass filter using a tapered resonator has been introduced. But, the manufactured filter has an extensive circuit size. In [8] a compact low pass filter using stepped-impedance hairpin resonator (SIHR), split-ring resonator defected ground structure (ISRR DGS), and elliptical DGSs is introduced. Such structure exhibits low insertion loss and sharp cutoff characteristic. But, it provides high having $3\,dB$ cutoff frequency of $f_c = 2.5\,GHz$. On these lines, an improved Defected Ground Structure using H-slot resonators and coupling matrix method are introduced for compact Low pass /Band pass filters design [9]. The H-slot is used to serve as a DGS cell element for the microstrip line. The DGS component provides size reduction and has capability of harmonics and spurious suppression.

In this paper, an arc-shaped defected ground structure with defected microstrip line is proposed for implementation of compact size, sharp cutoff, and wide stopband low pass filter. Besides DGS and DMS, the inset feed and stub matching technique are utilized to adjust the impedance matching between the feeding port and the transmission line to enhance the input reflection coefficient. The use of this structure allows sharp cutoff frequency response and high stopband attenuation. Furthermore, it provides compact filter size without the need for periodic DGS structures. The proposed LPF is designed using the CST-MICROWAVE STUDIO simulator. The filter is simulated using Rogers's RO4003 substrate of dielectric constant $\varepsilon_r = 3.38$ and thickness $h = 1.524$ mm.

2. PROPOSED FILTER STRUCTURE

In this section, a new design for minimized size low pass filter with relatively flat pass band characteristics and low cutoff frequency is proposed. Keeping in mind the end goal to exhibit the viability of the proposed design, it is utilized for LPF design which is delineated in Figure 1. The designed LPF comprises of two arc-shaped DGS cells with a similar radius however with various widths. The DGS cell is embedded to give high attenuation over a wide stopband. Using the sharp cutoff frequency response of the etched arc-shaped DGS cells and considering the coupling effect between

slots in the ground plane can give the required elliptical characteristics of the filter. Likewise, a shaped transmission line is put on the upper surface of the substrate. The transmission line comprises of two segments of various widths where two open circuit twofold stubs are joined. The expansion of these stub segments controls the transmission line impedance which for sure gives a mean to control the attenuation level of the stopband. Besides, to control the input impedance of the transmission line, an inset feed is etched at the input port. The blend between the stub matching and the inset feed techniques provides more opportunity to control the attenuation level in the stopband. The detailed description of the DGS structure and the transmission line is appeared in Figures (2-a) and (2-b) respectively.

The proposed filter has been simulated using the CST-MICROWAVE STUDIO software using Rogers RO4003 substrate of dielectric constant $\varepsilon_r = 3.38$ and thickness $h = 1.524\ mm$ as the same as the double equilateral U-shaped DGS filter presented in [5] and the LPF presented in [6]. The dimensions of both DGS and DMS are listed in table (1).

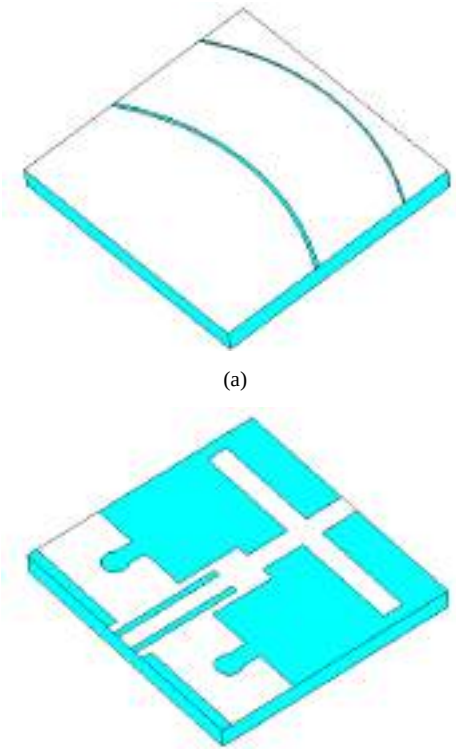

(a)

(b)

Fig. 1. (a) Back view and (b) Front view of the simulated CST design of the proposed low pass filter.

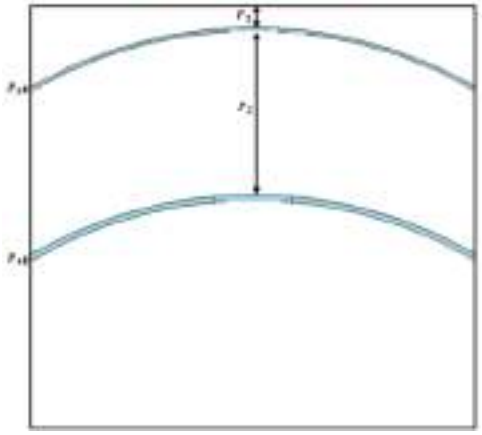

(a)

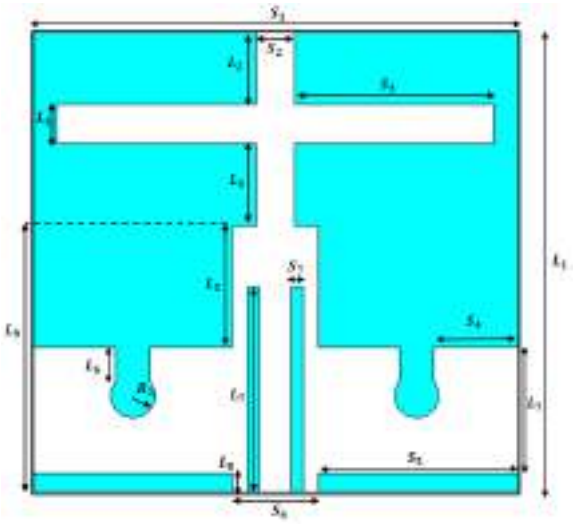

(b)

Fig. 2. Description of the (a) DGS and (b) DMS dimensions.

Table (1). The dimensions of both DGS and DMS

Dimension	Value in mm	Dimension	Value in mm	Dimension	Value in mm
L_1	19	S_1	20	R	20
L_2	3	S_2	1.6	p_3	0.17
L_3	1.6	S_3	8.2	p_4	0.29
L_4	3.4	S_4	3.5		
L_5	5	S_5	8.2		
L_6	1.39	S_6	3.5		
L_7	5.2	S_7	0.5		
L_8	0.8	p_1	1		
L_9	8.5	p_2	7.35		

3. SIMULATION RESULTS

In this section, the simulation results of the proposed arc-shaped DGS low pass filter is compared to both double equilateral U-shaped DGS low pass filter presented in [5] and

LPF presented in [6]. It is worth noting that the three filters are realized on the same Rogers RO4003 substrate with dielectric constant $\varepsilon_r = 3.38$, and thickness $h = 1.524\,\text{mm}$. Figure 3 shows the scattering parameters $|s_{11}|$ and $|s_{21}|$ of the proposed filter. The filter has low cutoff frequency of $f_c = 1.368\,GHz$. Lowering the cutoff frequency provides much wider stop band which indeed increases the noise and spurious harmonics suppression. The filter stop band extends from $1.368\,GHZ$ to more than $8GHz$ with $|s_{21}| \cong -20dB$. For comparison and showing the effectiveness of the designed filter, it is compared with the low pass filters introduced in [5] and [6] as shown in figure 4. The simulation results showed that the cutoff frequency is lowered from $2.58\,GHz$ and $2.7\,GHz$ to $1.368\,GHz$ that is for the filters presented in [5], [6], and the proposed one respectively. It is clear that the designed filter has sharp cutoff response in comparison to previous work. Besides these, it has a simple design structure.

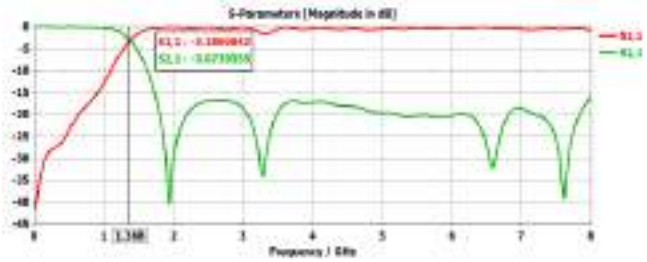

Fig. 3. The simulation results of the proposed low pass filter

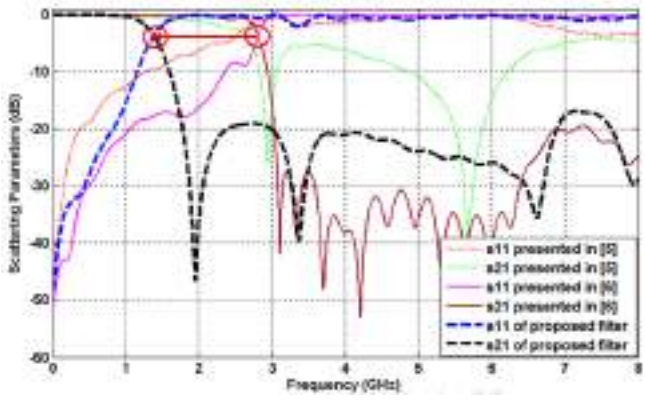

Fig. 4. Comparison between the scattering parameters of the proposed filter and the low pass filters presented in [5] and [6].

4. CONCLUSION

In this paper, an arc-shaped DGS and DMS are proposed for the execution of compact LPF filter with sharp cutoff frequency response and wide stopband. In addition, inset feed and stub matching techniques are used to adjust the input reflection coefficient of the filter. The proposed filter is realized on Rogers RO4003 substrate with dielectric constant $\varepsilon_r = 3.38$, and thickness $h = 1.524\,\text{mm}$. The filter stop band extends from $1.368\,GHZ$ to $8GHz$ with $|s_{21}| \cong -20dB$. The simulation results revealed that the designed filter has sharp cutoff response and much lower cutoff frequency in comparison with previous work. Besides these, it has a simple design structure.

REFERENCES

[1] WANG, J., CUI, H., ZHANG, G.,"Design of compact microstrip lowpass filter with ultra wide stopband", Electronics Letters, vol. 48, no. 14, pp. 854–856, 2012.

[2] WANG, J., XU, L. J., ZHAO, S., GUO, Y. X., et al. ,"Compact quasi-elliptic microstrip lowpass filter with wide stopband", Electronics Letters, vol. 46, no. 20, pp. 1384–1385, 2010.

[3] WANG, J. P., GE, L., GUO, Y. X., WU, W. ," Miniaturised microstrip lowpass filter with broad stopband and sharp roll-off ", Electronics Letters, vol. 46, no. 8, pp. 573–575, 2010.

[4]Mohsen HAYATI, Farzin SHAMA," A Compact Lowpass Filter with Ultra Wide Stopband using Stepped Impedance Resonator", RADIOENGINEERING, vol. 26, no. 1, pp. 269-274, APRIL, 2017.

[5] 10. Ting, S. W., K. W. Tam, and R. P. Martins, "Miniaturized microstrip lowpass filter with wide stopband using double equilateral U-shaped defected ground structure," *IEEE Microwave and Wireless Components Letters*, vol. 16, no. 5, pp. 240-242, 2006

[6] Abdulhadi AAA, Ashoka A, Jeberson W. Combined shaped microstrip line and DGS techniques for compact low pass filter design. Int. J. Eng. Technol., vol. 13, pp. 74–77, 2013.

[7] HAYATI, M., SHAMA, F., ABBASI, H. Compact microstrip lowpass filter with wide stopband and sharp roll-off using taper resonator. International Journal of Electronics, 2013, vol. 10 no. 12, pp. 1751–1759.

[8] Xi, D., Y.-Z. Yin, L.-H. Wen, Y. Mo, and Y. Wang, "A compact low-pass filter with sharp cutoff and low insertion loss characteristic using novel defected ground structure," Progress In Electromagnetics Research Letters, Vol. 17,pp. 133–143, 2010.

[9] A. Boutezdar et al., "An improvement of DGS lowpass/bandpass filters using H slot resonators and coupling matrix method," J. Microw. Opt. Electromagn. Appl., vol. 10, pp. 295–307, 2011.

Evaluation of Visual Performance of Religious Urban Open Spaces

(Case study: Al- Sayyida Nafisa Mosque Square in Cairo, Egypt)

تقييم الأداء البصرى للفراغات العمرانية ذات الطابع الدينى

(دراسة حالة فراغ مسجد السيدة نفسية بالقاهرة - مصر)

Nourhan Mahmoud Mohammed Ibrahim Ali

Teaching assistant at Tanta University, faculty of engineering, architectural department

Abstract

The visual performance of Al- Sayyida Nafisa Mosque Square in Cairo is analyzed in this paper. The aim of the present study is to derive a proposed evaluation model that service as a tool for evaluating the visual performance of religious urban open spaces. The research also tries to reach the best visual basics and criteria which support the design and planning process that must be taken in consideration when dealing with the religious urban open spaces. Research results showed that legibility, identity, determinants, aesthetics consistency, sense of nature, and supplements of urban open space help in enhancing the visual performance of urban spaces. We concluded that urban designers can enhance the visual performance by achieving the mentioned components appropriately.

1. Introduction

Designing attractive spaces could be achieved by understanding the visual structure around us. Definitely, we gain information about the space by using our senses, such as sight, smelling, hearing, tasting and some other complex ones. The sight is the most important sense, as it represents 87% of human perception to surrounding space (Bell, 2005). Visual perception is a major component in developing the image of the city. Accordingly, we can identify cultures, social mores and common values of the built space through visual resources (Radovic, 2003).

Several researchers in different fields were curious to the perception process: psychology (Gibson, 1950; Tomaszewski, 1986; Bańka, 1999), specifically behavioral and environmental psychology represented by H.M. Proshansky, T. O'Hanlon, W.H. Ittelson, L.G. Rivlin. (1977) and others, who analyzed the use of behavioral maps; anthropology and sociology (Hall, 1966; Sommer, 1967; Lawson, 2001) furthermore, geography (Wood, 1992), urbanism of cities and town planning (Lynch, 1960; O. Simonds, 1961; G. Cullen, 1961; D. Appeleyard & J.R. Meyer, 1964; Venturi,

1966; Krier, 1975; Ch. Alexander,1977; A. Rapoport, 1977; Stea, 1978; Winters, 1999; and many others) indicated the significance of the interaction between man and place, and the significance of how the images are created in the human memory. The Gestalt theory interested in the overall perception of the space, which means realizing the visual components as patterns which are related to each other, instead of many separated parts (Perusich, 2010).

Perception is an active process of gaining information from the environment through observation (Lang 1994). According to Sudarmadi, perception is a relationship between knowledge and awareness. Knowledge is the principles which are gathered through information. Awareness is an attention or sensitivity to different issues (Sudarmadi, 2001). Firstly, people discover the structure of the scene, to the stage where we understand what we observe. Secondly, we correspond our pre-existing knowledge with our new experience. Finally, we compose meanings or values for what we observe (Bell, 2005).

The type of activity in urban space defines the character of space. The present study focuses on religious urban open spaces which are distinctive at the city scale due to their centralized position, large size, and their association with religious buildings. They play a critical symbolic role, and are used for multiple purposes, such as cultural events, local trade, and social interaction. They are the cultural products of the city in which they always present social, cultural and religious meanings to a great variety of people (Stanley, 2012).

Many researchers have investigated urban open spaces from different sides, such as Kevin Lynch who concerned with the visual quality, the mental image (Lynch, 1960), performance characteristics, and psychological and sensual satisfactions (Lynch, 1990); Gordon Cullen who concerned with the visual sequence (Cullen, 1961); Robert Venturi who concerned with the social and cultural dimension (Venturi, 1966); Leon Krier who concerned with space determinants (Krier, 1975); Donald Appleyard who concerned with the physical and social complexities; Ralph Erskin who concerned with the social-cultural relations; Philip Johnson and et al. who concerned with the natural components of landscape (Trancik, 1986).

Generally, the life quality in the city is determined by the level of its visual performance. Sense of place is the result of the visual perception of the urban space details. Precisely, space is realized visually through three levels. The first level is to realize either physical or incorporeal space details such as colors, textures, shape, furniture, light, vegetation, scale, enclosure, etc. The second level is achieved by realizing the relationships between space details (e.g., unity, variety, balance, rhythm, hierarchy, Symmetry etc.). The third level is achieved as a result of using two or

more elements of the second level. When variety, balance, symmetry, etc. are achieved in urban open space, this leads to legibility, meaning, identity and sense of space.

2. The Aim of the Research

The main purpose of the present study is to derive a proposed evaluation model that service as a tool for evaluating the visual performance of religious urban open spaces. This model also helps to improve the visual image of these places, thus the improvement of city image. After studying several theories dealing with visual performance of urban open space, we reached to a proposed evaluation model based on a theoretical background **(Figure 1)**. This model will further be used for evaluation of Al- Sayyida Nafisa Mosque Square in Cairo **(Figure 2).** The importance of the study has additional strength in the fact that the religious urban spaces of Egypt are often criticized by the local population of the city, so, based on their perception, we can be reached to desirable objective visual elements in space.

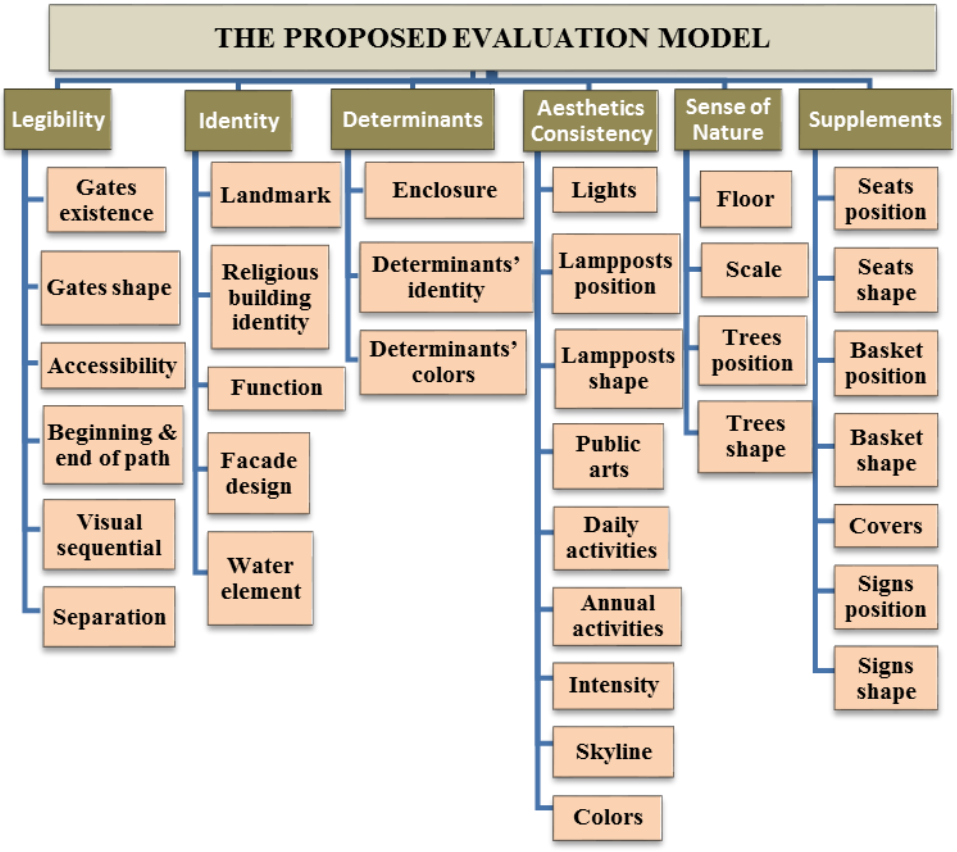

Figure 1. Shows the proposed evaluation model based on a theoretical background


Figure 2. Shows Al- Sayyida Nafisa Mosque Square in Cairo, Egypt

3. The Research Methodology

The research process consisted of several stages. The first stage included deriving a questionnaire which consisted of 34 items from previous approaches of studying space such as Kevin Lynch, Gordon Cullen, Robert Venturi, and etc. approach. The second stage: the questionnaire that consisted of 34 questions recording participants' perception for Al- Sayyida Nafisa Mosque Square. The participants were 50 Egyptian specialists in urban design, architectural design, and urban planning. They evaluated the space, by using a rating scale numbered from zero to four **(Table 1)**. This scoring method was derived from the one had been developed by CABE (2001), but was modified for the purpose of this research. The scale developed by CABE provided only a qualitative descriptor for the highest and lowest score and did not provide a descriptor that lent itself to numerical measurements. As some criteria in my checklist lend themselves to a subjective and qualitative response while others can be easily measured, and thus, quantified have included descriptors that address both situations.

Table 1. Shows the rating system

0	1	2	3	4
Not Existent (does not satisfy criterion at all)	**Poor** (satisfies criterion less than 25 percent of the time)	**Fair** (satisfies criterion 26 to 50 percent of the time)	**Good** (satisfies criterion 51 to 75 percent of the time)	**Excellent** (satisfies criterion 76 to 100 percent of the time)

Finally, we analyzed the answered questionnaire. The results showed that the space is suffer from the lack of its visual performance. Accordingly they need to be developed to enhance their visual performance.

4. The Results of the Research and Discussion

The research results show following:

Al- Sayyida Nafisa Mosque Square in Cairo (Table 2) (Figure 3)

Al- Sayyida Nafisa Mosque Square is a semi-circular square and has a total area of two acres. The space is surrounded by the mosque of Al- Sayyida Nafisa, youth center, school and the religious institution of Al-Sheikh Mohamed Metwally Al-Shaarawi. The space does not have fully developed shaped criteria that provide a desirable visual performance. The researcher evaluated it, and the majority of criteria were evaluated negatively. Also the reasons for negative evaluation are insufficient amount of natural elements, as well as the lack of gates, lights, seats, signs, and other supplements on the square. One of the essential problems there is the conflict between pedestrian movements and traffic that killing the space because they block pedestrian movement. The total result was 46/136 about 33.8%. The square needs to be developed to increase the efficiency of its visual performance.

Table 2. Shows summary of results

Legibility		**Identity**		**Determinants**		**Aesthetics Consistency**		**Sense of Nature**		**Supplements**	
Q1: Gates existence	1/4	Q7: Landmark	4/4	Q12: Enclosure	1/4	Q15: Lights	1/4	Q24: Floor	1/4	Q28: Seats position	0/4
Q2: Gates shape	1/4	Q8: Religious building identity	3/4	Q13: Determinants' identity	1/4	Q16: Lampposts position	1/4	Q25: Scale	1/4	Q29: Seats shape	0/4
Q3: Accessibility	3/4	Q9: Function	4/4	Q14: Determinants' colors	1/4	Q17: Lampposts shape	1/4	Q26: Trees position	0/4	Q30: Basket position	1/4
Q4: Beginning & end of path	1/4	Q10: Facade design	3/4			Q18: Public arts	0/4	Q27: Trees shape	1/4	Q31: Basket shape	1/4
Q5: Visual sequential	2/4	Q11: Water element	0/4			Q19: Daily activities	0/4			Q32: Covers	0/4
Q6: Separation	0/4					Q20: Annual activities	4/4			Q33: Signs position	1/4
						Q21: Intensity	3/4			Q34: Signs shape	0/4
						Q22: Skyline	3/4				
						Q23:Colors	2/4				
8/24		**14/20**		**3/12**		**15/36**		**3/16**		**3/28**	
Total result 46/136 =33.8 %											

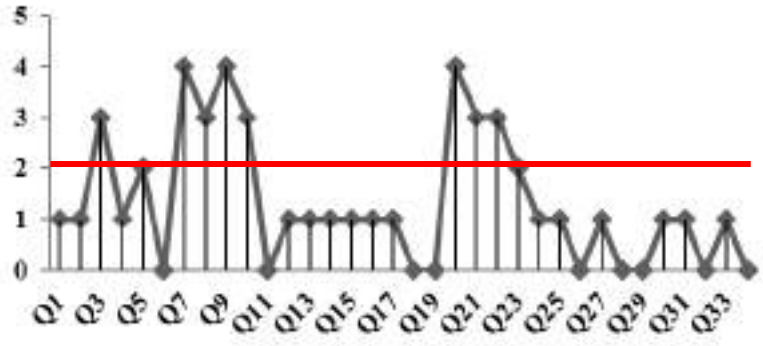

Figure 3. Diagram shows the lowest and highest scores of 50%

Finally, the results of the three urban spaces were convergent. The results showed that the three spaces are suffer from the lack of their visual performance. Accordingly they need to be developed to enhance their visual performance.

5. Conclusion

Visual performance of religious urban space directly reflects its value. Planning and design of the physical structure of the city, indicate the importance of an integrated approach to enhance the visual performance of religious urban open spaces. Religious urban open spaces of the city are seen as a visual aesthetic ambiences, as the center of religious activities, social interaction, as a place of rest, leisure, and inspiration that direct us for acquisitioning new impressions and experiences. Visual studies help in identifying the criteria for the design process of desirable religious urban spaces, with emphasis on visual - aesthetic dimension.

The analyzed religious urban open space (Al- Sayyida Nafisa Mosque Square) by specialists and experts, suggests that legibility, identity, determinants, aesthetics consistency, sense of nature, and supplement furniture of urban space, achieve desired visual effect on users. Spaces that do not have clearly defined visual identity in the structure of the city, and do not have legibility, were negatively evaluated. Also spaces which do not have aesthetic consistency between its components, and have low content of natural elements, were negatively evaluated. By the comparative analysis of results presented from Al- Sayyida Nafisa Mosque Square, it was concluded that there are many visual problems. Accordingly it need to be developed to enhance its visual performance.

Experts and users participate in the development of the city process. Religious urban open spaces are reflected as dominant through visual experience. Visual performance studies is indispensable factor in that process. It is concluded that a religious urban open spaces of Egypt as the primary visual resource of the city have potential, but it needs their revitalization, especially in terms of content and dynamics.

The contribution of this study is that the overall desirable visual performance of religious urban open space are identified on the basis of six factors (legibility, identity, determinants, aesthetics consistency, sense of nature, supplement furniture), which can serve as guidelines for the rehabilitation of existing and design of new religious urban open spaces of the city. Is desirable that the future directions of research would be based on the identification and analysis of specific religious urban open spaces independently and at the city level to identifying specific desired visual effects and criteria for the design of these spaces. Recommendations for appropriate design of religious urban spaces start from the fact that in this process should involve the user's premises and their needs. Visual performance of space is of primary importance for the creation of desirable urban spaces of the city.

References

- Asihara, Y. (1983). *The Aesthetic Townscape.* Cambridge, MA: MIT Press.
- Bal, Mansee. (2008). *Perceptions, Planning and Principles of Public Open Spaces (POS): Realities of Cape Town and Kosovo Informal Settlement, South Africa*. Erasmus University.
- Bell, Simon. (2005). *Elements of visual design in the landscape*. 2nd ed., Taylor & Francis e-Library.
- Cullen, Gordon. (1961). *The Concise Townscape*. Van Nostrand.
- Gibson, J.J. (1950). *Perception of the visual world*. Boston, Houghton Mifflin Company.
- Hall, Edward Twitchell. (1990). "The hidden dimension".
- Ittelson, W.H. (1960). *Visual Space Perception.* New York: Springer.
- Koffka, K. (1935). *Principles of Gestalt Psychology.* New York: Harcourt-Brace&World, Inc.
- Krier, Leon. (1975). "The reconstruction of the city".
- Lawson, Bryan. (2007). *Language of space*. Routledge.
- Lynch, K. (1960). *The image of the City.* Cambrige : MA:MIT, Pres.
- Lynch, Kevin. (1990). *City sense and city design: writings and projects of Kevin Lynch*. MIT press.
- Patil Resha, Patil Vinod. (2015). *Urban Spaces by Rob Krier-Review.* Research Paper.
- Perusich, Karl. (2010). *Cognitive Maps*. Purdue University, USA.
- Radovic, R. (2003). *Forma grada.* Beograd :Orion art; Novi Sad: Stylos.
- Trancik, Roger. (1986). *Finding lost space: theories of urban design*. John Wiley & Sons.
- Venturi, Robert. (1966). *Complexity and contradiction in architecture*. Vol. 1. The Museum of modern art.

Methodology to evaluate acoustic performance in educational spaces by Different Methods

Pro.Dr.Ahmed Abd-Alwahab Rezk[a], Pro. Dr. Huda Soliman Sideak[b], Dr. Hosny Ahmed Dewar[c], Dr. Mahmoud Muhamed Abd-Alrazik[d], Eng. Rania Abdo Aly-Aldean[e].

[a] Architecture Professor and Environmental design Architecture department, Tanta University, [b] Professor, Building Physics Institute Acoustic Department, (HBNC) [c] Lecturer of Architecture, Architecture department, Tanta University, [d] Lecture, Building Physics Institute, (HBNC), [e] Architecture department, Tanta University.

Abstract: Different methodologies used to evaluate acoustic performancein in educational lecture hall. Theses technical methods have been used in order to define the acoustic problems in lecture hall and suggest acoustic and architecture treatments to solve these acoustic problems. The methods that used for acoustic analysis were Sabin, Eyring, Arau-puchades and ODEON. This paper is foucing on acoustic performance in lecture hall 2 in Tanta Engineering. Acoustic study has been done for lecture hall as follows: Evaluation the acoustic performance by field measurements for reverberation time**,** manual calculation and acoustic simulation; ODEON software. Different acoustic performance analysis was performed. Different acoustic and architecture treatments were suggested based on the analysis. The final results of room acoustics of different cases carried on the hall were compered to the international requirements for educational spaces. The main problems based on the acoustic analysis are the increase of hall height, architecture design of ceiling and hard covering of the internal surfaces

Keywords: ODEON, Acoustic Performance, Reverberation Time, Acoustic Treatments, Acoustic simulation, ODEON, field measurments.

1. INTRODUCTION

Acoustic measuring and simulation are very important to determine acoustic performance and acoustic comfort in spaces.Computer simulations to predict acoustical parameters have been attracting renewed interest in recent years. New technologies for acoustic simulations and measurements have been developed, and it is now possible to predict and measure the acoustics of a room with good accuracy[i].

There are many acoustic software programs in room we will use ODEON because, it cares acoustic side only in first step. It gives complete impression of acoustic performance in space, and results are given out in both graphical representations and tables. It gives most important criteria in space acoustics are usually reverberation time (RT) by (Sabin, Eyring and Arau-puchades) and speech transmission index (STI), early reflection in room (C50), sound pressure level (SPL), sound transmission class (STC) in this study we will foucse on RT[ii].

Acoustic measurements are the obvious prerequisite of acoustic investigations; they are an important tool for the analysis of acoustical problems. Acoustics of educational spaces (classrooms, lecture halls or speech rooms and auditoria) engross the attention of the researchers in this field in the past years. Thus, researches in this field has been going n over the years with the aim of enhancement acoustic performance in educational spaces in universities through studying the most important factors affecting the acoustics performance in educational spaces is relation between RT and space hall. We will calculate RT for one of education spaces by manual equation, field measurement, and simulation by software, and compare final results of reverberation time (RT) with RT require for educational spaces[iii].

We scope this study on main lecture hall 2 in engineering faculty, Tanta University, it located in ground floor of college building (Workshop building), Engineering faculty, Sebrbay colleges' campus, next to Workshop spaces and main quad it`s known Eadady Modarg figure (1).

1. Preparatory Building, Department of Electrical powers And Administration
2. Architecture Department and Administration
3. Library , Mechanical Power Department, Math And Physics Department
4. Building and Construction Building
5. Civil Department
6. Workshops
7. Lecture hall 1&2 (Case study)
8. Main arene.
9. Green Area.

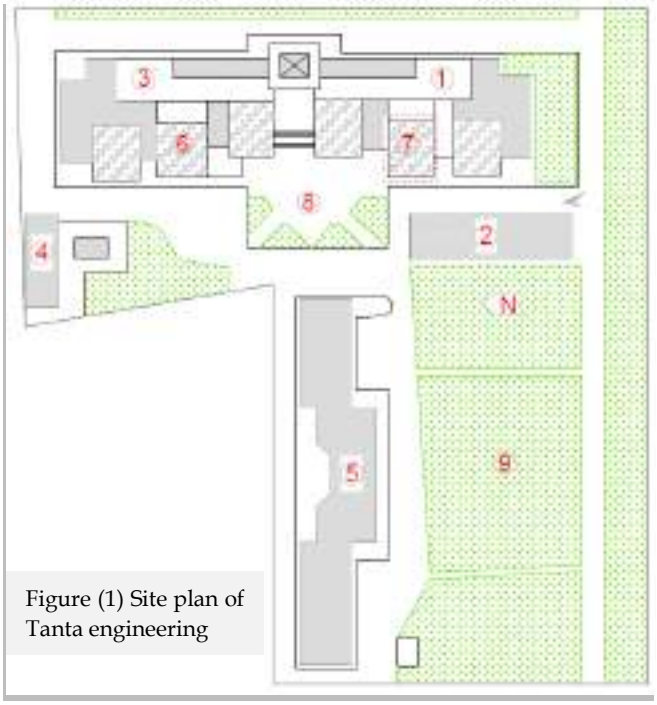

Figure (1) Site plan of Tanta engineering

Table (1) Description of Lecture hall 2

Dimensions

L	W	H	Area m^2	Volume m^3
29.7 **m**	19.3 m	10.6 **m**	573.2	6076

Statistical Data

Desks 19 wooden row, with 1m (W), 1m (H), 10 cm the row higher from row previous.
Stage, concrete, 2.65m (W), 13.10 (L), The distance to first row 2.35 m **.**
Hall is divided into 6 modules, width of each about 5m.
Interior surface are covered up with hard finishing, ceiling has skylight in each hall.
Sound system, amplifier, microphone and 8 loudspeakers, 4 at each side

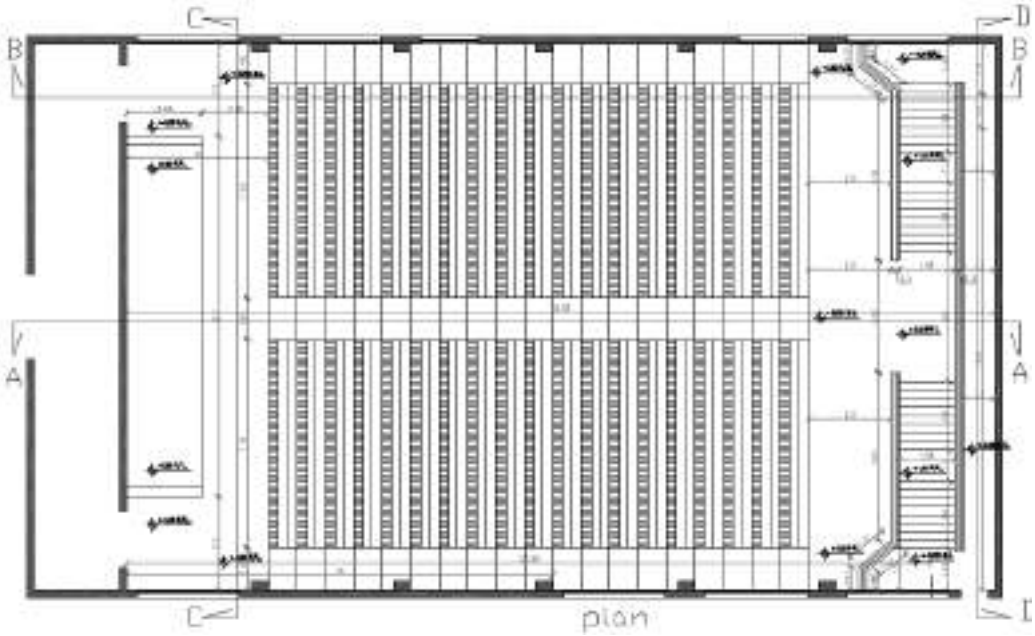

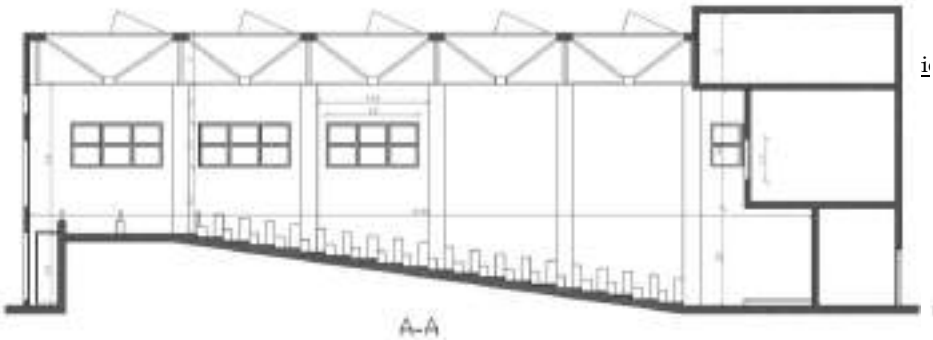

Fig (4) Elevation of side wall

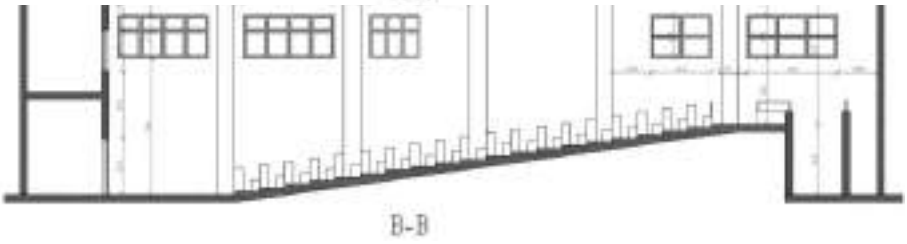

Fig (5) Elevation of side wall

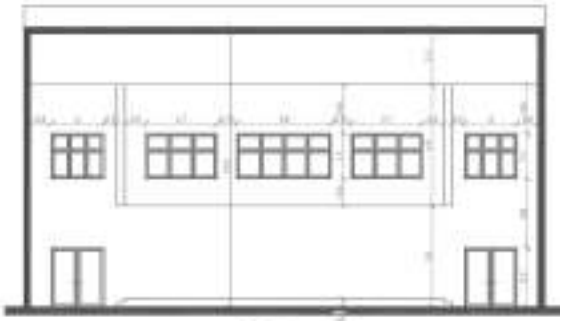

Fig (6) Elevation of front wall

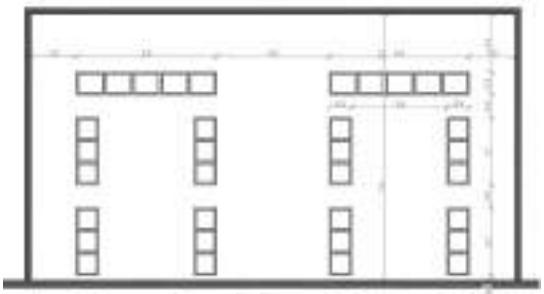

Fig (7) Elevation of rear wall

2- Methodology

a- Selection case study.
b- Architecture describe for case study.
c- Calculate requirement RT for case study by equation.
d- Done field measurement by devices in case study.
e- Evaluation basic case from field measurement results.
f- Entering architecture data for case study in acoustic software simulation.
g- Done acoustic simulation for case study model.
h- Evaluation basic case from acoustic software simulation results.
i- Calabrat acoustic software program and compare RT results by manual equation, field measurement, and acoustic program simulation.
j- Determin acoustic problems in case study.
k- Suggestion acoustic and architecture treatments

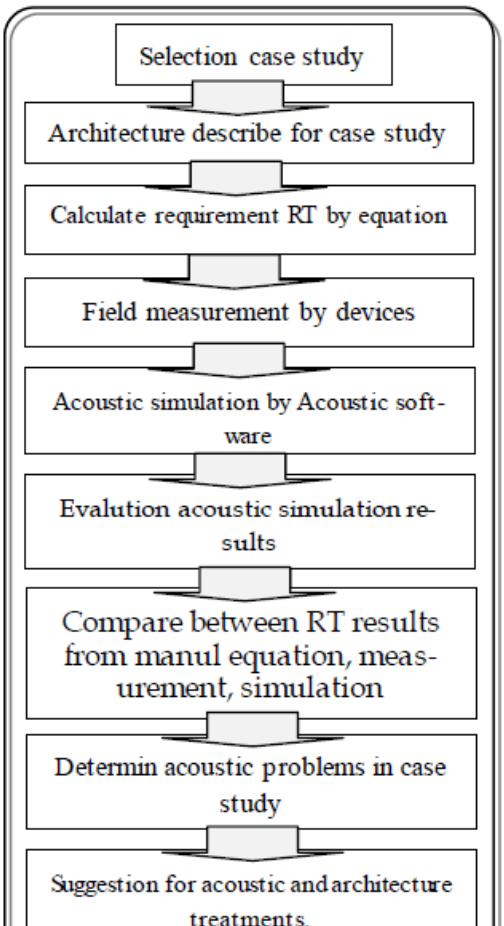

Figure (8) AcousticEvalution Methodology for space

2.1. RT by Manual equation

In previous paragraph we selected case study and architecture describe then determine requirement reverberation time for hall from equation

TR= [0.32 * lg (V) – 0.17]s , , (V) space size,

Whereas TR depends on space volume, required reverberation time is based on furnished occupied areas. When unoccupied TR, should no more than 0.2 s over required time. (Vary 20% in frequency range 250 Hz to 2000 Hz).the figure shown chart of Requirement reverberation time range for speech spaces[4].

Table (2) for RT require values at differnat frequency

	125 HZ	250 HZ	500 HZ	1000	2000	4000	8000
RT requirement	1.48	1.05	1	1	1	1	1

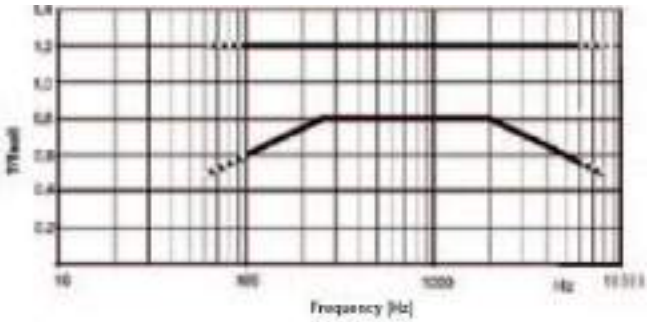

The frequency depending RT (Reverberation Time) range for speech.

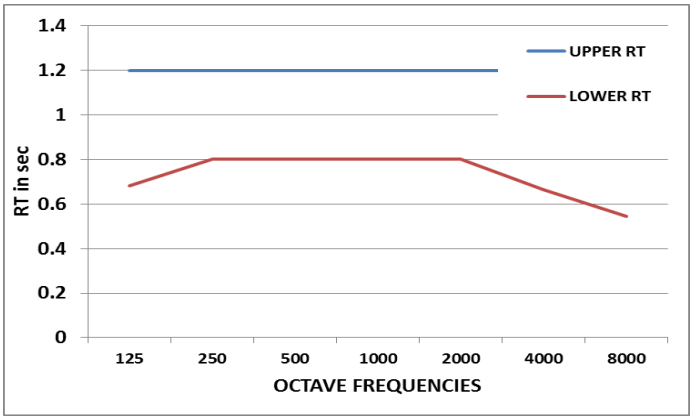

Fig (9) Chart of RT require for hall (case study) Range (0.6-1.2)

2.2. RT by Field measurement for basic case

Acoustic measurements are main prerequisite of acoustic investigations. In this research measurements depend on reverberation time measured, it is done through following**:**

1- **Used Devices:** there are a lot of types of acoustic measuring equipment but in this research we use Hand-held Analyzer Type 2270 (B&K) is use with connection of condenser microphone type 4189 (B&K) and omnidirectional loudspeaker type 4292 (B&K) with power amplifier 2716 (B&K). Using the reverberation time Software BZ-7227.

2- **Work Method:** analyzer generates noise test signal and excites the space of the room through third octave filtered noise signal figure (11). The reverberation time measured in different points through the room at the seating area figure (10). The reverberation time measured using white or pink noise at 1/3 octave band from 125 to 8000 Hz. And calculate the average reverberation time for measurements in space.

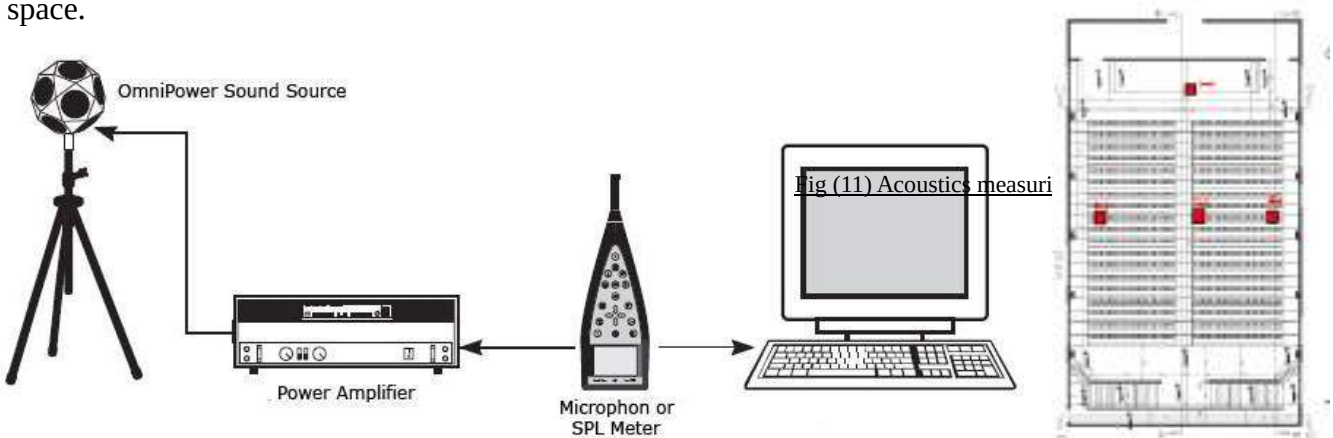

Fig (11) Acoustics measuri

Freq.HZ	point 1	point 2	Point 3	Point 4
125	3.44	3.64	4.75	3.4
250	4.44	3.76	3.66	3.11
500	6.58	4.36	3.98	3.8
1000	7.08	4.31	4.8	4.17
2000	3.8	3.63	3.59	3.26
4000	2.32	2.83	2.34	2.34
8000	1.4	1.33	1.24	1.31

Fig (10) Points for Reverbera-tion Measurements in hall

2.2.1. Results of field measurements

Table (3) Reverberation time measurements at 4 points in hall

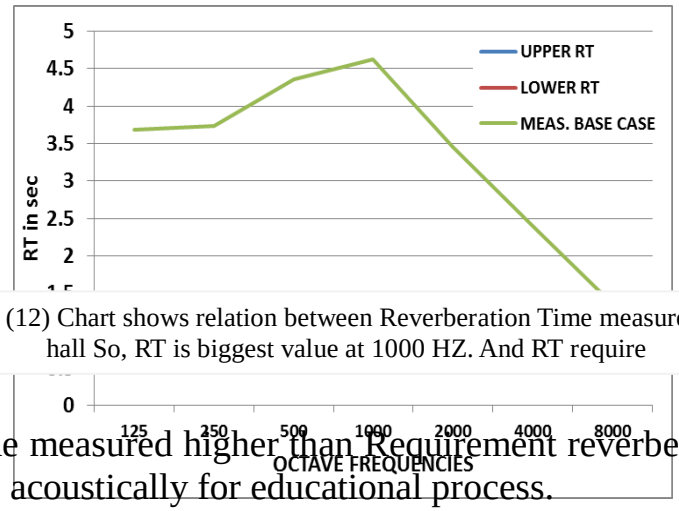

Fig (12) Chart shows relation between Reverberation Time measured in hall So, RT is biggest value at 1000 HZ. And RT require

From chart at figure (12) Reverberation time measured higher than Requirement reverberation time range for hall, thus the hall is unsuitable acoustically for educational process.

2.2. **RT by Computer software simulation for basic case**

We evaluate basic case acoustically by ODEON software version 9.2, and calibrate program, acoustic simulation at 3 point in different places, this is through several stages:

1- ODEON software
2- Create hall model and entering acoustic data
3- Simulation for hall acoustic performance
4- Results
5- Calibrate

2.3.1. Results of acoustic hall (BASICE CASE) by ODEON At receives 1, 2, 3

- Table (4) shown results of acoustic parameters RT

T30(s)sim

Rec. no.	63	125	250	Average 500	1000	2000	4000	8000
1	3.33	3.4	3.5	3.77	4.93	3.78	2.56	1.6
2	3.61	3.89	4.13	4.29	5.05	4.35	2.33	1.19
3	4	4.07	3.98	4.13	4.93	3.95	2.62	1.4

T30(s)	**63Hz**	**125**	**250**	**500**	**1000**	**2000**	**4000**	**8000**
	3.65	3.78	3.87	4.06	4.97	4.03	2.5	1.4

- Table (5) shown results average of acoustic parameters

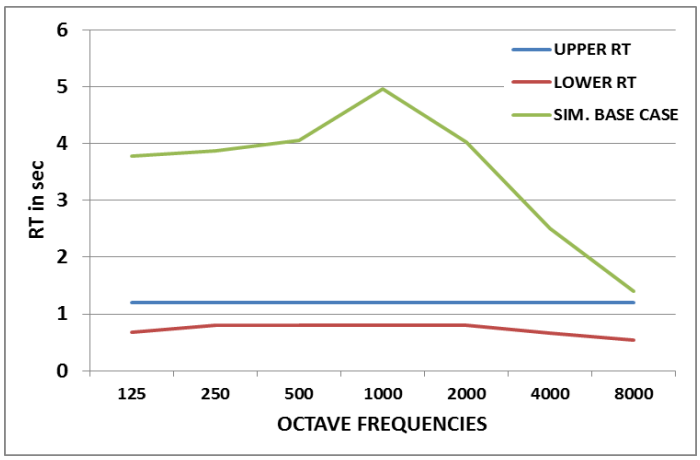

From chart figure (13) Reverberation time simulated higher than Requirement reverberation time range for hall, thus the hall is unsuitable acoustically for educational process.

Fig (13) Chart shows relation between Reverberation Time simulted in hall so; RT is biggest value at 1000 HZ. And RT require

2.3. R T by Sabin, Eyring, Arau-puchades

From figure (14) RT is higher than Requirement reverberation time range for hall

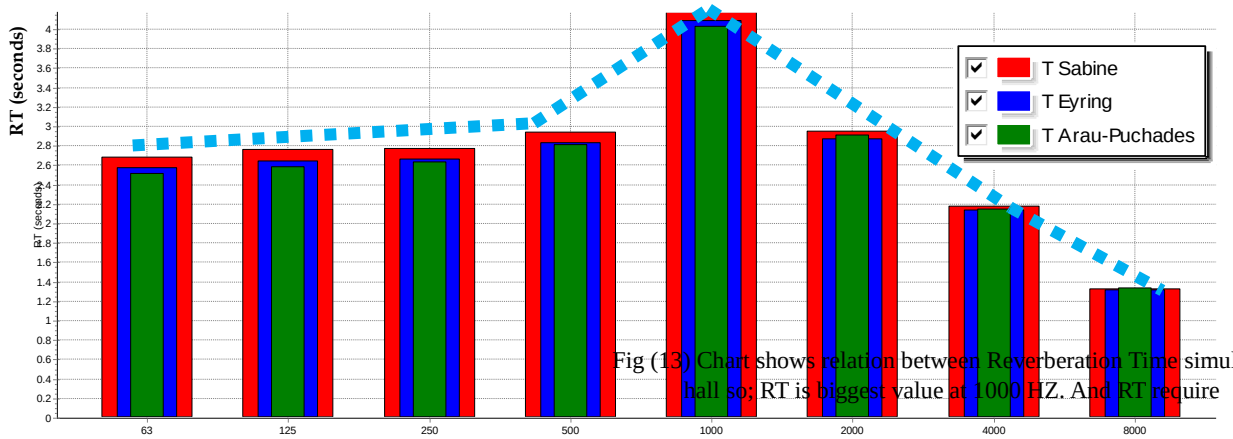

Fig (13) Chart shows relation between Reverberation Time simulted in hall so; RT is biggest value at 1000 HZ. And RT require

Figure (14) shows RT by Sabin, Eyring, Arau-puchades

From chart figure (13) Reverberation time simulated higher than Requirement reverberation time range for hall, thus the hall is unsuitable acoustically for educational process.

Final results through compare between RT require & RT measure & RT simulation.

- Table (6) shows RT values (requirement, measurement, simulation)

	125 HZ	250 HZ	500 HZ	1000	2000	4000	8000
RT requirement	1.48	1.05	1	1	1	1	1
RT average (Measuring)	3.68	3.73	4.36	4.62	3.46	2.4	1.36
RT average (Simulation)	3.78	3.87	4.06	4.97	4.03	2.5	1.4

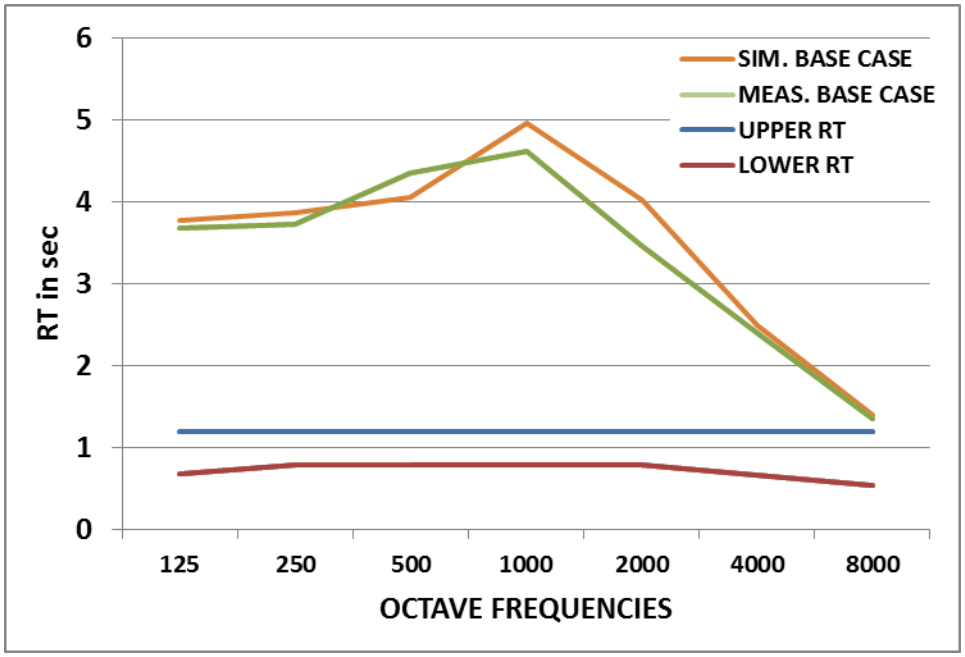

Fig (15) Chart shows relation between RT values for (requirement, measurement, and simulation)

From chart in figure (15)

- There is no high difference between RT mea & RT sim, thus the program was calibrated,
- RTmeasure & RTsimulate are higher than RTrequire.
- The hall is acoustically unsutable and has acoustic problems.
- The hall needs acoustic and architecture treatments to solve acoustic problems and enhancement acoustic performance in it..

3. Conclution

Methodology to evaluate acoustic performance in universities`educational spaces and selecation acoustic problems to suggeste acoustic and architecture treatments to solve this determined problems.

4. Acknowledgement

I`m thankful to alla then my doctors, Pro. Dr. Ahmed Rizk, Pro.Dr. Huda sideak, Dr. Hosny Dewar, Dr. Mahmud Abd-Alrazikfor for supporting and helping me.

5.Referances

Martín. R. S, Arregui. A, Machín. J and Arana. M, "Comparison of Measured and Simulated Room Acoustic Parameter Values Using High Resolution Grids" Acoustics Australia, 2014.

[1] Ying Ye, Qifan Fu, "Studies on the Accuracy of Acoustic Simulation based on EASE Software", IEEE, 2014.

[1] Mahdavi.A, Kainrath, B, Orehounig. K, Lechleitner, J, "Measurement and Simulation of Room Acoustics Parameters in Traditional and Modern Bath Buildings", Build Simul (2008).

[1] DIN 18041- Room Acoustic-

جامعة طنطا

كلية الهندسة

قسم الهندسة المعمارية

"تأثير الصوت والتهوية على البيئة التعليميه الخاصه بأطفال المتلازمه داون"

أ.د. أحمد عبدالوهاب رزق
رئيس قسم الهندسة المعمارية سابقا – كلية الهندسة
جامعة طنطا

د. أحمد حسين أبوالسعادات
مدرس بقسم الهندسة المعمارية – كلية الهندسة
جامعة طنطا

سهام على حامد الموزي
معيدة بقسم الهندسة المعماريه – كلية الهندسه - جامعة طنطا

الملخص :

دائما ما يبحث المعماري عن كيفية تنظيم الفراغ وتوظيفه واستغلاله بصورة جيده ليمكن المستخدم من أداء وظيفته وممارسة الأنشطة المختلفة في راحة وظروف ملائمة ، حيث نجد ان عناصر تصميم أى فراغ لها تأثير مباشر على المستخدم ، فكل ما نلمسه بأيدينا ويقع عليه بصرنا وتسمعه أذاننا وتتفاعل معه كافة حوسنا يعتبر جزء من التجربة الفراغية المعمارية .

كذلك فإن مصمم الفراغ يتجه دائما من خلال عناصر التصميم الى تلبيه الاحتياجات النفسية للمستخدم والتى تؤثر فى اتجاهاته وافكاره وأرائه وميوله وسمات شخصيته وتحقيق له الراحة الحسية والنفسية .

ويختص هذا البحث بدراسه وتتبع اهم الجوانب المحيطة بطفل المتلازمة داون ، والمؤثره على إدراكه وانطباعاته النفسية أثناء تواجده بالفراغ ، ويمكن تحديد أهم تلك العناصر فى الصوتيات والتهوية داخل الفراغ كجزء من قيمة الفراغ المحيط به .

الكلمات الأفتتاحيه : متلازمه داون – الفراغ المعماري .

المقدمة :

إن البيئة المحيطة بالأفراد تحتوى على العديد من العناصر المؤثرة عليه والتى تتفاعل مع حواسه المختلفة ، وقد ذكرت ميليسنت جابل أن التكوين العاطفى والجسدي للإنسان يتأثر بستة عناصر بيئيه وهى :

الصوت .
التهوية .
اللون .
الرائحة .
الشكل .
الملمس .

فهذه العناصر لها تأثير كبير على الصحة النفسية والجسدية للأفراد ، ولهذا فهى ترى أن التصميم الجيد لأى منشأة طبية لابد أن يراعى تلك العناصر والتى يمكن اعتبارها جزء مهم من العلاج . (1)

ويمكن تحديد أهم تلك العناصر والتى لها تأثير قوى على مستخدمى أى فراغ معمارى ويتم تركيز الدراسة البحثية عليها وهى : **الصوت ، التهوية .**

مشكلة البحث :

نجد أن من اهم الأمور التى تؤثر على سلوك أطفال المتلازمة داون هى المعالجة الصوتية للفراغ المعماري ، حيث نجد أن الفراغات التى لا تعالج مشاكل ارتداد الصوت وارتفاع مستويات الضجيج غير مقبولة على الأطلاق وتؤثر بصورة سلبية علي سلوك مستخدمى الفراغ .

كما نجد أن التهوية الطبيعية هى أفضل أنواع التهوية على الإطلاق لما لها من منافع عضوية جيدة على الفرد ، لذا يجب مراعاة تصميم فراغات ذات تهوية طبيعية جيدة .

الهدف من البحث :

يهدف البحث الي دراسة اهم الأمور التى تؤثر على سلوك أطفال المتلازمة داون وهى المعالجات الصوتية والتهوية الطبيعية للفراغ المعماري بهدف زيادة قدرة الأطفال وزيادة المهارات التعليمية لديهم أثناء تواجدهم داخل الفراغات التعليمية .

منهجية البحث :

تقوم منهجية البحث علي مايلي :

- تناول تعريف عام للمتلازمه داون وأهم إحصائيات تلك المرض ومدى إنتشاره عالميا ومحليا .
- تعريف الفراغ المعماري ودراسه توضيحية لكل من المعالجات الصوتية والتهوية كجزء من قيمة هذا الفراغ وكيفيه تأثيرهم على الصحة النفسية والجسدية لمستخدمى الفراغ .

تعريف المتلازمه داون :

تشير كلمة متلازمة إلى مجموعة من العلامات و الخصائص التي توجد و تظهر مجتمعه في أن واحد . أما كلمة داون فهي اسم العالم الانجليزي الدكتور جون لانغدون داون "DR.John.Langdon.Down".

والمتلازمة هذه هي عبارة عن شذوذ صبغي (كروموسومي) يؤدي وجود خلل في المخ والجهاز العصبي ،ينتج عنه عوق ذهني واضطراب في مهارات الجسم الإدراكية والحركية ، كما يؤدي هذا الشذوذ إلى ظهور ملامح وعيوب خلقية في أعضاء ووظائف الجسم ، وهي ليست مرضاً بل عرضاً يولد به الطفل . (4)

وهذا الشذوذ الصبغي ، لايحدث نتيجة خلل في وظيفة جهاز من أجهزة الجسم أو نتيجة للإصابة بمرض معين ،كما أنه ليس بالضرورة أن يكون حالة وراثية ، بل هو تقدير من الله تعالى يحدث أثناء انقسام الخلية عند بداية تكوين الجنين.وعلية فإن أي زوجين بدون تمييز معرضين لأن يولد لديهم طفل ذو متلازمة داون . (2)

وقد زاد متوسط العمر للأفراد الذين يعانون من متلازمة داون بشكل ملحوظ إلى 60 عام من العمر . و تتطلب هذه الحقيقة وحدها تحسين نوعية التعليم في المدارس ومواصلة التعليم، والتدريب على العمل، لتعزيز الإنجاز عبر مراحل العمر . (5)

إحصائيات عن المرض ومدى إنتشاره عالميا ومحليا :

يختص هذا الجزء بعرض إحصائيات عن مرض المتلازمه داون فى الفترة الزمنية الأخيره لبيان مدى إنتشاره وضروره الإهتمام بهذه الفئه عدم الإغفال عنها .

نسب حدوث متلازمه داون عالميا :

طبقا " لمراكز مراقبة الأمراض والوقاية منها " فى الولايات المتحدة ، نجد أن ما يقرب من 6000 طفل يولدون سنويا مصابين بالمتلازمه داون أى ما يقرب من 1 من كل 691 مولود ، كما يلاحظ أن 80 % من هؤلاء الأطفال لامهات دون سن 35 عام . (6)

ولكن يتراوح هذا المعدل من الإعاقة العقليه بين المعتدلة إلى الشديدة ، ووفقا لأخر إحصائيات حدثت فى عام 2012 نجد أن أكثر من 400 ألف شخص يعانون من متلازمه داون داخل الولايات المتحدة وفقا لما ذكره المجلس القومى لمتلازمه داون . (7)

نسب حدوث متلازمه داون محليا (فى مصر) :

نجد طبقا للجهاز المركزى للتعبئه العامه والأحصاء فى مصر عام 2006 وجد أن نسبه المعاقين فى مصر وصلت إلى 3,4 % من إجمالى عدد السكان ، كما أتضح أن الإعاقة العقلية تمثل مركز ثقل فى عدد ونسبه المعاقين حيث تصل النسبه إلى 73 % من إجمالى المعاقين يليها بعد ذلك الإعاقة الحركية بنسبه 0.14 % ثم بقيه الإعاقات بنسبه 0.13 % .

وطبقا لاخر إحصاءات للجهاز المركزى بمصر أن عدد المعاقين عقليا 106464 ينقسم الى 66945 من الذكور و 39519 من الإناث ، وهؤلاء يحتاجون إلي عناية خاصة من جانب الدولة والمجتمع والاسره ، خاصة وان الطفل المعاق ذهنياً في المجتمعات النامية ومنها مصر يمثل عبئاً علي الاسره والدولة ، ومن ثم تحتاج هذه المجتمعات إلي التقليل من أضرار مشكلة الاعاقه الذهنية التي ترتبط بالكفاءة العقلية للأفراد الذين يعتمد عليهم المجتمع في بنائه وتطوره. (3)

مفهوم الفراغ المعماري :

يمكن تعريف الفراغ المعماري بشكل مبسط، يفيد الدراسة الحالية، بأنه جزء من الفراغ العام، تم اقتطاعه بمواصفات ومحددات خاصة، تجعله يصلح لأن يمارس فيه الإنسان أنشطة حياتية خاصة، وتتوقف هذه الأنشطة وطريقة أدائها على طبيعة الجزء المقتطع وحجمه وهيئته التصميمية وعلاقته بالفراغ العام المحيط به.

ذلك هو التعريف الذي يرتبط في الأساس ببيان مكونات الفراغ المعماري وطريقة تصميمه وتشكيل هيئته الداخلية وانعكاس كل ذلك على الهيئة المعمارية الخارجية للمبنى، أو انعكاسه أيضاً على الإحساس بالفراغ . (8)

أولا الصوتيات :

من اهم الأمور التى تؤثر على سلوك أطفال المتلازمة داون هى المعالجة الصوتية للفراغ المعماري ، إذا أن الفراغات التى لا تعالج مشاكل ارتداد الصوت وارتفاع مستويات الضجيج غير مقبولة على الإطلاق ، ولاسيما الفراغات التى يتواجد بها الأطفال ذوي الإعاقة الحسية أو ممن لديهم صعوبات فى الاتصال . (9)

أشار كل من ماكسول وإيفانس فى دراستهما أن الضوضاء تؤثر سلبا على قدرة الأطفال على التركيز ، حيث قام المدرسون بتقييم مهارات الأطفال قبل إجراء المعالجة الصوتية للفراغ وبعدها ، وأوضحت النتائج – بعد استخدام ألواح ماصة للصوت داخل الفصل – ان معدل أداء الأطفال قد ارتفعت عنها قبل المعالجة الصوتية ، كما وجد ان الأطفال أكثر مشاركة فى الفصول الهادئة عنهم فى الفصول ذات الضوضاء. (10)

فللضجيج الذى يشعر به الاطفال داخل الفصول لها عدة مصادر منها : (11)

- الضوضاء الناتجة عن الأنشطة الدراسية .
- الضوضاء الناتجة من مصادر الضوضاء الخارجية .
- الضوضاء الناجمة عن الخدمات الهندسية بالمبنى مثل تكيفات الهواء والتدفئة والإضاءة .
- الضوضاء الصادرة من معدات التدريس .

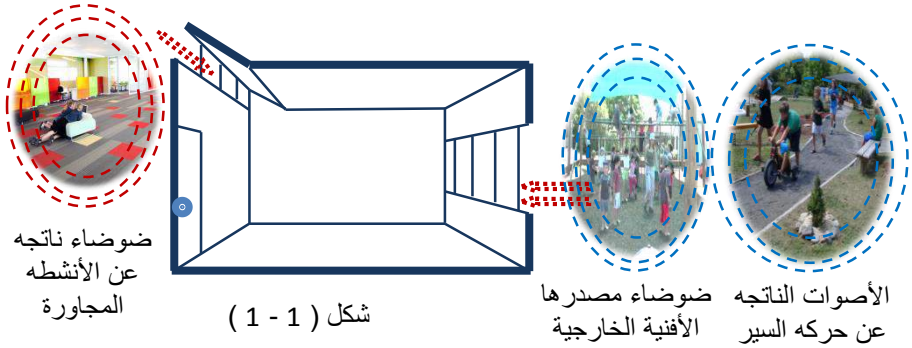

شكل (1 - 1)

مصادر الضوضاء المختلفه التى تؤثر على الطفل داخل الفصل

وقد أثبتت الدراسة التى قام بها كل من شيلد ودوكرل أن مستوي الضوضاء له تأثير كبير على المهام اللفظيه عند الأطفال داخل الفصل ، مما يزيد من الصعوبات التى يواجهها الأطفال مع المهارات اللغوية . (12)

ونجد أن الإنعكاسات الصوتيه الناتجه عن الأسطح ذات الخواص العاكسه تكون غير ملائمه لاحتياجات الأطفال لأنها تشتت انتباههم ، وهى أيضا تكون مزعجة للأطفال الذين يعانون من ضعف السمع .

ولهذا يمكن الأخذ فى الاعتبار عدة نقاط لتجنب الاثار السلبية للضوضاء على الاطفال أو مستخدمى الفراغ بشكل عام ، وذلك بواسطة : (12)

- اختيار موقع المدرسة ، والتخطيط الداخلى لها حيث تكون الفصول الدراسية بعيدة عن الضوضاء الصادرة من الخارج مثل حركة المرور ، بالإضافه إلى تحقيق أدنى حد ممكن من مستويات الضوضاء الداخلية فى الفصول الدراسية لضمان تحقيق أفضل الظروف للتعليم والتعلم .
- إستخدام مواد عازلة للصوت فى تشطيب الحوائط والأرضيات .

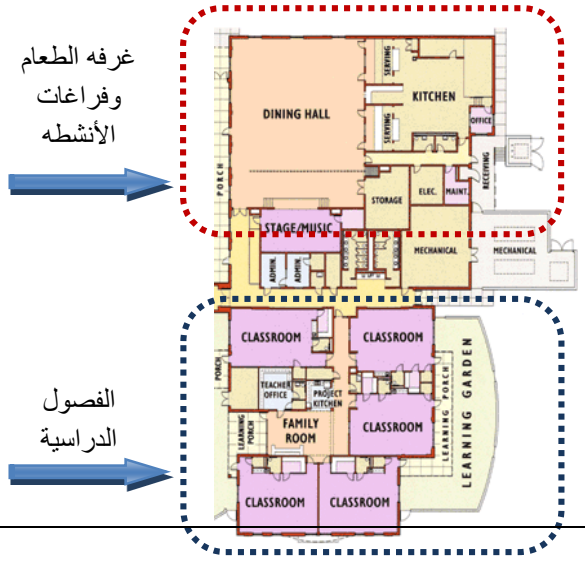

شكل (1 - 2)

مسقط أفقي لتوضيح إختيار موقع الفصول الدراسيه التى تحتاج إلى هدوء حيث تكون بعيده عن الفراغات التى تسبب الضوضاء .

المصدر:

http://www.designshare.com/Awards/2003/projects/file.asp?ID=2

ويمكن عزل الضوضاء الخارجية ، وذلك بواسطه : (13)

- فصل الأماكن المثيرة للضوضاء بعيدا عن الفراغات الدراسية التى تحتاج الى هدوء .
- وضع الفراغات الهادئة على أفنية داخلية ، مع مراعاة تصميم حوائط سميكة للجدران الخارجية .
- توفير فراغات منغلقة للحد من الضوضاء والتشويش الذى قد يصدر من الأنشطة الأخري .
- التحكم فى الضوضاء التى تنتج عن أجهزة التكييف وذلك عن طريق وضع المعدات الميكانيكية بعيد عن الفصول الدراسية أو بالقرب منها ، وهذا عن طريق وضعها على أسقف المبنى على سبيل المثال .
- زراعة الأشجار بالقرب من المبنى لمنع وتقليل الضوضاء الأتيه من الخارجي كتلك الناتجة عن حركة الطرق والسيارات .

شكل (1 - 3)

إستخدام الأشجار كحاجز صوتى لحجب الضوضاء الناشئه عن السيارات وحركه الطريق .

المصدر:

http://www.fhwa.dot.gov/environment/noise/noise_compatible_planning/federal_appro

- تصميم فراغات تسمح بانتقال الموجات الصوتية بشكل واضح وملائم لمستخدمى الفراغ وذلك من خلال :
  - تصميم فراغات متوسطة الحجم .
  - تفادى البؤر الصوتية وذلك بعدم تصميم الأسقف المنحنية .
  - إستخدام مواد عاكسة للصوت بكميات وأبعاد وزوايا خاصة وتوزيعها بداخل الفراغ بحيث لا تتركز فى جانب واحد منه .

ثانيا التهوية :

إن توفير التهوية الطبيعية والهواء النقي داخل الفراغات أمر ضروري فى جميع المدارس ، حيث تؤثر التهوية الطبيعية تأثيرا كبيرا على صحة الفرد وشعوره بالراحة داخل الفراغ ، وهناك بعض التوصيات الواجب مراعتها عند التصميم ، وهى كالتالى : (9)

- إحلال الهواء النقي محل الهواء الفاسد ، بمعنى إمداد المبنى بقدر كاف دائما من الاكسجين ومنع تزايد ثانى أكسيد الكربون ، فالهواء غير المتجدد الذى يحتوي على مستويات مرتفعة من ثانى أكسيد الكربون يؤثر على درجة التركيز ويسبب الشعور بالنعاس .
- التخلص من الأبخرة والروائح الكريهة والتى قد تؤثر سلبا على الأفراد وخاصة الأطفال ذو الحساسية المفرطة لحاسة الشم .
- تحقيق الراحة الحرارية للإنسان ، حيث أن ركود الهواء على الجلد يسبب الضيق وخاصة فى ظل ارتفاع نسبة الرطوبة لذلك يفضل تحريك الهواء فى الفراغ .
- يجب تصميم أنظمة للتهوية لمكافحة العدوى والحفاظ على معايير النظافة ، لانها قد تكون مصدرا محتملا للتلوث ، ويمكن تخفيض استهلاك الطاقة من خلال تقليل استخدام تكييف الهواء واستعادة الحرارة من أنظمة التهوية الميكانيكية .

التهوية الطبيعية :

فى دراسة قام بها إسكومب وأخرون فى ثمان مستشفيات بليما وبيرو ، وجدوا أن الإصابة بالعدوى فى الفراغات ذات أنظمة التهوية الطبيعية أقل منها فى الفراغات ذات التهوية الغير طبيعية ، وفى دراسة أخرى أجراها فينسنت وأخرون فى مباني إدراية

، وجد أن فرص إصابة العاملين بالأزمات الصحية داخل الفراغات ذات التهوية الصناعية أكبر منها داخل الفراغات ذات التهوية الطبيعية ، وأثبتت دراسات أخرى تأثير التهوية الصناعية فى إصابة الأفراد بمتلازمة مرض المبانى أى ظهور أعراض مرضيه على الأشخاص ، عند دخولهم مبنى معين قد تستمر لعدة ساعات ، ثم تتحسن الأعراض بعد ترك البناية نتيجة التهوية غير الجيدة للفراغ . (14)

وفى دراسة أجراها هسكونج وأخرون فى ثلاث مدارس بمناطق تعليمية مختلفة ، وجد أن درجات الطلاب المتواجدون بفصول ذات شبابيك منزلقة – قد حققوا زيادة بنسبة 7 %- 8 % فى إختبار تم إجراؤه – عن أقرانهم فى فصول ذات شبابيك ثابتة ، وقد استدلوا من هذه الدراسة على أن التهوية الطبيعية تساعد على التركيز وتزيد من كفاءة أداء الأفراد ، وبالتالى فإن التهوية الطبيعية تكون ضرورية لدى طفل المتلازمة داون لتساعده على التركيز فى النشاطات القائمه . (15)

هناك عدة توصيات وتقنيات يمكن من خلالها تحقيق تهوية طبيعية للفراغ المعمارى وهى : (9)

1- التوجيه : دراسة الموقع جيدا لتحقيق أفضل تهوية .
2- استخدام عناصر تنسيق الموقع ، مثل الأشجار والشجيرات وعناصر المياه وغيرها بحيث تكون فى اتجاه الرياح .
3- تصميم المبانى حول أفنية داخلية .
4- فتحات المبنى : وجود فتحتين متقابلتين مع بعض فى المبنى ، واحدة لدخول الهواء والأخرى لخروجه .

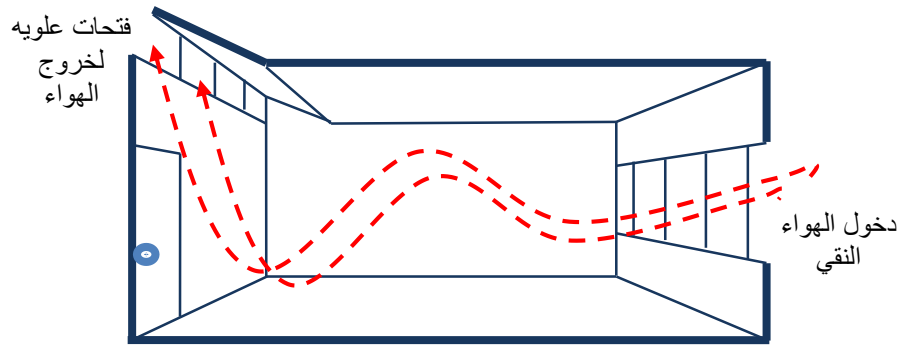

شكل (1 - 4)

تصميم فتحات مناسبة للتهوية الطبيعية مع مراعاة إرتفاعتها وتأثيرها على حركة الهواء داخل الفراغ .

5- التهوية باستخدام الظلال ، وذلك من خلال الظلال التى تسببها كتل المبانى المتقاربة والمتفاوتة فى الأحجام فترمى الكتلة الكبيرة بظلها على المبنى الصغير .

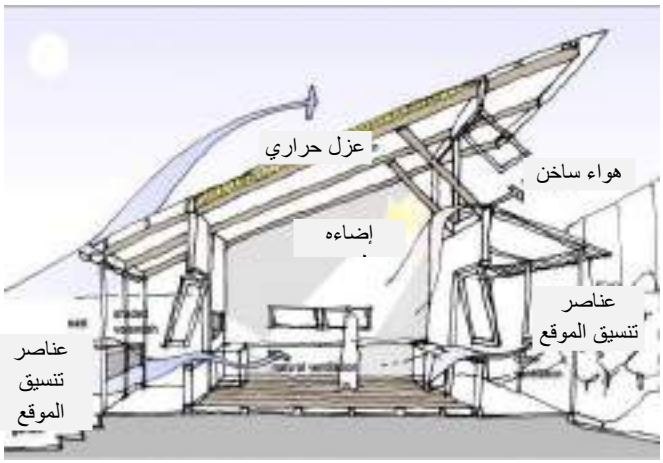

شكل (1 - 5)

يوضح أساليب التهوية وعزل الحراره داخل الفراغ .

التهوية الميكانيكية :

يلجأ المصمم إلى أنظمة التهوية الميكانيكية فى حالة عدم القدرة على توفير التهوية الطبيعية للفراغات المعمارية وذلك لإزالة الروائح أو الدخان أو الحرارة أو الغبار ، ينبغى أن تكون منافذ دخول الهواء مصممة بحيث تسمح للهواء النظيف بالدخول ،

ويجب مراعاة عدم إستخدام أنظمة التهوية التى تؤثر على الأداء الصوتي داخل الفراغ ، إذا أن الأطفال ذوى الإحتياجات التعليمية الخاصة قد تكون لديهم حساسية إضافية للأصوات عموما ومنها الضوضاء الخارجية .

لذا من الضرورى ان يتم تصميم اليات التشغيل لتكون منخفضة الصوت بقدر المستطاع ، وذلك لمنع التشتت الكبير الذى قد يحدث أثناء العملية التعليمية نتيجة لتلك الضوضاء . (9)

التدفئة والراحة الحرارية :

يتم التحكم فى التدفئة والراحة الحرارية عن طريق التحكم فى درجات حرارة الهواء ودرجة الحرارة المشعة وحركة الهواء ، وفقا لإحتياجات الأطفال الخاصة ، فإن درجات الحرارة العالية تسبب إزعاجا لأى فرد وخاصة للأطفال ذوى الحساسية الشديدة للمثيرات اللمسية ، وينبغى هنا على المعلمين ومقدمي الرعاية الصحية أن يكونوا قادرين على التحكم الداخلي قى درجة حرارة الفراغ .

النتائج :

من خلال الدراسة السابقه التي أشارت الى اهمية التهوية الطبيعية والمعالجات الصوتيه للفراغات التعليمية الخاصة بأطفال المتلازمه داون نجد أن :

- وجود عدة مصادر للضوضاء التى يشعر بها الأطفال داخل الفراغات التعليمية .
- هناك العديد من الإعتبارات الواجب مراعاتها لتجنب الإثار السلبية للضوضاء على أطفال المتلازمه داون وعلى مستخدمى الفراغ بشكل عام .
- هناك عدة طرق لعزل الضوضاء الخارجية قبل وصولها إلى الفراغ .
- هناك عدة توصيات يجب مراعتها عند التصميم من أجل توفير تهوية طبيعية للفراغات التعليمية لما لها تأثير كبير على نفسية مستخدمى الفراغ .
- هناك عدة توصيات وتقنيات يمكن من خلالها تحقيق تهوية طبيعية للفراغ المعمارى .

المراجع :

(1) عبد المنعم ، وليد ، " المفهوم الحديث لمباني الرعاية الصحية للمرضي النفسيين " ، ، رسالة دكتوراه – غير منشورة – جامعه القاهرة ، 2000م .

(2) أبو النصر، مدحت . "الإعاقة العقلية المفهوم والأنواع وبرامج الرعاية "، مجموعة النيل العربية ، القاهرة ، ص (155-159) – ٢٠٠٥م.

(3) الجهاز المركزى للتعبئه والأحصاء ، النتائج الأوليه للتعداد العام والإسكان والمنشات مصر 2006 ، منشورات الجهاز المركزى للتعبئه والإحصاء ، مارس 2007 ص2 .

(4) “Health Supervision for Children with Down Syndrome” clinical report from the American Academy of Pediatrics, was created in July 2013, available here: http://pediatrics.aappublications.org/content/128/2/393.full.

(5) Bittles, A. H., Bower, C., Hussain, R. & Glasson, E. (2007) The four ages of Down syndrome. European Journal of Public Health. 17 (2): 221-225 .

(6) CDC. (2012). World Down syndrome day. Retrieved June 11, 2012, from http://www.cdc.gov/ncbddd/features/DownSyndromeWorld Day-2012.html.

(7) NDSS. Down syndrome fact sheet. Retrieved June 11, 2012, fromhttp://www.ndss.org/en/About-Down-Syndrome/Down-Syndrome-Fact-Sheet .

(8) Ching , F.D.K ,"Architecture: Form , space and order " .New York : Van Nostrand Reinhold Company , 1979 .

(9) Department for Education and Employment , Building Bulletin 77 : Designing for people with Special Educational Needs and Disabilities in school , London : TSO , (1992) .

(10) Maxwell, L. E., & Evans, G. W. (2000). The effects of noise on pre-school children's pre-reading skills. Journal of environmental Psychology, 20(1), 91-97.

(11) Dockrell, J. E., Shield, B. M., & Rigby, K. (2004). Acoustic guidelines and teacher strategies for optimising learning conditions in classrooms for children with hearing problems. D. Fabry, CH. DeConde J.(Eds.), ACCESS: Achieving Clear Communication Employing Sound Solutions. Chigago: Phonak AG.

(12) Shield, B. M., & Dockrell, J. E. (2008). The effects of environmental and classroom noise on the academic attainments of primary school children. The Journal of the Acoustical Society of America, 123(1), 133-144.

(13) Seep, B., Glosemeyer, R., Hulce, E., Linn, M., & Aytar, P. (2000). Classroom Acoustics: A Resource for Creating Environments with Desirable Listening Conditions.

(14) Vincent, D., Annesi, I., Festy, B., & Lambrozo, J. (1997). Ventilation system, indoor air quality, and health outcomes in Parisian modern office workers. Environmental research, 75(2), 100-112.

(15) Heschong, L., Wright, R. L., & Okura, S. (2002). Daylighting impacts on human performance in school. Journal of the Illuminating Engineering Society, 31(2), 101-114.

"The Effect of Voice and Ventilation on the Educational Environment for Down Syndrome Children"

ABSTRACT

The architect is always looking for how to organize the space and use it well to enable the user to do his job and practice the various activities comfortably at appropriate conditions. It is known that elements of any space design have a direct impact on the user. Moreover, all the things can be touched by our hands, seen by our eyes, heard by our ears and interacted by all our senses which are part of the experience of architectural space.

So, The designer of space always move towards the elements of design to meet the psychological needs of the user, which affect his direction, ideas, views, tendencies and characteristics of personality and achieve the sensual and psychological comfort.

This study aims to search and follow the most important surrounding aspects for the child of Down syndrome, which affects his perception and psychological impressions when the child exists in the space. The most important of these elements can be identified by the voice and ventilation within the space as part of the value of the surrounding space.

THE ROLE OF SOFT MOBILITY TOWARDS STRENGTHENING URBAN TRANSFORMATION AND SUSTAINABLE WELL-BEING:
CASE STUDY: MANSOURA CITY, EGYPT

Mai Wahba Madkour [1], Alaa A. ELMANZLAWI [2]

[1] *Lecturer, Faculty of Engineering, Tanta University, Egypt*
[2] *Lecturer, Misr Higher Institute for Engineering and Technology (MET), Egypt*
Corresponding author: maimadkour@yahoo.com, A.Manzlawy@hotmail.com

ABSTRACT

This research investigates the method of soft mobility role on Egyptian neighborhood unit. It discusses its relationship with the main principles of New Urbanism. And proposes some objectives: Interpret Mobility new concepts in New Urbanism, cite urbanism principles and its trends to conclude soft mobility indicators, design a matrix inventories the compatibility of soft mobility indicators and behavioral dimension. And at last, the matrix tests the combination of indicators and dimensions in an Egyptian traditional urban fabric, at Mansoura City.

KEYWORDS: Soft Mobility, New urbanism, sustainable well-being, behavioral dimensions

1. INTRODUCTION

In the nineties of the last era, new urbanism & sustainable urban design and, as a new trend in Urbanism, emerged in synchronization (Duany, 2001). It integrated both functional, perceptual, and behavioral dimensions with environmental sustainable ideas. This paper is to make sense of many ideas and research that bear on urban ecology, sustainable development and mobility effects on them. Mobility is the pillar of the economy and a basic need of the contemporary urban lifestyle. The main question is if our cities can cope with using cars as a sign of mobility, independence, and modernity. The great number of cars on streets, manly solo driving, is jeopardizing the urban context, living, working and relaxing places for people.

The great growth in using cars in traffic with environmental problems also eroded people's possibilities to have free and safe roaming in open spaces. This research is a contribution to debate and discuss mobility patters effects on urban spaces. The idea is developing cities into good streetscapes quality and turn back from nonfunctional, bleak and unattractive urban spaces fairly. Negotiate uses of cars in urban spaces towards changing streetscape to an attractive and multifunctional landscape.

In this reseach, the role of soft mobility in sustainable well-being is explored and discussed against strengthening urban transformation. The main concept of soft mobility is based on the protection and enhancing nature and natural processes, and the benefits gained from nature to serve human needs, are integrated into spatial planning and territorial development, and in strategies of mobility. Soft mobility promotes many solutions and is complementary, to standard solutions.

1.1. Research problem

Due to modern architecture, it started changing, the dominance of cars on spatial relationships in city planning professional practice. After the World War II, this trend was named as

Conventional Suburban Development (CSD) (Duany, 2001). In this research, it was criticized because of the lacking of town centers and pedestrian priority (Urbanism, 1996, pg. 5-10), (Duany, 2001). (CSD) spreads out to large areas of the countryside whatever the population growth rate. It pushes the higher percentage of car ownership in the absence of any public transport system. Today, New Urbanism suggests action plans to (CSD) (Steuteviller, 2009). It starts with some principles of enhancing the communities within walking distances.

Fig. (1): A Photo showing the Mobility problems in Egypt (Increasing of population densities in urban and rural centers)

Source: Ministry of Housing, Utilities & Urban communities, 2014 "Urban Future: Egypt's Urban Policies", PowerPoint presentation.

On the other side, urban mobility, people, and goods transportation, is very essential for economic and social well-being but also is a growing concern. Nowadays urban development faces a great challenge of how to make soft mobility sustainable and environment-friendly and competitiveness (Figure 1). Sustainability has to cope with a steady concern in urban development. So, New Urbanism role is done to improve communities to develop car problems in the forefront of their priorities.

1.2. Research hypotheses

Although the Mobility principles of New Urbanism are the most important for many livable cities, therefore, the research suggests a hypothesis addressed as: "if each one of the groups of soft mobility indicators and behavioral dimensions make a livable city, the integration of them will provide convenience solutions to sustainable well-being ."

The paper inventories the indicators of soft mobility inside an Egyptian neighborhood. It provides a matrix addressed as "indicators of soft mobility to " to be tested upon the case study from the behavioral milieu; it is the most tangible to the sustainable wellbeing.

2. Mobility and Sustainable Wellbeing:

Mobility is the ability of people and freight to travel where they want to go; it can be measured by kilometers traveled per year: the greater the number, the more the society is mobile. For example, achieving a system for sustainable transport, drivers should drive less; as, driving a car is much more attractive than other transport modes, due to its convenience, independent, flexible, more comfort, fast, safe, and private; cars also provide more pleasure and status than other transport modes. In addition to using soft mobility as a new lifestyle, its main aim is improving

environmental benefits and urban livability. It includes all non-motorized transport as it is called "human-powered mobility". Such as pedestrian, bicycles as an alternative to using cars. Consequently, knowing how high or low does public accept elements of different sustainable development is very important.

2.1.Soft mobility "Slow Traffic":

Soft mobility includes all types of Non-Motorized Transportation methods (NMT) that depends only on human energy (Human Powered Mobility). Slow traffic guidelines drawn by the Federal Roads Office (FEDRO) in 2002, is a framework to define general conditions for improving mobility system at urban and regional level. Swiss is the most significant example of public policy involved in integrating slow traffic into mobility system globally. Soft mobility which includes: pedestrian, bicycle and other non-motorized methods are "zero impact" mobility as an alternative to using cars. According to what was mentioned, slow traffic or soft mobility is a different way of expressing the same concept. Soft mobility can be defined as a special form of sustainable mobility that optimizes urban livability, through keeping individual right moving.

The global concept for sustainable mobility aims to increase urban livability, keeping individual right moving. **Also, soft mobility can improve urban environment referring to:**

- Air pollution & noise Levels,
- Traffic congestion.
- Streets safety.

In general, soft mobility and its promotion in urban policies are linked to emissions problem generated by vehicular traffic. As is based on by increasing soft mobility this could reduce using private cars, with regard to short trips.

This should ensure highest levels of urban safety increasing occasions of public spaces regeneration. Despite this increase, network idea for soft mobility hasn't been carried out yet. Integrated facilities supply and services, being alternative to the car use, is still difficult to be accomplished.

2.2. Mobility in New Urbanism

New Urbanism, is a Nontraditional Design, and an urban design movement that started in the urban design field in the USA in 1980's, to enhance pedestrian movement in neighboring units. It had grown gradually in the direction of reforming the various aspects of urban planning and urban design. It influenced in urban areas according to standards of urban design to reform the built environment. Which had fostered life and placemaking quality? It had also retrieved the urban communities thought that includes various activities with short walking distance. New Urbanism provides walkable places, which give many options for people living an urban lifestyle in comfortable and enjoyable places. And drives the communities towards the utopian city.

New urbanism principles classification which is based on basis of three main levels:

1. Region: metropolis, city, & town.
2. Neighborhood, district, and corridor.
3. Block, road, & building.

According to a literature review pursued on CNU, new urbanism principles, at the neighborhood level are modified to be ten principles instead of nine (Carmona, 2010). Due to the scope of this research, only mobility in new urbanism principles related to neighborhood scale is addressed, and

foster the community which gives choices for pedestrian movement with various activities for all users. These are, firstly Walkability, Secondly, Connectivity.

2.2.1. Walkability:

Accessibility is used often in human geography for evaluating facilities and functions spatial distribution. When any place is reached easily by pedestrians or by an appropriate mode of transport it becomes accessible; it denotes the ease with which any land-use activity can be reached from a location, using a particular transport system. Accessibility is considered also as the opportunity available to an individual or type of person to take part in a particular activity or set of activities.

Typical accessibility measure is divided into two parts:

A. Transportation elements, which represent travel difficulty or impendence. It is measured by travel distance, time, or costs (usually walking distance is measured by kilometer or mile while the distance covered by vehicles is measured by travel time) - (El Wakil, 2007).

B. Activity element represents opportunities available at a particular zone. It is indicated by the amount and the location of activities of different types. Everyone should have access to outdoor environments. Lack of accessibility could reduce individual and community activities participation and reduce people's ability to take advantage of some opportunities such as social, economic and healthy lifestyle.

Table 1: Accessibility's indicators, basic needs, and general goals

Mobility and Sustainable Wellbeing			Accessibility
Indicator	**Toolbox for Measuring Indicator**	**Basic Need**	**General Goal**
Pedestrian Catchment Area	**Converting street into pedestrian thoroughfares**	Maximum walking distance before turning back or opting to drive a bike or a car rather than walk.	Improving public health by encouraging daily physical activity and reducing the negative effects of vehicle emissions.
	Pedestrian Catchment Area For Primary Facilities		
	Pedestrian Catchment Area for Secondary Facilities		
Connectivity	**Turn public lots into public square**	Measure the ease of access from one point to another within the development	
	Comfortable climatic conditions		
	Blocks Size & façade		
	Walk with dignity, integrity and without overcrowding		

2.2.2. Walkability and Cyclability:

Regular physical activity associated with enhanced health and reduces the risk of premature deaths. Physical activity reduces the risk of cardiovascular disease, stroke, diabetes type 2, colon cancer, osteoporosis, depression, and fall-related injuries. Walking is the most commonly promoted moderate-intensity physical activity, therefore walking and cycling are the most convenient and sustainable mode of transport for all local trips. The built environment has to provide a safe walkable and bicycle network in order to encourage people to walk or bike rather than use private cars.

The key to pedestrian-friendly neighborhood is to tame than to exclude cars. Which means reducing traffic speed and reclaiming more street area for pedestrians without removing the entire cars. Streets can be made more attractive by widening pavements, providing cycle lanes and calming traffic (Rudlin and Falk, 2009).

Table 2: Walkability and Cyclability's indicators, basic needs and general goals

<table>
<tr><th colspan="3">Mobility and Sustainable Wellbeing</th><th>Walkability and Cyclability</th></tr>
<tr><th>Indicator</th><th>Toolbox for Measuring Indicator</th><th>Basic Need</th><th>General Goal</th></tr>
<tr><td rowspan="5">Walkable Network</td><td>Sidewalk Network Coverage</td><td rowspan="5">Continues walkable network along both sides on streets that links the dwellings to diverse uses within the neighborhood.</td><td rowspan="7">Encourage pedestrian activity without excluding automobiles altogether.</td></tr>
<tr><td>Good walking rhythm with few interruptions</td></tr>
<tr><td>Well-situated cafes and outdoor restaurants</td></tr>
<tr><td>Beautiful and effective lighting</td></tr>
<tr><td>Good conditions</td></tr>
<tr><td rowspan="2">Cyclable Network and Facilities</td><td>Bicycle Lane Km</td><td rowspan="2">Continue cyclable network along the streets that link the dwellings to diverse uses within the neighborhood.</td></tr>
<tr><td>Bicycle Facilities</td></tr>
<tr><td>Traffic Calming</td><td>Reduce traffic and parking gradually</td><td>Reducing vehicle speeds within the neighborhood.</td></tr>
</table>

3. Behavioral Dimensions: BD

Behavior is defined and measured due to the importance to the success of any behavioral analysis. The target behavior characteristics must be sufficiently well defined to allow clear distinctions done between instances (cases where the target behavior has been emitted) and non-instances (cases where some other behavior has been emitted). Also, care must be exercised in behavioral selection dimension monitored to evaluate behavior changes over time.

Urban design through the classified documents relates to the relationship between man and the built environment can be represented in six common dimensions (UDD) (Carmona, 2010). Urban design documents (UDDs) are perceptual, functional, visual, temporal, behavioral and environmental dimension (Banerjee, 2001; Baran, 2003; Bartuska, 2007; Carmona, 2010), (Fig. 8). This research focuses on the criteria of behavioral dimension for the reason of being the most tangible dimension to the mobility of new urbanism principles. Table 3 illustrates the two main descriptive indicators of behavioral dimension (Desy,1990; Carr,1992; Gehl,2001; Berison,2008; Ilewelyn ,2010; Evans,2012).

Table 3: Behavioral Dimension

Sub-Issue	Indicators
Non-Physical Issues	**The interferes with the effect on human behavior are:** ▪ Users physiological abilities that affect the behavioral response. ▪ An individual's personality that distinguishes him from others and made him unique in interacting with the surrounding environment (personalization). ▪ Social context in which the individual resides determined by the rules which routes, and framework of relations between individuals which imposes on all of them. ▪ Cultural background as a set of social values and beliefs to which the individual belongs to and that guide the behavior and from the experience. ▪ Human needs such as social, Commercial, etc. ▪ Public participation in all design process. ▪ Equality between all users. ▪ Freedom to act within public spaces. ▪ Freedom in political practices.
Physical Issues	**It interferes with the mutual effect on human behavior and the built environment:** ▪ The range of ownership of the vacuum due to property ownership between public and semi-public. ▪ More limits of surrounding buildings and trees, the more powerful of the space (enclosure). Defined edges and connected to the greater sense of containment increase the positive interaction between man and environment. ▪ Movement system which affects the performance, and means of accessibility and movement to the parking area. ▪ Treatment quality used in space raises the efficiency quality.

4. Approach Apparatus

As mentioned, the research suggests a tool to analyze the role of soft mobility in making cities livable and favorite. Thus, the paper formulates a matrix which called (indicators of soft mobility vs. behavioral dimension), Table 4. The matrix tests behavioral milieu and soft mobility indicators based on the case study. It adopts a hypothesis concedes that the behavioral dimension is the most adjacent to the theory (Dunham, 2000). The matrix has two main axes: indicators of soft mobility and a general framework for behavioral dimensions. Table 4 shows indicators, which are concluded from the table. 1, and 2, list as five indicators within two main axes. Results achieved from the analysis of the matrix of relations between indicators and dimensions range is between high and low: The highest comes from high potentialities with low constrains; medium comes from low potentialities with low constraints, and the lowest comes from low potentialities with high constraints. The mutual impact of indicators versus dimensions showed as dots, no mutual impact showed as blanked cells.

Table (4): **A matrix which called (indicators of soft mobility vs. behavioral dimension)**
Source: Authors

No Relationship ● Mutual Relationship ☒ Conflicting Relationship

	Indicator	Toolbox for Measuring Indicator	The Quality of Treatment used inside	Movement system	Enclosure	The ownership	Freedom in the political practices	Freedom to act within the Public Spaces	Equality Between all users	Public Participation	Human Needs	Cultural Background	Social Context	Personalization
Accessibility	Pedestrian Catchment Area	Converting street into pedestrian thoroughfares		●	●	✕	●				●	●		
		Pedestrian Catchment Area For Primary Facilities		●	●						●	●	●	
		Pedestrian Catchment Area for Secondary Facilities		●	●						●	●	●	
	Connectivity	Turn public lots into a public square	●	●						●	●	●		
		Comfortable climatic conditions						●			●	●	●	
		Blocks Size & façade	●		●	✕					●		●	
		Walk with dignity, integrity and without overcrowding	●		●			●			●	●		
Walkability and Cyclability	Walkable Network	Sidewalk Network Coverage		●	●						●	●	●	
		Good walking rhythm with few interruptions	●	●	●						●	●	●	●
		Well-situated cafes and outdoor restaurants	●					●			●	●	●	●
		Beautiful and effective lighting	●				●				●		●	●
		Good conditions	●					●	●		●		●	
	Cyclable Network	Bicycle Lane Km		●							●			
		Bicycle Facilities	●		●		●				●		●	●
	Traffic Calming	Reduce traffic and parking gradually		●							●	●	●	

4.1. Field Survey

The surveying process aims and verifies indicators validity of soft mobility in Egypt. Table 5 shows surveying methods & techniques for the required task. Therefore, the field survey encompasses three main phases: appreciate the context, site analysis, and finally, getting concluded remarks Table 6.

Table 5: Survey techniques and related methods

Survey Technique	Methods.
Appreciate the context	Site visit & data collection.
Site analysis: indicators of soft mobility site characteristics	Designing a matrix collected data analysis: Site problems, potentialities, and constraints.
Concluded remarks	Further interpreting of analyzing the case study, survey outcomes.

Fig. (2): A Photo showing Mansoura city streets in The past and Now

Source: Authors, http://english.ahram.org.eg .

4.2.El-Seka El-Gededa "Commercial city center", Mansoura city: Appreciate the context

Mansoura* as many other cities of Egypt had been modernized in the 18th century and its development has been evolving through a series of political designs. The case study area named revolution street (El-Seka El-gededa Street) which was named Ismail Street is the first street to be constructed within Mansoura old quarter and that was during Khedive Ismail (1863- 1879) period according to in Mansoura old maps. Ismail's vision of modernization was to turn Egypt into a European country and Egyptian cities like Cairo, Alexandria, and Mansoura into European cities. He turned his back to the traditional quarter and started to build new districts and suburbs in European styles.

***El-Mansoura:** is an intermediate city in Egypt, Coordinates: 31°03′N 31°23′E. It is the capital of Dakahlia Governorate. Historically, Mansoura was the place where the crusaders were defeated and for this reason, its first name "The Rose Island" was converted to its recent name Mansoura "The Victorious". The City witnessed historical, political and economic development which affected the social life and communities in Mansoura. Now, the City is considered the third capital of Egyptian cities regarding its importance, population, economic activities, and political power.

Fig. (3): El-Mansoura historical center highlighting main valuable culture regions map

Source: El-Gizawy, L., Shawky, M. Fouda, M., " The Effect of the Urban Heritage Sites Sustainable On The Development Of Intermediate Cities – Case Study: Mansoura City, Egypt" the 7th international engineering conference International Mansoura University, Egypt, (2010).

This area is nearby the Hussaniya area (southern El-Seka El-Gededa) the first planned area with urban fabric in Modern Mansoura and at the north located "Met-Hader" area which is the main commercial market with about 35% of (residential/commercial) activities (vegetables and fish market). The study area is considered to present about 50 % of the Mansoura city commercial activities.

It is the oldest commercial area known in Dakahlia, which is divided into two parts as the first part; from Port-Said street where the Gold and Jewelry shops (AlSagha) (about 25%), then the second part with cloth shops in the middle (around 55%), and the shoe shops in the final part (20%). in addition to a mix of uses of commercial activities with people and salesmen.

Fig. (4): The map shows high-density points, landmarks, and the visual Sequence Source: Authors

From the property archives of the study area, most of the original owners were foreigners and now owned by Egyptians with mixed uses of commercial, residential and business activities (medical, offices and so on).

The area is faced by a set of influence factors; community priorities and needs (housing, infrastructure, and transport), the physical constraints (vacancies, potential, and obsolescence), regulatory constraints (authorities and legislation involved) and environmental constraints (air pollution and underground water). The ignorance of the existence of these constraints would discredit the practicality of any developmental actions and the sustainability.

El-Seka El-Gededa "Commercial city center" is the most predominance, functionally and visually, square in Mansoura city. Choosing El-Seka El-Gededa, as a case study, is due to its location as a focal point.

It contains various movement elements and behavioral aspects which could be analyzed from the perspective of indicators of soft mobility. In addition to its location, the cohabitation field of the researcher makes exploring the site more reliable. El-Seka El-Gededa locates within a distinctive place (Figure 4), as well as containing principles which contribute to configure responsive community. On the other hand, the master plan of El-Seka El-Gededa presents negative aspects from the perspective of the soft mobility that needs to be analyzed to overcome them.

4.3.Testing Indicators vs. dimensions: Site analysis

Analyzing the site aims to find out the current status of El-Seka El-Gededa. Table 6 represents the indicators of soft mobility versus the behavioral dimension. In addition to, this phase endeavor answers to the following question: to what extent does El-Seka El-Gededa conforms to the indicators of soft mobility?

Firstly, the pedestrian-friendly/walkability, and connectivity: The routs system achieves a high connectivity/permeability due to the street/block system which characterized by the medium size and street hierarchy. The site has several types of movement; these are the private cars, microbuses, and the pedestrian movement. The private car represents the main means of connectivity in this area. They benefit from the high connectivity realized by the street/block system. The street/block system gives all public spaces and places the quality of accessibility. Although this high connectivity is a positive factor for indicators of soft mobility, the car has the main dominance. This, in turn, affects the variety of activities and the exploitation of spaces by the other movement elements.

The shortage of parking places creates a basic problem that limits the capacity of urban spaces to achieve indicators of soft mobility; Cars can only park on the sides of the commercial axes. They even park sometimes on the sidewalks, these hazards in the pedestrian movement from the physical barrier to their movement.

Although public microbuses cover El-Seka El-Gededa, the dependency on this type is missing; quality of buses and bus stop locations are not suitable to the Mansoura inhabitants' way of life. In the initial layout of Mansoura, the routs appeared not separated from vehicle movement. Many factors enhance the efficiency of these paths and encourage people to use them; arcades to provide shadow for walkers. The site enjoys various types of landmarks. These enhance paths orientation, in addition to, exploring the place. The occupation of sidewalks by vendors and shops extensions represents another negative factor.

Table (6): **The matrix 'Pedestrian Friendly/Walkability, and Connectivity'' Vs. Behavioral dimensions**
Source: Authors

	Indicator	Toolbox for Measuring Indicator	The Quality of Treatment used inside	Movement system	Enclosure	The ownership	Freedom in the political practices	Freedom to act within the Public Spaces	Equality Between all users	Public Participation	Human Needs	Cultural Background	Social Context	Personalization	Total points of achievement	%
Accessibility	Pedestrian Catchment Area	Converting street into pedestrian thoroughfares **(total achievement 5 points)**		●	●	×	●				●	●			**2/5**	**40%**
				1	1		0				0	0				
		Pedestrian Catchment Area For Primary Facilities **(total achievement 5 points)**		●	●						●	●	●		**2/5**	**40%**
				0	1						1	0	0			
		Pedestrian Catchment Area For Secondary Facilities **(total achievement 5 points)**		●	●						●	●	●		**2/5**	**40%**
				0	1						1	0	0			
	Connectivity	Turn public lots into public square **(total achievement 5 points)**	●	●						●	●	●			**1/5**	**20%**
			0	1						0	0	0				
		Comfortable climatic conditions **(total achievement 4 points)**						●			●	●	●		**0/4**	**0%**
								0			0	0	0			
		Blocks Size & façade **(total achievement 4 points)**	●		●	×					●		●		**4/4**	**100%**
			1		1						1		1			
		Walk with dignity, integrity and without overcrowding **(total achievement 5 points)**	●		●			●			●	●			**4/5**	**80%**
			0		1			1			1	1				
Walkability and Cyclability	Walkable Network	Sidewalk Network Coverage **(total achievement 5 points)**		●	●						●	●	●		**2/5**	**40%**
				0	1						1	0	0			
		Good walking rhythm with few interruptions **(total achievement 7 points)**	●	●	●						●	●	●	●	**4/7**	**58%**
			0	1	1						1	0	0	0		
		Well-situated cafes and outdoor restaurants **(total achievement 6 points)**	●					●			●	●	●	●	**5/6**	**83%**
			1					1			1	1	1	0		
		Beautiful and effective lighting **(total achievement 5 points)**	●				●				●		●	●	**0/5**	**0%**
			0				0				0		0	0		
		Good conditions **(total achievement 5 points)**	●					●	●		●		●		**2/5**	**40%**
			0					1	1		0		0			
	Cycable Network	Bicycle Lane Km **(total achievement 2 points)**		●							●				**0/2**	**0%**
				0							0					
		Bicycle Facilities**(total achievement 6 points)**	●		●		●				●		●	●	**0/6**	**0%**
			0		0		0				0		0	0		
	Traffic Calming	Reduce traffic and parking gradually **(total achievement 4 points)**		●							●	●	●		**1/4**	**25%**
				1							0	0	0			
No of points			**2/8**	**4/8**	**7/8**	**-**	**0/3**	**3/4**	**1/1**	**0/1**	**7/15**	**2/10**	**2/11**	**0/4**		
Percentage %			**25**	**50**	**88**	**-**	**0**	**75**	**100**	**0**	**47**	**20**	**18**	**0**		

High Achievement | **Medium Achievement** | **Poor Achievement** | × **Conflicting Relationship**

Horizontally, the relationships between Blocks Size & façade comparing with behavioral milieu score a high percentage "100%". The same as the previous step, indicators such as

Comfortable climatic conditions, Beautiful and effective lighting, Bicycle Lane Km, Bicycle Facilities have zero% incompatibility with behavioral issues .

Therefore, these indicators should have the action priority in the re-designing process as they have the highest achievements in the study area.

Fig. (5): The characteristics movement pattern in El-Seka El-Gededa:

(a) The high capacity of traffic in El-Seka El-Gededa Street; (b) the occupation of sidewalks by shops extension and roadside parking; (c) bad treatment of sidewalks pavement; (d) The occupation of sidewalks by vendors (e)the unsafe pedestrian movement

Source: Authors

4.4.Concluding remarks: Survey outcomes

From Table 4, the paper concludes some remarks.

Vertically, the issues equal between all users; Equality Between all users, Freedom to act with Public Spaces, and Enclosure took high grades percentage.

Consequently, it leads to the percentage of a weak equity among all users. On the other hand, the grades percentage that follow express of Human Needs, and Movement system range from medium to high .

Ultimately, the following three Indicators; Blocks Size & façade, walk with dignity, integrity and without overcrowding, and Well-situated cafes and outdoor restaurants received the highest percentage . Furthermore, the last sub-issues of the behavioral dimensions received a weak percentage of the grade in comparison with indicators of soft mobility .

4.5.The Development Proposal:

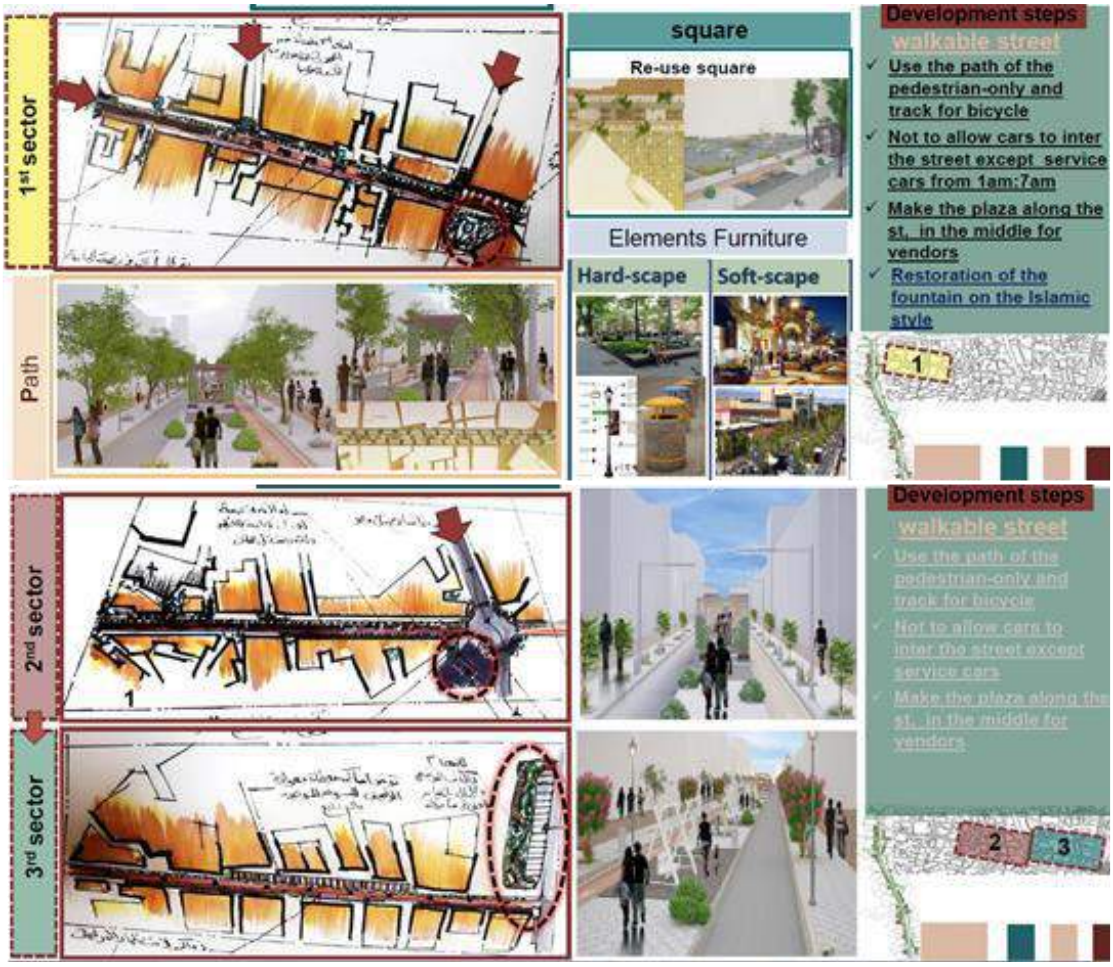

Fig. (6): The proposal of development by dividing in El-Seka El-Gededa Street **into 3 parts**

Source: Author

5.Conclusions

This research is done to find the relationship between indicators of soft mobility through one of the urban design dimensions under a certain hypothesis which might be true if taken into consideration the following:

- Public participation can play a great role in motivating the indicators and dimensions towards a real application
- Soft mobility indicators have to respect the cultural context of a certain context.
- Percentage of the mutual impact between indicators and dimensions numerically must be done by a digital model.

Current work followed the inductive analytically and an empirically approaches. focused on the quantitative analysis whereas a case study analysis depends on the results of the previous quantitative. This research was designed for this purpose, a matrix which addressed the indicators of soft mobility versus behavioral dimension and taking into account soft mobility to accommodate the change in human needs and rights.

This research proposes further researches as a way to develop the proposed integrated approach, test a matrix. In addition to indicators of soft mobility that may play an important role in neighborhood units' constructive integration.

6. References

1. Ameen, R.F.M.; Mourshed, M.; Li, H. **A critical review of environmental assessment tools for sustainable urban design**. Environ. Impact Assess. Rev. 2015.
2. Ayman Mohamad Mostafa, **(Quality of Life Indicators in Value Urban Areas: Kasr Elnile Street in Cairo)**. ASEAN Conference on Environment-Behavior Studies, Bangkok, Thailand, 16-18 July 2012.
3. Abeer Elshater, **(New Urbanism Principles versus Urban Design Dimensions towards Behavior Performance Efficiency in Egyptian Neighborhood Unit).** ASIA Pacific International Conference on Environment-Behavior Studies, Mercure Le Sphinx Cairo Hotel, Giza, Egypt, 31 October 2 November 2012.
4. Abu Dhabi Urban Planning Council, **"Abu Dhabi Urban Street Design Manual, Vision 2030"**, Abu Dhabi Urban Planning Council, Abu Dhabi, United Arab Emirates, 2011.
5. BRE Global, **"BREEAM Communities - Integrating sustainable design into master planning"**, Bucknalls Lane, Watford - United Kingdom, 2013.
6. Boeing, Geoff; Church, Daniel; Hubbard, Haley; Mickens, Julie; Rudis, Lili. **"LEED-ND and Livability Revisited"**. Berkeley Planning Journal, 2014.
7. E. Lora, A. Powell and others, **"The Quality of Life in Latin American Cities, Markets and Perception"**, the Inter-American Development Bank, Washington, United States, 2010.
8. Florian Steinberg, **Conservation and Rehabilitation of Urban Heritage in Developing Countries.** Institute for Housing and Urban Development Studies, Rotterdam, The Netherlands, 1996.
9. Hassan, A.M.; Lee, H. **Toward the sustainable development of urban areas: An overview of global trends in trials and policies**. Land Use Policy 2015.
10. Jungwon Yoon, Jiyoung Park, **"Comparative Analysis of Material Criteria in Neighborhood Sustainability Assessment Tools and Urban Design Guidelines: Cases of the UK, the US, Japan, and Korea"**, sustainability journal, ISSN 2071-1050,2015.
11. Sarah Abdel Moneim El Ariane, **‹Neighborhood Urban Quality of Life - Guidelines for Urban Planning and Development of New Assessment Tool›**, FACULTY OF ENGINEERING, CAIRO UNIVERSITY, 2012.
12. Sharifi, Ayyoob; Murayama, Akito **"A critical review of seven selected neighborhood sustainability assessment tools",** Environmental Impact Assessment Review 38. 2013.
13. Sharifi, Ayyoob; Murayama, Akito **"The potential of CASBEE for urban development for delivering sustainable communities: A case study from the "Koshigaya Lake Town" planning experience",** International symposium on Urban planning, Taiwan,2012.
14. El-Gizawy, L., Shawky, M.,; Fouda, M., **" The Effect of the Urban Heritage Sites Sustainable On The Development Of Intermediate Cities – Case Study: Mansoura City, Egypt"** the 7th international engineering conference International Mansoura University, Egypt, 2010.
15. A.Rashed, D.Elkerdany, M.Shawky **" Community Participatory for Sustaining Heritage Environments: Case Study Mansoura City"**, Mansoura University, Egypt, 2005.

مدينة طنطا التاريخية

قيم عمرانية وإدراجها في خطط التنمية المستقبلية

أ.د/ علاء الدين علوي الحبشي – م/ الزهراء عبدالوهاب محمد جبل

قسم الهندسة المعمارية– كلية الهندسة– جامعة المنوفية

الملخص

في أواخر القرن التاسع عشر عقب مجيء الخديوي إسماعيل للسلطة عام 1863،شهدت طنطاكسائر بلاد القطر المصري ضوءاً جديداً،و كان لفترة ولايته تأثيراً كبيراً على عمرانها وعمارتها لتضفي عليها روح عصر جديد فأنفتحت المدينةعلى العالم وتم توجيهها نحو الغرب لتصبح مدينة عصرية متكاملة (ثقافية –إدارية – صناعية) عاش فيها مختلف شعوب البحر المتوسط جنباً إلى جنب مع المصريين وشيدوا سوياً المدينة الحديثة ولعبت جميع الأديان والجنسيات دورًا في نسيج الحياة المصرية واحتفلت جميع طوابق المجتمع سوياً بالأعياد المختلفة على مدار العام، ولم تكن الجنسية أو الهوية هي التي تهم، وإنما العيش سويًا في تكامل وتناغم،فكان مجتمعها تعددياً منفتحاً وكريماً وقانعاً.(صالح 2016)

ويسعى البحث إلى تسليط الضوء على النسيج العمراني الأصيل لمدينة طنطا والذي يشكل هويتها التاريخية وإبراز القيم التراثية والعمرانية في المدينة والتي مازالت لها سمات (معبرات) موجودة ومؤثرة على الأرض حتى يتم الحفاظ عليها وإدراجها في الخطط التنموية المستقبلية للتأكيد على النسيج العمراني الأصيل للمدينة والذي يميزها عن باقي مدن إقليم الدلتا.

تهدف الدراسة لتوعيةالجيل الحالي بمدى عظمة ما أحدثه الخديوي إسماعيل في عمارة وعمران الدولة المصرية عموما وفي مدينة طنطا تحديدا لأن شكل المدينة لم يعد واضحا كما كان خاصة أن العمران المعاصر يشوه معالم المدينة وهذا الأمر يزداد سوءا يوما بعد يوم فلابد من وقفة للحد من التنمية العمرانية المتسارعة والغير مدروسة التي تقضي على أصالة العمارة والعمران، وإعادة صياغة المدينة لتصبح واضحة المعالم ويتم التفرقة بين النسيج القديم والحديث والتحكم في عمليات البناء في المناطق التراثية بحيث لا تشوه الشوارع ولا المباني ذات المدلول التراثي، وتعديل مسار التخطيط الحالي للمدن والقائم على المنفعة الوقتية فقط والذي ينتج عنه طمس ملامح المدينة الأصيلة، ويهدف البحث إلى إدراج المنطقة الخديوية في مدينة طنطا كمنطقة تراثية يجب حمايتها بقانون 119 لسنة 2008 ولائحته التنفيذية والتي تضبط كل مفردات عمران المناطق التراثية من ارتفاعات المباني ونمط الواجهات والإضاءة والتشجير والأرصفة واللافتات والإعلانات (حواس 2013)وغيرها التي من شأنها حماية وحدة المنطقة البصرية والحفاظ على سياقها الأصيل وعلاقتها بالمناطق المجاورة، والبدء عموما في تخطيط المدن التاريخية المصرية على أساس مميزاتها وتطور عمرانها التاريخي، وكذلك الحفاظ على المباني التراثية وذات الطابع المعماري المميز المسجلة ضمن قانون 114 لعام 2006 (حواس 2013) وإدراج المباني غير المسجلة للحفاظ عليها وإعادة استخدام كل المباني التراثية لضمان مستقبل مستدام لها وللمنطقة ككل.

وتكون النتيجة لذلك إعلاء قيمة المدينة وإضافة ميزة جديدة بها إلى جانب كونها مدينة السيد البدوي فيتعرف المجتمع المحلي على هويتها وتاريخها ورقيها مما يزيد من الترابط والانتماء للمكان ومن ثم يعمل المجتمع المحلي كقوة داعمة تساهم في استمرارية النسيج الأصلي وتحافظ عليه ويمكن بذلك تنشيط السياحة الثقافية الداخلية للمدينة حتى في غير أيام المولد.

Abstract

In the late of nineteenth century, the city of Tanta saw a new light, thanks to the seizing of power by Khedive Ismailin 1863. His reign had a great impact on the city and its architecture, ushering in a new, visionary era. He sought to open the city, and orient it westwards: making it an integrated modern city, open to the world, and a place where peoples from every corner of the Mediterranean once rubbed shoulders. Together with Egyptians, they created the modern city. All religions and nationalities played a part in the tapestry that was Egyptian life – all echelons of society celebrated the multitude of festivals that punctuated the year. However, it was not the multitude of nations or identities that mattered, but their conviviality and harmonious integration. It was a pluralistic society founded on the birth of a distinct xenophile: both generous, and content. (Saleh 2015)

This research seeks to shed light on the authentic and significant fabric of the city of Tanta, which makes its historical identity,Reveal and interpret heritage significance and values of the city and its urban fabric, which still have features and attributesin the city to be preserved and included in future development plans to emphasize the authentic urban fabric of the city that distinguish it from other cities of the Delta.

The purpose of the study is to raise awarenessof thepresent generation about the extent of the greatness of what Khedive Ismail caused in the architecture and theurban fabric of the Egyptian state specially in city of Tanta because the identity of the city is no longer evident as it was especially that contemporary urbanism distorts the features of the city andThe situation is getting worse and worse day by day.There must be a pause to reduceunplannedurban development to make a visualdisparity between old and new fabric, control the construction processes in heritage districts to make sure that it will not distort the urban fabric

One of the main prospective results of this research is to include the Khedive district in the city of Tanta as a heritage district which must be protected by Law 119 -2008, which governs all the features of the urban heritage districts(height of buildings, style of façades, lighting, landscaping, and sidewalks) (Hawas 2013) and others, which will protect the visual unity of the district and preserve its authentic context and its relation to the neighboring districts: generally to begin planning the historic Egyptian cities on the basis of its advantages and the development of its historical monuments. Heritage buildings registered under Law 114 - 2006 (Hawas2013) and the enrollment of unregistered buildings to be preserved and reuse all heritage buildings to achieve a sustainable future for them and for the whole district.

المقدمة

مدينة طنطا كانت تتمتع بشهرة دينية واسعة بسبب قدوم السيد أحمد البدوي إليها عام ١٢٤٠ وعاش بها حتى وفاته عام ١٢٧٦ وبقيت طنطا طوال ستة قرون مقتصرة على كونها مدينة السيد البدوي حتى ولي الخديوي إسماعيل عرش مصر فحظيت باهتمام لا يقل عن مدينتي القاهرة والاسكندرية فالجميع كان على درجة واحدة من الرقي والتميز، وكانت عناية الخديوي إسماعيل في البداية بعمارة وعمران القاهرة لكي تصبح الواجهة لدولة عصرية تحاكي وتنافس أكبر العواصم الأوروبية الحديثة –أرادها أن تصبح باريس الشرق– فتم تخطيط المدينة على أساس نسيج عمراني مبني على الشوارع المستقيمة الواسعة التي تتجمع لتصب في ميادين متدرجة في المقياس والأهمية وتم تشيد قصور ومباني بدورانات لتحمل سمات الجاذبية الباريسية وأجواء الروكوكو.(صالح ٢٠١٥) "صفحة٧"

[١] القاهرة الخديوية عام ١٩٨٤بشوارعها المستقيمة التي تتوسطها ميادين متدرجة في المقياس والأهمية (حواس٢٠٠٢)

التطور العمراني لمدينة طنطا

كانت طنطا عبارة عن بؤرة محددة تعود إلى العصور الوسطى يقع في قلبها الجامع الأحمدي، يحدها شرقًا وجنوبًا الترع والقنوات الملاحية وحدودها الشمالية مفتوحة للامتداد المستقبلي على طول المجرى الملاحي لقناة القاصد وحدودها الغربية مفتوحة أيضا، وكان يغلب عليها الاستعمال السكني التجاري وذات النسيج العمراني قوامه طرقات ضيقة غير مخططة تتنوع بين شوارع وحارات وعطفات، وكانت طنطا مشهورة قديما ببواباتها، إذ كان لها عدة بوابات تغلق على أهلها مساء كل يوم (وذلك على غرار بوابات القاهرة الشهيرة)، منها واحدة على الحد البحري وأخرى على الحد الغربي وثلاث بوابات على الحد الجنوبي الغربي للمدينة القديمة (البؤرة التاريخية) وقال عنها العالم الأثري الفرنسي ج.ف.شامبليون (١٧٩٠–١٨٣٢مكتشف حجر رشيد) "لم نكد نقترب من تلك الأسوار العالية العتيقة ذات البوابة التي انهارت حديثاً، لم أستطع قياس مدى التأثر الذي شعرت به بعد أن تجاوزنا تلك البوابة، ووجدنا تحت ناظرينا كتلاً هائلة بارتفاع ٨٠ قدمًا، إنها صخور متشابهة تهشمت بفعل الصواعق أو الهزات الأرضية".(وهبي ١٩٦٥)

– ولما اعتلى الخديوي إسماعيل عرش البلاد أعطا المدينة هوية جديدة فأقام ثورة عمرانية غير مسبوقة حيث اختار غرب المدينة القديمة ليكون محور اهتمامه ورعايته وكان اختيار مدروس لموقع استراتيجي يربط بين مركز النقل البري المتمثل في السكك الحديدية والنقل النهري المتمثل في المجرى الملاحي لقناة القاصد كما وتقع تلك المنطقة بجوار البؤرة التاريخية يفصلهما شارع وتحوي المنطقة المختارة مقر ديوان المديرية (مبنى مديرية الغربية قديما).

[٢] المنطقة الخديوية غربي ديوان المديرية وعلاقتها بمحطة السكك الحديدية والقناة الملاحية والمدينة القديمة من خريطة طنطا ١٨٨٧

وبالفعل صدر الإذن من طرف الخديوي لديوان الأوقاف بتقسيم الفضاء الواقع في غربي المدينة بجوار ديوان المديرية على الراغبين وتحكيره وعمل لذلك الرسومات اللازمة وجرت العمائر فيه طبق الأوامر الخديوية فبنيت هناك أبنية فاخرة وعمائر جليلة مما زاد من بهجة المدينة وعمارتها وكثرة سكانها. (مبارك ١٨٨٨)

- أقيم بالمنطقة أغلب المصالح الحكومية والإدارات والمدارس والمستشفيات وكان من أهم المصالح الحكومية التي أقيمت بها القنصليات الأجنبية وعلى رأسهم القنصلية الفرنسية والإيطالية واليونانية، حيث كانت توجد القنصلية اليونانية في شارع طه الحكيم والقنصلية الفرنسية في شارع الإمام الشافعي والقنصلية الإيطالية في شارع الأميرة فوزية (المدارس حاليا) (القنصليات الإيطالية في مصر كانت توجد في خمس مدن فقط هم الإسكندرية–القاهرة–طنطا–السويس–المنصورة) (Shlala 2017)كما تقع القنصلية الفارسية في الشمال الشرقي من تلك المنطقة التراثية، فأصبحت أهم وأرقى منطقة في المدينة وحتى وقت قريب (أواخر القرن العشرين).
- وقد تم توسعة بعض الحارات وفتح الشوارع المستقيمة ورتب لها مهندس تنظيم وحكيم صحة وفتحت فيها عدة شوارع وحارات ذات اتساع واعتدال فتمكنت دواعي الصحة من أزقتها وبيوتها وحسن حالها وكثرت فيها أنواع المتاجر و ازدادت الرغبة في سكناها.(مبارك ١٨٨٨) " صفحة ٤٥ الجزء الثالث عشر"
- هاجر إلى طنطا كثير من أهل الوطن والأغراب من شوام وأروام فرنساوية وانكليز وطليانية ونمساوية ومالطية ويهود حتى صار عدد أهلها كثيرا. (مبارك ١٨٨٨)

[٣] المنطقة الخديوية بعد تعميرها والخدمات التي أقيمت بها من خريطة ١٩٢٨
(مصدر خريطة ١٩٢٨ موقع انترنت ١)

ازدهار مجال القطن في طنطا تزامنا مع نهضتها العمرانية

إلى جانب النهضة العمرانية التي أحدثها الخديوي إسماعيل، حظيت طنطا بشهرة عالمية خاصة بها بسبب ريادتها في مجال القطن (الذي ظلت مصر الدولة رقم ١ في العالم في إنتاجه بأجود أنواعه حتى أوائل الخمسينات)، حيث أنشأ بها على مساحات كبيرة شون ومحالج وحلقات القطن ، فكانت طنطا تمثل منفذ تصريف محصول القطن في وسط الدلتا.

فانفردت طنطا قديماً بوجود بورصة القطن، وكان بها كل متعلقات صناعة القطن وتسويقه من آلات ومصانع، وكانت تلقب بـ(ملكة البورصة)، وإلى الآن يوجد بها شارع البورصة وامتداده حلقة القطن، واعتبر شارع حلقة القطن بها أكبر وأهم مركز لبيع القطن في وسط الدلتا.(وهي١٩٦٥)

[٤] شون ومحالج وحلقات القطن في المنطقة الصناعية بطنطا ١٩٢٨

وتمركزت هذه الصناعة في الجزء الشمالي الشرقي من المدينة وبذلك أصبحت المدينة تنقسم إلى مدينة قديمة حول الجامع الأحمدي ومنطقة إدارية وثقافية في الجزء الغربي ومنطقة صناعية في الشمال الشرقي وتحدد هذه الأقسام كل من القناة الملاحية والسكك الحديدية.

[٥] الأقسام العمرانية لمدينة طنطا من خريطة ١٩٢٨

فانفتحت المدينة على العالم وهاجر إليها الأوروبيون من جميع أنحاء اوروبا للعمل بها وجمع الأموال، مثل الاسكتلندي "جيمس إنجليس" الذي هاجر إلى طنطا هو وأسرته للعمل في مجال القطن، وحقق إنجليس ثروة هائلة في طنطا وكان ذلك في عهد الخديوي إسماعيل وعندما عاد إلى بلده أنشأ قصراً ومصنعا ودارا لرعاية الأطفال وكبار السن عام ١٨٨٤واسماهما باسمها Tantah Croft تأثراً بها وبمكانتها العالية وما زالا موجودين في بلدة بيبلز الاسكتلندية والقصر مسجل ضمن المباني ذات القيمة التاريخية الاقليمية في اسكتلندا ومشهور بحكاية صاحبه انجلس ومدى تأثره بالمدينة المصريةفي قلب وادي النيل.(موقع انترنت ٤)

[٦] قصر طنطا كروفت في اسكتلندا

بحر طنطا (المجرى الملاحي لقناة القاصد)

بحرطنطا كان ذو أهمية كبرى حتى أواخر القرن التاسع عشر حيث كان النقل النهري وسيلة المواصلات الرئيسية لأغلب المترددين على مدينة طنطا خصوصا أيام مولد السيد البدوي إلى أن دخلت السكك الحديدية في خمسينيات القرن التاسع عشر وقلت أهمية بحر طنطا شيئا فشيئا كوسيلة للانتقال فتم ردمه بعد أن ساهم بشكل كبير في تكوين المدينة و تحديد شكلها وامتدادها على طوله وتشكلت حوله القصور والمباني الفخمة لأغنى الشخصيات التي عاشت في طنطا لتعطي لهذا المسار ثقل عمراني ومعماري شكل هوية المدينة الحديثة ولايزال العديد من القصور التراثية قائما حتى الآن لم تطاله يد التخريب ليكون شاهدا على مدى ثراء العمارة في ذاك الزمان.

[٧] رسمة قديمة لطنطا في النصف الثاني من القرن التاسع عشر وتظهر بها القناة الملاحية بمسارها الأصلي كما تظهر المنطقة الصناعية قبل تعميرها وإنشاء المحالج والشون والحلقات وتظهر على يمين الرسمة مآذن الجامع الأحمدي (موقع انترنت ٣)

[٨]لقطة بانورامية لطنطا نهاية القرن التاسع عشر (موقع انترنت ٢)

[٩]صورة للقناة الملاحية ١٩١١وتطل عليها كلية سانت لويس وكنيسة الإفرنج الكاثوليك وجامع المنشاوي (موقع انترنت ٢)

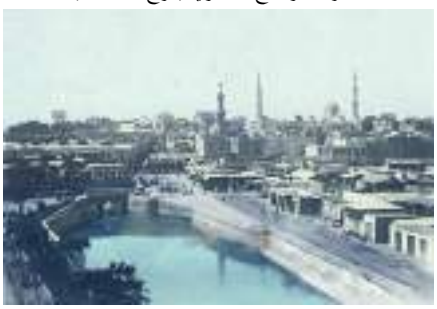

[١٠]لقطة بانورامية لطنطا بداية القرن العشرين (موقع انترنت ٣)

[١١] أماكن بعض الصور القديمة للقناة الملاحية على خريطة ١٩٢٨

وكما تم في مشروع القاهرة الخديوية من تحويل مجرى النيل بداية من ١٨٦٣ (حواس ٢٠٠٢) كذلك في طنطا تم ردم المجرى الملاحي لقناة القاصد وتحويل مجراها لتكون خارج الكتلة العمرانية، وقد بدأت أعمال تحويل المسار في منتصف العقد الثالث من القرن العشرين وانتهت في العقد الخامس حيث ردم أخر جزء من القناة عام ١٩٥٤ وتحولت إلى شارع أخذ منها الاسم فقط، وأصبح مسار الترع على حدود المدينة فقط.(أرشيف ٣)

[١٢]خريطة بتاريخ ١٩٣٣ لتحويل مسار القناة حيث يظهر المسار المقترح باللون الأحمر (أرشيف ٣) – خريطة ٢٠٠٨ ويظهر تحول المسار القديم للقناة إلى شارع (أرشيف ٤)

وكما يظهر في الخريطة النمو العمراني الهائل في المدينة وترامي أطرافها خارج الحدود القديمة لها، مما يؤثر على وضوح معالمها وتداخل النسيج القديم مع الحديث مما يحدث خلل في السياق العمراني الأصلي الذي نسعى لإبرازه والحفاظ عليه.

نماذج على الشوارع والمباني التراثية في الأقسام التراثية الثلاث لمدينة طنطا

في عام ٢٠٠٧ تم تسجيل ٢٧ مبنى تراثي ذوطراز معماري متميز في مدينة طنطا تبعا لقانون ١٤٤ لسنة ٢٠٠٦في جهاز التنسيق الحضاري والذي يحظر هدم هذه المباني هدم كلي أو جزئي وأغلب هذه المباني في المنطقة الخديوية (أرشيف ١)، كما تمتلك المدينة ستة مباني مسجلة كأثار إسلامية وقبطية تابعة لمنطقة أثار وسط الدلتا تم تسجيلها ابتداءا من عام ١٩٩٩ (الجامع الأحمدي والسبيل الأحمدي وسبيل على بك الكبير ومجموعة المنشاوي الإسلامية وجامع عز الرجال وقصر الأميرة فريال)، وقصر الأميرة فريال هو المبنى الوحيد المسجل في الجهتين (وزارة الأثار وجهاز التنسيق الحضاري) في آن واحد،كما يوجد الكثير من المباني التراثية غير المسجلة والتي تمثل في مجموعها ذاكرة للنسيج العمراني التراثي الأصيل، ويمكن القول أنه لولا استخدام بعض المباني التراثية كمقر لجهات حكومية وإدارية وبقاء بعض السكان في المباني القديمة لما دام هذا الرصيد التراثي الحالي (رغم قلته) من المباني حتى اليوم.

وهنا بيان مواقع المباني المسجلة وبعض المباني غير المسجلة في المدينة على خريطة ١٩٢٨ والموجودة حتى الآن

[١٣] المباني التراثية الموجودة في مدينة طنطا من ١٩٢٨ والباقية حتى الآن

أولا: نماذج لعمارة وعمران البؤرة التاريخية

في هذا البحث تم التركيز على المنطقة الخديوية والمنطقة الصناعية بشكل أوسع دون التعمق في تفاصيل البؤرة التاريخية حيث أنها تم دراستها بشكل مفصل في دراسات سابقة حديثة (زيدان ٢٠١٦)، ونكتفي هنا بعرض موجز لأبرز سمات عمارة وعمران البؤرة التاريخية على رأسها الجامع الأحمدي ومسجد سيدي مرزوق التاريخي وصور للنسيج العمراني للمنطقة من شوارع ضيقة وارتفاعات تتراوح بين دور واحد وثلاثة أدوار في غالبية البؤرة التاريخية حيث أنها تتمتع بطابع تراثي خاص معماريا وعمرانيا.

الجامع الأحمدي

تبلغ مساحته ١١٠٠٠م٢، بدأ فى شكل خلوة ١٢٧٦ ثم زاوية، ثم مسجدا بفضل على بك الكبير ١٧٧٣ وبعدها قام عباس باشا الاول عام ١٨٤٨ بإعادة بناؤه، وتقويته فى عهد عباس حلمى الثانى ١٩٠٢، توسعة فى ١٩٥٦، وأضيف إليه الرواق الجنوبي عام ١٩٧٥.(زيدان ٢٠١٦)

[١٤] الجامع الأحمدي وبجواره اللوكاندة الأحمدية في القرن العشرين (موقع انترنت ٣)

مسجد سيدي مرزوق

ثانى اقدم مسجد في مدينة طنطا بعد مسجد البهي ويرجع إلى عام٧٥٠م، ودفن به مرزوق الغازى ١٥٧٣، وتم إعادة بنائه ١٩٢٧م ،ويبعد ٢٥٠م عن الأحمدى (زيدان ٢٠١٦).

[١٥] مسجد سيدي مرزوق في البؤرة التاريخية

[١٦] الشوارع الضيقة والمباني ذات الطابع التراثي في البؤرة التاريخية

النسبة الأكبر من البؤرة التاريخية مازال محافظاً على النمط العمراني والمعماري خاصة في شرق الجامع الأحمدي مع وجود تغييرات كثيرة في الجهة الغربية منه وذلك لمجاورتها للمنطقة الخديوية فأخذت من طابعها الخدمي وشيدت العمائر المرتفعة وتم توسعة الشوارع في عهدالرئيس السادات (وهي ١٩٦٥) ولكن الطابع العام للبؤرة التاريخية مازال محافظاً على نمطه المعماري والعمراني.

ثانيا: نماذج للشوارع والمباني التراثية في المنطقة الخديوية

شارع المديرية

تم اختيار هذا الشارع كأبرز نموذج للمنطقة الخديوية لأهميته البصرية في الفصل بين المدينة القديمة والمنطقة الخديوية وهو شارع تجاري من أشهر وأهم شوارع طنطا ويصل بين أهم ميادين طنطا ميدان الساعة وميدان المحطة.

[١٧] شارع المديرية من خريطة ١٩٢٨ وتظه المباني التراثية الموجودة حاليا به باللون الأحمر وباللون الأزرق باقي عمارات البواكي التي هدمت- شارع المديرية أواخر القرن التاسع عشر(موقع انترنت ٢)

ويتميز شارع المديرية بالمباني ذات البواكي التي تغطي الرصيف للتظليل والحماية من الشمس والمعروفة في طنطا بعمارات الأوقاف بنيت في ثمانينات القرن التاسع عشر وبقى منها عمارتين، وفيما يلي عرض لبعض المباني التراثية في المنطقة الخديوية:

عمارات الأوقاف (المباني ذات البواكي): تسمى حاليا عمارة الإنشاء وعمارة المنزلين وفقا لهيئة الأوقاف

تاريخ الإنشاء: عمارة الإنشاء١٨٨٠- عمارة المنزلين١٨٩٠ (أرشيف٢)

الطراز المعماري: كلاسيك

الإستخدام الأصلي للمبنيان: سكني تجاري (أرشيف١)

الإستخدام الحالي: تجاري

المساحة: عمارة الإنشاء ٧٧٣م^2- عمارة المنزلين ٣٨٣م^2(أرشيف٢)

عدد الأدوار: ثلاثة أدوار علوية

[١٨] شارع المديرية أواخر القرن التاسع عشر(مواقع انترنت ٢) وحديثا ٢٠١٦ بمبانيه ذات البواكي التي تغطي الأرصفة

عقار رقم ١ شارع الأوقاف ويطل على شارع المديرية من جهتين (يطلق عليه عمارة ميتو حاليا)

تاريخ الإنشاء: تسعينات القرن التاسع عشر. الطراز المعماري: نيو باروك فرنسي.

الإستخدام الأصلي: إدراي سكني (الطابق الأرضي كان عبارة عن مكتب الري التابع للجمعية الملكية للزراعة).

الإستخدام الحالي للمبنى: سكني+ محلات تجارية.

عدد الأدوار: أرضي +أربعة ادور علوية ونصف دور بالسطح المساحة: ٣٨٠م^2 (أرشيف ١)

المبنى محافظ على الطراز المعماري لواجهاته مع بعض التغيرات في الدور الأرضي وإضافة نصف دور علوي مستحدث ليكون الدور الأخير بكامل المساحة.

[١٩] صورة قديمة في أوائل القرن العشرين للمبنى التراثي (موقع انترنت ٣) – صورة المبنى ٢٠١٧

عقار رقم ٢٩ شارع عثمان محمد متفرع من شارع المديرية

تاريخ الإنشاء: مطلع القرن العشرين

الطراز المعماري: نيو باروك فرنسي مع تأثير المدرسة التعبيرية.

الإستخدام الأصلي للمبنى: سكني تجاري (أرشيف١) الإستخدام الحالي: تم إخلاؤه باستثناء محل في الدور الأرضي. المساحة: ١٨٠م^2

عدد الأدوار: أرضي ودورين علويين ودور خدمات مستحدث.

المبنى محافظ على واجهاته ولكنه متضرر من الداخل (فراغي الحمام والمطبخ مهدمين بالكامل في كل الطوابق) بسبب محاولات المالك لهدمه باستخدام المياه الجارية ولكن باقي الفراغات بحالة سليمة وكذلك الواجهات الرئيسية والجانبية لم تتضررا.

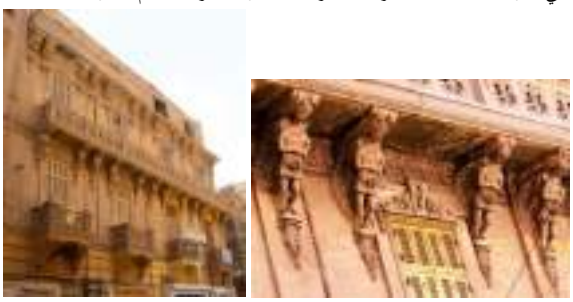

[٢٠]الواجهة الرئيسية للعقار المطلة على شارع عثمان محمد متفرع من شارع المديرية

قصر الأميرة فريال بشارع المدارس متفرع من شارع المديرية

تاريخ الإنشاء: بين ١٩٠٩و ١٩١٨ – الطراز المعماري: مزيج من نيو كلاسيك ونيو باروك فرنسي وإيطالي – الاستخدام الأصلي: سكني وأعيد استخدامه كمدرسة لمدة تقارب السبعين عاما – الاستخدام الحالي: مهجور.

عدد الأدوار: بدروم وأرضي ودور أول علوي ونصف دور ثاني علوي (بقية الدور الثاني مستحدث) – المساحة المبنية:٤٥٥م^{٢} المساحة الكلية للقصر مع الحديقة: ١٦١٥م^{٢}

"هو قصر سكني كان مملوك عام ١٩١٨ لإبراهيم بهجت واحد من أثرياء المدينة في ذلك الوقت ثم استأجرته وزارة المعارف العمومية (التربية والتعليم حالي) واستخدم كمدرسة بداية من عام ١٩٣٦" (من لقاء الباحثة مع مالك القصر أ/شوقي توكل)، وهومقفل الآن بعد أن استعاده المالك الحالي وسمي بروضة الأميرة فريال تيمنًا بالأميرة فريال ابنة الملك فاروق وسمي الشارع الذي يطل عليه بالأميرة فوزية تكريما لهما عندما جاءت الأميرة فوزية أخت الملك فاروق إلى طنطا في الأربعينيات لتفتتح مستشفى مبرة محمد علي والموجودة إلى الآن في شمال البؤرة التاريخية.

[٢١] قصر الأميرة فريال في شارعالأميرة فوزية (شارع المدارس حاليا)

[٢٢] الفرنتون أحد العناصر التشكيلية للواجهة الرئيسية لقصر الأميرة فريال

ثالثا: نماذج للمباني التراثية في المنطقة الصناعية

– كلية سانت لويس (مدرسة فرنسية) واحدة من أهم وأقدم المباني في المنطقة الصناعية والتي تحولت إلى مبنى إدارة جامعة طنطا وهدم المبنى الإداري الذي يطل على القناة سابقا شارع البحر حاليا وتم بناء مبنى أخر محله.

[٢٣] تحولات المدرسة الفرنسية التراثية على مر العصور (موقع انترنت ٣)

– قصر عائلة كوهين في طنطا (فيلا أسعد حاليا)

تاريخ الإنشاء: مطلع القرن العشرين – الطراز المعماري: باروك فرنسي.

الاستخدام الحالي والأصلي: سكني – عدد الأدوار: بدروم وأرضي ودورأول علوي– عنوان القصر: شارع البحر بجوار مبنى جامعة طنطا (كلية سانت لويس سابقا).

[٢٤] واجهة القصر من شارع البحر ٢٠١٦

القصر كان مملوكا لعائلة كوهين من أغنى العائلات اليهودية التي سكنت طنطا إلى منتصف القرن العشرين والذين شاركوا في انعاش الحركة الاقتصادية بالمدينة ثم انتقلوا إلى الاسكندرية وبعدها إلى فرنسا (أبو الغار ٢٠٠٦) وعرضوا القصر للبيع في اليانصيب بحيث كانت بطاقة اليناصيب الواحدة تساوي جنيه واحد (موقع انترنت ٣) وأصبح القصر من نصيب محمد أسعد المالك الحالي ومازال القصر يتمتع بحالة جيدة ويعد زاكرة للمكان.

[٢٥] قصر عائلة كوهين من كتاب يهود مصر (الصورة التي نشرت أثناء عرضه للبيع) (أبو الغار ٢٠٠٦)

– أماكن المحالج والشون وحلقات القطن حاليا وبقاياها المعمارية

أماكن المحالج والشون وحلقات القطن القديمة مستغلة حاليا كمساكن وخدمات مختلفة ولم يتبق في المنطقة الصناعية سوا فراغ كان يمثل جزءًا من محلج قديم وبه بقايا أجزاء من المحلج.

[٢٦] الفراغ والبقايا المعمارية من محلج قديم في المنطقة الصناعية

[٢٧] المناطق الصناعية تحول أغلبها إلى مساكن ومشار بالسهم على المنطقة المتبقية من محلج قديم.

المدلول التراثي لطنطا الخديوية (القيم المتمثلة في المنطقة):

تتمتع المنطقة بطابع تراثي يكاد يندثر لولا بقاء بعض المباني التي تمثل هذه الحقبة فللوهلة الأولى يمكن للزائر أن يدرك بأن المنطقة تختلف عن المدينة القديمة في طابعها العمراني (من اتساع الشوارع واتجاهاتها وتخطيط وتقسيم الأراضي) والمعماري ولكنه لن يدرك مدى رقي هذه المنطقة قديما إلا إذا أمعن النظر وحاول ربط المعطيات الباقية مع بعضها البعض فهناك العمائر ذات طراز شب موحد على النيو باروك فرنسي وإيطالي واستخدمت فيها نفس الكوابيل واعتمدت على الزوايا الدائرية كما شوارع باريس والمباني ذات البواكي التي تغطي الأرصفة والباقي منها عمارتين في شارع المديرية التراثي والذي يفصل بين المدينة القديمة والمدينة الحديثة التي أسسها الخديوي إسماعيل ويمكنه بعد ذلك أن يدرك حدود المنطقة شرقا وجنوبا واستقراء القيم التاريخية والجمالية المعمارية والعمرانية والوظيفية بها.

القيمة التاريخية:

أن تاريخ تخطيط المنطقة يعود إلى ولاية الخديوي إسماعيل الذي وضع أسس تخطيطها فهي تمثل بداية العمران المصري في صورته الحديثة في النصف الثاني من القرن التاسع عشر فيقترب عمر المنطقة من المائة وأربعين عاما.

فأمر بتخطيطها على نسيج عمراني يعتمد على المحاور الرئيسية المحددة للبؤرة التاريخية والشرايين الرئيسية بداخلها فتم الالتزام بها لتخطيط المنطقة الخديوية وشيدت الشوارع الواسعة المستقيمة والمباني إما قصور وفيلات أو عمارات فخمة تطل على الشوارع الرئيسية، وهنا يختلف النمط العمراني المتبع في طنطا الخديوية عن القاهرة الخديوية فقد اعتمدت القاهرة على الميادين الواسعة والمتدرجة التي تتوسط تلك الشوارع المستقيمة.

القيمة الرمزية:

حركة البناء والتعمير في ذلك العصر لم يكن قوامها فقط القصور الخاصة بطبقة الأمراء والنبلاء، وإنما أيضا خدمة شرائح اجتماعية مختلفة واستحداث أنماط وظيفية جديدة من المباني.

تميز المجتمع بوجه عام في ذلك العصر بالذوق الرفيع والحس الجمالي الواضح في عمارة وعمران المدينة الحديثة بطنطا.

إبداع الأيدي العاملة المصرية والأجنبية في إنتاج التفاصيل المعمارية التي تزخر بها واجهات المباني التراثية والتي تضفي على الواجهات فخامة وثراء.

القيم العمرانية والمعمارية:

تعبر المنطقة الخديوية ومبانيها التراثية عن طرز ومدارس معمارية عالمية تتناغم فيما بينها وتجتمع مع بعضها أحيانا في واجهة مبنى واحد ممثله مزيج بديع من التفاصيل العالية الدقة والانسيابية وكذلك العناصر المشتركة المكررة في كثير من المباني والتي تعطي وحدة بصرية مميزة للمنطقة.

القيمة الوظيفية:

تحتوي المنطقة الخديوية على رصيد عمراني لا بأس به قوامه المباني ذات القيمة التراثية التي تقف راسخة رغم ما مر عليها من عقبات كادت أن تقضي عليها وعدد هذه المباني يجاوز الأربعين مبنى منهم المسجل ومنهم الغير مسجل بعض منها لازال يؤدي وظيفته الأصلية التي أنشئ من أجلها والبعض الأخر أعيد استخدامه لوظائف أخرى، والأخر مهجور ينتظر مشروع إعادة استخدام.

وتنبع الأهمية الوظيفية للمنطقة الخديوية من تمركز المباني الخدمية والعامة بها فمنها الإداري والتعليمي والثقافي والتجاري والصحي والترفيهي بها مما يرفع بقيمتها الوظيفية في إطار رصيدها العظيم من التراث العمراني الذي يحتفظ بدوره النفعي والحيوي، على سبيل المثال لا الحصر:

- المصالح الحكومية (مجلس المدينة وإدارة الحي، مكتب الشهر العقاري، الضرائب العقارية، هيئة الأوقاف، مديرية التربية والتعليم، مديرية الشئون الاجتماعية، مركز معلومات الرقم القومي، التأمينات والمعاشات، مديرية الشئون الصحية، مديرية الإصلاح الزراعي، تفتيش الري،...إلخ)
- مبان البنوك والمصارف الرئيسية (بنك مصر والبنك الأهلي وبنك الاسكندرية...
- المدارس الابتدائية والإعدادية والثانوية والجامعة العمالية والمعهد الفني الصحي واكاديمية تدريب المعلمين
- المستشفيات (مستشفى الحميات قديما كانت الاسبتالية الأميرية، مستشفى الهلال الأحمر، مستشفى ٥٧٣٥٧ لأورام الأطفال.
- مجمع المحاكم و المطافي والإسعاف ومباحث النقل والقسم الشرطي
- السنيمات (سنيما أمير، ريفولي، الجمهورية) ومسرح مدينة طنطا
- المباني الخدمية الكثيرة (مكاتب محاماة وعيادات طبية) والمباني التجارية

[٢٨] استعمالات الأراضي الحالية في المنطقة الخديوية ونلاحظ أنها مازالت محتفظة بطابعها الخدمي الإداري والتعليمي وبجوارها المدينة القديمة التي يغلب عليها الاستعمال التجاري والسكني

وللحفاظ على هوية مدينة طنطا لابد من الحفاظ على هذه القيم وإبرازها من خلال التوصيات التالية:

التوصيات

إدراج القيم العمرانية المتمثلة في النسيج الأصلي لمدينة طنطا التراثية لمخطط المدينة لعام ٢٠٣٠ من خلال إبراز السمات –المعبرات– التي مازالت موجودة على أرض الواقع ويمكن تقسيم المقترح إلى أربعة محاور بناءا على مكونات النسيج الأصلي وهي:

- المجرى الملاحي لقناة القاصد
- البؤرة التاريخية
- المنطقة الخديوية الإدارية
- المنطقة الصناعية

[٢٩]المناطق التراثية الثلاث في قلب المدينة الحديثة

[٣٠] خطة الحفاظ على السمات التراثية المعبرة عن النسيج العمراني المحاور الأربعة للمدينة

أولا القناة الملاحية

يتم عمل حزام أخضر مستمر على مسار المجرى الملاحي الأصلي للقناة يحدد البؤرة التاريخية من الغرب والشمال الغربي ويستمر شمالا على طول المدينة، وكان شارع البحر قبل عام ٢٠١٢ يحتوي على جزيرة عريضة (متوسط عرضها ١٥م) في منتصفه تقترب من فكرة الحزام الأخضر المطلوب ولكن تم توسيع الشارع في الاتجاهين وتضييق الجزيرة إلى أن أصبحت مجرد فاصل فنقترح إعادة إدراج الحزام الأخضر كما كان من قبل وذلك لتحسين الظروف البيئية للكتلة العمرانية وليصبح واجهة للمنطقة الصناعية والبؤرة التاريخية ومتنفس يتخلل النسيج العمراني ولإبراز التطور التاريخي للمدينة والفصل البصري بين البؤرة التاريخية والمنطقة الصناعية والمنطقة الإدارية.

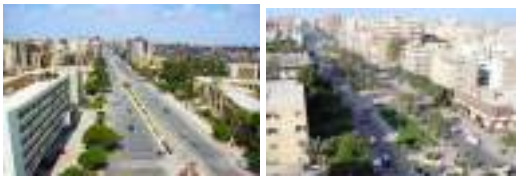

[٣١] شارع البحر قبل تضييق الجزيرة في الوسط وبعده (موقع انترنت ٣)

كما ويقترح عمل بحيرة صغيرة في قلب الحزام الأخضر أو سلسة من البحيرات للتعبير عن المجرى القديم للقناة الملاحية في المكان المشار إليه بحيث تقابل بقايا المنطقة الصناعية القديمة والبؤرة التاريخية وتستخدم في أنشطة ترفيهية ورياضية ويتسع الحزام الأخضر حولها لتصبح متنزه ترفيهي للمنطقة.

ثانيا البؤرة التاريخية

الحفاظ على هذه المنطقة يبدأ من الحفاظ على الفعالية الأهم على مستوى المدينة وهي مولد السيد البدوي كتراث غير مادي له معبراته وسماته المعمارية الموجودة والمؤثرة بشكل كبير على أرض الواقع بداية من الجامع الأحمدي والمساجد الأثرية بالمطنقة منها ما يعود إلى ما عصر ما قبل الجامع الاحمدي ومنها ما بني بعده وكذلك اللوكاندات والفنادق التي يبيتبها زوار ومريدي المولد كل عام والذين قارب عددهم في إحدى السنوات الاثنين مليون زائر وعلى الجانب الأخر إحياء الحرف التراثية في المنطقة والتي مازال بعضها موجود إلى الآن وتنمية الأسواق والأماكن التجارية والتي تمثل النسبة الأكبر من استعمالات الأراضي في المنطقة حيث أنها تعتبر تجارية من الدرجة الأولى، لذا لابد من: ١– الحفاظ على النسيج العمراني القديم للبؤرة التاريخية.

٢– إعادة تأهيل المباني داخلها واستغلالها لخدمة السياحة الدينية والثقافية.

٣– إبراز السمات المعمارية والعمرانية المرتبطة بالمولد (الجامع الأحمدي ومسار موكب الخليفة في المولد والمساجد التاريخية التي يمر بها واللوكاندات).

٤– إحياء الحرف التراثية وتوفير أماكن لعرضها في مسار موكب الخليفة في المولد.(زيدان ٢٠١٦)

ثالثا المنطقة الخديوية

الحفاظ على النسيج العمراني للمنطقة الخديوية بداية من الحفاظ على الشوارع والميادين التراثية والتي مازالت بنفس سياقها الأصلي ومنع التعدي عليها.

إعادة استخدام القصور والمباني التراثية في وظائف تخدم المدينة من الناحية الإدارية والثقافية (مثل الإدارات الحكومية والمكاتب والمتاحف ومراكز الثقافة والمسارح وغيرها).

حماية المنطقة من عمليات البناء الغير متوافقة مع أصالتها العمرانية والمعمارية من حيث طراز الواجهات وارتفاعات المباني التي تؤثر سلبا على الصورة البصرية للمنطقة وتفقدها طابعها التراثي.

إعادة تأهيل المباني التراثية المستخدمة بحيث نضمن عدم الاساءة إليها والتأكيد على استمراريتها واستدامتها.

رابعا المنطقة الصناعية

بما أن أماكن المحالج والشون وحلقات القطن القديمة أغلبها أعيد استخدامه كمساكن وخدمات مختلفة فلابد من استغلال الدليل الوحيد الباقي المرتبط بالصناعة في المنطقة والذي كان جزءًا من محلج قديم فنقترح أن يتم استخدام هذا الفراغ خصوصا مع وجود بقايا للمحلج كجزء متحفي عن المدينة الصناعية القديمة للدلالة عليها ويكون ذلك

بربط هذا الفراغ مع شارع حلقة القطن الموجود إلى الآن في البؤرة التاريخية والذي مازال يوجد به محلات بيع القطن (ولكن قطن مستورد من محافظة الجيزة)، ويتميز هذا الفراغ بقربه من مسار القناة الملاحية القديمة مما يسهل من ربط محاور الحفاظ ببعضها فتكون البحيرة الصغيرة المقترحة في قلب الحزام الأخضر أقرب ما يكون للعرض المتحفي في فراغ المحلج القديم والجميع على ممقربة من البؤرة التاريخية والمنطقة الخديوية.

[٣٢] محلات بيع الأقطان من شارع حلقة القطن في البؤرة التاريخية

الخلاصة

- تناولت الدراسة مدينة طنطا وتاريخها ومراحل نموها وتطورها الثلاث (البؤرة التاريخية – المنطقة الخديوية– المنطقة الصناعية).
- السمات المعبرة عن كل منطقة مازالت موجودة وبشكل مؤثر على أرض الواقع على المستويين المعماري والعمراني مثل القصور والمباني الفاخرة في المنطقة الخديوية وكذلك الشوراع والميادين التراثية بها، والمساجد القديمة والجامع الأحمدي واللوكاندات في البؤرة التاريخية وأيضا الشوارع القديمة، وبالنسبة للمنطقة الصناعية النسيج العمراني التراثي موجود بسياقه الأصلي والقصور والمنشئات المطلة على القناة سابقا مازال أغلبها بحالته الأصيلة.
- إحياء المجرى الملاحي الأصلي لقناة القاصد والذي يشكل فصل بصري واضح بين المناطق الثلاث وواجهة مميزة لكل منها.
- التفرقة بين المناطق الرئيسية الثلاث والحفاظ على سياق كل منطقة يبرز هوية المدينة وبعظمها.
- إبراز هوية المدينة وأصالتها يوجه المدينة نحو التنمية المستدامة وبالتالي ضمان مستقبل عمراني يدعم التراث الأصيل.
- تمثيل المناطق العمرانية الثلاثة وشريان القناة لإحياء تاريخ المدينة من خلال إبراز السمات الموجودة على الأرض والتدليل على العناصر المندثرة كعمل حزام أخضر وبحيرات في مسار القناة القديم وعمل عرض متحفي في بقايا المحلج.
- تسجيل المناطق بشكل واضح كمناطق تراثية تبعا لقانون ١١٩ لسنة ٢٠٠٨ على المستوى العمراني وتسجيل المباني التراثية الغير مدرجة في قانون ١٤٤ لسنة ٢٠٠٦ وإعادة تأهيلها واستخدامها لدعم الوظيفة الأساسية لكل منطقة.

المراجع

أ– الكتب العربية

- مبارك، علي "الخطط التوفيقية الجديدة لمصر ومدنها وبلادها القديمة والشهيرة" الجزء الثالث عشر –ترجمة الشيخ الشرف الطنبدي ١٨٨٨–١٨٨٩.
- وهبي، سيد "السجل الذهبي لطنطا" الجزء الأول –دار سفير للنشر بالغربية الطبعة الأولى ١٩٦٥.
- حواس، سهير زكي "القاهرة الخديوية: رصد وتوثيق عمارة وعمران القاهرة – منطقة وسط البلد" مركز التصميمات الهندسية– المهندسين الطبعة الأولى ٢٠٠٢.
- أبو الغار، محمد "يهود مصر من الازدهار إلى الشتات" دار الهلال الطبعة الأولى ٢٠٠٦.
- صالح، فتحي دليل بعنوان "القاهرة :حولة معمارية إيطالية حول المباني التاريخية التي قام بتصميمها وبنائها إيطاليين خلال القرنين التاسع عشر والعشرين" المعهد الثقافي الإيطالي بالقاهرة والمكتب العلمي بالسفارة الإيطالية بالقاهرة ٢٠١٥.
- حواس، سهير زكي "الحفاظ العمراني وإحياء المناطق التراثية فى مصر– مشروع الدرب الأحمر" مؤسسة الأغا خان–القاهرة ٢٠١٣.

ب– الكتب الإنجليزية

- Shlala, Elizabeth H "The Late Ottoman Empire and Egypt: Hybridity, Law and Gender" Routledge Oxon and New York-USA 2017.

ت– أرشيف هيئات حكومية

١. الإدارة الهندسية/ حي أول طنطا/ محافظة الغربية/ منطقة وسط الدلتا.
٢. الإدارة الهندسية/ هيئة الأوقاف – منطقة أوقاف طنطا.
٣. تفتيش ري / القسم الثاني– مدينة طنطا.
٤. هيئة المساحة/ القسم الأول – مدينة طنطا.

ث– مواقع الانترنت

1. American Geographical Society Library Digital Map Collection University of Wisconsin. http://collections.lib.uwm.edu
2. www.delcampe.net
3. http://newtanta.blogspot.com.eg/
4. www.tantahcroft.co.uk/?c=Tantah_Story

ج– الدراسات السابقة

- زيدان، علياء خليل "الحفاظ على القيم غير المادية في مواقع التراث الثقافي: دراسة لمسجد السيد البدوي بطنطا" رسالة ماجستير بقسم الهندسة المعمارية –كلية الهندسة جامعة المنوفية ٢٠١٦.